January 2009

A Quest for Meaning in Spontaneous Brain Activity - From fMRI to Electrophysiology to Complexity Science

Biyu He
Washington University in St. Louis

Recommended Citation

He, Biyu, "A Quest for Meaning in Spontaneous Brain Activity - From fMRI to Electrophysiology to Complexity Science" (2009). *All Theses and Dissertations (ETDs)*. 149.
https://openscholarship.wustl.edu/etd/149

WASHINGTON UNIVERSITY

Division of Biology and Biomedical Sciences

Program in Neurosciences

Dissertation Examination Committee:
Marcus E. Raichle, Chair
Maurizio Corbetta
Steven E. Petersen
Abraham Z. Snyder
David C. Van Essen
John M. Zempel

A QUEST FOR MEANING IN SPONTANEOUS BRAIN ACTIVITY
- From fMRI to Electrophysiology to Complexity Science

by

Biyu Jade He

A dissertation presented to the
Graduate School of Arts and Sciences
of Washington University in
partial fulfillment of the
requirements for the degree
of Doctor of Philosophy

December 2009

Saint Louis, Missouri

ABSTRACT

The brain is not a silent, complex input/output system waiting to be driven by external stimuli; instead, it is a closed, self-referential system operating on its own with sensory information modulating rather than determining its activity. Ongoing spontaneous brain activity costs the majority of the brain's energy budget, maintains the brain's functional architecture, and makes predictions about the environment and the future. I have completed three separate studies on the functional significance and the organization of spontaneous brain activity. The first study showed that strokes disrupt large-scale network coherence in the spontaneous functional magnetic resonance imaging (fMRI) signals, and that the degree of such disruption predicts the behavioral impairment of the patient. This study established the functional significance of coherent patterns in the spontaneous fMRI signals. In the second study, by combining fMRI and electrophysiology in neurosurgical patients, I identified the neurophysiological signal underlying the coherent patterns in the spontaneous fMRI signal, the slow cortical potential (SCP). The SCP is a novel neural correlate of the fMRI signal, most likely underlying both spontaneous fMRI signal fluctuations and task-evoked fMRI responses. Some theoretical considerations have led me to propose a hypothesis on the involvement of the neural activity indexed by the SCP in the emergence of consciousness. In the last study I investigated the temporal organization across a wide range of frequencies in the spontaneous electrical field potentials recorded from the human brain. This study demonstrated that the arrhythmic, scale-free brain activity often discarded in human and animal electrophysiology studies in fact contains rich, complex structures, and further provided evidence supporting the functional significance of such activity.

ACKNOWLEDGEMENTS

This thesis is dedicated to Marcus Raichle, my advisor over the past three and a half years. Marc is a man of great brilliance and wisdom, who has taught me not only how to do science, but also how to be a scientist; who has provided me the most enviable support; who has given me an incredible degree of freedom to pursue the questions that interest me; who has demonstrated, not by words but by his own actions, the way of living of a dedicated scientist; who has seen me grow in the past few years, both scientifically and personally…It was Marc's words, and a little book that he recommended, that were the most comforting of all when I was stranded in Australia for a second winter in a year after a conference due to visa issues. It was Marc's encouragements that sustained me through some of the most difficult, and quite depressing stages of my last project involving complex topics in complexity science. It was the hours and hours of afternoons spent in Marc's office, chatting about data initially but quickly the conversation spinning onto all possible topics in science and the doing of science and all kinds of books that we both enjoy, that mark many of the most enjoyable moments in my life in the past few years. It is fair to say that I am where I am because of Marc. I hope that 20 years from now, wherever I am, I will be coming back (or to Seattle) to report to Marc what I am working on every step of the way.

Profound thanks also go to Maurizio Corbetta, who led me into cognitive neuroscience. I joined Maurizio's lab when I was 19, knew nothing of human brain imaging, had little experience writing programs and dealing with data processing. I came from the world of Drosophila behavioral genetics – which I loved, and thought I would just give it a try in systems neuroscience, but I was immediately hooked. Maurizio was a

fantastic mentor in every respect. In his lab, I went from a blank novice to someone who

not only was able to write programs, understood all the basics of fMRI data processing,

but also had a reasonable idea of the concepts of attention systems, and published two

good first-author articles, one research one review, all within a short time of one year.

How lucky was I!! Nine months after I joined his lab, Maurizio announced at the lab

meeting that he was going on a sabbatical in Sep., and there was a chance that he might

stay in Italy – to this day I hold such high regard for Maurizio's openness and integrity.

Afraid of being without a mentor, I switched to Marc's lab next door, after a long time of

very difficult decision process, but I chose to stay in the closest cubicle to Maurizio's lab.

I could not have been any more fortunate than having had two such amazing mentors at

the beginning of my scientific career.

I am grateful to Avi Snyder, a fantastic mentor, colleague and friend. I learned

how to program, and many of the mathematical tools I use from Avi. Without Avi, I

would not have been able to do what I do now. Avi has also been a great friend. Some

wonderful times in the past few years were spent talking about classical music,

composers and going to concerts together.

Very special thanks go to John Zempel. John has been a most wonderful

collaborator and mentor, who has not only provided me the opportunity to do research

with invasive EEG, but has also taught me a great deal about EEG signals. As busy as he

is clinically, he has always put my projects at high priority, and has spent an enormous

amount of time and effort helping me acquire data, making sure everything runs

smoothly. I have been so fortunate to have John's help over the past few years.

TABLE OF CONTENTS

LIST OF TABLES

CHAPTER I: Overview of Background and Significance of Spontaneous Brain activity

Why study the intrinsic activity of the brain?

Historically, there have been two alternative perspectives for understanding brain function: the first perspective views the brain as a complex input/output system driven by the momentary demands of the environment; the second perspective views the brain as a closed, self-referential system operating on its own with the sensory information modulating rather than determining its activity (Llinas, 2001). The former view has motivated the majority of systems neuroscience research, but the later perspective is gaining increasing appreciation. A consideration of various aspects including energy cost, anatomical wiring and signal magnitude emphasizes the importance of intrinsic brain activity beyond that of evoked activity.

From a metabolic perspective, the cost of intrinsic activity far exceeds that of evoked activity (Raichle, 2006; Raichle and Mintun, 2006). The adult human brain represents about 2% of the body weight, but accounts for about 20% of the body's total energy consumption. Out of this enormous energy budget, 60-80% spent at rest is devoted to intrinsic brain activity. The additional energy burden associated with momentary demands of the environment may be as little as 0.5% to 1.0% of the total energy budget.

From a view of cortical anatomy (Braitenberg and Schuz, 1998), even in layer IV of primary sensory regions, less than 10% of the synapses represent inputs from outside the brain (Peters and Feldman, 1976); the vast majority of cortical neurons are neither

directly under influence of sensory input nor directly involved in motor output. The information flow from sensory to motor areas, if there is such a thing, must pass through a very large network of interconnected neurons (Braitenberg and Schuz, 1998). It is thus more reasonable to think that the dynamic state of this large network determines motor output, whereas various sensory inputs only play a role in continually updating this dynamic state (Braitenberg and Schuz, 1998).

From a physiological standpoint, the magnitude of task-evoked responses in either electroencephalography (EEG) or functional brain imaging is very small compared to the magnitude of spontaneous signal fluctuations. Thus, conventional studies of brain's responses to carefully controlled sensory, cognitive and motor events require averaging over many trials to obtain consistent result. The brain is not a silent system waiting to be driven by external inputs, but rather one that constantly exhibits large-amplitude activity fluctuations regardless of the state of external inputs (Raichle, 2006). Corroborating the above perspective derived from cortical anatomy, this dynamic state of the brain is only updated, or informed, by sensory inputs (Petersen et al., 2003). Further, the pattern of these spontaneous fluctuations sometimes resembles that of evoked activity (Kenet et al., 2003; Tsodyks et al., 1999), supporting the idea that the brain's ultimate function is to predict the environment (Llinas, 2001).

Lastly, from a phenomenological perspective, neither the neural activity in sensory afferents nor that in motor pathways is necessary for conscious experience (Tononi, 2005). For example, a person who becomes retinally blind as an adult continues to have vivid visual images and dreams; similarly, patients with locked-in syndrome or

normal people during dreaming sleep are fully conscious despite the complete paralysis and absence of behavior (Tononi, 2005).

Spontaneous BOLD fMRI signal and its correlation structure

Spontaneous slow (< 0.1 Hz) fluctuations in the blood oxygen level-dependent (BOLD) signals of functional magnetic resonance imaging (fMRI) appear to reflect a fundamental aspect of the brain's organization (Biswal et al., 1995; Vincent et al., 2007). These fluctuations are temporally covariant within large-scale functional brain networks such as those associated with visual (Lowe et al., 1998), auditory (Cordes et al., 2000), sensorimotor (Biswal et al., 1995), language (Hampson et al., 2002), attention (Fox et al., 2006) and executive (Seeley et al., 2007) functions as well as the 'default network' (Greicius et al., 2003). These covariant relationships (i.e., correlation structures) of spontaneous BOLD signals exist during restful waking (Biswal et al., 1995; Fox et al., 2006; Greicius et al., 2003; Hampson et al., 2002; Seeley et al., 2007), task performance (Hampson et al., 2002; He et al., 2007), sleep (Larson-Prior et al., 2006) and even general anesthesia (Vincent et al., 2007). Moreover, the spontaneous fluctuations of fMRI BOLD signal contribute substantially to variability in behavioral performance (Fox et al., 2007).

Electrophysiological correlate of BOLD signal

Studies employing simultaneous recordings of BOLD signal and electrophysiological activity have found that BOLD responses evoked by sensory stimuli appear to reflect synaptic activity as reflected in local field potentials (LFPs), especially the strength (i.e., modulated power) of gamma frequency LFP response (Logothetis et al.,

2001; Mukamel et al., 2005; Niessing et al., 2005; Shmuel et al., 2006; Viswanathan and Freeman, 2007). Such a relation between BOLD signal and gamma frequency LFP power holds true for both positive (Logothetis et al., 2001; Mukamel et al., 2005; Niessing et al., 2005; Viswanathan and Freeman, 2007) and negative (Shmuel et al., 2006) task-evoked responses. Recently, a similar correlation was found between the spontaneous fluctuations of BOLD signal and those of gamma frequency LFP power in monkeys (Shmuel et al., 2007). Potentially related to the issue of electrophysiological correlates of spontaneous BOLD correlation structure, gamma frequency LFP power remain coherent in its spontaneous fluctuations at distances up to 1 cm, unlike spontaneous raw gamma oscillations which are correlated only locally (Leopold et al., 2003).

In a separate vein, an early study, by recording electrocorticography (ECoG) and regional cerebral blood flow (CBF, measured by laser-Doppler flowmetry) simultaneously in anesthetized rats, showed that spontaneous waves of CBF faithfully followed bursts of ECoG activity at a frequency of < 0.1 Hz (Golanov et al., 1994). This suggests that the burst suppression pattern of cortical surface potential may be what underlies CBF fluctuations under anesthesia.

Brain oscillations and "1/*f* noise"

Since the first human brain rhythm, alpha waves, was described by Berger (Berger, 1929), a host of other brain rhythms have been studied under various physiological and cognitive states (Buzsaki, 2006). These oscillatory patterns cover a wide range of frequencies from infra-slow oscillations (< 0.1 Hz) to ultra-fast ripples (> 200 Hz) (Buzsaki and Draguhn, 2004). Generally, higher frequency oscillations are

confined to a smaller neuronal space, whereas lower frequency oscillations recruit larger

brain networks (Buzsaki and Draguhn, 2004; von Stein and Sarnthein, 2000).

Interestingly, it has recently been found that phase of theta frequency (4-8 Hz)

oscillations modulates amplitude of gamma frequency (>30 Hz) oscillations (Canolty et

al., 2006) and unit activity (Jacobs et al., 2007). During deep sleep, the slow oscillation,

an oscillatory alternation of membrane potential between a hyperpolarized "down" state

and a depolarized "up" state at about 0.8 Hz (Steriade et al., 1993b), strongly modulate

power of higher frequency activity (Mukovski et al., 2007; Steriade et al., 1996). Further,

it has been shown that the phase of theta or gamma oscillations influence the

development of synaptic long-term potentiation or long-term depression (Holscher et al.,

1997; Wespatat et al., 2004).

The power spectrum of brain activity, whether it is measured by

electroencephalography (EEG), magnetoencephalography (MEG), ECoG, LFP, or fMRI,

obeys a power law distribution (Buzsaki, 2006; Fox and Raichle, 2007; Freeman and

Zhai, 2009), that is, the power density (P) is inversely proportional to frequency (f), as

expressed by the relationship, $P \sim 1/f^{\beta}$, where β is an exponent that normally varies in the

range of $0 - 3$. This $1/f^{\beta}$ power relationship implies that perturbations occurring at slow

frequencies can cause a cascade of energy dissipation at higher frequencies and that

widespread lower frequency activity may modulate faster local events (Bak et al., 1987;

Buzsaki and Draguhn, 2004). Indeed, the low-frequency end (< 0.1 Hz) of the "$1/f$

noise", termed infra-slow fluctuations or slow cortical potentials (SCP), appear to

modulate power of higher frequencies, with the trough of SCP corresponding to increased

power of higher frequency field potentials (Vanhatalo et al., 2004) as well as increased

multiple-unit activity (Birbaumer et al., 1990).

<u>Spontaneous brain activity across the awake-sleep cycle</u>

The transition from wakefulness to sleep is accompanied by striking changes in

neural activity patterns measured at all levels of electrophysiological recordings, from

intracellular membrane potential to scalp EEG. The characteristic oscillatory waveforms

of non-rapid eye movement (NREM) sleep include sleep spindles (12-15 Hz), delta

waves (1-4 Hz), the K-complex waveform, and slow oscillations (~ 0.8-1 Hz) (Hobson

and Pace-Schott, 2002). The early stage of NREM sleep is associated with spindles and

K-complex. As sleep deepens, power of slower frequencies (< 4 Hz) increases, deep

NREM sleep (stages 3 and 4) is dominated by delta waves and slow oscillations and thus

is also named slow-wave sleep (SWS) (Steriade et al., 1993a). Slow waves seen in the

scalp EEG are a signature of the slow oscillation, at the same frequency, of membrane

potential in virtually all cortical neurons (Mukovski et al., 2007). As the SWS transits

into rapid-eye-movements (REM) sleep that is associated with dreaming episodes, the

large-amplitude slow waves disappear and the EEG patterns show low-amplitude fast

activity similar to those during waking. These changes in spontaneous brain activity

parallel the phenomenon that consciousness is present during both waking and REM

sleep but is diminished during NREM sleep, especially SWS.

Given these dramatic changes of neuronal activity patterns, it may come as a

surprise that the spontaneous correlation structures of fMRI signals are maintained in

light sleep (Horovitz et al., 2007b), deep sleep (Horovitz et al., 2007a), as well as deep

anesthesia associated with burst-suppression EEG patterns (Vincent et al., 2007).
Potentially helpful in reconciling these results, the spontaneous fMRI signals are at a
much lower frequency (< 0.1 Hz) than the electrophysiological oscillatory patterns
mentioned in the previous paragraph, among which the slowest, the "slow oscillation"
(Steriade et al., 1993b) (i.e., the 'up' and 'down' states), is around 0.8 – 1 Hz.

In summary, the sleeping brain presents a fantastic model for studying intrinsic,
self-organized neuronal activity, as it is a natural physiological state with minimal
interaction with the environment. Understanding which patterns of spontaneous brain
activity change across awake-sleep cycle and which do not will be a critical piece in the
endeavor of elucidating how the brain maintains its intrinsic functional architecture
despite changing levels of consciousness.

References

Bak, P., Tang, C., and Wiesenfeld, K. (1987). Self-organized criticality: An explanation
of the 1/f noise. Phys Rev Lett *59*, 381-384.

Berger, H. (1929). Uber das Elektroenkephalogramm des Menschen. Arch. Psyhiatr.
Nervenkr. *87*, 527-570.

Birbaumer, N., Elbert, T., Canavan, A.G., and Rockstroh, B. (1990). Slow potentials of
the cerebral cortex and behavior. Physiol Rev *70*, 1-41.

Biswal, B., Yetkin, F.Z., Haughton, V.M., and Hyde, J.S. (1995). Functional connectivity
in the motor cortex of resting human brain using echo-planar MRI. Magn Reson
Med *34*, 537-541.

Braitenberg, V., and Schuz, A. (1998). In Cortex: Statistics and Geometry of Neuronal Connectivity (Germany: Springer), pp. 179-180.

Buzsaki, G. (2006). Rhythms of the Brain. (New York, NY: Oxford University Press), pp. 111-135.

Buzsaki, G., and Draguhn, A. (2004). Neuronal oscillations in cortical networks. Science *304*, 1926-1929.

Canolty, R.T., Edwards, E., Dalal, S.S., Soltani, M., Nagarajan, S.S., Kirsch, H.E., Berger, M.S., Barbaro, N.M., and Knight, R.T. (2006). High gamma power is phase-locked to theta oscillations in human neocortex. Science *313*, 1626-1628.

Cordes, D., Haughton, V.M., Arfanakis, K., Wendt, G.J., Turski, P.A., Moritz, C.H., Quigley, M.A., and Meyerand, M.E. (2000). Mapping functionally related regions of brain with functional connectivity MR imaging. AJNR Am J Neuroradiol *21*, 1636-1644.

Fox, M.D., Corbetta, M., Snyder, A.Z., Vincent, J.L., and Raichle, M.E. (2006). Spontaneous neuronal activity distinguishes human dorsal and ventral attention systems. Proc Natl Acad Sci U S A *103*, 10046-10051.

Fox, M.D., and Raichle, M.E. (2007). Spontaneous fluctuations in brain activity observed with functional magnetic resonance imaging. Nat Rev Neurosci *8*, 700-711.

Fox, M.D., Snyder, A.Z., Vincent, J.L., and Raichle, M.E. (2007). Intrinsic fluctuations within cortical systems account for intertrial variability in human behavior. Neuron *56*, 171-184.

Freeman, W.J., and Zhai, J. (2009). Simulated power spectral density (PSD) of background electrocorticogram (ECoG). Cogn Neurodyn *3*, 97-103.

Golanov, E.V., Yamamoto, S., and Reis, D.J. (1994). Spontaneous waves of cerebral

blood flow associated with a pattern of electrocortical activity. Am J Physiol *266*,

R204-214.

Greicius, M.D., Krasnow, B., Reiss, A.L., and Menon, V. (2003). Functional connectivity

in the resting brain: a network analysis of the default mode hypothesis. Proc Natl

Acad Sci U S A *100*, 253-258.

Hampson, M., Peterson, B.S., Skudlarski, P., Gatenby, J.C., and Gore, J.C. (2002).

Detection of functional connectivity using temporal correlations in MR images.

Hum Brain Mapp *15*, 247-262.

He, B.J., Snyder, A.Z., Vincent, J.L., Epstein, A., Shulman, G.L., and Corbetta, M.

(2007). Breakdown of functional connectivity in frontoparietal networks underlies

behavioral deficits in spatial neglect. Neuron *53*, 905-918.

Hobson, J.A., and Pace-Schott, E.F. (2002). The cognitive neuroscience of sleep:

neuronal systems, consciousness and learning. Nat Rev Neurosci *3*, 679-693.

Holscher, C., Anwyl, R., and Rowan, M.J. (1997). Stimulation on the positive phase of

hippocampal theta rhythm induces long-term potentiation that can Be

depotentiated by stimulation on the negative phase in area CA1 in vivo. J

Neurosci *17*, 6470-6477.

Horovitz, S.G., Fukunaga, M., Carr, W.S., Picchioni, D., De Zwart, J.A., Van Gelderen,

P., Balkin, T.J., Braun, A.R., and Duyn, J.H. (2007a). Functional connectivity

during deep sleep: a simultaneous EEG-fMRI study. In 13th Annual meeting of

the organization for human brain mapping.

Horovitz, S.G., Fukunaga, M., de Zwart, J.A., van Gelderen, P., Fulton, S.C., Balkin, T.J., and Duyn, J.H. (2007b). Low frequency BOLD fluctuations during resting wakefulness and light sleep: A simultaneous EEG-fMRI study. Hum Brain Mapp.

Jacobs, J., Kahana, M.J., Ekstrom, A.D., and Fried, I. (2007). Brain oscillations control timing of single-neuron activity in humans. J Neurosci *27*, 3839-3844.

Kenet, T., Bibitchkov, D., Tsodyks, M., Grinvald, A., and Arieli, A. (2003). Spontaneously emerging cortical representations of visual attributes. Nature *425*, 954-956.

Larson-Prior, L.J., Zempel, J.M., Vincent, J.L., Nolan, T.S., Snyder, A.Z., and Raichle, M.E. (2006). An EEG-fMRI study of the default network in light sleep. Abstracts Society For Neuroscience.

Leopold, D.A., Murayama, Y., and Logothetis, N.K. (2003). Very slow activity fluctuations in monkey visual cortex: implications for functional brain imaging. Cereb Cortex *13*, 422-433.

Llinas, R.R. (2001). I of the vortex (Cambridge, MA: MIT press).

Logothetis, N.K., Pauls, J., Augath, M., Trinath, T., and Oeltermann, A. (2001). Neurophysiological investigation of the basis of the fMRI signal. Nature *412*, 150-157.

Lowe, M.J., Mock, B.J., and Sorenson, J.A. (1998). Functional connectivity in single and multislice echoplanar imaging using resting-state fluctuations. Neuroimage *7*, 119-132.

Mukamel, R., Gelbard, H., Arieli, A., Hasson, U., Fried, I., and Malach, R. (2005). Coupling between neuronal firing, field potentials, and FMRI in human auditory cortex. Science *309*, 951-954.

Mukovski, M., Chauvette, S., Timofeev, I., and Volgushev, M. (2007). Detection of active and silent states in neocortical neurons from the field potential signal during slow-wave sleep. Cereb Cortex *17*, 400-414.

Niessing, J., Ebisch, B., Schmidt, K.E., Niessing, M., Singer, W., and Galuske, R.A. (2005). Hemodynamic signals correlate tightly with synchronized gamma oscillations. Science *309*, 948-951.

Peters, A., and Feldman, M.L. (1976). The projection of the lateral geniculate nucleus to area 17 of the rat cerebral cortex. I. General description. J Neurocytol *5*, 63-84.

Petersen, C.C., Hahn, T.T., Mehta, M., Grinvald, A., and Sakmann, B. (2003). Interaction of sensory responses with spontaneous depolarization in layer 2/3 barrel cortex. Proc Natl Acad Sci U S A *100*, 13638-13643.

Raichle, M.E. (2006). Neuroscience. The brain's dark energy. Science *314*, 1249-1250.

Raichle, M.E., and Mintun, M.A. (2006). Brain work and brain imaging. Annu Rev Neurosci *29*, 449-476.

Seeley, W.W., Menon, V., Schatzberg, A.F., Keller, J., Glover, G.H., Kenna, H., Reiss, A.L., and Greicius, M.D. (2007). Dissociable intrinsic connectivity networks for salience processing and executive control. J Neurosci *27*, 2349-2356.

Shmuel, A., Augath, M., Oeltermann, A., and Logothetis, N.K. (2006). Negative functional MRI response correlates with decreases in neuronal activity in monkey visual area V1. Nat Neurosci *9*, 569-577.

Shmuel, A., Augath, M., Oeltermann, A., and Logothetis, N.K. (2007). Spontaneous fluctuations in functional MRI signal reflect fluctuations in the underlying local neuronal activity. In 13th Annual meeting of the organization for human brain mapping.

Steriade, M., Contreras, D., Amzica, F., and Timofeev, I. (1996). Synchronization of fast (30-40 Hz) spontaneous oscillations in intrathalamic and thalamocortical networks. J Neurosci *16*, 2788-2808.

Steriade, M., McCormick, D.A., and Sejnowski, T.J. (1993a). Thalamocortical oscillations in the sleeping and aroused brain. Science *262*, 679-685.

Steriade, M., Nunez, A., and Amzica, F. (1993b). A novel slow (< 1 Hz) oscillation of neocortical neurons in vivo: depolarizing and hyperpolarizing components. J Neurosci *13*, 3252-3265.

Tononi, G. (2005). Consciousness, information integration, and the brain. Prog Brain Res *150*, 109-126.

Tsodyks, M., Kenet, T., Grinvald, A., and Arieli, A. (1999). Linking spontaneous activity of single cortical neurons and the underlying functional architecture. Science *286*, 1943-1946.

Vanhatalo, S., Palva, J.M., Holmes, M.D., Miller, J.W., Voipio, J., and Kaila, K. (2004). Infraslow oscillations modulate excitability and interictal epileptic activity in the human cortex during sleep. Proc Natl Acad Sci U S A *101*, 5053-5057.

Vincent, J.L., Patel, G.H., Fox, M.D., Snyder, A.Z., Baker, J.T., Van Essen, D.C., Zempel, J.M., Snyder, L.H., Corbetta, M., and Raichle, M.E. (2007). Intrinsic functional architecture in the anaesthetized monkey brain. Nature *447*, 83-86.

Viswanathan, A., and Freeman, R.D. (2007). Neurometabolic coupling in cerebral cortex

  reflects synaptic more than spiking activity. Nat Neurosci *10*, 1308-1312.

von Stein, A., and Sarnthein, J. (2000). Different frequencies for different scales of

  cortical integration: from local gamma to long range alpha/theta synchronization.

  Int J Psychophysiol *38*, 301-313.

Wespatat, V., Tennigkeit, F., and Singer, W. (2004). Phase sensitivity of synaptic

  modifications in oscillating cells of rat visual cortex. J Neurosci *24*, 9067-9075.

CHAPTER II: Breakdown of functional connectivity in frontoparietal networks underlies behavioral deficits in spatial neglect

Summary

Spatial neglect is a syndrome following stroke characterized by attentional deficits in perceiving and responding to stimuli in the contralesional field. Here we examined the integrity of attentional systems in patients with spatial neglect by measuring coherent fluctuations of blood oxygen level-dependent (BOLD) signals (functional connectivity) with functional magnetic resonance imaging (fMRI). Inter-regional connectivity in two largely separate attention networks located in dorsal and ventral fronto-parietal regions was assessed at both acute and chronic stages of recovery. Consistent with the fact that strokes causing neglect often damage the ventral attention network, connectivity between regions in this network was diffusely disrupted and showed no recovery. The extent of residual connectivity correlated with visual detection deficits in both visual fields, consistent with the hypothesized role of the ventral network in mediating non-lateralized deficits of spatial neglect. In the structurally intact dorsal attention network functional connectivity between left and right posterior parietal cortex was acutely disrupted, but fully recovered at the chronic stage. This acute disruption correlated with a behavioral 'disengagement' deficit in responding to unattended stimuli in the neglected field, which again is consistent with the role of this region in directing spatial attention. Finally, the impairment of functional connectivity within dorsal and ventral attention networks, and the associated behavioral deficits, were positively correlated, and depended on the disconnections of the white matter tracts connecting frontal and parietal cortices. These

findings demonstrate the behavioral significance of BOLD functional connectivity and its relevance for explaining the pathophysiology of spatial neglect and potentially of other stroke-related behavioral deficits.

Introduction

Functional connectivity (FC) magnetic resonance imaging (MRI) studies temporal correlations between the blood oxygenation level-dependent (BOLD) signals in different brain regions. These temporal correlations are readily demonstrated in the resting state (i.e. in the absence of an explicit task) (Biswal et al., 1995) and are contributed predominantly by low frequency (<0.1 Hz) fluctuations (Cordes et al., 2001). Coherent BOLD fluctuations within widely distributed but anatomically discrete networks recapitulate the spatial topography of task-evoked BOLD responses commonly observed with a variety of behavioral paradigms [e.g. somatosensory (Biswal et al., 1995), language (Hampson et al., 2002), default (Greicius et al., 2003; Laufs et al., 2003) and attention (Fox et al., 2005; Laufs et al., 2003)].

The behavioral significance of BOLD FC is poorly understood (but see (Hampson et al., 2006a; Hampson et al., 2006b) for two recent studies). One goal of the current study was to assess the behavioral significance of BOLD FC by measuring the relationship between FC and performance deficits in stroke patients longitudinally. The primary question was whether the degree of disruption in FC correlated with the severity of behavioral deficits at the acute stage, and whether this correlation was maintained over the course of recovery.

A second goal of this study was to gain insights into the role of coherent BOLD fluctuations in the pathophysiology of neglect. Neglect is a common syndrome following right hemisphere that includes both rightward biases in spatial sensory-motor processing, as well as several non-lateralized deficits of arousal, capacity, and working memory [for reviews see (Heilman et al., 1985; Hillis, 2006; Husain and Rorden, 2003; Mesulam, 1999; Robertson, 2001)]. Neglect has been traditionally explained in terms of localized damage of specific brain structures [inferior parietal lobule (IPL) (Mort et al., 2003; Vallar and Perani, 1987), superior temporal gyrus (STG) (Karnath et al., 2001; Karnath et al., 2004), subcortical nuclei (Karnath et al., 2002; Vallar and Perani, 1987), and the inferior frontal cortex (Husain and Kennard, 1996; Vallar and Perani, 1987). The present work fits within a more recent perspective that emphasizes the importance of distributed dysfunction in fronto-parietal cortical networks (Corbetta et al., 2005; Thiebaut de Schotten et al., 2005).

We have recently proposed that spatial neglect reflects dysfunction of two fronto-parietal networks involved in the control of attention. The dorsal attention network controls the allocation of spatial attention to extra-personal space, and the selection of stimuli and responses predominantly in contra-lateral space, and includes as core regions the intraparietal sulcus (IPS) and the frontal eye field (FEF). The ventral attention network is necessary for target detection and reorienting toward salient unexpected events in either space, is localized predominantly in the right hemisphere, and is centered around the temporo-parietal junction (TPJ) and ventral frontal cortex (VFC) [for review see (Corbetta and Shulman, 2002)]. Strokes that cause neglect often structurally damage the ventral network while sparing the dorsal network (Corbetta et al., 2005; Husain and

Rorden, 2003; Malhotra et al., 2006a; Milner and McIntosh, 2005). We have recently demonstrated, using a visuo-spatial attention task, that such strokes may lead to a functional imbalance of evoked responses in left (hyperactive) and right (hypoactive) dorsal parietal cortex, even though these areas are structurally intact (Corbetta et al., 2005). This imbalance correlates with the degree of contra-lesional inattention and recovers over time. These observations suggest that structural damage of the ventral network leads to functional impairment of the posterior parietal nodes of the dorsal network.

However, this previous fMRI study of neglect only examined task-evoked responses of individual regions. Inferences regarding network-level interactions were purely qualitative. Because stroke injury to part of a network may result in network dysfunction, direct assessments of functional interactions among brain areas using FC MRI should provide a better understanding of neglect. The dorsal and ventral attention networks were originally defined on the basis of task-evoked responses; more recently, using FC MRI acquired in healthy resting adults, Fox and colleagues showed that the same two networks emerge from an analysis of coherent spontaneous fluctuations of BOLD signals (Fox et al., 2006a). Here, we measured inter-regional functional connectivity in these two attention networks in patients with neglect at both acute and chronic stages after the ictus. Performance measures on a visuospatial attention task were correlated with FC measures across subjects. The obtained results show that disrupted FC in the dorsal and ventral attention networks constitutes a critical mechanism underlying the pathophysiology of neglect.

Methods

Subjects

Eleven patients (2 female), mean age 59 years, with right fronto-parietal stroke and initially demonstrated neglect participated in the study. All provided informed consent according to procedures established by the Washington University Institutional Review Board. All patients underwent standard rehabilitation for at least 3 months after the stroke. Patients were tested twice: once in the acute stage, i.e., ~4 weeks (mean 30 days) after the stroke and once at the chronic stage, i.e., more than 6 months (mean 40 weeks) after the ictus. Inclusion criteria: 1. Age 18 or greater. No upper age limit applied. 2. Single right hemisphere lesion, ischemic or hemorrhagic. 3. Clinical evidence of neglect on clinical screening. 4. Awake, alert, and capable of understanding and participating in research. 5. Able to tolerate the scanner environment for 2 hours within the first 4 weeks after the stroke. Exclusion Criteria: 1. Evidence by CT or MRI of other strokes, although up to 2 lacunes were allowed in the subcortical white matter. 2. Inability to maintain wakefulness. 3. Presence of other neurological, psychiatric or medical conditions precluding active participation in research or altering the interpretation of behavioral/imaging studies (e.g., dementia, schizophrenia), or limited life expectancy to less than 1 year (e.g., cancer or congestive heart failure class IV). 4. Carotid stenosis greater than 50% by Doppler studies or angiogram (as the BOLD response in the hemisphere ipsilateral to a carotid stenosis may not reliably track neuronal activity). 5. Claustrophobia.

Twelve young (6 female; age 18-38 years) and twelve older (7 female; mean age 57.4, range 41-71) healthy subjects were recruited from the Washington University

community to serve as control subjects. All control subjects were right-handed, and had no neurological history. All gave informed consent following guidelines set by the WU Institutional Research Board and were compensated for their time.

Apparatus and stimuli

Stimuli were generated by an Apple Power Macintosh computer and projected onto a screen at the head of the magnet bore by a Sharp LCD projector. Participants viewed the stimuli through a mirror attached to the head coil. Stimuli were white on a black background.

Task

The Posner task was implemented as follows in patients and elderly controls. The display contained two boxes (unfilled squares) each 1° on a side, centered 3.3° to the right and to the left of the central fixation point. Each trial started with the fixation point changing color from red to green. After 800 ms an arrow cue pointing left or right was presented at the fixation locus for 2360 ms. Following a delay ranging from 1500 to 3000 ms, an asterisk target was presented for 100 ms in one of the two boxes. Left and right targets were equally probable. On 75% of the trials the target was presented at the location indicated by the cue (valid), while on 25% of the trials it was presented at the opposite location (invalid). The subject indicated target detection as quickly as possible with a right hand key-press. Reactions times (RTs) were measured in milliseconds from the appearance of the target to the key-press. The next trial began after an inter-trial interval (ITI) that was randomized between 4760-9440 ms. The standard session involved

eight fMRI runs of 5 minutes each, where each run contained about 20 trials. At the acute

stage, we obtained between 6 and 12 fMRI runs (mean=8.9) per subject. At the chronic

stage, the number of fMRI runs ranged from 7 to 12 (mean=9.6). Eight fMRI runs were

obtained in each elderly control subject.

The Posner task procedure for young controls differed slightly. 1) 20% of trials

ended immediately after the cue. In another 20% of trials the cue was followed by a test

period lasting 4.72 sec in which no target was presented; 2) the cue-target interval varied

between 3860 and 5360 ms; 3) the ITI lasted for 2, 3 or 4 frames. The number of fMRI

runs ranged from 11 to 16 (mean 15.1).

fMRI Scan Acquisition

Scanning was performed with a Siemens (Erlangen, Germany) 1.5 T Vision MRI

scanner. Functional data were acquired using an asymmetric spin-echo, echoplanar

imaging sequence sensitive to blood oxygen level-dependent (BOLD) contrast (TE = 37

ms, TR = 2.36 s, flip angle = 90°; 16 contiguous 8mm slices with 3.75x3.75mm in-plane

resolution). The functional data slice tilts and field of view were prescribed parallel to the

AC-PC plane on the basis of a short (< 2 minute) pre-functional coarse MP-RAGE scan.

Each fMRI run included 128 frames (volumes). Compensation for asynchronous

(interleaved) slice acquisition was accomplished by sinc interpolation. The functional

data were realigned within and across fMRI runs to correct for head motion. Each fMRI

run was intensity scaled to yield a whole brain mode value of 1000 (not counting the first

4 frames). Anatomical images were acquired using a sagittal MP-RAGE sequence (TR =

97ms, TE = 4ms, flip angle = 12°, inversion time = 300ms). For each subject, an atlas

transformation to the atlas representative template was computed on the basis of an average of the first frame of each fMRI run and MP-RAGE structural images. Our template was produced by mutual co-registration of images obtained in 12 normal subjects and represents the Talairach coordinate system (Talairach and Tournoux, 1988). Each fMRI scan was interpolated to 3mm cubic voxels in atlas space. Time series were combined within each session and event-related responses were extracted using the general linear model making no assumptions regarding the hemodynamic response shape. Regional time courses were extracted by averaging within the regions. Magnitudes were computed as the inner product of the timecourses with a canonical hemodynamic response function of the gamma type (Boynton, 1996).

Anatomical Imaging and Lesion Segmentation

Multiple anatomical images were acquired using a sagittal T1-weighted MP-RAGE sequence (TR = 97ms, TE = 4ms, flip angle = 12°, inversion time = 300ms, 1x1x1.25 mm voxels) and a T2-weighted fast spin echo sequence. All anatomical data acquired in each subject were spatially mutually coregistered and resampled in atlas space to 1mm^3 voxels. Atlas registration error attributable to the presence of a lesion was measured by computing the transformation with and without excluding the lesion and determined to be less than 2 mm for the largest lesion in this group of patients. The coregistered MP-RAGE images were averaged to increase the contrast to noise ratio. Artifactual intensity heterogeneity was corrected using a 3D parabolic (10 free parameters) model of the gain field. Lesion boundaries were determined with the aid of an unsupervised bi-spectral (T1-weighted plus T2-weighted) fuzzy class means (FCM)

procedure that classified voxels into one of four categories: air, cerebrospinal fluid (CSF), gray matter and white matter. Expert judgment was required to correctly segment the lesion on the basis of the automatic classification, e.g., to distinguish CSF representing a cystic lesion vs. lateral ventricle.

Functional Connectivity Analyses

Additional preprocessing. In preparation for FC analysis, the BOLD volumetric timeseries were passed through several additional pre-processing steps: 1) spatial smoothing using a 6 mm full width at half maximum Gaussian blur; 2) temporal filtering retaining frequencies in the 0.009-0.08 Hz band; 3) removal by regression of several sources of variance unlikely to reflect spatially-specific functional correlations: i) six parameters obtained by correction of head motion; ii) the signal averaged over the whole brain (excluding the ventricles and, in patients, the stroke lesion); iii) the signal from a ventricular region; iv) the signal from a white matter region. Temporal derivatives of these regressors were included in the linear model, thereby accounting for the time-shifted versions of spurious variance (e.g., delayed whole brain BOLD signal in venous structures). Deterministic task-evoked response components were removed by including, for each distinct trial type (left-valid, left-invalid, right-valid, right-invalid), 8 regressors corresponding to frames 0 through 7 following the trial onset (cue presentation) (for an evaluation of the efficacy of this manoeuvre see Supplementary Note 2). Trials of varying cue-target interval were lumped together as the difference between the shortest and longest interval (1.5 sec) was less than one frame TR (2.36 sec). The total number of regressors used to remove spurious sources of variance as well as deterministic responses

thus was $2*(6 + 1 + 1 + 1) + 4*8 = 50$, the first factor of 2 corresponding to inclusion of temporally differenced as well unmodified waveforms. The present regression strategy was accomplished in one step, which differs modestly from the previously described serial regression strategy (Fox et al., 2005).

Construction of regions of interest. ROI for functional connectivity analyses were determined from a meta-analysis of four previously published event-related fMRI studies of young adults performing the Posner task (Astafiev et al., 2003; Astafiev et al., 2004; Corbetta et al., 2000; Kincade et al., 2005). For each study, responses to the cue were identified by a whole-brain voxel-wise ANOVA using MR frame as factor. The resulting F-score maps were converted to equally probable Z-scores that were then combined using a fixed-effects analysis and the resulting map then subjected to automatic peak search. Peaks closer than 10 mm were consolidated by algebraically averaging their coordinates. ROI were defined around peaks by thresholding the map at thresholds chosen to yield regions of approximately constant volume. Eight ROIs were selected on the basis of *a priori* knowledge as representing the dorsal attention network (DAN). Five regions representing the ventral attention network (VAN) were similarly defined on the basis of differential responses to the target following invalid vs. valid cues (MR frame × cue validity interaction effect). All ROIs are listed in Supplementary Table 1.

FC MRI correlation analysis. The first step in all FC analyses was to extract BOLD time courses from each ROI (defined as described above) by averaging over voxels within each region. To compute FC maps corresponding to a selected seed ROI, the regional timecourse was correlated against all other voxels within the brain as originally described by (Biswal et al., 1995). The present main results (regional FC) were

obtained by computing Pearson correlation coefficients (r) for region pairs. Statistical tests on regional FC results were computed after application of Fisher's z transform ($z = 0.5\ln((1+r)/(1-r))$), which yields variates that are approximately normally distributed (Zar, 1996).

Diffusion Tractography Imaging (DTI)

DTI data was acquired on 6 subjects in 48 directions, 2.5 mm cubic resolution, b = 800 s/mm^2, with 5 averages and was analyzed similar to (Shimony et al., 2006). The images were realigned across encodings and datasets to correct for electronic shift and head movement. Full brain streamline tractography was performed on all subjects after placing starting seed points on 1 mm resolution grid. The SLF tracks were filtered by selecting tracks that pass through a large region in the deep white matter of the posterior frontal lobe and through the deep white matter of the parietal lobe. The AF tracks were selected to pass through the same region in the posterior frontal and a region in the deep white matter of the temporal lobe. A consensus volume was created from the tracks in all 6 subjects, which was then surface rendered for display. For the probabilistic tracking the data was analyzed using Bayesian probability theory (Behrens et al., 2003). The lesion spot in Fig. 7b (red) was transformed to each subject's individual space and used as a seed region for probabilistic tracking. Probability in each voxel was normalized to the voxel with highest connectivity. These results were then transformed to atlas space and averaged across subjects. For display purposes voxels with probabilities above 5% or 10% were colored with two shades of blue and they follow the expected location of the SLF and AF.

Results

Overview

To measure inter-regional FC, it was necessary first to identify regions of interest (ROIs) representing nodes in the dorsal and ventral attention systems. To this end, we reanalyzed data obtained in four previously published fMRI studies of visuospatial attention. Two sets of ROIs were defined and validated by FC mapping using data acquired in young healthy subjects, which showed that fluctuations were coherent within each system and largely independent across systems. Having defined two sets of functionally connected regions involved in attention-related functions, we measured inter-regional FC in patients and age-matched controls and determined whether temporal correlations within fMRI signals correlated with behavioral performance across patients.

Normal Functional Connectivity of Dorsal and Ventral Attention Networks

ROIs in the dorsal and ventral attention networks were determined from a meta-analysis of four previously published event-related fMRI studies of young healthy adults in which spatial attention was manipulated using a Posner-like paradigm [(Astafiev et al., 2003; Astafiev et al., 2004; Corbetta et al., 2000; Kincade et al., 2005) see Methods and Supplementary Fig. 1]. In each experiment the locus of attention was indicated on each trial by a central arrow pointing toward a left or right location on the computer screen. After a variable delay, a target appeared at either the cued location (75% of trials, "valid trials") or the opposite location (25% of trials, "invalid trials"). Subjects were instructed to maintain fixation on a central cross-hair and to detect targets as quickly as possible. In

different experiments, detection was signaled by a right hand key-press, a saccadic eye movement, a pointing hand movement, or object identification. Whole-brain ANOVA was conducted on each of the four studies (activation during cue period for dorsal attention regions, activation × validity during the period following target presentation for ventral attention regions) to identify significantly modulated voxels. The Z-score maps were combined using a fixed-effects meta-analysis and ROIs were then identified by an automated peak search algorithm.

Eight ROIs in the dorsal attention network (DAN) were consistently recruited in responses to the cue: bilateral FEF, posterior IPS (pIPS), ventral IPS (vIPS), and middle temporal area (MT+) (Fig. 1a yellow; Supplementary Table 1, top). Several regions in the ventral attention network (VAN) were identified by consistently stronger activation to unexpected than expected targets: a precentral sulcus region (PrCe), middle frontal gyrus (MFG), anterior insula, TPJ, and superior temporal sulcus (STS) (Fig. 1a orange; Supplementary Table 1, bottom). All ventral regions were lateralized to the right hemisphere.

To confirm that these regions constitute separate FC networks, inter-regional temporal correlations of BOLD signals were examined in a data set of young healthy subjects (N = 12) performing the Posner task. Time courses were extracted from all regions in the right hemisphere, and the consistent task-evoked BOLD responses were removed by regression (see Methods and Discussion). The inter-regional correlation matrix then was computed (Supplementary Fig. 2). Correlations between regions in different networks were significantly weaker than correlations between regions within the DAN (P< .0001) or within the VAN (P < .0003), indicating that the two networks are

dissociable. To explore the distributed spatial topography of the correlated activity, seed ROI-driven FC maps were computed on a voxel-wise basis for each of the 9 *a priori* attention regions in the right hemisphere. For each network, FC maps were combined using a conjunction analysis that identified voxels correlated with at least 3 of 4 regions in the DAN (Fig 1b) or 4 of 5 regions in the VAN (Fig 1c). Although only right hemisphere regions were used as seeds, the FC defined DAN network was largely bilaterally symmetric. Regions consistently correlated within the DAN included FEF, MT+, and a large swath of cortex extending along IPS into extrastriate visual cortex. Consistent with task-activation studies, the FC-defined VAN network was strongly right lateralized and included the TPJ extending into the inferior parietal lobule, MFG, PrCe, and anterior insula. A small region also was detected in the left supramarginal gyrus (SMG). Interestingly, the largely-bilateral DAN included a right-lateralized region in the middle and inferior frontal lobe (see arrow in Figure 1b), which overlapped with the VAN, suggesting this region may function as a link between networks [see also (Fox et al., 2006a)].

These two *a priori* sets of ROIs were then applied to the comparison of FC in patients versus in age-matched controls. Defining the ROIs in a separate group of young adults minimized the possibility of bias in the patient vs. control comparison. The selected ROIs were complete in the sense that no other brain region outside the two networks showed robust attention-related BOLD response in patients at either stage (Supplementary Fig. 1).
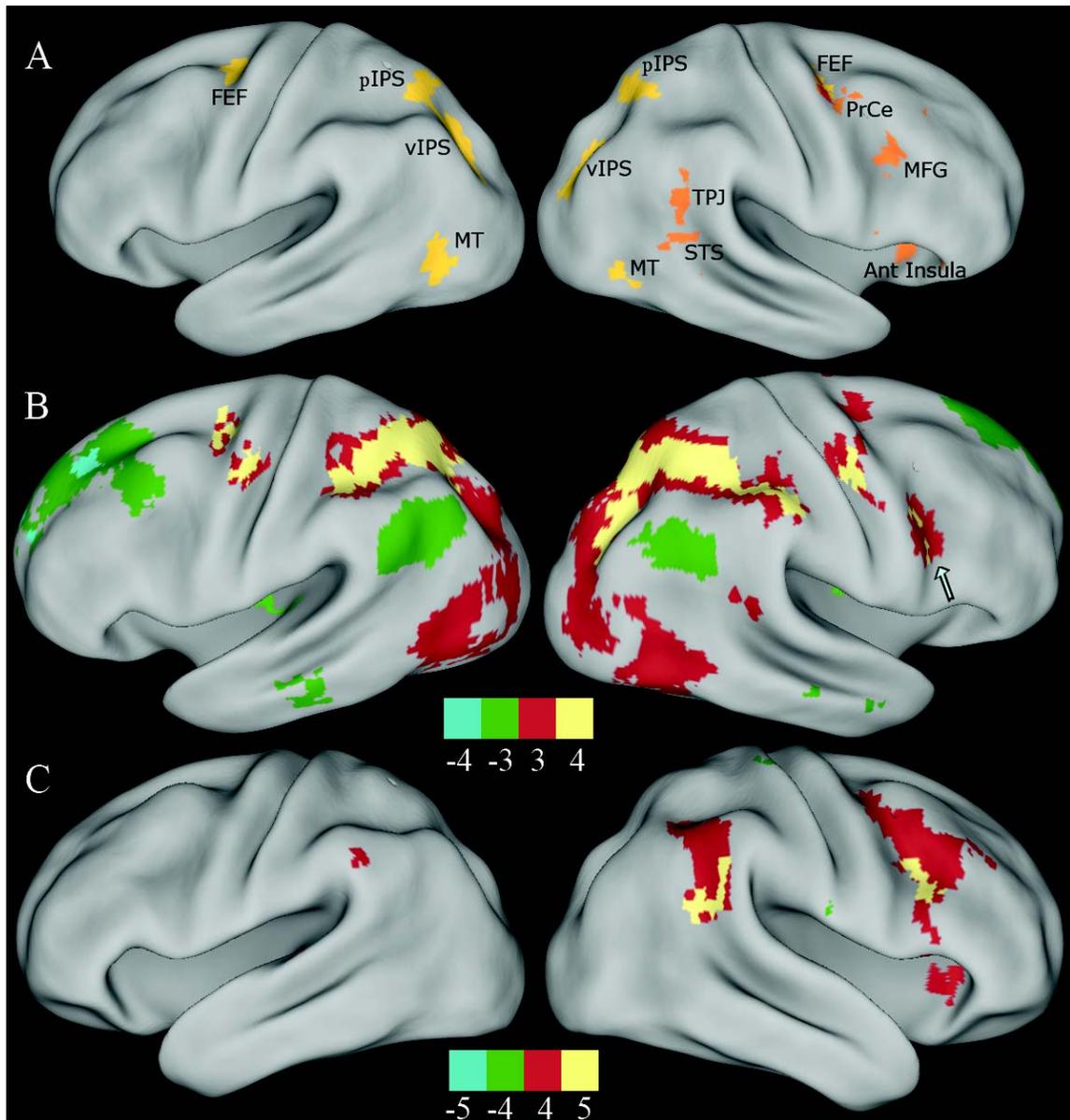
Figure 1 Dorsal and ventral attention networks. **(a)** ROIs defined by activation fMRI studies and used as ROIs for FC analyses. Dorsal network regions: yellow; ventral network regions: orange. Region sizes were controlled to be about 900 mm^3. **(b)** For each of the four right hemisphere DAN ROIs, group statistical maps were obtained using a random-effects analysis on the Fisher-transformed correlation maps and corrected for multiple comparisons at a significance level of P<0.05 (z=3, cluster size = 17 voxels). The four FC maps were combined to produce the conjunction map shown. Voxels in yellow are positively correlated with all 4 ROIs; red: positively correlated with 3 of 4 ROIs; green: negatively correlated with 3 of 4 ROIs; blue: negatively correlated with all 4 ROIs. Arrow points to the major right-lateralized region in the DAN, which overlaps with the VAN. **(c)** FC maps from the 5 VAN ROIs were used to produce the conjunction map. Color code similar to (b).

Patients: Lesion Anatomy and Behavior

We longitudinally studied eleven patients with spatial neglect following right hemisphere stroke (mean age 59, range 42-73, 2 female). Lesions were centered in the IPL, STG, frontal operculum, insula, as well as subcortical nuclei and white matter (Fig. 2a). The distribution of lesions in this group is typical of larger samples (Karnath et al., 2004; Mort et al., 2003). All ROIs in the DAN were spared by the lesions, whereas ROIs in the VAN were damaged to various degrees. PrCe, MFG, TPJ, STS, and anterior insula were damaged in 0, 2, 4, 3, and 3 patients, respectively (Fig 2a).

Patients performed the Posner task both in and out of the scanner at both the acute (30 ± 23 (mean $\pm$ s.d.) days post stroke) and the chronic (40 ± 11 weeks post stroke) stages of recovery. A group of twelve age-matched normal subjects (mean age 57.4, range 41-71, 7 female) were scanned while performing the Posner task in the same way as the patients.

Three types of behavioral deficits in the Posner task were assessed. A visual field (VF)-independent component of neglect was defined as increased misses and slowed reaction times (RT) across both visual fields as compared to controls. A VF-dependent component was defined as more misses and slower RTs in the contralesional than ipsilesional VF. Finally, a "disengagement deficit", common in neglect patients, was defined as specific impairment in detecting targets in the left VF following an invalid cue as this condition requires disengaging attention from the good VF and reorienting to the bad VF (Friedrich et al., 1998; Morrow and Ratcliff, 1988; Posner et al., 1984).

The behavioral performance of the patients was compared to age-matched controls using a three-way ANOVA, with group (control or patient), VF (left or right), and cue validity (valid or invalid) as factors (Fig. 2b). Patients had significantly more misses than controls (VF-independent impairment, Acute: $F_{1,22}$= 19.5, P = .0002; Chronic: $F_{1,22}$ = 7.4, P = .01), were particularly impaired in the left VF (lateralized impairment, VF x Group, Acute: hit rates, $F_{1,22}$ = 13.6, P = .001; RT, $F_{1,22}$ = 17.8, P = .0004; Chronic: hit rates, $F_{1,22}$ = 2.45, P = .1; RT, $F_{1,22}$ = 15.1, P = .0008), and had a significantly greater disengagement deficit (Group × VF × Validity, Acute: hit rates, $F_{1,22}$ = 3.9 P = .06; RT, n.s.; Chronic: hit rates, n.s.; RT, $F_{1,22}$ = 4.27, P = .05).

The improvement of behavioral performance from acute to chronic stage was not significant at the P < 0.05 level using the data from the scanner session, although the trends were in the expected direction (Fig. 2b). A significant improvement was observed in separate acute and chronic sessions conducted in a regular testing room. Target detection improved overall in both visual fields (Stage: hit rates, $F_{1,9}$= 5.6, P = .04; RT, $F_{1,10}$ = 5.3, P = .04), and both rightward bias (Stage × VF: RT, $F_{1,10}$ = 6.4, P < .03) and disengagement deficit (Stage × VF × Validity, RT: $F_{1,10}$ = 8.3, P=.016) were significantly reduced. Therefore, behavioral impairment including VF-independent, VF-dependent, and disengagement deficits recovered significantly over the interval between the acute and chronic sessions.
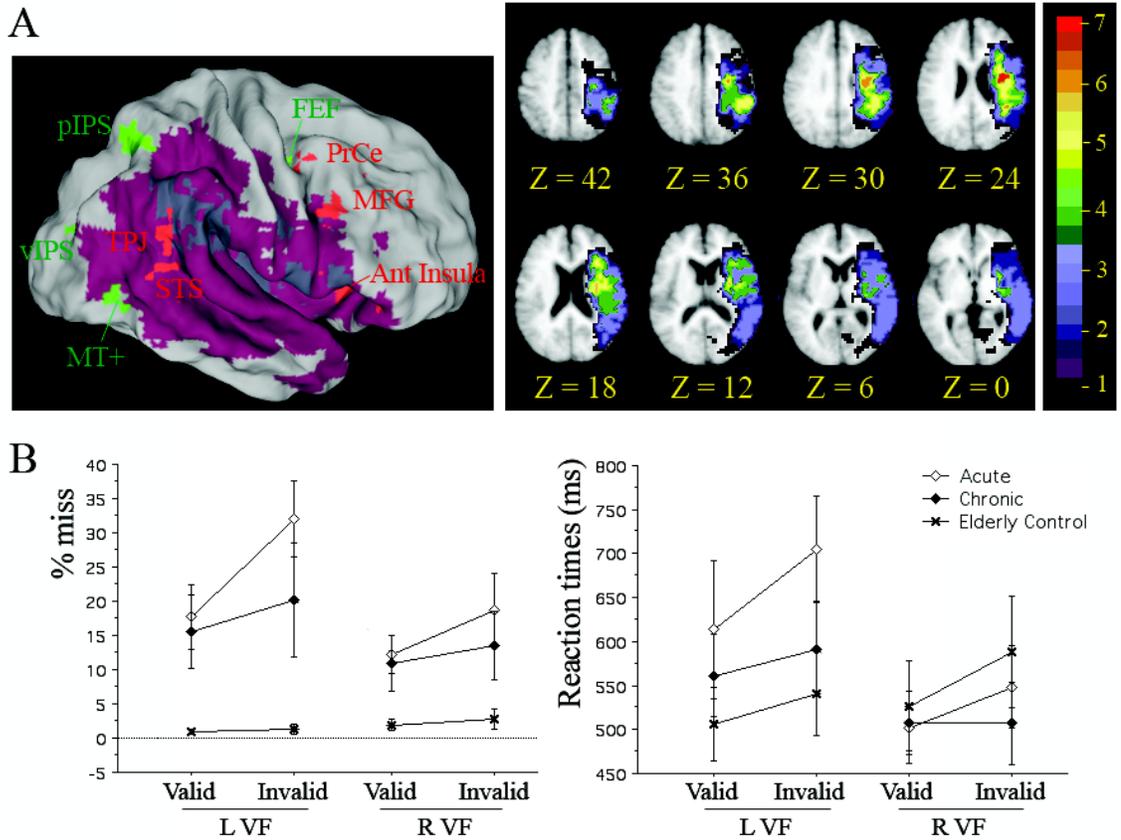
Figure 2 Lesion and task performance of patients. **(a) Left panel:** Overlap of lesion (N = 11, purple: damaged in 1-3 patients; blue: damaged in 4-7 patients) and ROIs constructed for FC analyses (DAN: green, VAN: red). **Right panel:** Lesion overlap (N=11) overlaid on patients' average anatomical image. Values denote the number of patients in which the particular voxel was damaged by lesion. **(b)** Performance in the Posner task, compared with age-matched controls. Left: percent miss; Right: RTs averaged across hit trials. Error bars denote s.e.m.

Functional Connectivity in Dorsal Attention Network (DAN)

We conducted several analyses to determine whether stroke affected basic characteristics of the BOLD signals, specifically, variance and temporal frequency distribution. These observations helped to rule out the possibility that the results presented below were artifact attributable to higher signal variance, more movement or

abnormal neural-vascular coupling in patients (See Supplementary Note 1 and Supplementary Fig. 3 for methods and results).

We measured functional connectivity in the DAN after consistent task-related responses were removed from the time series (see Methods and Discussion), and found a specific breakdown of FC between left and right pIPS. Left-right pIPS FC was reduced in acute patients as compared to age-matched controls (Fig. 3a, P = .04, unpaired t-test, two-tailed), but fully recovered at the chronic stage (Fig. 3a, acute vs. chronic: P < 0.03; chronic vs. control: 0.72±0.22 vs. 0.70±0.16). The disruption of inter-hemispheric FC was restricted to pIPS among the four homologous region pairs in the DAN (Fig. 3c).

As noted above, we have previously shown an inter-hemispheric imbalance in task-evoked BOLD responses in dorsal posterior parietal cortex at the acute stage of neglect that recovers over time (Corbetta et al., 2005). This finding was reproduced in the current data set (with 2 subjects not included in the previous study): The right pIPS was less recruited than left pIPS at the acute stage, but the two sides showed balanced activation at the chronic stage (Fig. 3b).

Critically, the breakdown of FC in dorsal parietal cortex was behaviorally significant. At the acute stage, there was a strong correlation between the strength of left-right pIPS FC and detection of unattended targets in the left visual field (Fig. 3d, hit rates: r = 0.846, P = .0005; RT: r = -0.593, P = .05), such that the lower the inter-hemispheric FC in dorsal parietal cortex, the more impaired patients were in reorienting attention toward the neglected visual field. This correlation remained highly significant after correction for both lesion size and movement (hit rates: r = 0.699, P < .05). The data from the other three trial types (left valid, right valid and invalid) showed a similar trend

that failed to reach significance (Supplementary Table 2). The correlation between behavior and FC was specific to dorsal parietal cortex; no significant correlation with behavioral measures was found for the other three homologous region pairs in the DAN (for correlation with hit rates see Supplementary Table 2).

Given that task-evoked responses are also abnormal in pIPS, an important question concerns whether the impairment of FC makes a difference beyond the abnormal evoked responses. Two analyses suggested that disrupted functional connectivity correlated with poor performance independently of task-evoked responses. First, there was no significant correlation between decreased FC and imbalanced task-evoked responses in pIPS (all $P > .2$, Supplementary Table 3a). Second, partial correlation analyses demonstrated that controlling for the degree of abnormal task-evoked responses did not decrease and, in some cases, even slightly increased the FC-performance correlation (Supplementary Table 3b).

At the chronic stage, the majority of patients showed improvement in both inter-hemispheric pIPS FC and performance, but 3 patients continued to show persistent impairments in both measures, resulting in a significant group correlation between these two measures (hit rates, left VF, valid: $r = 0.619$, $P = .04$; left VF, invalid: $r = 0.587$, $P = .057$; right VF, invalid: $r = 0.712$, $P = .01$). Behavioral relevance remained specific to inter-hemispheric pIPS FC; neither vIPS, FEF nor MT FC showed correlation with performance (either hit rates or RTs).
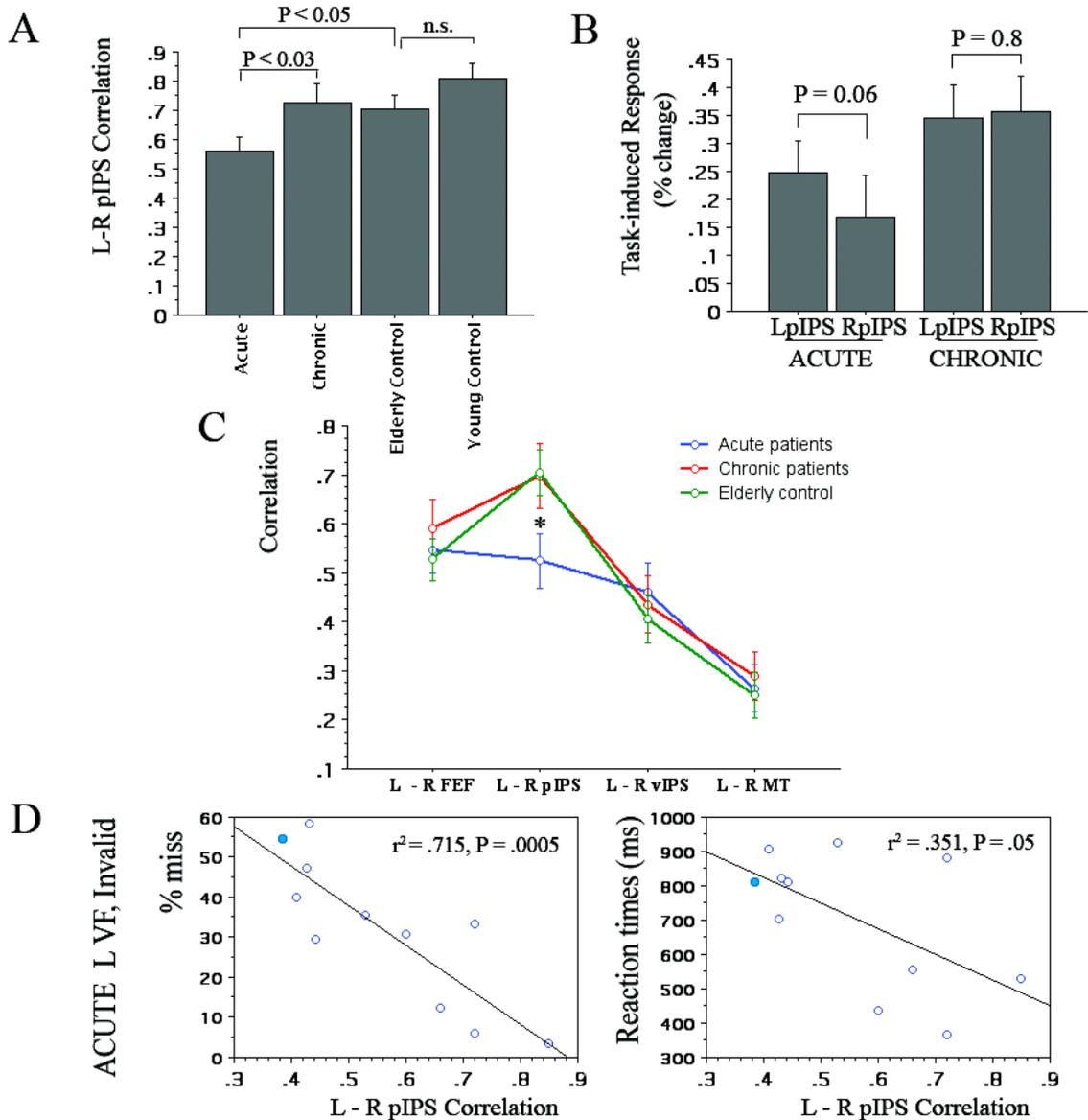
Figure 3 Left-right pIPS FC. **(a)** Temporal correlation between left and right pIPS in patients (N=11), elderly controls (N = 12) and young controls (N = 12). **(b)** Rebalancing of task-evoked responses between left and right pIPS at chronic stage. **(c)** Temporal correlations of all homologous pairs of regions in DAN, only left–right pIPS correlation was impaired acutely. **(d)** Across acute patients, left-right pIPS FC significantly correlated with % miss (left panel) and RT (right panel) in detecting targets in the left VF following an invalid cue. Filled circle indicates the subject with largest lesion (200,928mm^3). Error bars denote s.e.m.

Functional Connectivity in Visual Cortex

Consistent with models of attention that posit feedback interactions from attention-controlling dorsal parietal regions to data-processing visual regions (Corbetta and Shulman, 2002; Kastner and Ungerleider, 2000), an imbalance of task-evoked activity similar to that demonstrated in dorsal parietal cortex has been recorded in visual cortex in patients with left neglect (Corbetta et al., 2005). Accordingly, we measured temporal correlations between left and right visual cortex, using ROIs in retinotopic occipital cortex defined by functional and anatomical criteria [as in (Corbetta et al., 2005)]. Interestingly, inter-hemispheric FC in visual cortex was completely intact (acute vs. chronic vs. age-matched controls: dorsal retinotopic ROIs, 0.77 ± 0.07 vs. 0.77 ± 0.07 vs. 0.78 ± 0.07; ventral retinotopic ROIs, 0.74 ± 0.10 vs. 0.72 ± 0.16 vs. 0.69 ± 0.07). Thus, an inter-hemispheric imbalance in task-evoked activity was not necessarily accompanied by a breakdown of inter-hemispheric FC, indicating that abnormal task-evoked activity does not lead to abnormal FC. The observation of intact FC in visual cortex but disrupted FC in dorsal parietal cortex, however, does not contradict the presence of top-down modulation, which might be more dynamic and task-dependent, i.e., manifesting within task-induced responses. Neither task-evoked responses (Corbetta et al., 2005) nor FC in visual cortex correlated with behavioral performance, indicating that spatial neglect is less related to the functioning of visual cortex than to parietal cortex.

Functional Connectivity in Ventral Attention Network (VAN)

The structural integrity of regions in the VAN and, presumably, of their respective anatomical connections, was compromised by strokes to different degrees in different

patients. Correspondingly, we found a global impairment of functional connectivity in the ventral network, which did not recover (see Fig. 4a for MFG-STS FC, see Supplementary Fig. 4 for all pair-wise FC within the VAN).

Behavioral correlations with FC at the acute stage were largely restricted to MFG-STS and MFG-TPJ (Supplementary Table 2). MFG-STS FC correlated significantly with hit rates in both visual fields in the valid condition (left VF: $r = 0.693$, $P = .016$; right VF: $r = 0.652$, $P = .027$) and in the left visual field, invalid condition ($r = 0.775$, $P = .003$) (Fig. 4c). MFG-TPJ FC correlated with hit rates only in the valid conditions, but again in both visual fields (L VF: $r = 0.747$, $P = .006$; R VF: $r = 0.731$, $P = .008$, not shown). Results after correction for both movement and lesion size are shown in Supplementary Table 3.
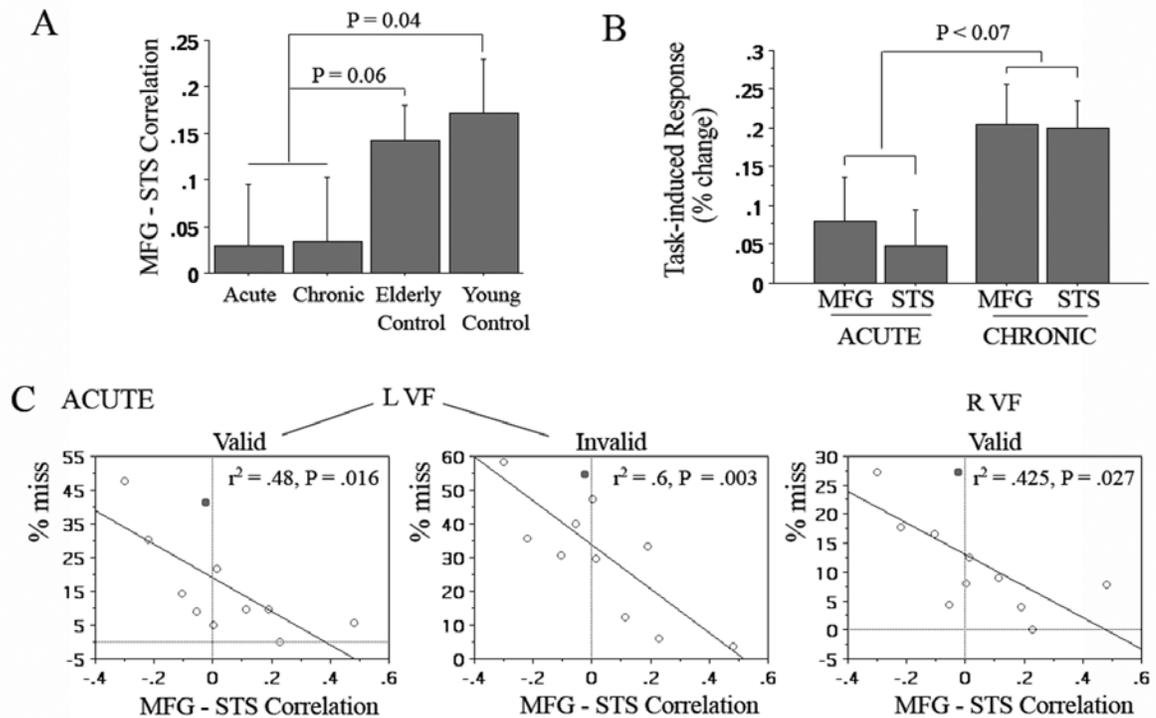
Figure 4 MFG-STS FC. **(a)** Temporal correlations between MFG and STS was significantly impaired in patients compared with controls and did not recover at the chronic stage. Error bars denote s.e.m. **(b)** Task-evoked responses in MFG and STS. **(c)** Across acute patients, MFG − STS FC significantly correlated with % miss in detecting

targets in the left VF following valid (left panel) or invalid (middle panel) cues and in right VF following valid cues (right panel).

Interestingly, the task-evoked responses in these areas did show some evidence of recovery (e.g., Fig 4b, P = 0.067), indicating that these regions might have independently partially regained function.

So far we have assessed all pair-wise FC between the five *a priori* ROIs in the VAN. Since the VAN as defined by FC also included a left SMG region (see Figure 1c), we assessed the FC between this L SMG region and its homologous right hemisphere region (R SMG). (This L SMG region showed a significant validity × time effect in the meta-analysis of young adult fMRI (Supplementary Figure 1b), but did not pass the threshold used in the peak-search algorithm, and therefore was not included in the *a priori* set of ROIs.) First, voxel-wise FC maps obtained by seeding the L SMG (Supplementary Figure 5a) and R SMG (Supplementary Figure 5b) confirmed the right hemisphere laterality of the VAN. The inter-hemispheric SMG FC, as most of other pair-wise FC in the VAN (Supplementary Fig. 4), was acutely disrupted and did not recover (Fig. 5a). Task-evoked responses in SMG were similar to those in pIPS in the sense that an acute imbalance recovered at the chronic stage, although these effects did not reach statistical significance (Fig. 5b). Inter-hemispheric FC of the SMG significantly and specifically correlated with disengagement deficit at the acute stage (Fig. 5c, with %miss: P < .001, significant after correction for both movement and lesion size (Supplementary Table 4); with RT: P = .03). In this characteristic the SMG was also similar to the pIPS. Moreover, there was a significant positive correlation between decreased pIPS FC and

decreased SMG FC (Fig. 5d). However, unlike inter-hemispheric pIPS FC, inter-

hemispheric SMG FC showed no recovery from acute to chronic stages.
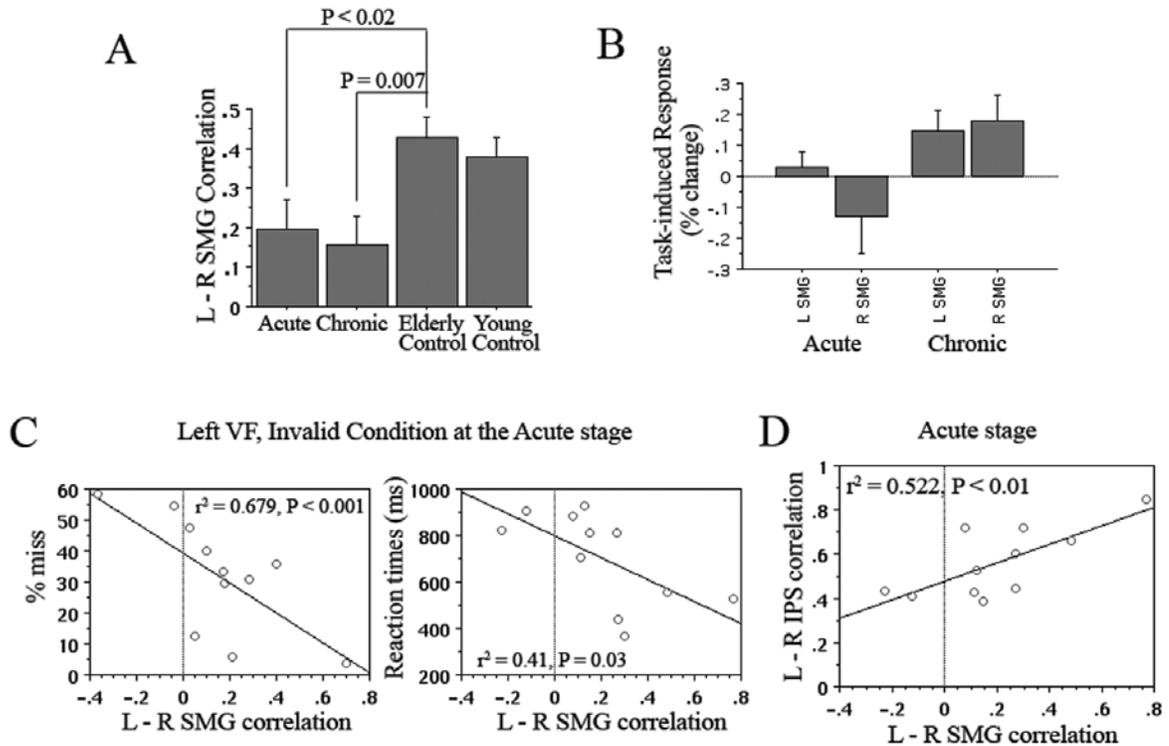
Figure 5 Left-right SMG FC. **(a)** Temporal correlation between left and right SMG was significantly impaired in patients compared with controls and did not recover at the chronic stage. Error bars denote s.e.m. **(b)** Task-evoked responses in left and right SMG. **(c)** Across acute patients, L – R SMG FC significantly correlated with % miss (left) and RT (right) in detecting targets in the left VF following an invalid cue. **(d)** Across acute patients, inter-hemispheric FC in pIPS and in SMG correlate with each other.

Interaction between DAN and VAN

The results presented up to this point indicate that strokes associated with spatial

neglect cause an acute disruption of FC between left and right dorsal parietal cortex,

persistent breakdown of FC between several regions of the VAN, and robust correlation

of disrupted FC with impaired performance in a spatial attention task. Below we consider

whether spatial neglect was associated with a deficit in the interaction between pIPS and the VAN.

First, we found that the physiological impairments in the two networks were highly correlated. Decreased MFG-STS FC (Fig 6a, r = 0.781, P = .003) and decreased inter-hemispheric SMG FC (Fig. 5d, r = 0.722, P < .01) each significantly correlated with decreased inter-hemspheric pIPS FC at the acute stage. Although this correlation might result from inter-subject variability in fMRI signal quality, FC of no other pair of regions within the VAN correlated with left-right pIPS FC, strongly arguing against this possibility. These correlations between pIPS FC and VAN FC were not observed in either the young or old control groups, suggesting this relationship was specific to the pathophysiology in patients.
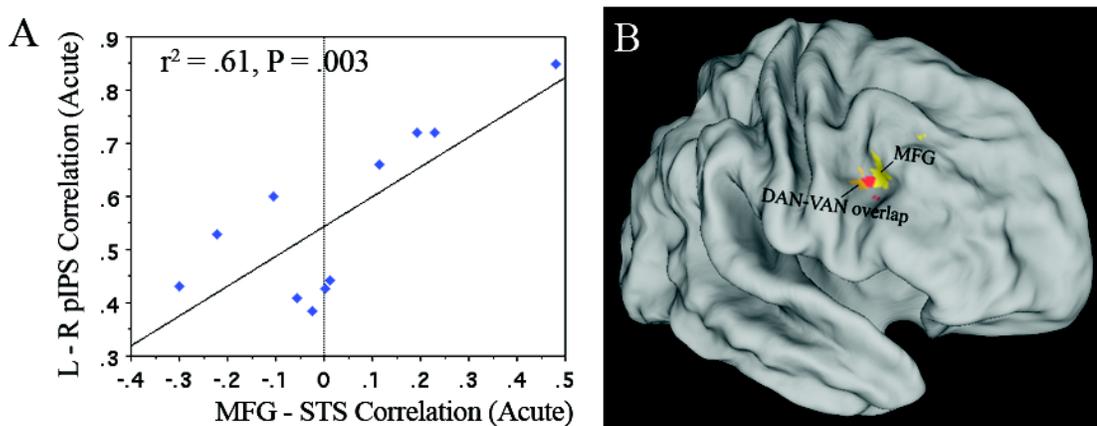
Figure 6 MFG as a potential link between DAN and VAN. **(a)** Correlation between MFG–STS FC and left-right pIPS FC across acute patients. **(b)** Part of MFG ROI is in temporal correlated with both networks.MFG ROI used in FC analyses (yellow) and the overlap region (blue) between DAN (thresholded as 3/4) and VAN (thresholded as 4/5). Overlap between MFG ROI and the DAN-VAN overlap region is shown in red.

Second, we investigated the anatomical basis of spatial neglect and its relation to disrupted FC. We divided the patients into two subgroups (each N=5) based on a median-split of the severity of left sided neglect at the acute stage (calculated as %miss and RT (Left – Right VF), averaged across valid and invalid trials). The two subgroups significantly differed at the acute stage in leftward neglect (VF × Group: hit rates, $F_{1,8} =$ 20.7, P < .002; RT, $F_{1,8} = 35.1$, P = .0004) and in overall detection speed across both visual fields (RT: $F_{1,8} = 8.14$, P = .02) (Fig. 7a). Moreover, consistent with results presented earlier, at the acute stage, inter-hemispheric pIPS FC (P < .04), MFG-STS FC (P < .07), and inter-hemispheric SMG FC (P < .01), but not MFG-TPJ FC (P = .89), were all lower in patients with more severe neglect (Fig. 7c). When we contrasted voxel-wise the distributions of anatomical damage in the two groups, we discovered that a region located at the arcuate fasciculus (AF) and the superior longitudinal fasciculus (SLF) was damaged in all patients with more severe neglect, but was spared in all patients with milder neglect (Fig. 7b). The AF connects middle frontal areas with superior temporal areas (Petrides and Pandya, 2002), providing a possible structural basis for the disruption of MFG-STS FC. Since part of MFG is temporally correlated with both networks (Fig. 6b), interruption of the MFG-STS connectivity might also affect communication between the VAN and pIPS. The SLF connects both the superior and inferior parietal lobules with dorsolateral prefrontal cortex (Schmahmann and Pandya, 2006), providing a plausible structural basis for the disruption of fronto-parietal FC in the VAN. More importantly, disrupted SLF may also damage the communication between ventral frontal component of the VAN and posterior parietal component of the DAN. Supporting this hypothesis,

FC between MFG and pIPS was strongly disrupted and did not recover (Supplementary Figure 4).
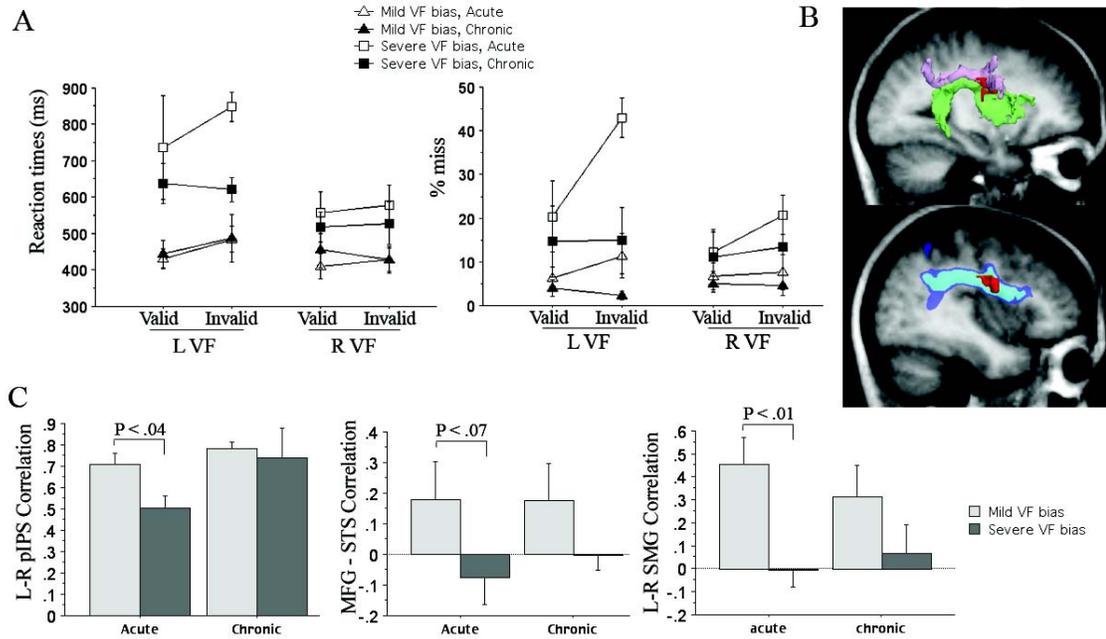
Figure 7 Median-split of all patients based on VF bias in the acute stage. **(a)** Behavioral performance of each subgroup at acute and chronic stages. **(b)** A white matter region (red) was damaged in all patients from the severe subgroup but spared in all patients from the mild subgroup. Top: streamline diffusion tensor tractography (sDTT) of the superior longitudinal fasciculus (SLF, pink) and the arcuate fasciculus (AF, green), with the lesion spot shown in red. The relatively abrupt anterior ending of the SLF was likely due to the crossing corticospinal tracts. Bottom: probabilistic DTT seeded in the lesion (red). Voxels in which > 5% of all tracts from the seed pass through are shown in dark blue. Voxels in which > 10% of tracts from the seed pass through are shown in light blue. **(c)** The subgroup with severe VF bias also had more impaired left-right pIPS FC, MFG – STS FC and left-right SMG FC.

Finally, results from a single case not included in the previous analyses indicated that disrupted inter-hemispheric pIPS FC alone does not lead to severe neglect. This patient (age 36) suffered a right dorsal medial parietal lesion that extended into the corpus callosum and presumably partially damaged the fibers connecting left and right posterior parietal cortices (Fig. 8a). As might be predicted, inter-hemispheric FC in pIPS was 2.8

standard deviations (SD) lower than the mean of the whole group at the acute stage (1.5 SD lower at chronic stage) (Fig. 8b left). However, this patient had a very mild VF bias (Fig. 8b middle & right, ~ 1 SD below the mean of the patient group and not significantly different from controls). Therefore, our data suggest that decreased pIPS inter-hemispheric BOLD FC alone is not sufficient to cause severe neglect. In other words, it appears that the severity of left neglect robustly correlates with decreased inter-hemispheric pIPS FC only in the presence of a damaged VAN. This clinical case, together with similar previous observations (e.g., (Quigley et al., 2003)), support a view that cortico-cortical connections provide a structural basis of BOLD functional connectivity.
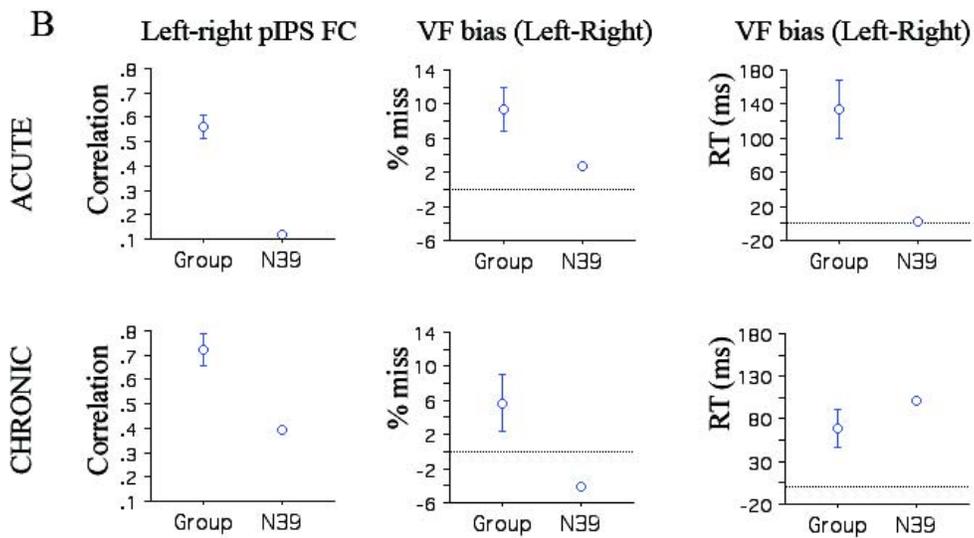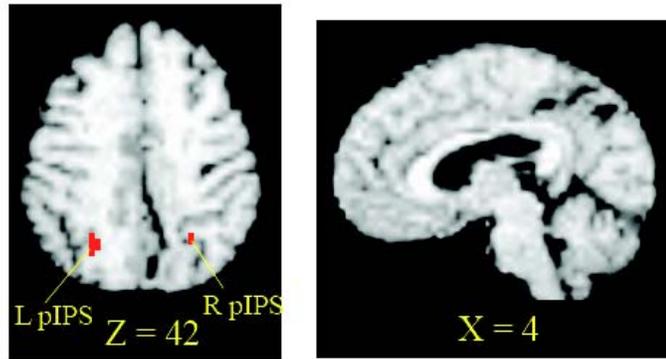
Figure 8 Single case with right dorsal medial parietal lesion. **(a)**pIPS ROI (red) overlaid on patient's own anatomical image. **(b)** Comparison of the single case to the mean of all the other patients (N = 11). Left: Inter-hemispheric pIPS FC. Middle (% miss) and Right (RT): Measurements of rightward visual field bias (% miss and RT) evaluated as (left VF) – (right VF), collapsed across valid and invalid trials. Error bars denote s.e.m..

<u>Discussion</u>

We have demonstrated the behavioral significance of BOLD functional connectivity by showing an across-subject correlation of disrupted FC and the severity of spatial neglect. The results also suggest that disrupted functional connectivity in the two

attention networks underlies different components of the syndrome, and yet correlate with each other. These findings emphasize a network view of neglect and, more generally, stroke. Below, we discuss how these results enhance our understanding of the neural basis of spatial neglect and support the use of FC MRI as a clinical tool.

Understanding spatial neglect with connectivity in mind

We have proposed that it is the conjunction of structural and functional damage to the ventral and dorsal frontoparietal attention networks that causes neglect. This view explains why neglect patients usually show both spatially lateralized (i.e., neglect of contralesional space) and non-lateralized (i.e., low arousal, impaired working memory, lower attentional capacity) deficits. Previous studies in healthy subjects indicate that the dorsal network mediates control of spatial attention with a contralateral bias (Corbetta et al., 2002; Macaluso et al., 2002; Sereno et al., 2001; Silver et al., 2005), while the ventral system is involved in non-lateralized attentional functions, including spatial and temporal capacity (Husain and Rorden, 2003; Peers et al., 2005; Shapiro et al., 2002) vigilance (Pardo et al., 1991; Rueckert and Grafman, 1996; Wilkins et al., 1987), saliency detection (Downar et al., 2000; Serences et al., 2004) and re-orienting of attention (Arrington et al., 2000; Corbetta et al., 2000; Macaluso et al., 2002). According to this account, structural damage to the right hemisphere ventral regions, which is the most commonly lesioned area in spatial neglect, causes non-lateralized deficits directly, and lateralized deficits indirectly, through distant effects on the dorsal parietal cortex that induce functional abnormalities therein.

This general framework is well supported by the current results. The pIPS was the only region in the dorsal network showing (at the acute stage) both a breakdown of inter-hemispheric FC and an imbalance (left>right) of task-evoked responses. Critically, both abnormalities were associated with behavioral performance, especially detection and reorienting in the left VF, and both abnormalities recovered completely at the chronic stage. The pIPS region normally is recruited by allocation of attention covertly or overtly (Corbetta et al., 1998), is adjacent to regions involved in planning arm movements (Astafiev et al., 2003), and contains a complete representation of the contralateral visual field (Schluppeck et al., 2005; Silver et al., 2005). It is therefore well positioned to mediate spatially lateralized deficits of neglect that typically involve attention, perception and responding. Consistently, inter-hemispheric pIPS FC most strongly correlated with the disengagement deficit, which reflects the lateralized component of neglect (i.e., left hemi-inattention).

In the VAN, significant correlations between MFG-TPJ FC and behavioral deficits were the same in both visual fields, consistent with the hypothesized contribution of the VAN to the non-lateralized component of neglect. Interestingly, MFG-STS FC showed a similar, albeit weaker, behavioral correlation pattern as inter-hemispheric pIPS FC, suggesting that TPJ and STS, although both part of the ventral network, may have distinct attentional functions. Another interesting result was that the degree of inter-hemispheric SMG FC closely correlated with the disengagement deficit in the left visual field, a correlation similar to that observed for left/right pIPS. This result may suggest that, at the acute stage, successful re-orienting to unattended targets requires inter-hemispheric coordination between ventral parietal areas involved in detecting unattended

targets (Astafiev et al., 2006; Corbetta et al., 2000; Macaluso et al., 2002), and dorsal parietal areas involved in shifts of attention. However, at the chronic stage, an improvement in the disengagement deficit was accompanied with a recovery of inter-hemispheric FC in dorsal parietal, but not ventral parietal cortex.

While these results suggest some dissociation of the neural systems underlying lateralized and non-lateralized deficits, to the extent that greater VAN damage causes greater disruption in pIPS FC, lateralized and non-lateralized deficits should be correlated. Indeed, multiple studies have indicated an interaction between these two components of neglect (Robertson, 2001; Robertson et al., 1998), consistent with the strong correlation between lateralized (e.g., difference between left and right VFs) and non-lateralized (e.g., averaged across VFs) behavioral deficits observed here (RT: $r = 0.68$, $P = .01$). Clinical interventions that enhance non-spatial vigilance improve leftward spatial neglect (Malhotra et al., 2006b; Robertson et al., 1995; Robertson et al., 1998), again suggesting a functional interaction between ventral and dorsal attention networks.

What is the functional-anatomical locus of this interaction? The close association between ventral structural damage and pIPS functional abnormalities suggests that pIPS is the major component of the dorsal network receiving input from the ventral network. Several converging results suggest that this input might come from right MFG. First, in the intact brain, right MFG shows BOLD signal temporal correlations with both VAN and DAN (Fig. 6b), suggesting it may function as a node shared between the two networks. Second, MFG-pIPS FC was as strong as within-VAN FC in elderly controls, but was severely and persistently disrupted in patients. In concert, the median-split lesion analyses indicated that patients with more severe spatial neglect sustained damage of the

SLF, which connects dorsolateral prefrontal cortex to superior and inferior parietal lobules, providing a plausible structural basis for the disruption of MFG-pIPS FC and MFG-TPJ FC. Third, disrupted FC between left and right dorsal parietal cortex was positively correlated with disrupted FC between STS and MFG. Fourth, behaviorally significant FC within the right hemisphere ventral network almost always involved the MFG. More speculatively, there is evidence that stimulation of a tract that could plausibly connect MFG to the posterior parietal cortex produces neglect-like symptoms (Thiebaut de Schotten et al., 2005). Furthermore, lesions causing neglect in both monkeys and humans tend to involve intra-hemispheric white matter long-range tracts bi-directionally connecting parietal and frontal cortices (Gaffan and Hornak, 1997) (Paolo Bartolomeo, personal communication).

Slightly complicating this picture, recovery of pIPS FC and task-evoked responses depended neither on the recovery of FC in the ventral network nor on the recovery of FC between MFG and pIPS. Speculatively, recovery of dorsal parietal cortex function, paralleling behavioral recovery, may reflect a stronger volitional control of the locus of spatial attention that results from the clinical rehabilitation and treatment of neglect patients (Diller and Weinberg, 1977).

Lastly, we revisit the long-standing puzzle that neglect is more frequent, severe and enduring following right than left hemisphere lesions. Traditionally, theories of neglect have proposed that the lateralization of neglect reflects an asymmetrical representation of space in the two hemispheres (Heilman and Van Den Abell, 1980; Hillis, 2006; Mesulam, 1999). In the current view, spatial representations are contained in the DAN, which is bilaterally symmetric. It is the VAN, which encodes non-spatial

functions, that is strongly lateralized to the right hemisphere, as suggested by task-activation (summarized in (Corbetta and Shulman, 2002)) and FC ((Fox et al., 2006a) and the present results) studies. Even when a left SMG region was selected as seed ROI, we found a lateralization to the right hemisphere of the ventral frontoparietal FC (Supplementary Fig. 5). Therefore, right hemisphere strokes are more likely to damage the VAN, and through its connections with the DAN via intra-hemispheric white matter tracts, more likely to cause a significant functional imbalance in posterior parietal cortex that will secondarily cause a rightward bias with left field detection deficits. Furthermore, non-spatial functions mediated by the VAN will be more permanently damaged after a right hemisphere stroke. Our model suggests that the right lateralization of neglect reflects primarily a lateralization of non-spatial functions, rather than spatial functions, which when disrupted also produce asymmetrical deficits in spatial functions.

Dissociation of FC and task-activation measures

Our data suggest that abnormal task-evoked responses and functional connectivity represent different and complementary physiological indicators of dysfunction. Supplementary Table 3 shows that the correlations between FC and performance were independent of task-evoked responses. Moreover, impairments in these two measurements could occur independently: imbalanced inter-hemispheric task-evoked responses occurred in the presence (e.g., pIPS) or absence (e.g., visual cortex) of disrupted FC; recovery of task-evoked responses in two regions was accompanied (e.g., left-right pIPS) or not accompanied (e.g., MFG-STS) by recovery of functional

connectivity. At this stage we note that a thorough understanding of these dissociations will need further experimental work.

FC MRI of resting state data vs. task state data

It is important to note that our FC analyses were conducted on fMRI data that was acquired while subjects performed an event-related attention task rather than at rest, but with the deterministic (i.e., consistent) task-evoked effects removed. For a detailed discussion on the potential difference between FC results using the current method and those using resting-state data see Supplementary Note 3.

Functional connectivity vs. anatomical connectivity

The current work is also relevant to understanding the relation of functional connectivity to anatomical connectivity. BOLD functional connectivity produces networks with spatial patterns similar to those of anatomical connectivity [for discussion see (Vincent et al., 2006)], i.e., coherent BOLD relationships appear to depend on anatomical connectivity. However, functional connectivity between regions can be disrupted in the absence of anatomical damage to those regions or their connections (e.g., inter-hemispheric pIPS FC in all the 11 patients), suggesting that anatomical connectivity may be necessary but not sufficient for normal functional connectivity; excitatory/inhibitory neuronal inputs from other regions are also needed.

FC MRI as a tool for studying patient populations

FC MRI is a promising new tool for the investigation of brain-behavior relationships in patient populations. It makes no demands on the subject other than holding still and possibly maintaining fixation and therefore can be acquired even in patients that cannot perform a task (for some examples of resting-state FC studies in patients see (Greicius et al., 2004; Lowe et al., 2002; Quigley et al., 2001; Waites et al., 2006); for a study using similar approach as the current study see (Whalley et al., 2005)). This significantly widens the range of patients that can participate in functional brain imaging protocols. Moreover, FC measures are less confounded by differences in task performance between patient and control groups or between patient groups at different stages of recovery, as compared to conventional task-activation measures. This is particularly true for resting-state FC MRI. Finally, FC MRI is robust and reliable in individual subjects after relatively short (5-15 minutes) scanning sessions, and is therefore suitable to clinical applications.

Previous studies of FC in patient populations have usually described group differences in the spatial pattern or strength of FC between patients and controls. Our study, which shows that across subjects the disruption of FC indexes the severity of impaired performance, (see (Hampson et al., 2006a; Hampson et al., 2006b) for similar correlations in healthy subjects), provides stronger evidence that intact BOLD FC is critical for normal brain function.

Supplementary data

Supplementary Note 1: BOLD signal quality in stroke patients

Movement was assessed by summing the deviations (3 translations plus 3 rotations at a radius of 50 mm) used to compensate for head motion within fMRI runs. The presently reported quantity is head movement rms mm averaged over runs and subjects. This quantity was 0.73±.030 mm for patients at the acute stage, 0.60±0.28 mm for patients at the chronic stage and 0.42±0.08 mm for age-matched controls. Acute patients moved more than age-matched controls (P = .003); the following comparisons were not significantly different: chronic patients vs. age-matched controls; and patients in the two stages of recovery. Critically, rms movement was not correlated with inter-regional FC measures (see the following figure for two examples). Hence, it is unlikely that patient vs. control movement differences account for the present main FC results. Further, a significant pIPS FC – performance correlation persisted after regressing out both rms movement and lesion size using partial correlation. Supplementary Table 4 shows that other major FC – behavior correlational results also remained significant after correcting for both movement and lesion size.
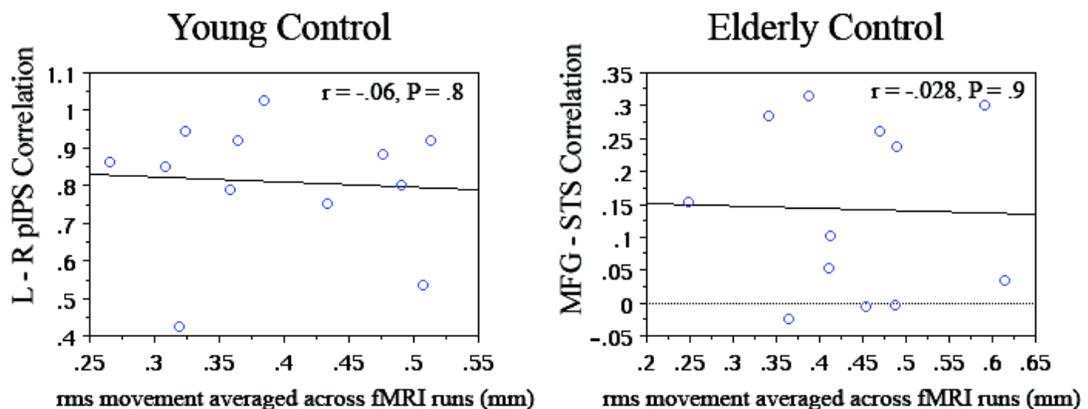
We also conducted several analyses to determine whether stroke affected basic characteristics of the BOLD signal, specifically, its variance and temporal frequency distribution. The BOLD signal s.d. averaged throughout all voxels in the brain (excluding

51

ventricles) was significantly higher in patients than in age-matched controls (Supplementary Fig. 3a).Two likely sources of higher signal variance in patients can be identified: more movement and more cerebrospinal fluid in the brain owing to the presence of lesions. To examine whether greater signal variance in patients was evenly distributed across different regions in the brain, we assessed signal s.d. in 15 widely separated ROIs, including all *a priori* attention ROIs as well as bilateral motor cortices (Supplementary Fig. 3b). In all regions, signal s.d. was higher in patients at the acute stage than in controls (difference significant in 10 out of 15 ROIs). Thus, increase of signal variance in patients was approximately evenly distributed across the brain. From acute to chronic stage, signal s.d. dropped in 13 out of 15 regions. BOLD signal power spectral density distributions (i.e., temporal frequency content) were not different in comparisons of age-matched controls vs. stroke patients in both stages of recovery (Supplementary Figure 3c).

The following considerations argue that the results in this paper are not artifacts attributable to movement, high signal variance, or abnormal neural-vascular coupling in the patient group. More movement might decrease signal quality throughout the brain by contributing to higher signal variance. However, our results were highly regionally specific. For instance, decreased inter-hemispheric FC was observed in pIPS but not in FEF, vIPS, or MT+. This regional specificity is not easily explained on the basis of gross head movement. The critical point, however, is that our main results concern highly specific *correlations* between inter-regional FC measures and behavioral performance. Thus, more movement may explain a uniform increase in signal variance and decreased

signal-to-noise ratios, but is not expected to affect FC measure correlations with performance in a regionally specific fashion.

An excellent question regards whether BOLD signal accurately reflects neuronal activity in post-stroke population. Although caution has to be taken when using fMRI to study patients with cerebrovascular disease (Carusone et al., 2002; D'Esposito et al., 2003; Hamzei et al., 2003; Krainik et al., 2005; Murata et al., 2006), the current findings cannot be explained by potential abnormal neurovascular coupling in the patient group. First, decremented BOLD response in stroke, if present, is a relatively diffuse problem (Murata et al., 2006; Pineiro et al., 2002; Rossini et al., 2004). The above-discussed considerations regarding the specificity of the present findings in relation to globally compromised image quality apply also to the question of neurovascular coupling. It seems to us implausible that abnormal vessels would appear only around the pIPS but not in other regions in the DAN, and only in patients with worse performance. Also, it is unlikely that abnormal neurovascular coupling could lead to artifactually high correlations between BOLD synchrony and performance. Third, in ventral attention regions, although both task responses and synchrony were impaired at acute stage, only the former recovered at chronic stage. Since both measures depend on neurovascular coupling, this dissociation argues against an account of the results by abnormal vasculatures. Fourth, the frequency distribution of the power of BOLD signals was no different in patients than in controls as shown by power spectral density (Supplementary Fig. 3c), suggesting there was no other alteration in signal quality in stroke patients beyond higher signal variance. Finally, recomputing the BOLD FC-performance correlation statistics excluding all the patients with lacunes - the type of stroke associated

with artifactual decrement of BOLD response (Pineiro et al., 2002) - did not alter the

main results. Three patients that had one lacune, three others with two lacunes (all in the

subcortical area or white matter) were excluded. On the basis of the remaining 6 patients,

at the acute stage, inter-hemispheric pIPS FC correlated with % miss in L VF, invalid

condition: r = -.915, P = .007; MFG-STS FC with % miss in L VF, invalid condition: r =

-.804, P = .05; inter-hemispheric SMG FC with % miss in L VF, invalid condition: r = -

.915, P = .007.

Supplementary Note 2: Efficacy of Task regression

To emphasize the intrinsic functional connectivity, we performed FC analyses

after removing deterministic task-evoked responses. Removal of task-evoked responses

was achieved by including the event-related design matrix not assuming hemodynamic

response shape (Ollinger et al., 2001) in the procedure that removed variance attributable

to nuisance regressors (e.g., head movement). We examined the effect of task removal by

computing residual task-evoked responses, signal variances, and inter-regional

correlations in pIPS, MFG and STS as well as left and right motor cortex.

The following analyses demonstrate that deterministic BOLD responses time-

locked to the task were effectively eliminated. After task removal, the modeled evoked

response residual did not differ from baseline (e.g., see Supplementary Fig. 5a for left

pIPS averaged across acute patients). Task-removal significantly reduced signal variances

in nearly all regions investigated (11 out of 12, all P < .003). Task regression also

reduced more variance in left than right motor cortex, (region × maneuver, signal s.d.:

$F_{1,10}$ = 31.7, P = 0.0002), as expected, given that left motor cortex is more strongly

activated by the task (right hand key-presses). Task removal did not change left-right

pIPS FC ($F_{1,10}$= 0.013, P = .9) (Supplementary Fig. 6b left) or MFG – STS FC ($F_{1,10}$=

0.88, P = .4,, data not shown). However, temporal correlation between left and right

motor cortices was significantly enhanced by task-removal (Supplementary Fig. 6b right).

This is expected, since removing task-evoked responses should increase the

proportionality of intrinsic activity in left motor cortex that is correlated with activity in

right motor cortex (Fox et al., 2006b).

Supplementary Note 3: FC MRI of resting state data vs. task state data

It is important to note that our FC analyses were conducted on fMRI data that was

acquired while subjects performed an event-related attention task rather than at rest, but

with the deterministic (i.e., consistent) task-evoked effects removed. Below, we discuss

factors that could produce differences between FC analyses conducted on data collected

during a task with consistent task-evoked activations removed, and at rest.

Our linear model of the task-evoked response did not assume a shape for the

hemodynamic response, thereby enabling maximal removal of *consistent* task-evoked

effects (see Supplementary Note 2 for an evaluation of the efficacy of this regression).

However, this modeling cannot account for trial-to-trial variability in task-evoked

responses, which cannot be distinguished from spontaneous fluctuations of the intrinsic

activity. Such variability could be due to primary variability in the response itself or non-

linear addition of task-evoked response and intrinsic activity. Theoretically, trial-to-trial

variability of task-evoked response, if present in the residual, could contribute to FC

measures. However, this contribution is likely to be small, since the variable component

of task-evoked BOLD responses should be smaller than the mean response, which itself is small compared to intrinsic fluctuations. Experimental evidence suggests that inter-hemispheric FC in motor cortex obtained during a bilateral motor task with task-evoked responses removed is very similar to that obtained at rest (Arfanakis et al., 2000). Empirically, we note that the spatial patterns of FC-defined attention networks obtained in this experiment (after task-regression, Fig. 1) were very similar to those observed during rest (Fox et al., 2006a). Additionally, recent data suggest that intrinsic BOLD fluctuations and deterministic task-evoked BOLD responses superpose approximately linearly (Fox et al., 2006b). Such linear superposition has also been previously reported using optical imaging, albeit at a much faster time scale (Arieli et al., 1996).

Another potential mechanism contributing to difference between task-state data with task-related variance removed and resting-state data concerns general effects that are not time-locked to the paradigm. For example, the task state might alter intrinsic fluctuations by maintaining arousal. Indeed, it has recently been shown that intensive continuous task performance may alter intrinsic fluctuations (Fransson, 2006). Finally it should be acknowledged that our GLM model assumes that the deterministic response is constant through the entire session. Thus, we did not model potential systematic change in the evoked response over time due, e.g., to fatigue or learning (for discussions of such effects see (Caclin and Fonlupt, 2006)). In summary, caution should be attached to the notion that FC measured after regression of task-evoked responses is identical to that measured at rest. We believe that the essential findings reported here are most likely not contingent on task performance but this prediction awaits future testing.

Supplementary Figures

a) Main effect of time

Young healthy subjects

0.0   10.0

Acute patients

Chronic patients

b) Validity x Time effect

Young healthy subjects

0.0   5.0
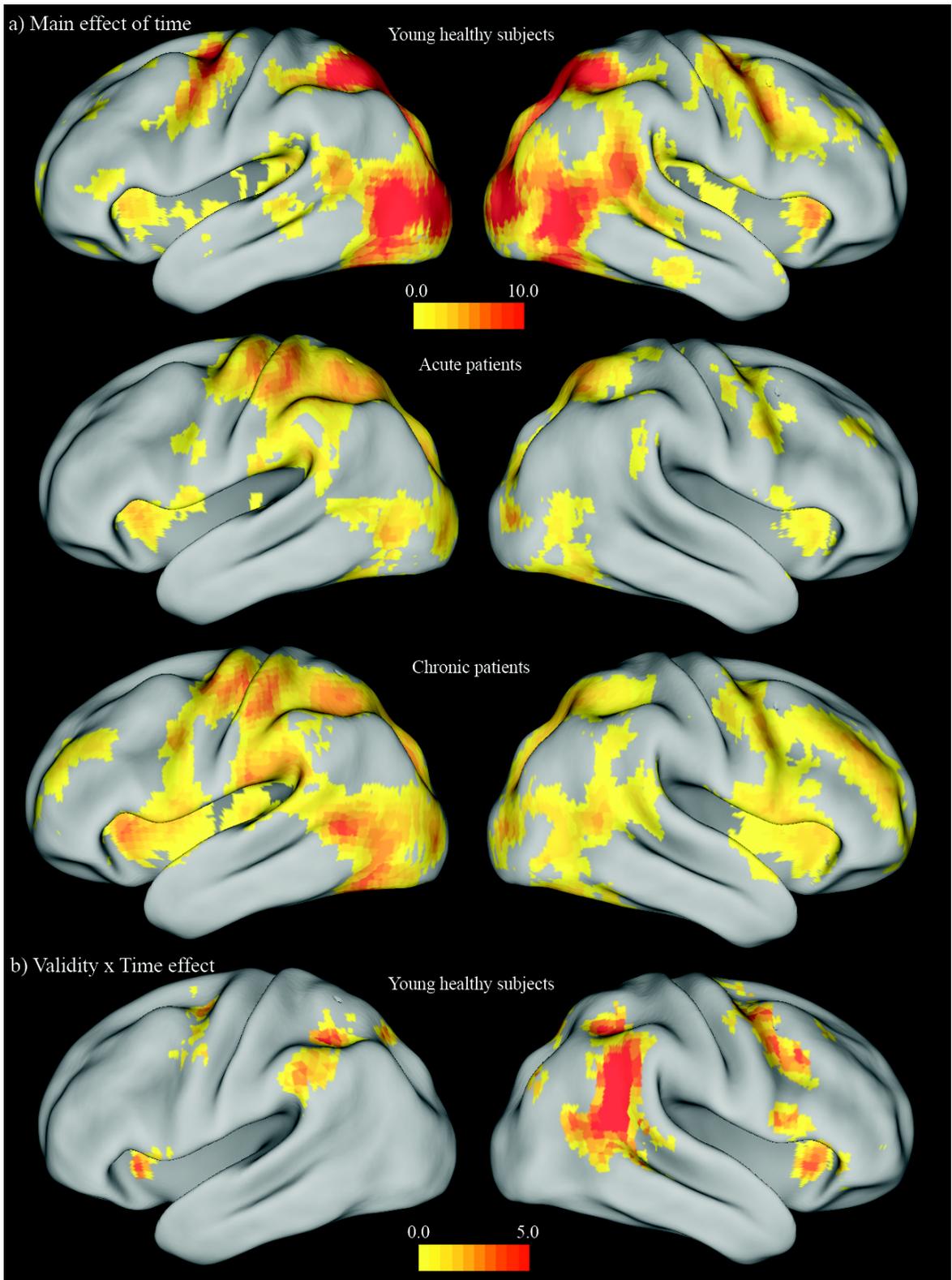
Supplementary Figure 1. Whole-brain voxel-wise analyses on task activation patterns. **(a)** Response to the cue. Top: meta-analysis of four previous studies of young healthy subjects performing Posner-like tasks, used for generating DAN ROIs. Middle: acute patients. Bottom: chronic patients. All maps are thresholded at P < 0.05 after correction for multiple comparison (Z=3, cluster size = 17 voxels). **(b)** Regions showing differential activations to the invalid versus valid targets. Shown is meta-analysis on the four previous studies used for generating VAN ROIs. Maps are thresholded similarly as in (a). No brain voxel was significant after multiple comparison correction in this analysis on patients at either stage.

r Values	FEF	pIPS	vIPS	MT	PrCe	MFG	Ant Insula	TPJ	STS
FEF	1.00	0.34	0.21	0.08	0.60	0.25	0.14	0.18	0.15
pIPS	0.34	1.00	0.59	0.38	0.18	0.17	0.07	0.01	0.08
vIPS	0.21	0.59	1.00	0.41	0.05	0.11	0.01	0.03	0.04
MT	0.08	0.38	0.41	1.00	-0.08	-0.05	0.01	-0.07	0.03
PrCe	0.60	0.18	0.05	-0.08	1.00	0.41	0.26	0.38	0.16
MFG	0.25	0.17	0.11	-0.05	0.41	1.00	0.34	0.34	0.17
Ant Insula	0.14	0.07	0.01	0.01	0.26	0.34	1.00	0.28	0.11
TPJ	0.18	0.01	0.03	-0.07	0.38	0.34	0.28	1.00	0.33
STS	0.15	0.08	0.04	0.03	0.16	0.17	0.11	0.33	1.00

Supplementary Figure 2 Correlation coefficients between all possible pairs of right-hemisphere *a priori* ROIs were computed for each subject in the young control group. Shown is the correlation matrix averaged across 12 subjects (top and middle). Across-network (DAN·VAN) correlations were significantly weaker than within-network correlations (DAN-DAN: P < .0001; VAN-VAN: P = .0009) (bottom panel). The spatial overlap beween FEF and PrCe was excluded from each ROI, but the two regions are still spatial adjacent. Due to spatial smoothing used in preprocessing of the images, there is likely spill over of signals from one region to the other, which explains the high FEF – PrCe correlation, as well as the relatively high correlations between FEF and VAN ROIs and between PrCe and DAN ROIs. The next highest across-network correlation appears between MFG and pIPS.
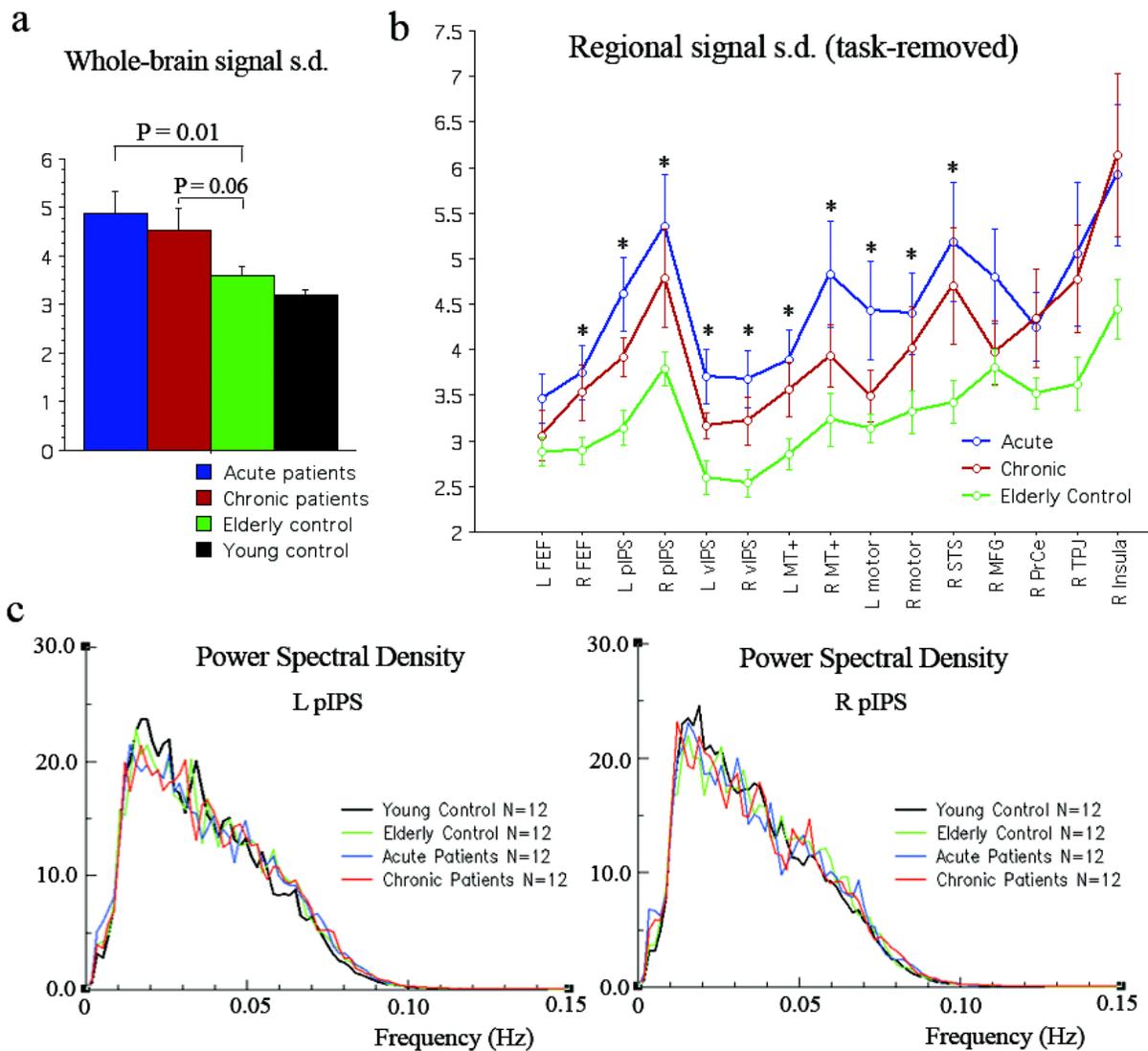
Supplementary Figure 3 Quality of BOLD signal in stroke patients. **(a)** Signal variances averaged across whole brain, excluding ventricles (acute vs. elder control: P = .01, chronic vs. elder control: P = .06). **(b)** Signal s.d. averaged within each ROI. Both the enhancement of s.d. in patients relative to control, and the drop of s.d. from acute to chronic stage were approximately evenly distributed across the brain. Regions marked with asterisks had significantly higher signal s.d. in acute patients compared to controls (all P < .04). **(c)** Power spectral density (normalized by total signal variance) of BOLD signal from pIPS. There were no obvious effects of either aging or stroke on frequency content.
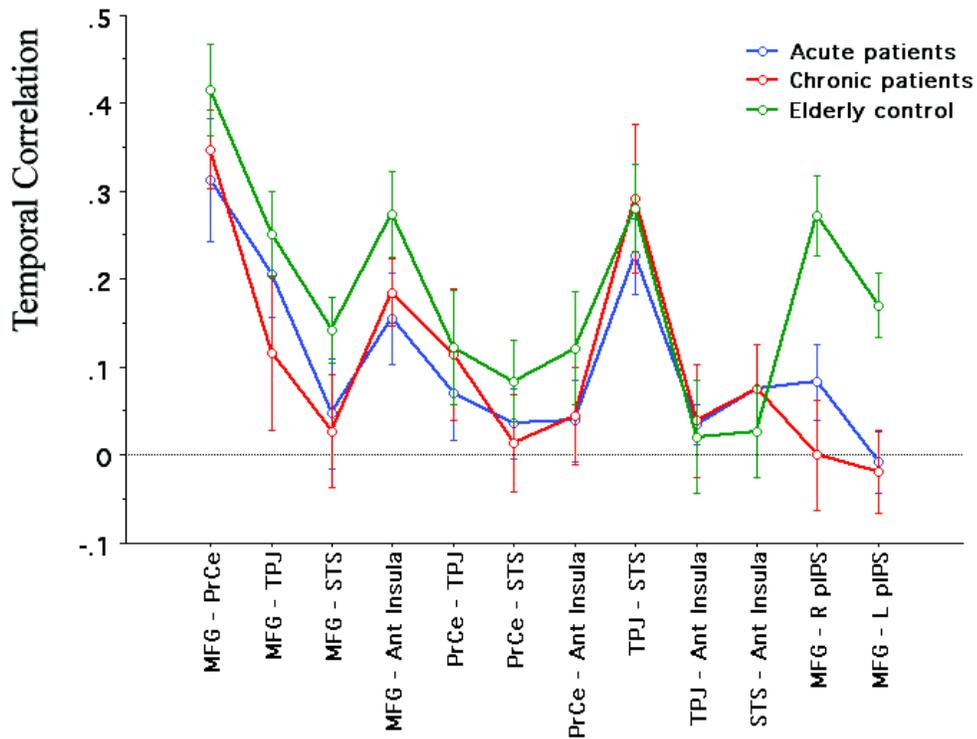
Supplementary Figure 4 FC within VAN in patients and age-matched controls. Error bars denote s.e.m. FC between MFG–PrCe, MFG–Insula, MFG–R pIPS, and MFG–L pIPS was significantly reduced in patients vs. controls. Although other correlations (including MFG–TPJ, MFG–STS, PrCe–Ant Insula) were also lower in patients, these differences were not significant at the 5% leve. One important observation was that no pairwise FC in the VAN showed significant recovery from the acute to chronic stages.
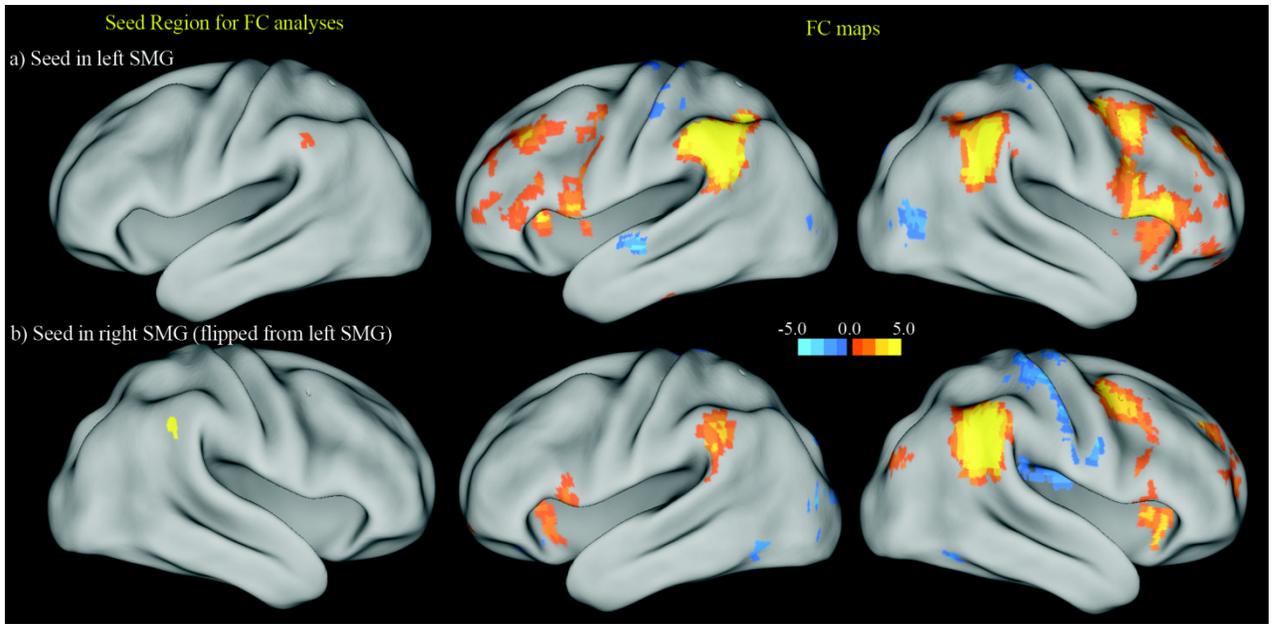
Supplementary Figure 5 (a) Left: left SMG region defined from normal FC patterns of the VAN (Fig. 1c). Middle and right: voxel-wise FC map generated by seeding in L SMG from the young control group, shown are Z scores from random-effects analysis, corrected for multiple comparison at a significance level of $P < 0.05 (Z > 3.0$, cluster size >17 voxels). **(b)** Left: right SMG region defined as homologous region of the L SMG. Middle and right: voxel-wise FC map generated by seeding in R SMG from the young control group, values are the same as in (a).
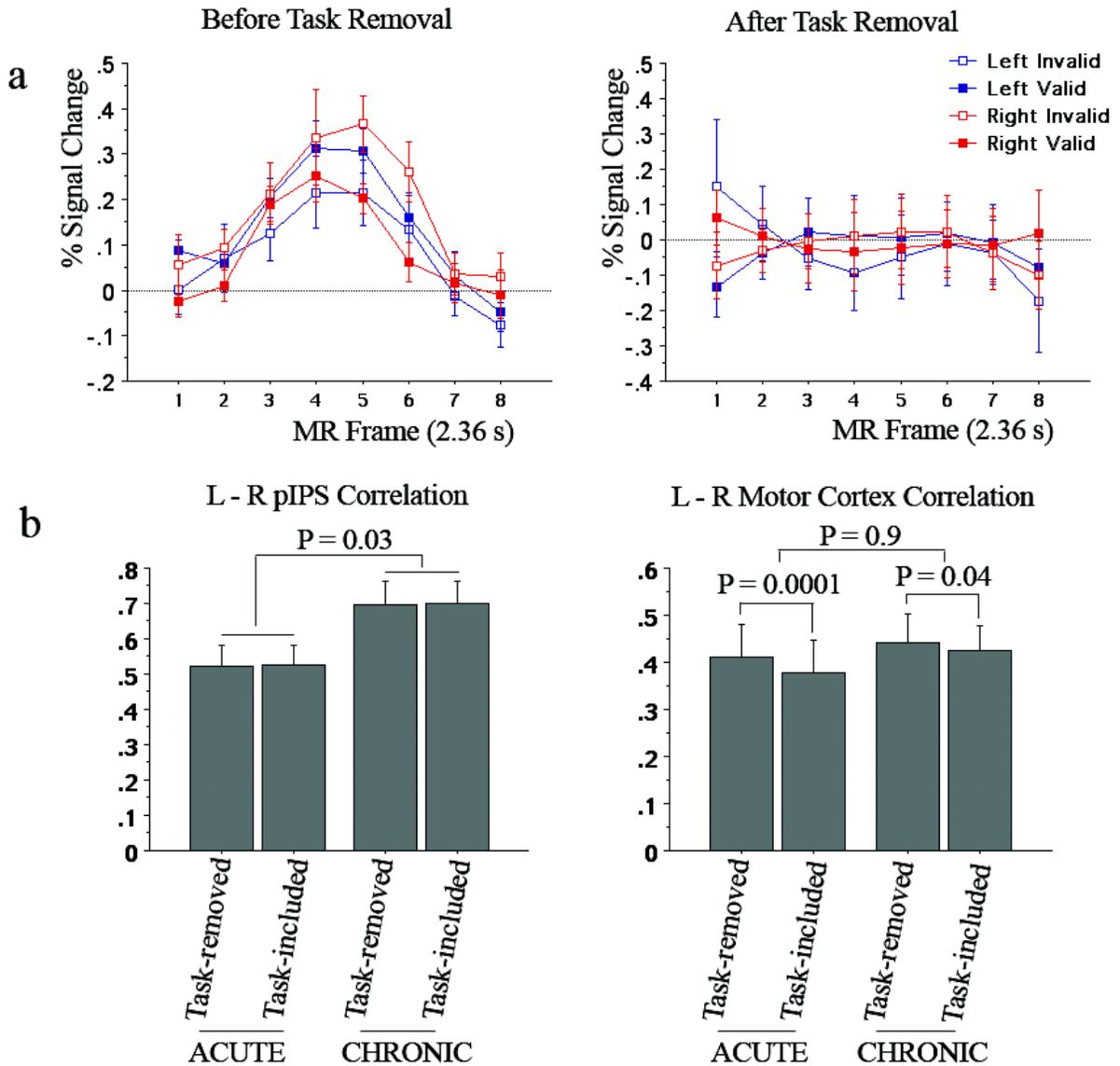
Supplementary Figure 6 Validation of task-evoked response regression procedure. **(a).** Averaged responses in L pIPS to various trial types before (left) and after (right) task removal. The response evoked by each event type was modeled without constraints over 8 frames following the cue, i.e., without prior assumptions regarding the hemodynamic response profile. Residual time courses were averaged over the 11 acute stage patients. **(b)** Task removal significantly increased correlation values between left and right motor cortex, but did not change left-right pIPS correlation. Left-right pIPS correlation significantly recovered from the acute to chronic stages ($F_{1,10}= 6.254$, $P = .03$), while L – R motor correlation did not significantly change with stage.

Dorsal Attention ROIs	Talairach coordinates			Volumn
	x	y	z	(mm3)
L frontal eye field (FEF)	-26	-9	48	918
R frontal eye field (FEF)	32	-9	48	729
L posterior intraparietal sulcus (pIPS)	-25	-63	47	918
R posterior intraparietal sulcus (pIPS)	23	-65	48	945
L ventral IPS (vIPS)	-24	-69	30	918
R ventral IPS (vIPS)	30	-80	16	999
L middle temporal region (MT+)	-43	-70	-3	918
R middle temporal region (MT+)	42	-68	-6	837
Ventral Attention ROIs	Talairach atlas coordinates			Volumn
	x	y	z	(mm3)
R precentral sulcus (PrCe)	38	-3	50	918
R middle frontal gyrus (MFG)	39	12	34	864
R Anterior Insula	38	16	1	918
R temporal-parietal junction (TPJ)	49	-50	28	810
R superior temporal sulcus (STS)	55	-50	11	891

Supplementary Table 1. Seed regions defined for FC analyses.

An automated peak search algorithm was run on the combined Z score map from meta-analysis, separately for dorsal and ventral networks. Coordinates were computed as center of mass for a cluster of peak foci within a ROI, not weighted by Z scores. Region sizes were controlled by including only 30-37 voxels with highest Z values.

Correlation between functional connectivity and hit rates		Left				Right			
		Valid		**Invalid**		**Valid**		**Invalid**	
		r	P	r	P	r	P	r	P
Homologous Pairs of Regions in Dorsal	**L-R pIPS**	0.577	0.06	0.846	**0.0005***	0.534	0.09	0.556	0.076
	L-R FEF	0.579	0.06	0.353	0.3	0.517	0.1	0.333	0.3
	L-R vIPS	-0.171	0.6	0.005	1	-0.128	0.7	-0.368	0.3
	L-R MT	0.023	0.9	0.374	0.3	0.055	0.9	0.192	0.6
All Pairs of Regions in Ventral Attention Network	**MFG-STS**	0.693	**0.016***	0.775	**0.003***	0.652	**0.027***	0.404	0.2
	MFG-TPJ	0.747	**0.006***	0.317	0.4	0.731	**0.008***	0.338	0.3
	MFG-PrCe	0.624	0.039*	0.298	0.4	0.578	0.06	0.024	0.9
	MFG-Ant Insula	0.051	0.9	-0.374	0.3	-0.037	0.9	-0.319	0.3
	TPJ-PrCe	0.539	0.09	-0.026	0.9	0.552	0.08	0.291	0.4
	TPJ-STS	-0.358	0.3	-0.024	0.9	-0.289	0.4	-0.387	0.2
	TPJ-Ant Insula	-0.274	0.4	-0.448	0.2	-0.409	0.2	-0.703	0.01*
	STS-PrCe	0.541	0.09	0.527	0.1	0.452	0.2	0.232	0.5
	STS-Ant Insula	0.072	0.8	0.071	0.8	-0.058	0.9	-0.482	0.1
	PrCe-Ant Insula	0.536	0.09	0.291	0.4	0.307	0.4	0.166	0.6

Supplementary Table 2.Correlation between inter-regional FC and hit rates across acute patients (N = 11).

	Correlation with inter-hemispheric pIPS FC	r-Value	P-Value
Acute	Difference between the magnitudes of evoked responses in left and right pIPS	.127	.72
	Normalized magnitude difference of evoked responses [(left – right)/(left + right)]	-.351	.3
Chronic	Difference between the magnitudes of evoked responses in left and right pIPS	-.414	.21
	Normalized magnitude difference of evoked responses [(left – right)/(left + right)]	-.377	.26

Supplementary Table 3a. Across-subject correlation between inter-hemispheric FC and the degree of imbalanced task-evoked responses (with two different measurements) in pIPS.

Acute, Left VF, Invalid cue		Correlation	Partial correlation (controlling for absolute magnitude difference)	Partial correlation (controlling for normalized magnitude difference)
Correlation with %miss	Inter-hemispheric pIPS FC	R = -.846, P = .0005	R = -.868	R = -.856
	Magnitude difference (left pIPS – right pIPS)	R = .090, P = .80		
	Normalized magnitude difference [(left - right)/(left + right)]	R = .151, P = .67		
Correlation with reaction times (ms)	Inter-hemispheric pIPS FC	R = -.593, P = .05	R = -.645	R = -.593
	Magnitude difference (left pIPS – right pIPS)	R = .234, P = .50		
	Normalized magnitude difference [(left - right)/(left + right)]	R = .119, P = .74		

Supplementary Table 3b. Correlation (across patients at acute stage) between disengagement deficit and inter-hemispheric pIPS FC or between disengagement deficit and imbalanced task-evoked responses in pIPS, as well as partial correlation between disengagement deficit and pIPS FC when controlling for imbalanced evoked responses.

Correlation with hit rates	MFG-STS		MFG-TPJ		L – R SMG	
Left VF, valid	r = 0.552	n.s.	r = 0.776	P < .02		
Left VF, invalid	r = 0.755	P < .02			r = .711	P < .01
Right VF, valid	r = 0.519	n.s.	r = 0.768	P < .02		

Supplementary Table 4. Correlation between functional connectivity and hit rates at

acute stage, after correction for both movement and lesion size.

References

Arfanakis, K., Cordes, D., Haughton, V.M., Moritz, C.H., Quigley, M.A., and Meyerand, M.E. (2000). Combining independent component analysis and correlation analysis to probe interregional connectivity in fMRI task activation datasets. Magn Reson Imaging *18*, 921-930.

Arieli, A., Sterkin, A., Grinvald, A., and Aertsen, A. (1996). Dynamics of ongoing activity: explanation of the large variability in evoked cortical responses. Science *273*, 1868-1871.

Arrington, C.M., Carr, T.H., Mayer, A.R., and Rao, S.M. (2000). Neural mechanisms of visual attention: object-based selection of a region in space. Journal of Cognitive Neuroscience *12*, 106-117.

Astafiev, S.V., Shulman, G.L., and Corbetta, M. (2006). Visuospatial reorienting signals in the human temporo-parietal junction are independent of response selection. Eur J Neurosci *23*, 591-596.

Astafiev, S.V., Shulman, G.L., Stanley, C.M., Snyder, A.Z., Van Essen, D.C., and Corbetta, M. (2003). Functional organization of human intraparietal and frontal cortex for attending, looking, and pointing. J Neurosci *23*, 4689-4699.

Astafiev, S.V., Stanley, C.M., Shulman, G.L., and Corbetta, M. (2004). Extrastriate body area in human occipital cortex responds to the performance of motor actions. Nat Neurosci *7*, 542-548.

Behrens, T.E., Woolrich, M.W., Jenkinson, M., Johansen-Berg, H., Nunes, R.G., Clare, S., Matthews, P.M., Brady, J.M., and Smith, S.M. (2003). Characterization and

propagation of uncertainty in diffusion-weighted MR imaging. Magn Reson Med *50*, 1077-1088.

Biswal, B., Yetkin, F.Z., Haughton, V.M., and Hyde, J.S. (1995). Functional connectivity in the motor cortex of resting human brain using echo-planar MRI. Magn Reson Med *34*, 537-541.

Caclin, A., and Fonlupt, P. (2006). Effect of initial fMRI data modeling on the connectivity reported between brain areas. Neuroimage *33*, 515-521.

Carusone, L.M., Srinivasan, J., Gitelman, D.R., Mesulam, M.M., and Parrish, T.B. (2002). Hemodynamic response changes in cerebrovascular disease: implications for functional MR imaging. AJNR Am J Neuroradiol *23*, 1222-1228.

Corbetta, M., Akbudak, E., Conturo, T.E., Snyder, A.Z., Ollinger, J.M., Drury, H.A., Linenweber, M.R., Petersen, S.E., Raichle, M.E., Van Essen, D.C., and Shulman, G.L. (1998). A common network of functional areas for attention and eye movements. Neuron *21*, 761-773.

Corbetta, M., Kincade, J.M., Ollinger, J.M., McAvoy, M.P., and Shulman, G.L. (2000). Voluntary orienting is dissociated from target detection in human posterior parietal cortex. Nat Neurosci *3*, 292-297.

Corbetta, M., Kincade, J.M., and Shulman, G.L. (2002). Neural systems for visual orienting and their relationships to spatial working memory. J Cogn Neurosci *14*, 508-523.

Corbetta, M., Kincade, M.J., Lewis, C., Snyder, A.Z., and Sapir, A. (2005). Neural basis and recovery of spatial attention deficits in spatial neglect. Nat Neurosci *8*, 1603-1610.

Corbetta, M., and Shulman, G.L. (2002). Control of goal-directed and stimulus-driven

    attention in the brain. Nat Rev Neurosci *3*, 201-215.

Cordes, D., Haughton, V.M., Arfanakis, K., Carew, J.D., Turski, P.A., Moritz, C.H.,

    Quigley, M.A., and Meyerand, M.E. (2001). Frequencies contributing to

    functional connectivity in the cerebral cortex in "resting-state" data. AJNR Am J

    Neuroradiol *22*, 1326-1333.

D'Esposito, M., Deouell, L.Y., and Gazzaley, A. (2003). Alterations in the BOLD fMRI

    signal with ageing and disease: a challenge for neuroimaging. Nat Rev Neurosci

    4, 863-872.

Diller, L., and Weinberg, J. (1977). Hemi-inattention in rehabilitation: the evolution of a

    rationale remediation program. In Hemi-inattention and hemisphere

    specialization, E.A.F. Weinstein, R.P., ed. (New York: Raven).

Downar, J., Crawley, A.P., Mikulis, D.J., and Davis, K.D. (2000). A multimodal cortical

    network for the detection of changes in the sensory environment. Nat Neurosci *3*,

    277-283.

Fox, M.D., Corbetta, M., Snyder, A.Z., Vincent, J.L., and Raichle, M.E. (2006a).

    Spontaneous neuronal activity distinguishes human dorsal and ventral attention

    systems. Proc Natl Acad Sci U S A *103*, 10046-10051.

Fox, M.D., Snyder, A.Z., Vincent, J.L., Corbetta, M., Van Essen, D.C., and Raichle, M.E.

    (2005). The human brain is intrinsically organized into dynamic, anticorrelated

    functional networks. Proc Natl Acad Sci U S A *102*, 9673-9678.

Fox, M.D., Snyder, A.Z., Zacks, J.M., and Raichle, M.E. (2006b). Coherent spontaneous

    activity accounts for trial-to-trial variability in human evoked brain responses. Nat

    Neurosci *9*, 23-25.

Fransson, P. (2006). How default is the default mode of brain function? Further evidence

    from intrinsic BOLD signal fluctuations. Neuropsychologia *44*, 2836-2845.

Friedrich, F.J., Egly, R., Rafal, R.D., and Beck, D. (1998). Spatial attention deficits in

    humans: a comparison of superior parietal and temporal-parietal junction lesions.

    Neuropsychology *12*, 193-207.

Gaffan, D., and Hornak, J. (1997). Visual neglect in the monkey. Representation and

    disconnection. Brain *120 (Pt 9)*, 1647-1657.

Greicius, M.D., Krasnow, B., Reiss, A.L., and Menon, V. (2003). Functional connectivity

    in the resting brain: a network analysis of the default mode hypothesis. Proc Natl

    Acad Sci U S A *100*, 253-258.

Greicius, M.D., Srivastava, G., Reiss, A.L., and Menon, V. (2004). Default-mode

    network activity distinguishes Alzheimer's disease from healthy aging: evidence

    from functional MRI. Proc Natl Acad Sci U S A *101*, 4637-4642.

Hampson, M., Driesen, N.R., Skudlarski, P., Gore, J.C., and Constable, R.T. (2006a).

    Brain connectivity related to working memory performance. J Neurosci *26*,

    13338-13343.

Hampson, M., Peterson, B.S., Skudlarski, P., Gatenby, J.C., and Gore, J.C. (2002).

    Detection of functional connectivity using temporal correlations in MR images.

    Hum Brain Mapp *15*, 247-262.

Hampson, M., Tokoglu, F., Sun, Z., Schafer, R.J., Skudlarski, P., Gore, J.C., and

    Constable, R.T. (2006b). Connectivity-behavior analysis reveals that functional

    connectivity between left BA39 and Broca's area varies with reading ability.

    Neuroimage *31*, 513-519.

Hamzei, F., Knab, R., Weiller, C., and Rother, J. (2003). The influence of extra- and

    intracranial artery disease on the BOLD signal in FMRI. Neuroimage *20*, 1393-

    1399.

Heilman, K.M., and Van Den Abell, T. (1980). Right hemisphere dominance for

    attention: the mechanism underlying hemispheric asymmetries of inattention

    (neglect). Neurology *30*, 327-330.

Heilman, K.M., Watson, R.T., and Valenstein, E. (1985). Neglect and related disorders.

    In Clinical Neuropsychology, K.M. Heilman, and E. Valenstein, eds. (New York:

    Oxford), pp. 243-293.

Hillis, A.E. (2006). Neurobiology of unilateral spatial neglect. Neuroscientist *12*, 153-

    163.

Husain, M., and Kennard, C. (1996). Visual neglect associated with frontal lobe

    infarction. J Neurol *243*, 652-657.

Husain, M., and Rorden, C. (2003). Non-spatially lateralized mechanisms in hemispatial

    neglect. Nat Rev Neurosci *4*, 26-36.

Karnath, H.O., Ferber, S., and Himmelbach, M. (2001). Spatial awareness is a function of

    the temporal not the posterior parietal lobe. Nature *411*, 950-953.

Karnath, H.O., Fruhmann Berger, M., Kuker, W., and Rorden, C. (2004). The anatomy of spatial neglect based on voxelwise statistical analysis: a study of 140 patients. Cereb Cortex *14*, 1164-1172.

Karnath, H.O., Himmelbach, M., and Rorden, C. (2002). The subcortical anatomy of human spatial neglect: putamen, caudate nucleus and pulvinar. Brain *125*, 350-360.

Kastner, S., and Ungerleider, L.G. (2000). Mechanisms of visual attention in the human cortex. Annu Rev Neurosci *23*, 315-341.

Kincade, J.M., Abrams, R.A., Astafiev, S.V., Shulman, G.L., and Corbetta, M. (2005). An event-related functional magnetic resonance imaging study of voluntary and stimulus-driven orienting of attention. J Neurosci *25*, 4593-4604.

Krainik, A., Hund-Georgiadis, M., Zysset, S., and von Cramon, D.Y. (2005). Regional impairment of cerebrovascular reactivity and BOLD signal in adults after stroke. Stroke *36*, 1146-1152.

Laufs, H., Krakow, K., Sterzer, P., Eger, E., Beyerle, A., Salek-Haddadi, A., and Kleinschmidt, A. (2003). Electroencephalographic signatures of attentional and cognitive default modes in spontaneous brain activity fluctuations at rest. Proc Natl Acad Sci U S A *100*, 11053-11058.

Lowe, M.J., Phillips, M.D., Lurito, J.T., Mattson, D., Dzemidzic, M., and Mathews, V.P. (2002). Multiple sclerosis: low-frequency temporal blood oxygen level-dependent fluctuations indicate reduced functional connectivity initial results. Radiology *224*, 184-192.

Macaluso, E., Frith, C.D., and Driver, J. (2002). Supramodal effects of covert spatial orienting triggered by visual or tactile events. J Cogn Neurosci *14*, 389-401.

Malhotra, P., Coulthard, E., and Husain, M. (2006a). Hemispatial neglect, balance and eye-movement control. Curr Opin Neurol *19*, 14-20.

Malhotra, P.A., Parton, A.D., Greenwood, R., and Husain, M. (2006b). Noradrenergic modulation of space exploration in visual neglect. Ann Neurol *59*, 186-190.

Mesulam, M.M. (1999). Spatial attention and neglect: parietal, frontal and cingulate contributions to the mental representation and attentional targeting of salient extrapersonal events. Philos Trans R Soc Lond B Biol Sci *354*, 1325-1346.

Milner, A.D., and McIntosh, R.D. (2005). The neurological basis of visual neglect. Curr Opin Neurol *18*, 748-753.

Morrow, L.A., and Ratcliff, G. (1988). The disengagement of covert attention and the neglect syndrome. Psychobiology *16*, 261-269.

Mort, D.J., Malhotra, P., Mannan, S.K., Rorden, C., Pambakian, A., Kennard, C., and Husain, M. (2003). The anatomy of visual neglect. Brain *126*, 1986-1997.

Murata, Y., Sakatani, K., Hoshino, T., Fujiwara, N., Kano, T., Nakamura, S., and Katayama, Y. (2006). Effects of cerebral ischemia on evoked cerebral blood oxygenation responses and BOLD contrast functional MRI in stroke patients. Stroke *37*, 2514-2520.

Ollinger, J.M., Shulman, G.L., and Corbetta, M. (2001). Separating processes within a trial in event-related functional MRI. Neuroimage *13*, 210-217.

Pardo, J.V., Fox, P.T., and Raichle, M.E. (1991). Localization of a human system for sustained attention by positron emission tomography. Nature *349*, 61-64.

Peers, P.V., Ludwig, C.J., Rorden, C., Cusack, R., Bonfiglioli, C., Bundesen, C., Driver, J., Antoun, N., and Duncan, J. (2005). Attentional Functions of Parietal and Frontal Cortex. Cereb Cortex.

Petrides, M., and Pandya, D.N. (2002). Association Pathways of the Prefrontal Cortex and Functional Observations. In Principles of Frontal Lobe Function, D.T. Stuss, and R.T. Knight, eds. (New York, NY: Oxford University Press), pp. 31-50.

Pineiro, R., Pendlebury, S., Johansen-Berg, H., and Matthews, P.M. (2002). Altered hemodynamic responses in patients after subcortical stroke measured by functional MRI. Stroke *33*, 103-109.

Posner, M.I., Walker, J.A., Friedrich, F.J., and Rafal, R.D. (1984). Effects of parietal injury on covert orienting of attention. J Neurosci *4*, 1863-1874.

Quigley, M., Cordes, D., Turski, P., Moritz, C., Haughton, V., Seth, R., and Meyerand, M.E. (2003). Role of the corpus callosum in functional connectivity. AJNR Am J Neuroradiol *24*, 208-212.

Quigley, M., Cordes, D., Wendt, G., Turski, P., Moritz, C., Haughton, V., and Meyerand, M.E. (2001). Effect of focal and nonfocal cerebral lesions on functional connectivity studied with MR imaging. AJNR Am J Neuroradiol *22*, 294-300.

Robertson, I., Tegner, R., Tham, K., Lo, A., and Nimmo-Smith, I. (1995). Sustained attention training for unilateral neglect: Theoretical and rehabilitation implications. Journal of Clinical and Experimental Neuropsychology *17*, 416-430.

Robertson, I.H. (2001). Do we need the "lateral" in unilateral neglect? Spatially nonselective attention deficits in unilateral neglect and their implications for rehabilitation. Neuroimage *14*, S85-90.

Robertson, I.H., Mattingley, J.B., Rorden, C., and Driver, J. (1998). Phasic alerting of neglect patients overcomes their spatial deficit in visual awareness. Nature *395*, 169-172.

Rossini, P.M., Altamura, C., Ferretti, A., Vernieri, F., Zappasodi, F., Caulo, M., Pizzella, V., Del Gratta, C., Romani, G.L., and Tecchio, F. (2004). Does cerebrovascular disease affect the coupling between neuronal activity and local haemodynamics? Brain *127*, 99-110.

Rueckert, L., and Grafman, J. (1996). Sustained attention deficits in patients with right frontal lesions. Neuropsychologia *34*, 953-963.

Schluppeck, D., Glimcher, P., and Heeger, D.J. (2005). Topographic organization for delayed saccades in human posterior parietal cortex. J Neurophysiol *94*, 1372-1384.

Schmahmann, J.D., and Pandya, D.N. (2006). Fiber Pathways of the Brain (New York, NY: Oxford University Press).

Serences, J.T., Yantis, S., Culberson, A., and Awh, E. (2004). Preparatory activity in visual cortex indexes distractor suppression during covert spatial orienting. J Neurophysiol *92*, 3538-3545.

Sereno, M.I., Pitzalis, S., and Martinez, A. (2001). Mapping of contralateral space in retinotopic coordinates by a parietal cortical area in humans. Science *294*, 1350-1354.

Shapiro, K., Hillstrom, A.P., and Husain, M. (2002). Control of visuotemporal attention by inferior parietal and superior temporal cortex. Curr Biol *12*, 1320-1325.

Shimony, J.S., Burton, H., Epstein, A.A., McLaren, D.G., Sun, S.W., and Snyder, A.Z. (2006). Diffusion tensor imaging reveals white matter reorganization in early blind humans. Cereb Cortex *16*, 1653-1661.

Silver, M.A., Ress, D., and Heeger, D.J. (2005). Topographic maps of visual spatial attention in human parietal cortex. J Neurophysiol *94*, 1358-1371.

Talairach, J., and Tournoux, P. (1988). Co-Planar Stereotaxic Atlas of the Human Brain (New York: Thieme Medical Publishers, Inc.).

Thiebaut de Schotten, M., Urbanski, M., Duffau, H., Volle, E., Levy, R., Dubois, B., and Bartolomeo, P. (2005). Direct evidence for a parietal-frontal pathway subserving spatial awareness in humans. Science *309*, 2226-2228.

Vallar, G., and Perani, D. (1987). The anatomy of spatial neglect in humans. In Neurophysiological and Neuropsychological Aspects of Spatial Neglect, M. Jeannerod, ed. (North-Holland: Elsevier Science Publishers), pp. 235-258.

Vincent, J.L., Snyder, A.Z., Fox, M.D., Shannon, B.J., Andrews, J.R., Raichle, M.E., and Buckner, R.L. (2006). Coherent Spontaneous Activity Identifies a Hippocampal-Parietal Mnemonic Network. J Neurophysiol.

Waites, A.B., Briellmann, R.S., Saling, M.M., Abbott, D.F., and Jackson, G.D. (2006). Functional connectivity networks are disrupted in left temporal lobe epilepsy. Ann Neurol *59*, 335-343.

Whalley, H.C., Simonotto, E., Marshall, I., Owens, D.G., Goddard, N.H., Johnstone, E.C., and Lawrie, S.M. (2005). Functional disconnectivity in subjects at high genetic risk of schizophrenia. Brain *128*, 2097-2108.

Wilkins, A.J., Shallice, T., and McCarthy, R. (1987). Frontal lesions and sustained

attention. Neuropsychologia *25*, 359-365.

Zar, J.H. (1996). Biostatistical Analysis, 3 edn (Upper Saddle River, New Jersey:

Prentice-Hall, Inc.).

CHAPTER III: Electrophysiological correlates of the brain's intrinsic large-scale functional architecture

Summary

Spontaneous fluctuations in the blood oxygen level-dependent (BOLD) signals demonstrate consistent temporal correlations within large-scale brain networks associated with different functions. The neurophysiological correlates of this phenomenon remain elusive. Here we show in humans that the slow cortical potentials recorded by electrocorticography demonstrate a correlation structure similar to that of spontaneous BOLD fluctuations across wakefulness, slow-wave sleep and rapid-eye-movement (REM) sleep. Gamma frequency power also showed a similar correlation structure, but only during wakefulness and REM sleep. Our results provide an important bridge between the large-scale brain networks readily revealed by spontaneous BOLD signals and their underlying neurophysiology.

Introduction

Spontaneous slow (< 0.1 Hz) fluctuations in the blood oxygen level-dependent (BOLD) signals of functional magnetic resonance imaging (fMRI) appear to reflect a fundamental aspect of the brain's organization (Biswal et al., 1995; Vincent et al., 2007). These fluctuations are temporally covariant within large-scale functional brain networks such as those associated with sensorimotor (Biswal et al., 1995), language (Hampson et al., 2002), attention (Fox et al., 2006) and executive (Seeley et al., 2007) functions as well as the 'default network' (Greicius et al., 2003). These covariant relationships (i.e.,

correlation structures) of spontaneous BOLD signals exist during restful waking (Biswal et al., 1995; Fox et al., 2006; Greicius et al., 2003; Hampson et al., 2002; Seeley et al., 2007), task performance (Hampson et al., 2002; He et al., 2007), sleep (Horovitz et al., 2008) and even general anesthesia (Vincent et al., 2007). Furthermore, their integrity appears to be essential to normal brain function (He et al., 2007). However, in contrast to evoked BOLD responses (Logothetis et al., 2001; Mukamel et al., 2005; Niessing et al., 2005; Shmuel et al., 2006), the electrophysiological basis of these spontaneous covariant BOLD fluctuations is unknown. Here we investigated this question in five patients with intractable epilepsy undergoing evaluation with surgically implanted grids of subdural electrodes. Each patient underwent about a week of continuous video-monitored electrocorticography (ECoG) for the purpose of determining the epileptic focus prior to surgical resection.

The present analyses were based on ECoG data recorded in three distinct arousal states: 1) extended awake periods during which patients were in bed or seated, typically watching TV, eating or engaged in social interactions; 2) slow-wave sleep (SWS); and 3) rapid-eye-movement (REM) sleep. Representative ECoG data are shown in Fig. S1. Resting-state (maintaining visual fixation) BOLD fMRI was acquired in a separate session either before or after surgical intervention. Patient information and data details are included in the Supplementary Table. In what follows we present analyses using four different strategies to compare the correlation structures of BOLD and ECoG signals.

METHODS

Subjects

Five patients undergoing surgical treatment for intractable epilepsy participated in the study. To localize epileptogenic zones, patients underwent a craniotomy for subdural placement of electrode grids and strips followed by 1-2 weeks of continuous video and ECoG monitoring. The placement of the electrodes and the duration of monitoring were determined entirely by clinical considerations. All patients gave informed consent according to the procedures established by Washington University Institutional Review Board. Exclusion criteria were: (1) widespread interictal spike-and-wave discharges; (2) age < 10 years old; (3) severely impaired cognitive capability; (4) diffuse brain tissue abnormality, e.g., tuberous sclerosis, cerebral palsy; (4) limited electrode coverage, e.g., only temporal lobe strips. See Supplementary Table for demographic and clinical information.

Electrophysiology data acquisition

The electrode arrays (typically 8×8, 4×5 or 2×5) and strips (typically 1×6 or 1×8) consisted of platinum electrodes of 4 mm diameter (2.3 mm exposed) with a center-to-center distance of 10 mm between adjacent electrodes (AD-TECH Medical Instrument Corporation, Racine WI). ECoG signals were recorded using a standard clinical monitoring system (Proamp, LaMont Medical Inc., 0.1 to 500 Hz bandpass, 18 dB/octave roll-off). Sampling frequency was 512 Hz for Patients 1 through 4 and 200 Hz for Patient 5. Noisy electrodes and electrodes overlaying pathologic tissue (including both the primary epileptogenic zone and areas showing active interictal spike-wave discharges) were eliminated from all analyses.

Artifact-free and interical-spike-free segments of ECoG data were clipped off the clinical recordings obtained in three distinct arousal states: quiet wakefulness, SWS (stages 3/4) and REM sleep. The length of data segments ranged from 2.7 to 112 min (mean 20.6 min). Arousal state determination was based on the conjunction of ECoG and video recordings. REM sleep was identified by (1) active eye movements in the video record and/or the electrooculogram and (2) low power in the < 4 Hz band. Time courses of < 4 Hz BLP were computed over entire night-time records using Fast Fourier transform (FFT) applied to half-overlapping windows of 1 sec length. Periods with < 4 Hz BLP as low as the waking state were selected, excluding those preceded by a sharp (as opposed to gradual) transition from SWS (marked by high < 4 Hz BLP), which were more likely to represent arousal/awakening rather than REM sleep. Total lengths of data collected for each patient are listed in Supplementary Table.

Electrode localization

Plain X-ray films and CT scans were acquired postoperatively with the subdural electrodes in place to define the electrode positions in relation to the skull. The CT images were co-registered to subject's own MP-RAGE and then to the atlas-representative image. The Talairach coordinates of the center of each electrode then were determined using a locally developed automated procedure. 3-D renderings of the pial surface were generated from atlas-transformed MP-RAGE images using MRIcro (http://www.sph.sc.edu/comd/rorden/mricro.html) (Fig. 1b) and Freesurfer (http://surfer.nmr.mgh.harvard.edu) (Fig. 1c). Displays showing BOLD correlation maps

and electrode locations overlaid on the pial surface (from Freesurfer) were generated using CARET (http://brainmap.wustl.edu/caret).

For each electrode, the corresponding BOLD sensorimotor correlation map Z-score (thresholded at a significance level of $P < 0.05$ corrected for multiple comparisons, see Supplementary Information) was evaluated by averaging over a 5-mm-radius sphere centered on the electrode, excluding voxels outside the pial surface. Electrodes with a Z-score greater than 3 were classified "sensorimotor". Electrodes with a Z-score equal to or less than 0 were classified as "control". A group of contiguous "sensorimotor" electrodes constituted a sensorimotor ROI. A group of contiguous "control" electrodes constituted a control ROI. The distance between two ROIs was computed in Talairach space as the distance between the center of mass of each group of electrodes. The distances between ROIs were carefully controlled such that i) all ROIs were separated by > 2 cm, to focus on large-scale brain functional connectivity; ii) the distribution of inter-ROI distances was comparable between the sensorimotor-sensorimotor and sensorimotor-control groups (see Supplementary Note 4 and Fig. 3). In addition, widespread, strong negative correlations to the sensorimotor network were avoided as control ROIs, because their physiological meaning is as yet unclear.

ECoG correlation analyses and comparison with BOLD correlation structure

ECoG signals were re-referenced to the common mean before further analyses. In Patient 2, results obtained using such average reference derivation were compared to those obtained using a modified Laplacian derivation (see Supplementary Note 1). A 60-Hz notch filter was used for ECoG signals filtered in 50 – 100 Hz.

Analysis of filtered regional ECoG signals

Analysis was performed separately in eight different frequency ranges: < 0.5 Hz, 1 – 4 Hz, 5 – 10 Hz, 10 – 20 Hz, 20 – 50 Hz, 50 – 100 Hz, 100 – 150 Hz and 150 – 200 Hz. Regional ECoG time series were extracted by averaging over the electrodes constituting each ROI, and were made zero-mean and detrended. Data were Fourier transformed, the cross- and auto- spectra corresponding to ROI pairs were computed and averaged over half-overlapping windows of 10-sec length across the entire data set (data segments from the same arousal state were averaged together). The averaged cross- and auto- spectra for each ROI pair were filtered in each of the above frequency ranges (18 dB/octave) and inverse Fourier transformed to yield the lagged cross- and auto-covariance functions for each frequency band. The lagged cross-covariance functions then were normalized to obtain the lagged cross-correlation functions. This approach is similar to that used in von Stein et al. (von Stein et al., 2000). Lagged cross-correlation functions are shown in Figs. 2a, S3 and S4.

Analysis of regional γ-BLP signals

Regional γ-BLP timeseries (2 sec sampling interval) were obtained by FFT of successive half-overlapping 4 sec windows and summing over frequency bins in the range 50 to 100 Hz (excluding 60-Hz bin). For each ROI pair and arousal state, lagged cross-correlation functions were conventionally computed in the time-domain for each data segment and averaged across segments in the same arousal state.

Analyses of regional BOLD signals

Regional BOLD timeseries were computed by averaging over voxels under electrodes constituting each ROI (see **Electrode localization** above). For each ROI pair,

lagged BOLD cross-correlation functions were conventionally computed in the time domain for each fMRI run and then averaged across runs.

Statistical testing of all cross-correlations was performed after application of Fisher's r-to-z transform.

Spatial correlation of temporal correlation maps

Spatial correlation was employed to assess spatial similarity of correlation maps (Fox et al., 2006). Here, correlation maps were obtained by computing temporal correlations of the signal (BOLD or ECoG) at one (seed) electrode against all other electrodes. Thus, we obtained r_{ik}^{B} and r_{ik}^{E}, the (zero-lag) temporal correlation map corresponding to seed electrode i, where k indexes all other electrodes and the superscript indicates modality (BOLD or ECoG). ECoG correlation maps (r_{ik}^{E}) were computed on signals that were low-pass filtered at < 0.5 Hz and down-sampled to 8 Hz (Figs. 5b and S6) or by using γ-BLP timeseries (Fig. S10). The r_{ik}^{B} and r_{ik}^{E} were subjected to Fisher's r-to-z transformation to obtain z_{ik}^{B} and z_{ik}^{E}. Within-modality and cross-modality spatial correlations, $R_{ij}^{B:B}$, $R_{ij}^{E:E}$ and $R_{ij}^{B:E}$, then were computed for pairs of seed electrodes. Thus, for seed electrodes i and j, the spatial correlation was computed as

$$R_{ij}^{X:Y} = \frac{\sum_{k \neq i,j}(z_{ik}^{X} - \bar{z}_{i}^{X})(z_{jk}^{Y} - \bar{z}_{j}^{Y})}{\sqrt{\sum_{k \neq i}(z_{ik}^{X} - \bar{z}_{i}^{X})^{2}\sum_{k \neq j}(z_{jk}^{Y} - \bar{z}_{j}^{Y})^{2}}},$$

where X and Y each range over B (BOLD) and E (ECoG).

MRI data acquisition and pre-processing

MR imaging was conducted at the Washington University Neuroimaging Laboratories either before admission or after discharge from the hospital. Patients were compensated for their time. Scanning was performed with a Siemens (Erlangen, Germany) 3 Tesla Trio MRI scanner. Functional data were acquired using the standard Siemens echoplanar BOLD fMRI sequence (TE = 27 ms, TR = 2 s, flip angle = 90°; 32 contiguous 4 mm slices with 4×4 mm in-plane resolution). The functional data slice tilts and field of view (256 mm) were prescribed parallel to the AC-PC plane on the basis of a short pre-functional coarse MP-RAGE scan. Each fMRI run included 150 or 200 frames (volumes). Number of frames acquired per patient ranged from 1200 to 2400. BOLD data preprocessing included compensation for asynchronous (interleaved) slice acquisition and realignment within and across fMRI runs to correct for head motion. Each fMRI run was intensity scaled to yield a whole brain mode value of 1000. Anatomical images were acquired using a sagittal T1-weighted MP-RAGE sequence (TR = 2200 ms, TE = 2.34 ms, flip angle = 7°, inversion time = 1000 ms, $1 \times 1 \times 1$ mm^3 voxels) and a T2-weighted fast spin-echo sequence. Atlas transformation was computed on the basis of an average of the first frame of each fMRI run and MP-RAGE structural images. Our atlas representative template was produced by mutual co-registration of MP-RAGE images obtained in 12 normal subjects (as described in (Lancaster et al., 1995)) and represents the Talairach coordinate system (Talairach and Tournoux, 1988). The functional data were resampled in atlas space to 3 mm^3 voxels.

Voxel-wise BOLD correlation analyses

Additional preprocessing

In preparation for correlation analyses, the BOLD time series were passed through several additional pre-processing steps, essentially as previously described (He et al., 2007): 1) spatial smoothing using a 6 mm full width at half maximum Gaussian blur; 2) low-pass filtering at 0.1 Hz; 3) removal by one-step linear regression of several sources of variance unlikely to reflect spatially-specific functional correlations: i) six parameters obtained by correction for head motion; ii) signal averaged over the whole brain; iii) signal from a ventricular region; iv) signal from a white matter region. Temporal derivatives of these regressors were included in the linear model, thereby accounting for the time-shifted versions of spurious variance.

Correlation analysis

To compute voxel-wise sensorimotor network correlation maps, a seed ROI in the hand representation of primary sensorimotor area was anatomically defined for each subject. The BOLD time course was extracted from this ROI by averaging over all included voxels. This time course then was correlated against all other voxels in the brain to obtain Pearson correlation coefficient (r) images. The r images were transformed by application of Fisher's r-to-z transformation ($z = 0.5\ln[(1+r)/(1-r)]$) and then normalized by the estimated variance to yield Z-score maps. Variance was estimated as $1/\sqrt{(df - 3)}$, where $df = n/c$, n being total number of time points (frames) in the dataset. The factor, c, corrects for autocorrelation in the BOLD timeseries according to Bartlett's theory (computed as as the time integral of the squared lagged autocorrelation function)(Jenkins and Watts, 1998) and, in the present data, had the value 3.3722. Z-score maps were thresholded at a significance level of $P < 0.05$ corrected for multiple comparisons on the

basis of Monte Carlo simulation (Z ≥ 3, cluster size ≥ 17 voxels); voxels not meeting this significance criterion were set to 0.

The sensorimotor networks defined by these BOLD correlation maps were concordant with the clinical electrophysiological localization results (using somatosensory evoked potentials and motor cortical stimulation).

Statistical testing of covariance matrix similarity by eigenvector decomposition

Eigenvector decomposition (diagonalization) factors a multivariate process into components. Let $B(t)$ be a time-dependent, $n \times 1$ column vector representing the BOLD time series measured under the n ECoG electrodes on the interval, $0 < t \leq T_B$. The BOLD:BOLD covariance matrix,

$$C_B = (1/T_B) \int_0^{T_B} B(t)B'(t)dt, \tag{1}$$

can be expressed as

$$C_B = W_B L_B W_B', \tag{2}$$

where W_B is a $n \times n$ array of column eigenvectors, L_B is a diagonal $n \times n$ array of eigenvalues, $\{\lambda_{Bi}, i = 1,2,...,n\}$, and W_B' is the transpose of W_B. Suppose without loss of generality that the eigenvectors have been sorted in order of decreasing variance, i.e., $\lambda_{B1} > \lambda_{B2} > ... > \lambda_{Bn}$. Inverting Eqn 2 yields

$$(1/T_B) \int_0^{T_B} [W_B'B(t)][B'(t)W_B]dt = W_B'C_B W_B = L_B. \tag{3}$$

Thus, eigenvector-weighted linear sums of the BOLD timeseries form a new set of n signals, $W_B'B(t)$, with covariance matrix, L_B. In other words, if w_{Bi} is the ith column of W_B, then

$$(1/T_B)\int_0^{T_B} [w_{Bi}'B(t)][B'(t)w_{Bi}]dt = \lambda_{Bi}. \tag{4}$$

Completely analogous expressions can be written for the ECoG data, $E(t)$. Thus, the ECoG:ECoG covariance matrix is

$$C_E = (1/T_E)\int_0^{T_E} E(t)E'(t)dt = W_E L_E W_E'. \tag{5}$$

The preceding constitutes the foundation for a measure of covariance structure similarity. Specifically, suppose, as in Eqn 3, that the BOLD eigenvectors are used to form weighted sums of the ECoG timeseries, $W_B'E(t)$. If the BOLD and ECoG covariance structures are completely similar then they share the same eigenvectors ($W_B = W_E$) and their eigenvalues ($\{\lambda_{Bi}\}$ and $\{\lambda_{Ei}\}$) are identically ordered. Then, the covariance matrix of the transformed ECoG data must be L_E and the variances of the transformed ECoG data computed as in Eqn 4,

$$\phi_{Ei} = (1/T_E)\int_0^{T_E} [w_{Bi}'E(t)][E'(t)w_{Bi}]dt, \tag{6}$$

must be ordered as the $\{\lambda_{Bi}\}$, i.e., $\phi_{E1} > \phi_{E2} > ... > \phi_{En}$. In other words, if the two covariance structures are similar, eigenvectors that account for more BOLD variance also account for more ECoG variance. Conversely, if the covariance structures are unrelated, eigenvector decomposition of one covariance matrix conveys nothing about the other and the $\{\phi_{Ei}\}$ ordering will be random. A test of covariance structure similarity therefore can

be formulated as the Spearman rank order correlation test (Zar, 1984). The relevant statistic is

$$r_s = 1 - \frac{6 \sum_{i=1}^{n} d_i^2}{n^3 - n}, \tag{7}$$

where d_i is the difference in rank orders of the $\{\phi_{Ei}\}$ and $\{\lambda_{Bi}\}$, i.e., $d_i = O(\phi_{Ei}) - i$. No relation between the two covariance structures corresponds to the null hypothesis: $r_s = 0$. The Spearman rank order test is nonparametric. Its application in the present context involves no assumptions concerning either BOLD or ECoG signals other than each has a diagonalizable covariance matrix.

Highly significant results were obtained in all patients (Figs. 5c and S8) indicating that the covariance structures of BOLD and slow (< 0.5 Hz) ECoG signals are similar. These results were strikingly invariant with respect to the state of arousal during ECoG recording.

Examining the relation between BOLD and ECoG correlation structures as a function of ECoG frequency

In our initial analysis to determine the correspondence between BOLD and ECoG correlation structures as a function of ECoG signal frequency (main text Fig. 2a), we filtered the ECoG signal in eight different frequency bands. Here we present an analysis addressing the same question but with a fine spectral resolution.

First, complex coherence spectrum was computed for each SM-SM and SM-C ROI pair from all patients using a 1-sec length, half-overlapping moving window. Then,

for each 1-Hz-width frequency bin from 1 to 100 Hz, results from all ROI pairs were

plotted in a complex coherency plane, such as those shown in Fig. S5b. The separation

between SM-SM and SM-C clusters in this coherency plane represents how well the

correlation structure of ECoG signal at the particular frequency corresponds to that of

BOLD. This is so because the ROI-pair type was defined based on BOLD correlation

structure. Hence, if ECoG signal has a similar correlation structure as BOLD, the SM-

SM, but not SM-C, ROI pairs should be in-phase on average. The statistical evaluation of

such a separation between SM-SM and SM-C ROI pairs in the complex coherence plane

was tested using a two-sample Hotelling's T^2 test

(http://www.philender.com/courses/multivariate/notes3/groups.html) against the null

hypothesis that the SM-SM and SM-C ROI pairs constitute one cluster.

The MATLAB code for performing this test is presented below. The input values,

a, b, c, d, are the vectors containing the abscissa values for SM-SM ROI pairs, the

ordinate values for SM-SM ROI pairs, the abscissa values for SM-C ROI pairs, and the

ordinate values for SM-C ROI pairs, respectively. T2 returns the Hotelling's T^2 value. F

returns the converted $F_{2, n1+n2-3}$ value, in which n1 and n2 are the number of SM-SM and

SM-C ROI pairs respectively.

```
function [T2 F] = TwoSample_Hotelling(a,b,c,d)
meanA = mean(a)
meanB = mean(b)
meanC = mean(c)
meanD = mean(d)
n1 = length(a)
n2 = length(c)
C = n1 * n2 * (n1 + n2 -2) / (n1 + n2)

X1 = [a b]
for i = 1:n1
X1bar(i,:) = [meanA meanB];
end
S1 = (X1 - X1bar)' * (X1 - X1bar)

X2 = [c d]
for i = 1:n2
```

```
X2bar(i,:) = [meanC meanD];
end
S2 = (X2 - X2bar)' * (X2 - X2bar)

W = S1 + S2
x = [meanA meanB]' - [meanC meanD]'
D2 = x' * inv(W) * x
T2 = C * D2
F = T2 * (n1 + n2 - 2 - 1)/((n1 + n2 -2)*2)
```

RESULTS

Correlation structures of spontaneous BOLD signal and slow cortical potential

In the first three analyses we focused on the sensorimotor network, because the ECoG electrodes provided adequate coverage of the sensorimotor network in all presently studied patients but much poorer coverage of the other networks known to exhibit covariant BOLD fluctuations. For each patient, we first computed a voxel-wise BOLD correlation map of the sensorimotor network (Figs. 1 and S2, for methods see Supplementary Information). Electrodes then were categorized according to the underlying BOLD correlation map: Electrodes within the sensorimotor network as defined by this map (Z-score > 3, $P < 0.05$) were labeled "sensorimotor". Electrodes outside this network ($Z \leq 0$, see Methods) were labeled "control". To increase signal-to-noise ratio, in the first two analyses, we defined sensorimotor and control ROIs as contiguous groups of sensorimotor and control electrodes, and averaged ECoG and BOLD signals within each ROI. Several ROIs of each type were defined in all patients (Figs. 1 and S2).
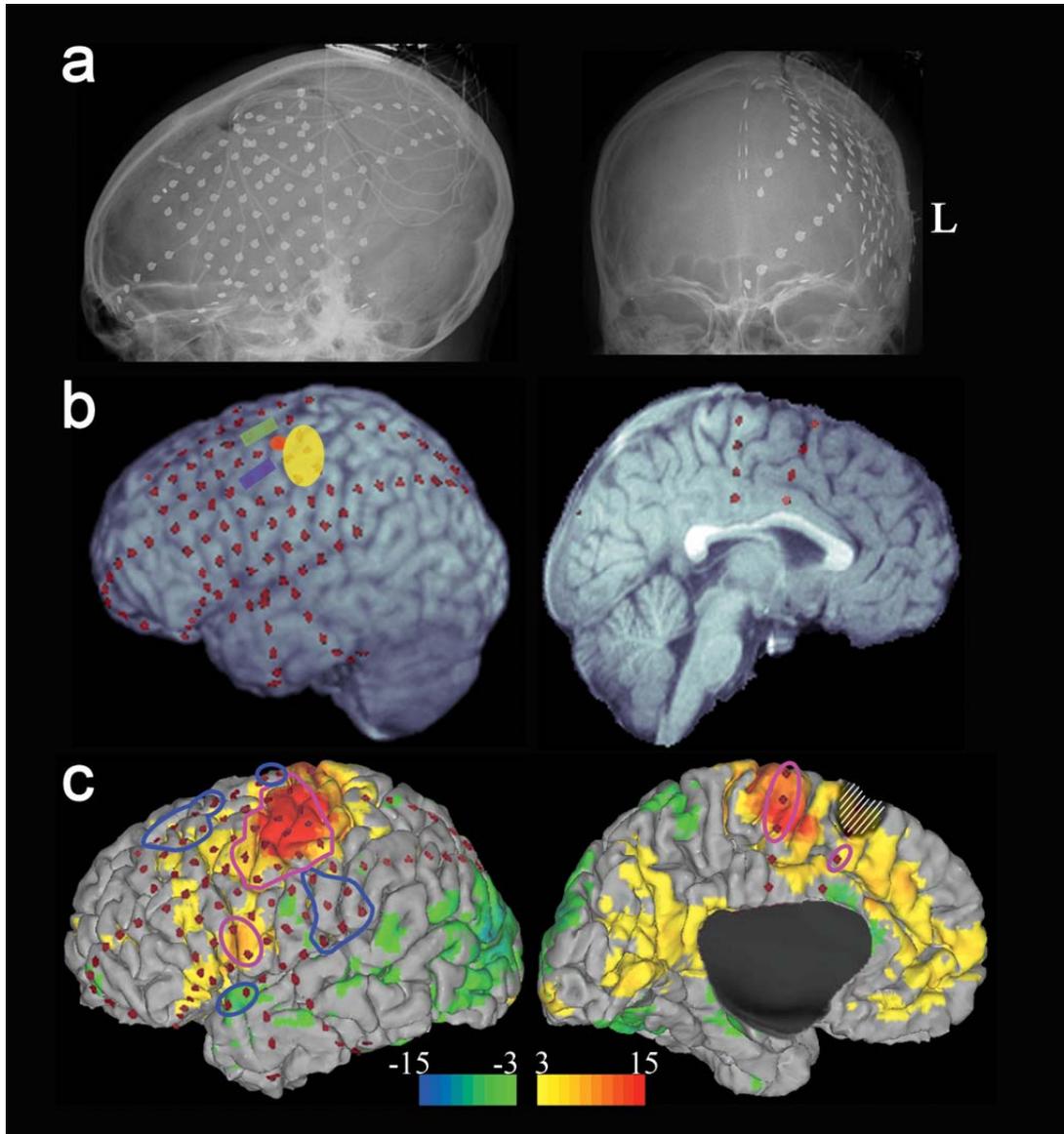
Figure 1 Spatial topography of electrode coverage and sensorimotor network in Patient 1. (**a**) X-ray showing electrode placements. (**b**) 3-D rendering of anatomical MRI and projection of electrode locations onto the 3-D surface. Clinical mapping of the sensorimotor cortex is indicated by color patches. Red: hand motor area based on median nerve somatosensory evoked potential (SSEP); Yellow: hand sensory area based on SSEP; Blue: facial twitching in response to cortical stimulation; Green: hand grasp in response to cortical stimulation. (**c**) BOLD sensorimotor correlation map (Z-score, thresholded at $P < 0.05$, corrected for multiple comparisons) and electrode locations overlaid on the pial surface reconstructed from anatomical MRI. Two bad electrodes in the anterior temporal strip were eliminated. Four sensorimotor ROIs (delineated by magenta contours) and four control ROIs (blue contours) were determined in this patient. The cross hatching indicates the epileptogenic zone that was subsequently resected.

In the *first analysis*, we computed lagged cross-correlation functions for all possible sensorimotor-sensorimotor and sensorimotor-control ROI pairs using BOLD and filtered ECoG signals. Since the sensorimotor ROIs were located within a common network defined by BOLD correlation structure whereas the control ROIs were outside this network, BOLD correlations between sensorimotor ROIs should be by definition higher than correlations between a sensorimotor ROI and a control ROI (see Figs. 2b and S3). The question was whether some type of electrophysiological activity may similarly differentiate sensorimotor-sensorimotor from sensorimotor-control correlations. To pursue this question, ECoG signals filtered in eight different frequency bands (< 0.5 Hz, $1 - 4$ Hz, $5 - 10$ Hz, $10 - 20$ Hz, $20 - 50$ Hz, $50 - 100$ Hz, $100 - 150$ Hz and $150 - 200$ Hz) were used to compute the lagged correlation functions (see Methods). These correlation functions then were compared across the two types of ROI pairs. ECoG activity in the two slowest frequency bands (< 0.5 Hz and $1 - 4$ Hz bands) distinguished sensorimotor-sensorimotor from sensorimotor-control ROI pairs: the sensorimotor-sensorimotor ROI pairs were positively correlated whereas the sensorimotor-control ROI pairs were negatively or not correlated. Remarkably, this distinction was present in all arousal states (Figs. 2a and S3). Similar findings were absent in higher frequency bands (Figs. 2a and S4). These results were consistent across all five subjects. Considering only the waking data, across all patients 86% of the sensorimotor-sensorimotor correlation functions (using either < 0.5 Hz or $1 - 4$ Hz band ECoG) had a positive peak with r value > 0.1 in the lag range within ±0.5 sec; in contrast, only 19% (< 0.5 Hz band) or 16% ($1 - 4$ Hz band) of sensorimotor-control correlations showed similar positive peaks. For statistical results see Fig. 2c. Importantly, this

difference in slow ECoG signal correlation between sensorimotor-sensorimotor and sensorimotor-control ROI pairs cannot be accounted for by a difference in their respective inter-ROI distances, as the distribution of inter-ROI distances were the same for the two groups of ROI pairs (Fig. 3).
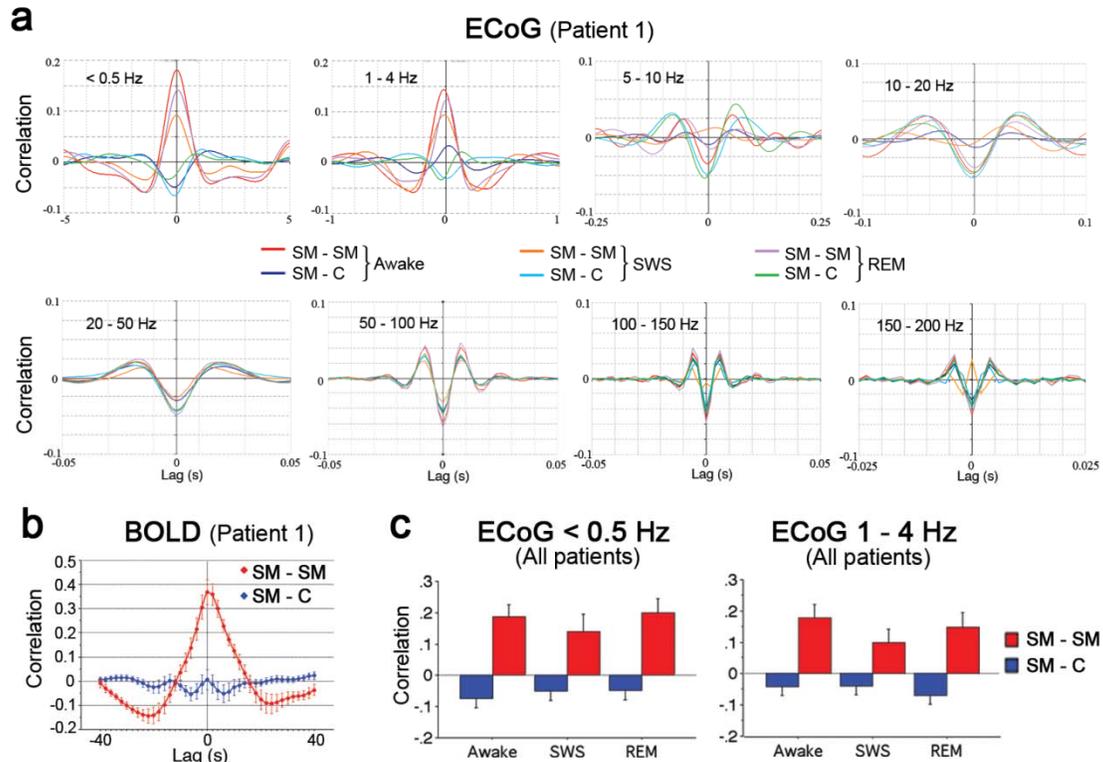
Figure 2 (a) Patient 1: Lagged cross-correlation functions were computed using ECoG signal filtered in eight frequency bands for all possible sensorimotor-sensorimotor (SM-SM, N = 6) and sensorimotor-control (SM-C, N = 16) ROI pairs. ROI pairs of similar type were averaged together after Fisher's r-to-z transformation. Red hues: sensorimotor-sensorimotor; blue/green hues: sensorimotor-control. **(b)** Patient 1: BOLD lagged cross-correlation functions averaged separately for sensorimotor-sensorimotor (red) and sensorimotor-control (blue) ROI pairs. **(c)** Combining data over all patients: Peak ECoG cross-correlation values (within ±500ms lag) as a function of ROI-pair type (SM-SM vs. SM-C) and arousal state (awake, SWS and REM). Two-way ANOVA yielded a highly significant main effect of ROI-pair type (< 0.5 Hz: $F_{1,47} = 20.1$, P < 0.0001; 1 − 4 Hz: $F_{1,47} = 17.8$, P = 0.0001). Neither the effect of arousal state nor the interaction of ROI-pair type × arousal state was significant (P > 0.1). All error bars denote SEM.
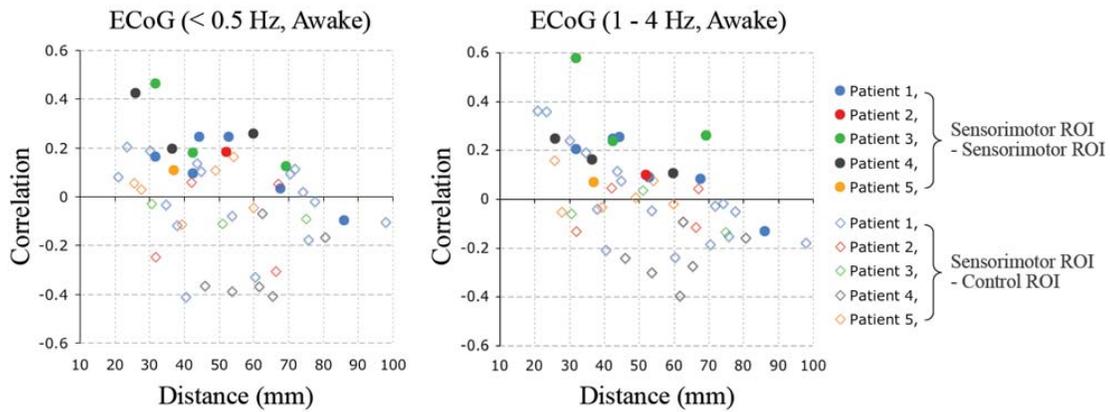
Figure 3 Effect of inter-ROI distance on ECoG peak cross-correlation values (within lag of ±500 ms). Left: < 0.5 Hz band; Right: 1 – 4 Hz band. ECoG data were from the waking state. Each ROI pair is represented by one symbol. Filled circle: sensorimotor-sensorimotor ROI pair. Open diamond: sensorimotor-control ROI pair.

Whereas the above analyses filtered the ECoG signal in eight different frequency bands and thus had a crude spectral resolution, converging results from an independent analysis employing coherence measurement with a fine spectral resolution are presented in Fig. S5 (for methods see "Examing the relation between BOLD and ECoG correlation structures as a function of ECoG frequency" in Supplementary Information).

In the *second analysis*, to quantitatively assess the similarity between the correlation structures of BOLD signal and slow ECoG activity, we plotted ECoG (filtered at < 0.5 Hz, Fig. 4a; 1 – 4 Hz, Fig. 4b) vs. BOLD correlation values across all sensorimotor-sensorimotor and sensorimotor-control ROI pairs in all patients. Highly significant correlations between BOLD and ECoG correlation measures were found for ECoG signals in the < 0.5 Hz and 1 – 4 Hz bands from all three arousal states (all $P < .002$), thereby demonstrating a correspondence between the correlation structures of spontaneous BOLD signal and slow (< 4 Hz) cortical potential (*SCP*) recorded by ECoG.
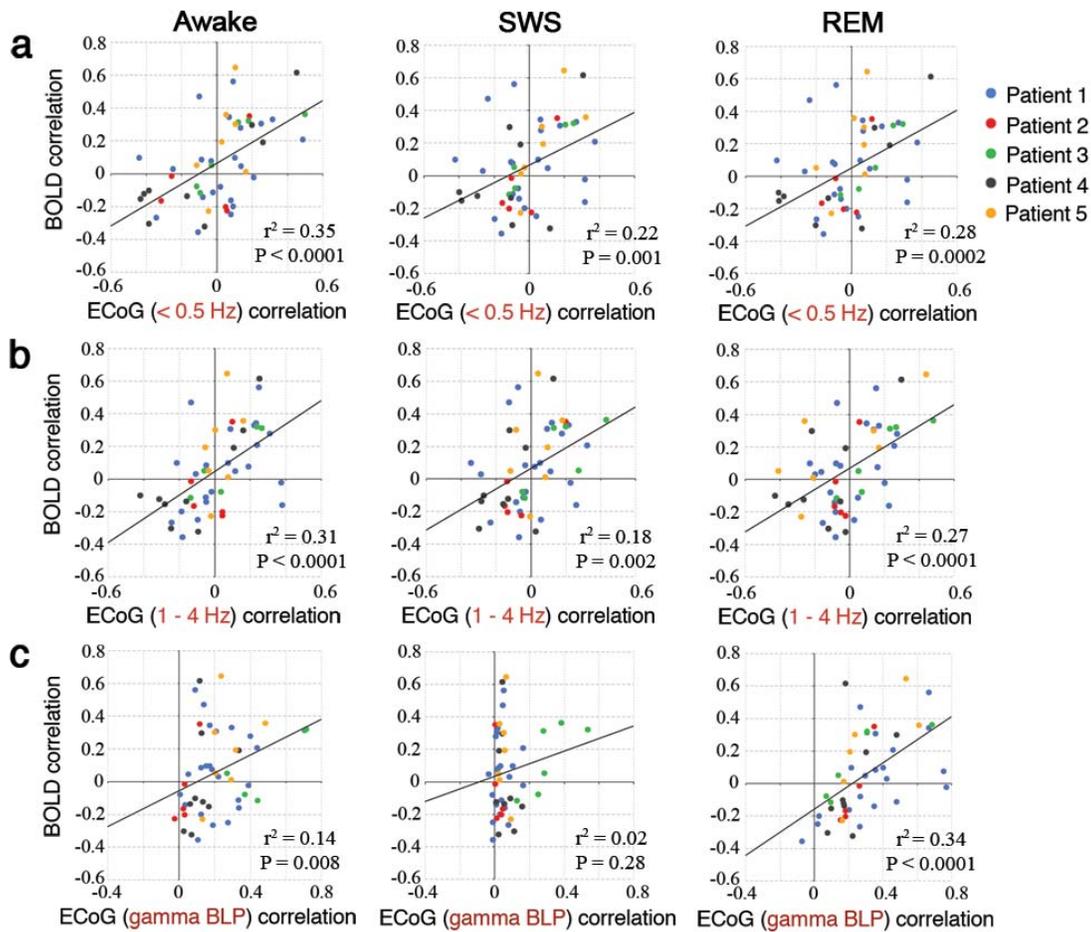
Figure 4 BOLD vs. ECoG cross-correlation function peak values. Peak correlations of filtered (< 0.5 Hz and 1 − 4 Hz) ECoG activity were evaluated for lags in the range±500 ms. Peak correlations of BOLD and γ-BLP (both sampled at 2 sec interval) were evaluated at zero-lag. Each ROI pair is represented by one symbol. All sensorimotor-sensorimotor and sensorimotor-control ROI pairs from all patients are shown. In Patient 2, the ECoG derivation was modified Laplacian; in all other patients it was average reference. (**a**) < 0.5 Hz ECoG; (**b**): 1 − 4 Hz ECoG; (**c**) γ-BLP ECoG. P values represent the significance of the measured correlation between BOLD and ECoG peak correlations.

In the *third analysis*, we computed spatial correlations between BOLD and slow ECoG (< 0.5 Hz band) correlation maps to compare their spatial patterns on an electrode-by-electrode basis. Voxel-wise BOLD correlation maps were spatially sampled by the electrode coverage to compare with ECoG correlation maps (for each electrode, the corresponding BOLD correlation value was evaluated by averaging over a 5-mm-radius

sphere centered on that electrode, excluding voxels outside the pial surface). For correlation map examples see Fig. 5a. All sensorimotor and control electrodes were used as seed electrodes, thus this analysis did not depend on ROIs. We found that the great majority of BOLD and ECoG correlation maps obtained by seeding at the same electrode were highly similar (98.3% of such comparisons had a spatial correlation value that was significant at the $P < 0.05$ level, uncorrected for potential dependence of signals at neighboring electrodes). Next, we examined similarity of correlation maps obtained with different seed electrodes within the sensorimotor system, the outcome measure being the mean spatial correlation averaged over pairs of seed electrodes. As shown in Figs. 5b and S6, this measure was significantly positive, regardless of whether the spatial correlations were computed within modality (BOLD:BOLD or ECoG:ECoG) or across modalities (BOLD:ECoG). In contrast, the spatial correlation measures comparing maps obtained by seeding at "sensorimotor" electrodes vs. those obtained by seeding at "control" electrodes were on average around zero, again regardless of whether the comparison was within or across modalities. These spatial correlation results cannot be accounted for by the effect of distance between seed electrodes (see Fig. S7). They confirmed the above finding that the correlation structures of spontaneous BOLD and slow (< 0.5 Hz) ECoG signals are similar, at least within the framework of the sensorimotor system.

In the *fourth analysis*, to extend our finding beyond the sensorimotor system, we evaluated the similarity of BOLD and slow ECoG (< 0.5 Hz band) covariance structures using an eigenvector decomposition strategy (for details of the method see "Statistical testing of covariance matrix similarity by eigenvector decomposition" in Supplementary Information). In brief, this strategy tested whether the eigenvectors accounting for more

variance in the BOLD data also accounted for more variance in the ECoG data, which, if true, would strongly reinforce the impression of a similarity between the BOLD and ECoG covariance structures derived from our other analyses. This analysis included all ECoG electrodes providing technically satisfactory recording, and hence was independent of the distinction between sensorimotor and non-sensorimotor networks. Statistical significance was assessed using a non-parametric test (Spearman rank order correlation) requiring no correction or qualification. The results again showed that the covariance structures corresponding to the two types of signals (BOLD and < 0.5 Hz ECoG) were similar in all five patients, for ECoG data acquired in all three arousal states (all $P <$ 0.005, Figs. 5c and S8).
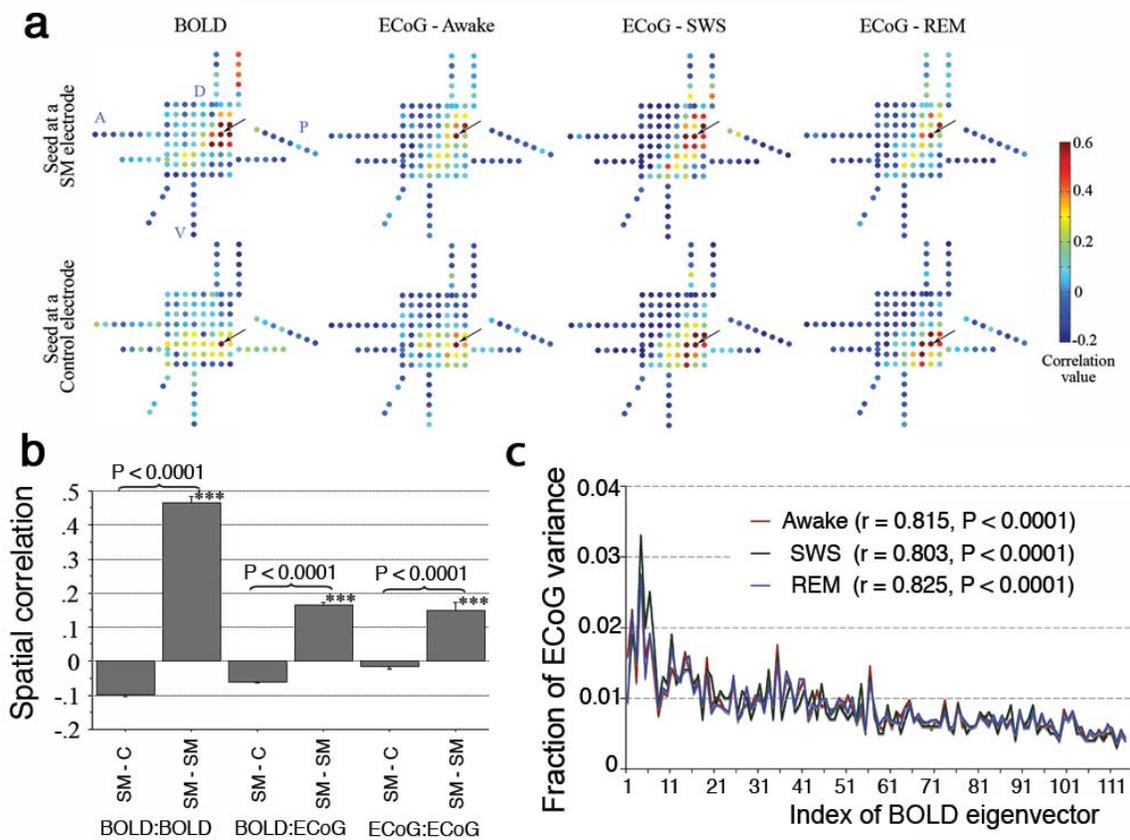
Figure 5 Similarity of BOLD and ECoG (< 0.5 Hz band) correlation structures assessed by spatial correlation and eigenvector decomposition strategies in Patient 1. **(a)** Raw representative BOLD and ECoG (< 0.5 Hz) correlation maps that were used for spatial correlation analyses. Each dot represents one electrode, arrow points to the seed electrode. Color represents Fisher's z-transformed correlation value between each electrode and the seed electrode, computed using BOLD signal or <0.5 Hz ECoG signal from each arousal state. BOLD correlation maps were spatially sampled by the electrode coverage to compare with ECoG correlation maps. The maps in the top row seed at a same sensorimotor electrode, those in the bottom row seed at a control electrode. Note that these two seed electrodes are separated only by 2 cm. A: anterior; P: posterior; D: dorsal; V: ventral. This 2-D presentation of the electrode grid was extrapolated from Fig. 1c. **(b)**Statistical results of spatial correlation analysis. Spatial correlations were computed between two BOLD correlation maps (BOLD:BOLD), between two ECoG correlation maps (ECoG:ECoG), or between a BOLD and a ECoG correlation map (BOLD:ECoG). Each bar represents the mean spatial correlation averaged over seed-electrode pairs. SM–C: One correlation map obtained by seeding at a sensorimotor (SM) electrode, the other map by seeding at a control (C) electrode. SM–SM: both maps were obtained by seeding at a sensorimotor electrode. Error bars denote SEM. ***: significant non-zero mean spatial correlation (P < 0.0001; one-sample *t*-test). The over-bracketed P values indicate unpaired *t*-tests comparing seed electrodes within (SM-SM) vs. across (SM-C) functional systems. ECoG data were from the waking state. Comparable results were obtained in all patients and for ECoG data from all states of arousal (Fig. S6). **(c)** Eigenvector decomposition analysis comparing BOLD and ECoG (from all three states) covariance structures. The ordinate shows the fraction of ECoG variance captured by eigenvectors derived by diagonalization of the BOLD covariance matrix. These eigenvectors were sorted by the rank-ordering of their corresponding eigenvalues (index shown in abscissa), such that the eigenvector with the smallest index was associated with the largest eigenvalue and hence accounted for most variance in the BOLD data. The variable range of abscissa reflects the number of eigenvectors, which is the same as the number of usable electrodes in each patient. The decreasing trend of the plot indicates that eigenvectors accounting for more BOLD variance also accounted for more ECoG variance. Statistical significance of the covariance structure similarity (tested by Spearman rank order correlation) is listed in the inset. Comparable results were obtained in all patients (Fig. S8).

Correlation structures of spontaneous BOLD signal and gamma band-limited power

So far we have demonstrated a correspondence between the correlation structures

of spontaneous BOLD signal and SCP representing the slowest component of raw ECoG

signals (< 4 Hz). However, power of gamma frequency (> 30 Hz) has not only been

demonstrated to correlate with BOLD in stimulus-evoked activity (Logothetis et al.,

2001; Mukamel et al., 2005; Niessing et al., 2005; Shmuel et al., 2006) but has also been shown to remain coherent in its spontaneous fluctuations at distances up to 1 cm, unlike spontaneous raw gamma oscillations that are correlated only locally (Leopold et al., 2003). Hence, we tested, in an additional analysis, whether gamma (50 – 100 Hz) band-limited power (γ-BLP) also had a correlation structure similar to spontaneous BOLD signals. Fig. 4c shows scatter plots of BOLD correlations against γ-BLP correlations across all ROI pairs. A significant correlation with BOLD was found for γ-BLP in waking (P = 0.008) and REM (P < 0.0001) but not SWS (P = 0.28) data. We note that the lack of correspondence during SWS was not due to a reduction in the amount of gamma frequency power, which was invariant across arousal states (Fig. S9) (Steriade et al., 1996). Consistent results from spatial correlation analysis comparing BOLD and γ-BLP correlation maps are shown in Fig. S10.

Given the correlation between γ-BLP and BOLD signal in stimulus-evoked responses (Logothetis et al., 2001; Mukamel et al., 2005; Niessing et al., 2005; Shmuel et al., 2006), it is possible that the waking γ-BLP result presented above was partly driven by environmental stimuli present during data recording. However, a similar result was obtained for γ-BLP during REM sleep, in which neuronal activity arises completely from within. Therefore, it appears that endogenous brain activity during REM sleep, and presumably also wakefulness, modulates γ-BLP in a spatial pattern similar to that of spontaneous BOLD fluctuations. Equally telling, γ-BLP during SWS did not show a similar correlation structure. This result is consistent with the view that coherent patterns in gamma frequency activity are related to conscious experiences (Rodriguez et al., 1999; Singer, 2001) that are more prevalent in wakefulness and REM sleep than in SWS

(Hobson et al., 2000; Llinas and Ribary, 1993). An alternative but not contradictory explanation is that the bistability of thalamocortical circuits between up- and down- states during SWS (Massimini et al., 2004) is responsible both for the fading of consciousness and for the collapse of gamma power correlations.

Interestingly, whereas the BOLD and SCP correlations included both negative and positive values, gamma-BLP correlations were mainly positive (Fig. 4). One possible explanation is that the removal of global signal in BOLD signal processing and the usage of average reference in ECoG analysis forced the appearance of negative BOLD and SCP correlations, whereas no equivalent maneuver was done in the BLP analysis. However, negative SCP correlations also emerged when modified Laplacian montage was used (see results from Patient 2 in Fig. 4 and Supplementary Note 1), in which case there was no numerical mandate of negative correlations. An alternative explanation is that the positive correlations of BOLD/SCP mean that the two regions are in the same network, which, as if crossing a threshold, "enables" the correlated γ-BLP relationship; by contrast, no γ-BLP relationship exists when this threshold is not crossed. Undoubtedly a better understanding of the above phenomenon awaits future investigation.

Discussion

To summarize, we have identified two types of neurophysiological signals that demonstrate a similar correlation structure to that of the spontaneous fMRI BOLD signal: SCP and γ-BLP. For SCP the correspondence with BOLD was state-invariant. For γ-BLP the correspondence was present in wakefulness and REM but not SWS. This leads us to suggest that spontaneous fMRI BOLD signals and SCPs both reflect a fundamental

stratum of the brain's intrinsic organization that transcends levels of consciousness. The more labile, state-dependent structures of γ-BLP, while similar, appear to be built on scaffolding provided by the more fundamental processes represented in the BOLD signals and the SCPs.

A remaining question regards whether the spontaneous BOLD signal, SCP and gamma-BLP are correlated on a time-varying basis. This could not be directly addressed in the present study for the lack of simultaneous BOLD and ECoG recordings. However, since these three signals have comparable frequency ranges (see Supplementary Note 2), it is not unreasonable to speculate that they may indeed be temporally coherent. Unfortunately, to date relevant empirical observations remain scarce. Nevertheless, it has been shown in anesthetized rats that spontaneously fluctuating total hemoglobin concentration and low-pass filtered local field potential are temporally correlated (Jones et al., 2007); when the anesthesia level was deepened to producing burst-suppression ECoG patterns, the spontaneous fluctuating blood flow faithfully followed bursts of ECoG activity at a frequency of ~ 0.1 Hz (Golanov et al., 1994). Whereas non-neuronal factors have been shown to contribute to spontaneous BOLD signal variance (Birn et al., 2006; Shmueli et al., 2007; Wise et al., 2004), the above studies and the present work suggest an important neural origin of these signals. Furthermore, numerous early EEG studies have shown that the negative shift of SCP occurs in response to various task demands much in the same way as the BOLD signal activation does (for a recent review see Khader et al. (Khader et al., 2008)). Hence, SCP may be a fundamental neural basis of the BOLD signal – a basis for both the spontaneous BOLD fluctuations and task-evoked BOLD responses alike.

Our results and the foregoing interpretations are consistent with well-established neuroanatomical and neurophysiological observations. The negative shift of SCPs reflects depolarization of apical dendrites in cortical superficial layers, e.g., by excitatory, nonspecific thalamic inputs (Birbaumer et al., 1990; Mitzdorf, 1985). Therefore, spontaneous SCP and the correlated BOLD signal fluctuations likely reflect endogenous fluctuations of cortical excitability within functional systems. (For a discussion on the relation between SCP and the "up-and-down states", which also reflects fluctuations of cortical excitability, see Supplementary Note 3.) Interestingly, glial cells become depolarized by local excitatory dendritic activity and contribute to negative SCP regardless of cortical depth because of their syncytial connections (Birbaumer et al., 1990; Goldring, 1974); these glial cells also concurrently take up synaptically released glutamate and contribute to locally increased glycolysis, which, in turn, increases the BOLD signal (Raichle and Mintun, 2006).

It has been shown that the trough of SCP is associated with increased power of higher frequency field potentials (Vanhatalo et al., 2004)as well as increased multiple-unit activity (Birbaumer et al., 1990). Hence, the correlated noise in unit recordings (Averbeck et al., 2006) may be regulated by the correlated, spontaneous fluctuations of SCPs confined within the large-scale brain functional networks. Furthermore, a long-established line of research showing the influence of spontaneous variations of SCPs on psychological performance is especially intriguing. Tasks presented on the negative shifts of spontaneous SCP fluctuations are solved faster (Stamm et al., 1987), more accurately (Stamm and Gillespie, 1978) and had lower sensory threshold (Devrim et al., 1999), supporting the role of spontaneous activity in facilitating responses to stimuli. Similar

investigations in the fMRI domain have only begun to blossom (Boly et al., 2007; Fox et al., 2007).

Supplementary Data

Supplementary Table.
Demographic, clinical and data collection information of the patients.

Patient no.	Age	Gender	Handedness	Intellectual functioning (WASI) Full-scale IQ	Academic functioning (WRAT-3)		
					Reading	Spelling	Arithmetic
1	15	M	R	93/average	102/average	106/average	112/high average
2	12	M	R	109/average	104/average	107/average	100/average
3	13	F	R	Not tested	Not tested	Not tested	Not tested
4	15	F	R	108/average	111/high average	113/high average	95/average
5	14	F	L	113/high average	132/very superior	115/high average	80/low average

Patient no.	Seizure type	Seizure focus/ Resection area	Total length of ECoG data, min			Length of BOLD data, min, Awake	Time of fMRI scan relative to the epilepsy surgery
			Awake	SWS	REM		
1	Complex partial	L SMA	327.3	54.7	33.3	46.7	4 mo after
2	Simple/complex partial	R SMA	202.6	56.0	56.0	40	4 mo after
3	Complex partial	L temporal	175.3	56.7	70.6	80	2 wk before
4	Complex partial	L anterior temporal	194.0	70.0	30.7	66.7	3 wk before
5	Complex partial	L anterior temporal	180.8	157.0	62.8	60	16 mo after

L, left; R, right; SMA, supplementary motor area; WASI, Wechsler Abbreviated Scale of Intelligence; WRAT-3, Wide Range Achievement Test-Revision 3.

Supplementary spatial correlation analyses results

Spatial correlation analyses comparing BOLD and < 0.5 Hz ECoG correlation maps are shown in Fig. S6. The first question addressed was similarity of BOLD and ECoG correlation maps corresponding to the same seed electrode within the sensorimotor system. Summing over all patients, there were 79 such seed electrodes. For 78 of them,

the BOLD and awake ECoG correlation maps were spatially similar (as indicated by a significant $R_{ii}^{B:E}$ value, $i \in$ sensorimotor; $P < 0.005$, uncorrected for potential dependence of adjacent electrodes). Similar results were obtained for SWS ($P < .01$ for 78/79 of sensorimotor electrodes) and REM ($P < .02$ for 77/79). Next, we examined similarity of correlation maps for seed electrode pairs within the sensorimotor system. In all patients, the correlation maps corresponding to two sensorimotor seed electrodes were on average spatially similar. Critically, this similarity held regardless of whether assessed within or across modalities. Thus, as shown in Fig. S6, sensorimotorBOLD:sensorimotorBOLD as well as sensorimotorECoG:sensorimotorECoG and sensorimotorBOLD:sensorimotorECoG spatial correlations were all significantly positive, as assessed by t-tests applied to Fisher z-transformed spatial correlations $\{R_{ij}, i, j \in$ sensorimotor, $i \neq j\}$ against the null hypothesis of zero mean ($P < 0.05$ for all patients and all arousal states). In contrast, mean spatial correlations for seed electrodes of unlike type $\{R_{ij}, i \in$ sensorimotor, $j \in$ control$\}$ were close to zero, again regardless of modality-association (see Fig. S6).

Spatial correlation analyses comparing BOLD and γ-BLP ECoG correlation maps are shown in Fig. S10. The distinction between sensorimotor:sensorimotor and sensorimotor:control spatial correlations was most pronounced during REM, the conscious state in which brain activity is exclusively endogenous.

Supplementary Note 1. Effect of reference on ECoG signal analysis

Electrophysiological activity sensed by a shared reference electrode leads to artifactually elevated correlation and coherence measures. In the present study, we used

an average reference derivation, which eliminates the influence of the physical reference electrode. The computed average reference potential typically is close to zero when many widespread electrodes are used (Nunez et al., 1997), as in our data. Hence, the effect of reference on our results should be small.

This was confirmed in one subject (Patient 2) in whom the sensorimotor system topography (as determined by BOLD correlation map) and electrode coverage permitted ECoG regional analysis using a modified Laplacian derivation. In the modified Laplacian derivation, each regional ECoG signal is computed by averaging over electrodes constituting the ROI and subtracting the signal averaged over the surrounding electrodes (see Fig. S2a). The modified Laplacian derivation effectively isolates local vertical currents underneath the ROI and eliminates all dependence on a reference. Thus, it provides an approximation to what would be obtained with trans-cortical recording (i.e., surface recording referenced to the underlying white matter).

Prerequisites for modified Laplacian recording are: 1) presence of surrounding electrodes, meaning that the ROI cannot be on the edge of the grid or on a strip; 2) the electrodes within the ROI must carry a common signal of interest, not carried by the surrounding electrodes. In the present context, this means the electrodes within a sensorimotor ROI must be over positive areas in the BOLD sensorimotor correlation map, while the surrounding electrodes are over nonsignificant or negative areas. Both these conditions were met in Patient 2 (Fig. S2a). The results obtained using such modified Laplacian derivation (Fig. S4) were very similar to those using the average reference derivation (Fig. S3, Patient 2).

Supplementary Note 2. Frequency content of spontaneous BOLD, SCP and γ-BLP fluctuations

Spontaneous BOLD (Cordes et al., 2001; Hathout et al., 1999) and γ-BLP (Leopold et al., 2003) fluctuations are both dominated by frequencies of < 0.1 Hz. The SCPs shown herein that correlated with BOLD are< 4 Hz but have exponentially increasing power towards lower frequency (Vanhatalo et al. (2004) and our unpublished data using DC-coupled recording). Our measurements are affected by the lower frequency cutoff (0.1 Hz, 18dB/octave roll-off) of our clinical FDA-approved EEG amplifier. Nevertheless, exponentially increasing power towards the low frequency end still allows substantial low frequency (< 0.1 Hz) ECoG power to be collected (Fig. S9).

Supplementary Note 3. The relation between SCP and the slow oscillation

"Slow oscillation" is a rhythmic, synchronized oscillation of neuronal membrane potential between a hyperpolarized "down" state and a hypopolarized "up" state (Steriade et al., 1993). It is observed spontaneously during anesthesia (Steriade et al., 1993), slow-wave-sleep (Massimini et al., 2004; Steriade, 1997) and quiet wakefulness (Petersen et al., 2003). The slow oscillation has been postulated as a possible neuronal correlate underlying spontaneous BOLD signal fluctuations (Raichle, 2006). However, in light of the present results, we do not think the slow oscillation contributes to the SCP correlate of spontaneous BOLD signal for the following reasons:

(1) The frequency content of slow oscillation is distinct from that of SCP or BOLD signals. Whereas both SCP and BOLD signal demonstrate a power spectrum that obeys power-scaling law ($P \propto 1/f^{\alpha}$) (see Note 3 above), the slow oscillation has a narrow

frequency range that centers around 0.8 Hz in natural SWS (Massimini et al., 2004; Steriade, 1997).

(2) Among natural physiological states, the slow oscillation is most prominent in SWS, and often is not observed in the waking state or REM sleep (Steriade, 1997). To the contrary, the spontaneous fluctuations of SCP and BOLD signals and their correlation structures are maintained across a wide range of arousal states, certainly including wakefulness.

(3) The slow oscillation during SWS has been shown to propagate across the scalp in traveling wave fashion, without apparent relation to network topography (Massimini et al., 2004). In contrast, the spatial patterns of BOLD signal and SCP are tightly linked to functional systems.

(4) Existing evidence hints at a relation of SCP modulating the slow oscillation, as during SWS there is increased power of slow oscillation at the trough of SCP (Fig. 2C of Vanhatalo et al. (2004)), reinforcing the impression that SCP and slow oscillation are distinct phenomena.

Supplementary Note 4. Effect of distance on ECoG correlations

The distributions of inter-ROI distances were the same for sensorimotor-sensorimotor and sensorimotor-control ROI pairs (Fig. 3). Therefore, although field potential correlations may fall off with increasing distance (Nunez et al., 1997), such an effect does not account for the observed difference between sensorimotor-sensorimotor and sensorimotor-control ECoG correlations. Further, it should be noted that all ROI

pairs were separated by at least 2 cm, hence, the correlation structures investigated herein belong to the category of large-scale brain networks.

A related topic, the effect of inter-seed distances on spatial correlation results, was also investigated, the result of which is shown in Fig. S7. Similarly, the difference between sensorimotor-sensorimotor and sensorimotor-control spatial correlations cannot be accounted for by a difference in the distances between seed electrodes.

Supplementary Note 5. Can results from epilepsy patients be extrapolated to normal subjects?

Despite the enormous scientific insights gained from research using epilepsy patients (e.g., Engel et al., 2005; Gazzaniga et al., 1965), there is always the question of whether results from neurological patients can be extrapolated to normal subjects. Nonetheless, the present results are most likely extendable to normal physiology for the following reasons. (a) This group of patients had average or above intellectual and academic functioning, as tested by standard neuropsychological battery (see supplementary table). (b) In all patients the epileptic focus was focal. (Otherwise they would not have been candidates for surgery, which involves focal resection of epileptic brain region.) (c) Patients with diffuse brain tissue abnormality, including widespread interictal spike-wave discharges, were excluded from the study. (d) Considerable care was taken to exclude any interictal spikes and other ECoG phenomena associated with seizure from the collected data. (e) Three out of five patients had localized temporal lobe seizures, yet coherent SCP and gamma-BLP fluctuations confined within the sensorimotor system were found in every single patient.

Supplementary Figures
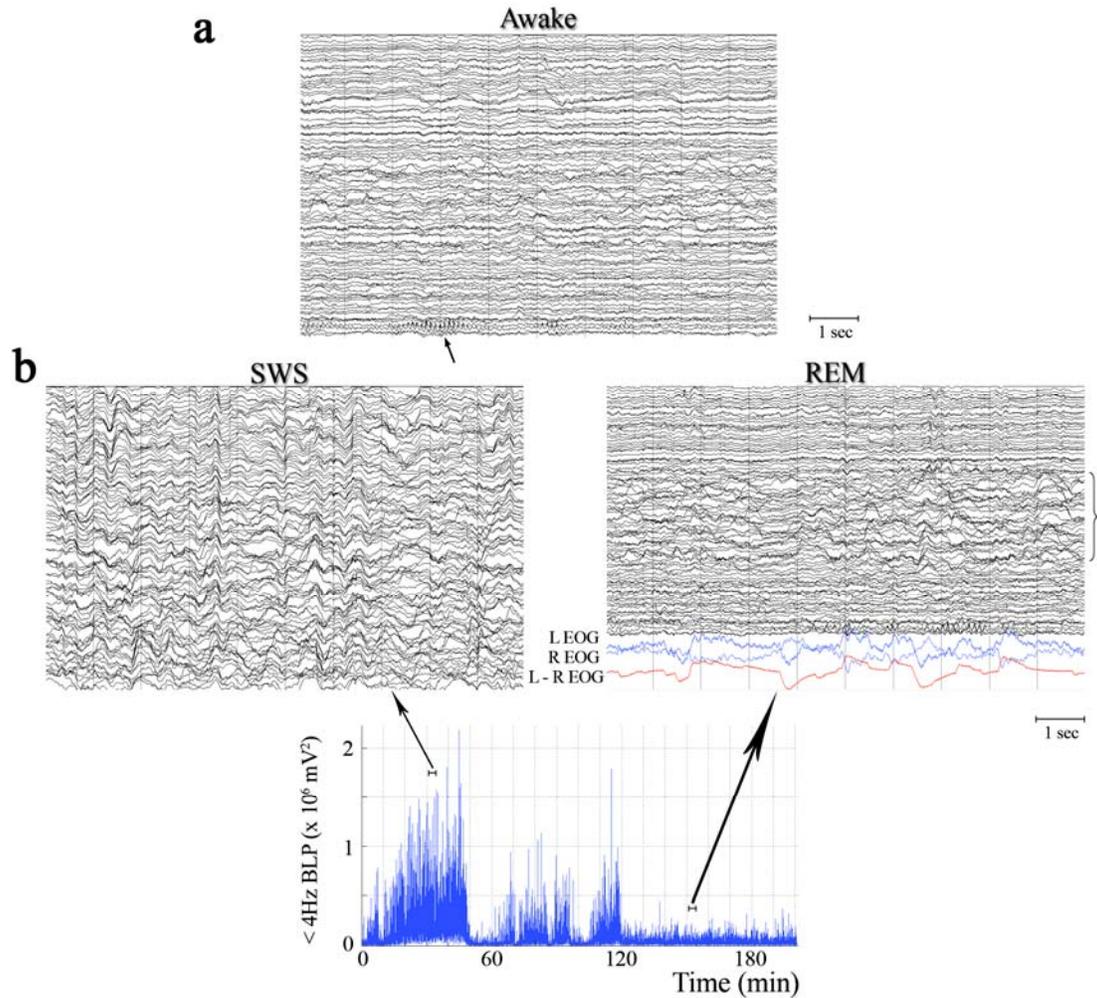
Supplementary Figure 1 Samples (10 sec duration) of raw ECoG data from Patient 3.(**a**) Awake record. Channels over sensorimotor cortex display a μ rhythm (arrow). (**b**) SWS and REM. In the REM segment, the three channels at the bottom are left eye EOG, right eye EOG, and the subtraction between the two, respectively. Note presence of μ rhythm during REM. Channels in the central portion of the display (bracketed) were over occipital areas and show slow activity that may represent PGO waves. Bottom: Power in the < 4 Hz band computed for a continuous record of 3 hr and 20 min, starting at 2:33AM. Times corresponding to the 10 sec samples shown in **b** are marked.

a) Patient 2
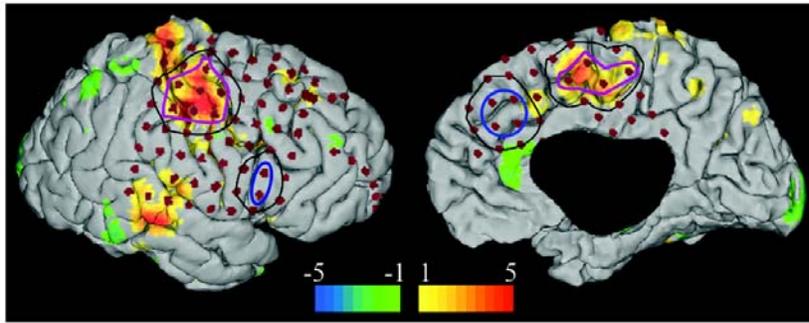
b) Patient 3
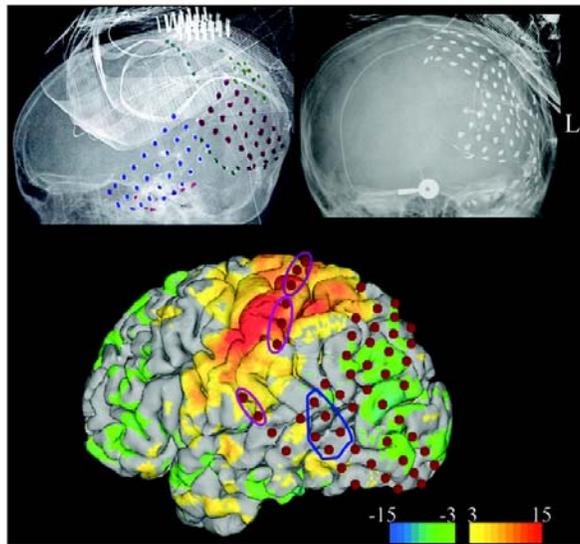
c) Patient 4
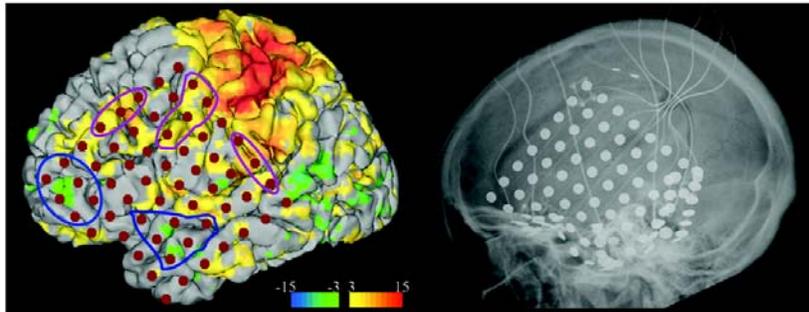
d) Patient 5
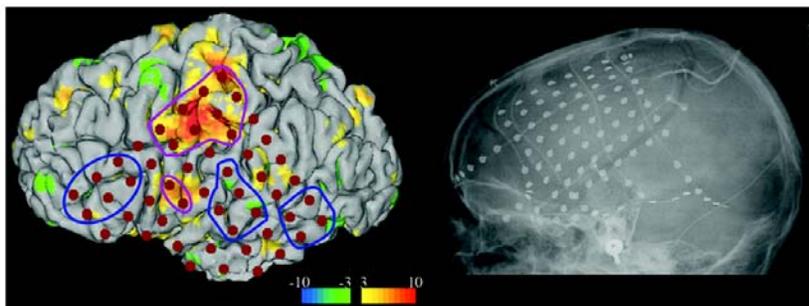
Supplementary Figure 2 Complement of Main Text Fig. 1 for Patients 2 through 5: Spatial topography of electrode coverage and BOLD correlation map of the sensorimotor network. Format as in Main Text Fig. 1. Electrodes excluded due to bad signal or covering pathological tissue are eliminated from the reconstructed figures but not the plain X-ray images. For Patient 2, plain X-ray images were not available. Also in Patient 2, in addition to average reference derivation used in all patients, a modified Laplacian derivation was tested, meaning the signal averaged over all electrodes constituting each ROI (delineated by magenta or blue contour) was subtracted by the signal averaged over the surrounding electrodes (on black contour).
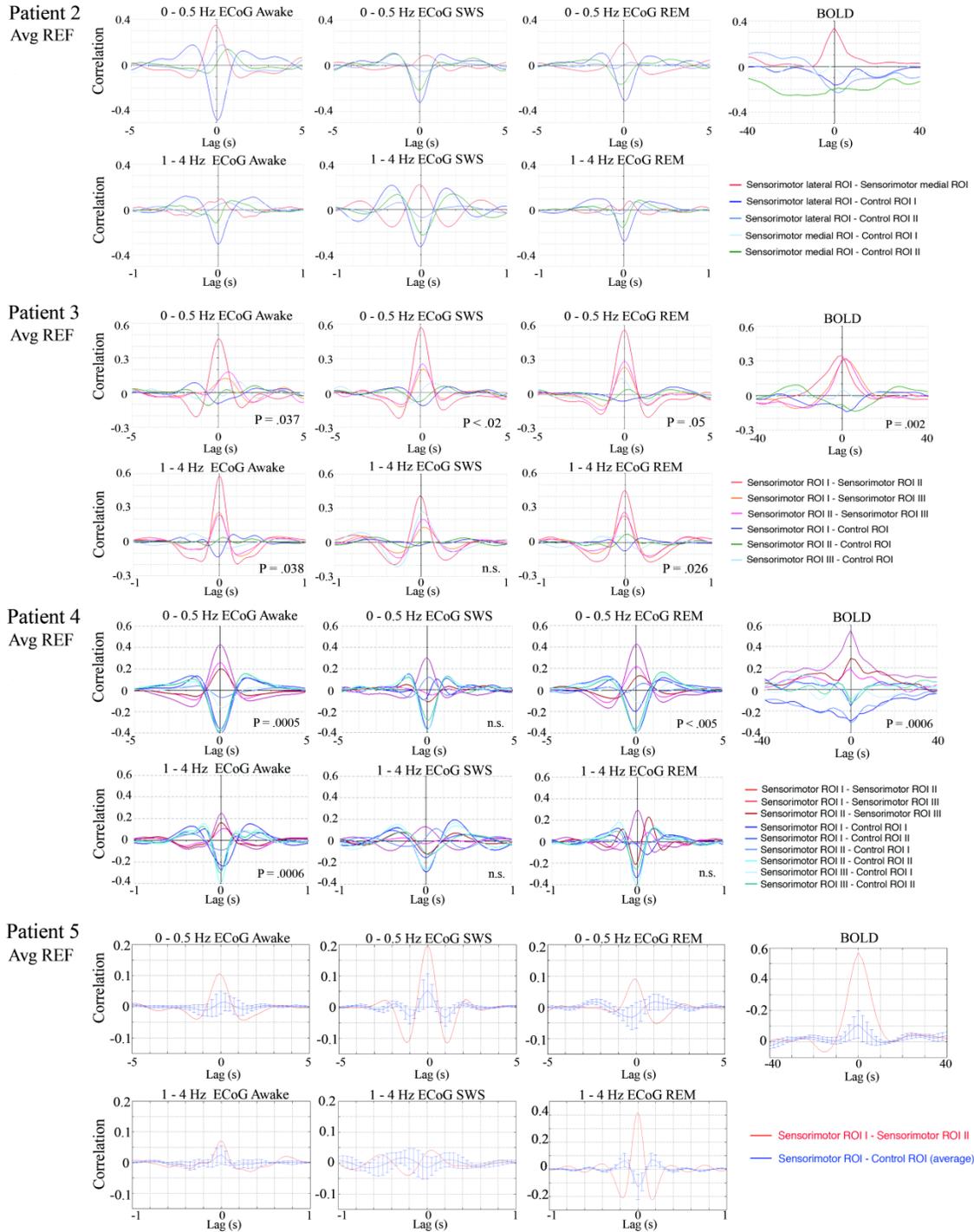
Supplementary Figure 3 Complement of Main Text Fig. 2 for Patients 2 through 5: Lagged ROI cross-correlation functions corresponding to < 0.5 Hz and 1 − 4 Hz band ECoG activity as well as BOLD signals. Format as in Main Text Fig. 2, but with different arousal states separately plotted for ECoG results. Red hues: sensorimotor–sensorimotor ROI pairs; Blue/green hues: sensorimotor–control ROI pairs. All data were analyzed using the average reference derivation. P values reflect significance of unpaired *t*-tests

comparing sensorimotor-sensorimotor vs. sensorimotor-control cross-correlation peak values. Similar statistical testing was not possible in Patients 2 and 5 because each had only one sensorimotor-sensorimotor ROI pair.
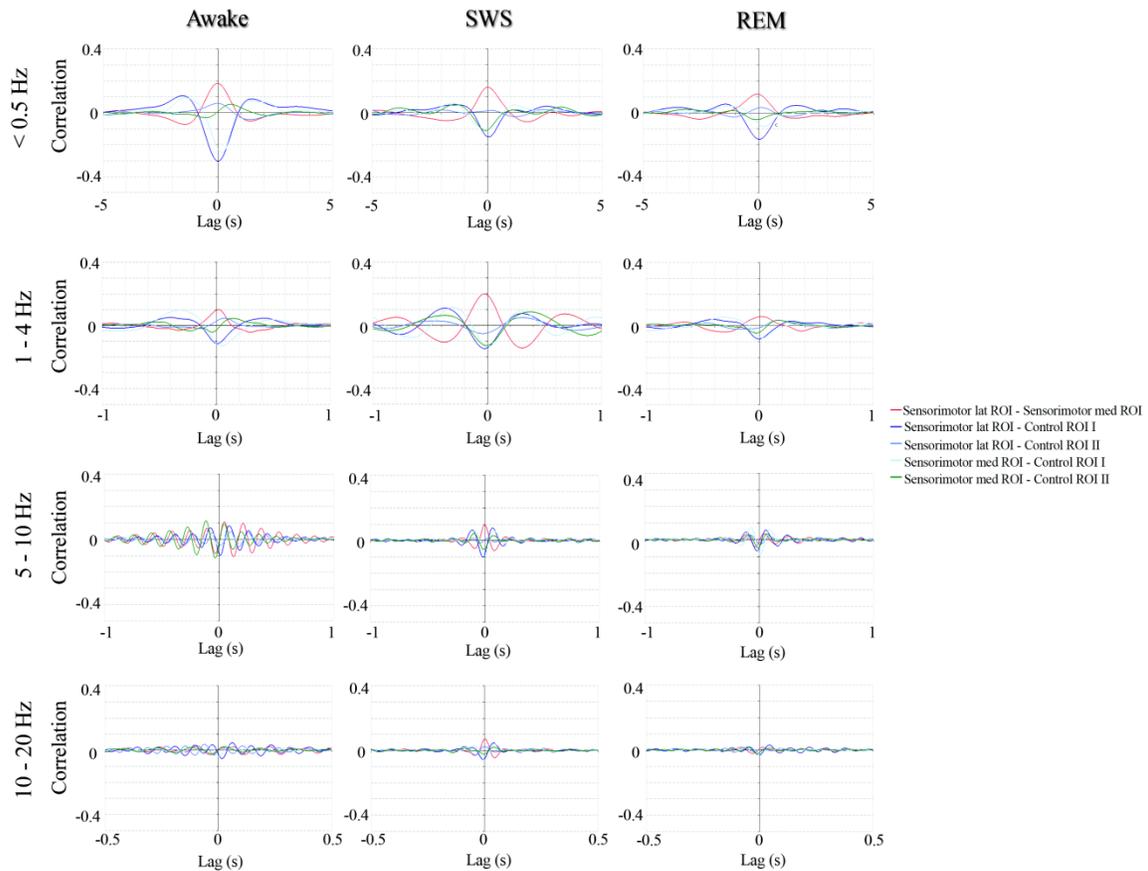
Supplementary Figure 4 ECoG cross-correlation functions obtained in Patient 2 using the modified Laplacian derivation. ECoG signals were filtered in four different frequency bands. Comparable results for the two slowest frequency bands obtained using the average reference derivation are shown in Fig. S3.
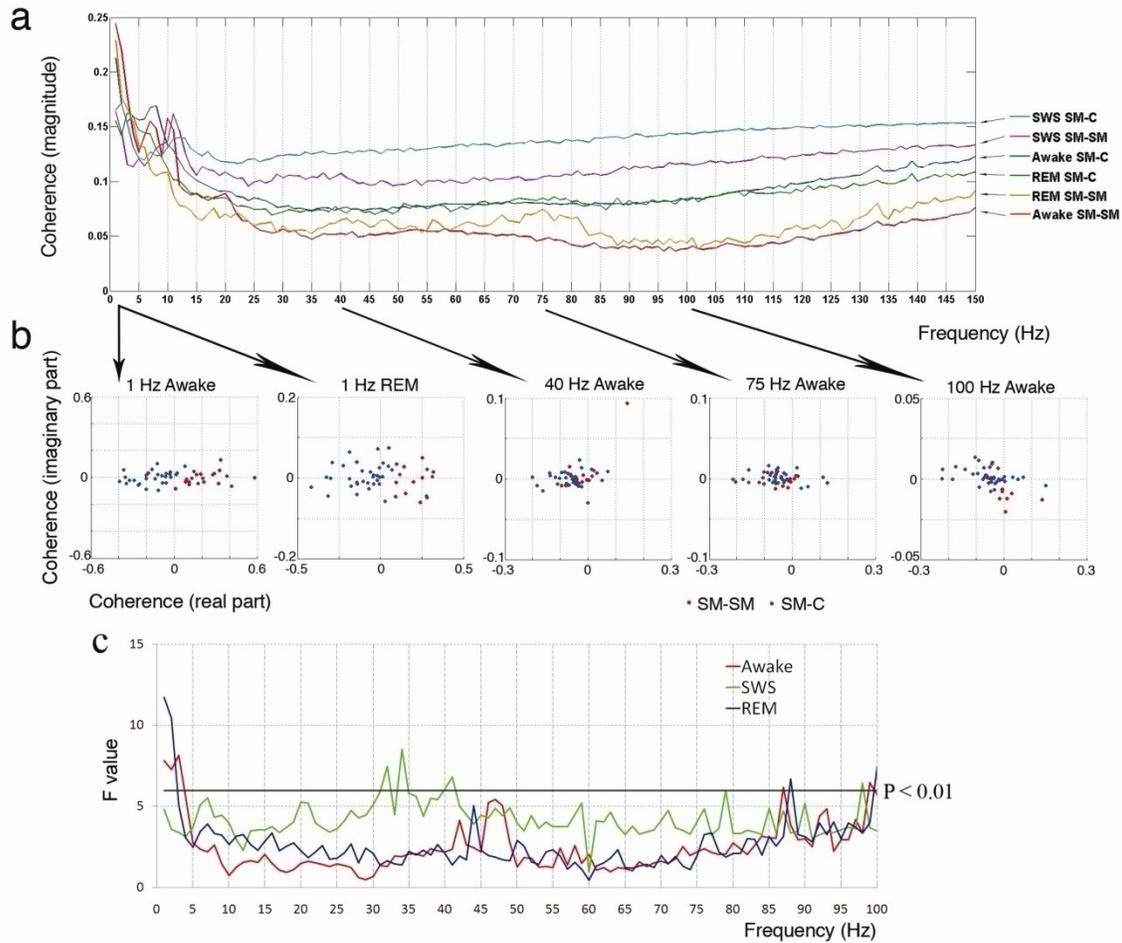
Supplementary Figure 5 Results from coherence analysis (using 1-sec length, half-overlapping moving windows). (**a**) Spectra of coherence magnitude averaged across Patients 1-4, separately for SM-SM ROI pairs and SM-C ROI pairs. Patient 5 was not used here because of a different sampling frequency (200 Hz, as opposed to 512 Hz). (**b**) Scatter plots showing the coherence magnitude and phase for each ROI pair, using ECoG data filtered in 1-Hz bins centered around 1 Hz, 40 Hz, 75 Hz, or 100 Hz. Each dot represents one ROI pair. All SM-SM (red) and SM-C (blue) ROI pairs from all 5 patients are included. The distance of each dot to (0,0) is the magnitude of coherence. The angle of this vector represents the phase difference between the two ROIs. Using 1 Hz ECoG signal, SM-SM ROI pairs are generally in phase, which corresponds to positive correlations as seen in Figs. 2a & S3, in contrast, the phase values of SM-C ROI pairs are scattered across the midline and on average out-of-phase. A similar separation between SM-SM and SM-C clusters is absent in gamma frequency bands. (**c**) The separation between SM-SM and SM-C ROI pairs in the complex coherency plane (as shown in b) was tested for each 1-Hz-width frequency bin from 1 to 100 Hz using ECoG data from each arousal state, using a two-sample Hotelling's T^2 test (see Supplementary methods). The T^2 values were converted to F values ($F_{2,46}$) and plotted. All ROI pairs from all 5 patients were included in the test. The black line indicates significance level of $P < 0.01$, assuming independence between ROI-pairs. The F-spectrum significance for waking and REM sleep data dropped below $P < 0.01$ above 4 and 3 Hz, respectively, which

corresponds well with results shown in Figs. 2a & S4. The result for SWS ECoG data is noisier, which may be due to the strong presence of up-down states during SWS (see Supplementary Note 4 for detailed discussions). The lack of statistically significant result for < 4 Hz ECoG data from SWS in this analysis does not invalidate our conclusion that SCP shows a similar correlation structure to BOLD across all three arousal states, which is a convergent result from analyses using four different strategies (Figs. 2c, 4, 5, S6, S8). Nevertheless, the correspondence between SCP and BOLD correlation structures may be weaker in SWS compared to that during waking or REM sleep.
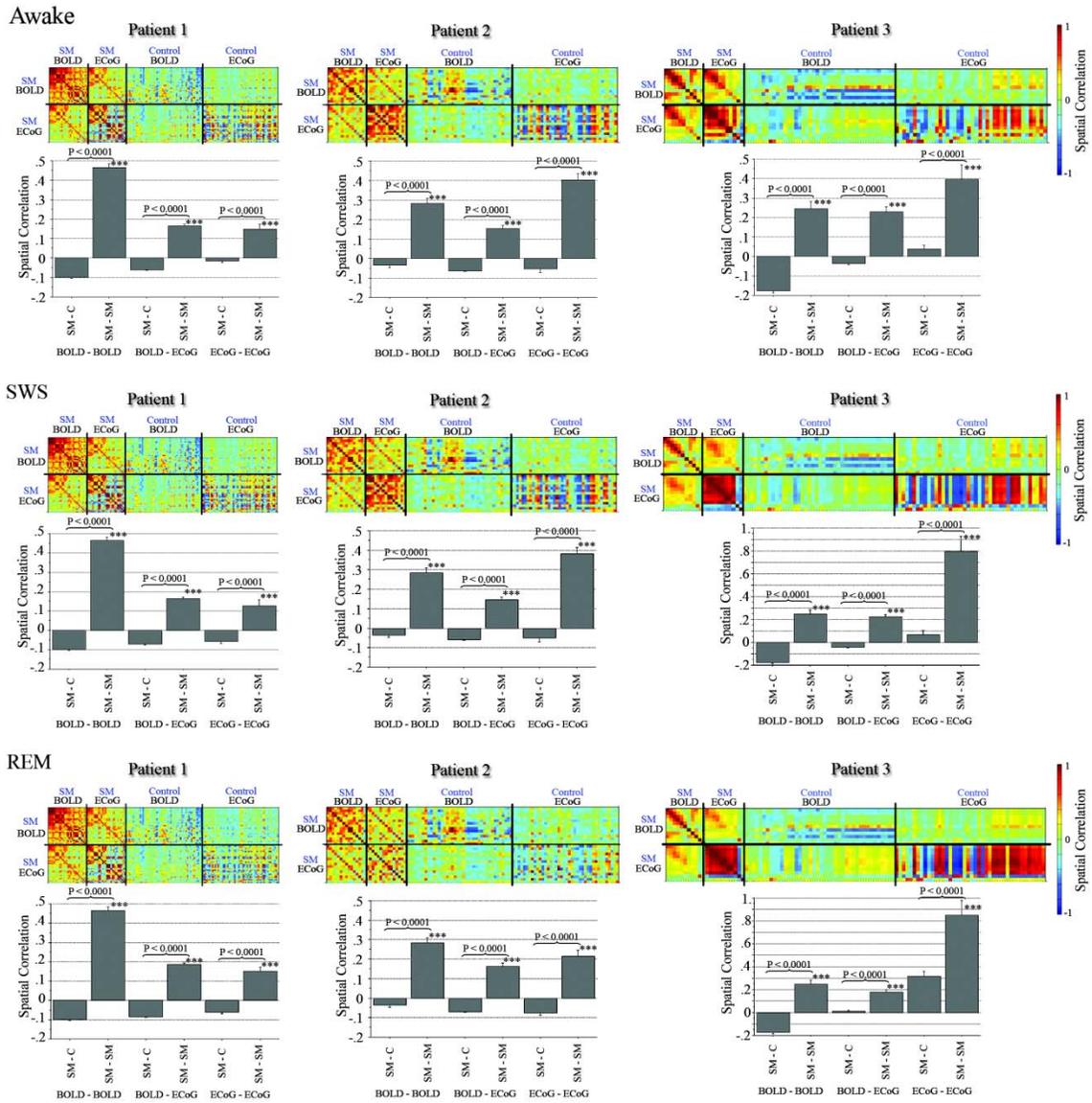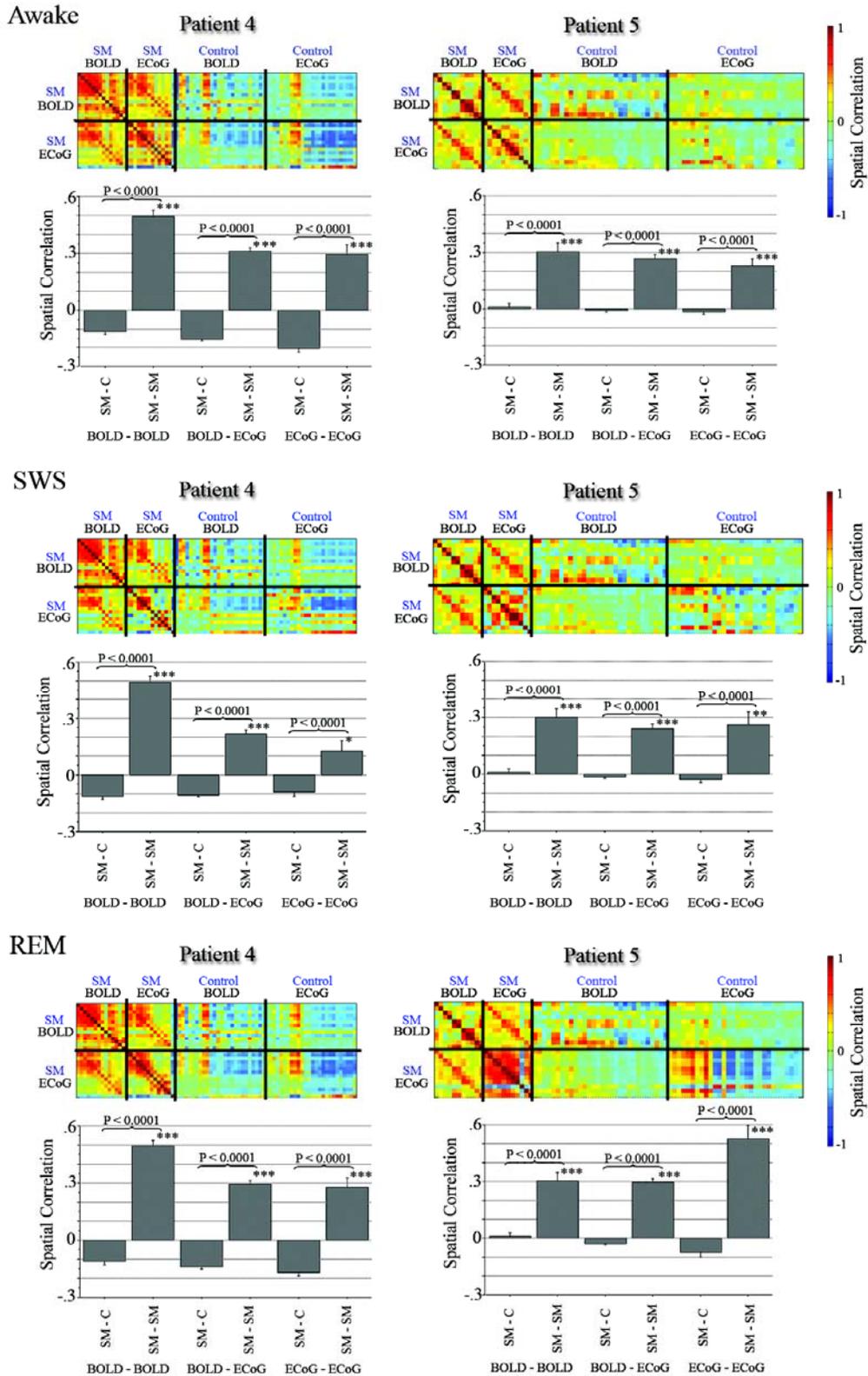
Supplementary Figure 6 BOLD and ECoG (< 0.5 Hz band, from all three arousal states) spatial correlation results obtained in all 5 patients. Relevant formulae are given in the

Methods section of the online pdf. For each patient and arousal state, spatial correlation grids are shown on top; each color-coded element corresponds to $R_{i,j}^{B:B}$, $R_{i,j}^{B:E}$, or $R_{i,j}^{E:E}$, where the superscript indicates modality pair (BOLD or < 0.5 Hz ECoG) and the subscript indexes seed electrode pair. The R values are arranged in blocks corresponding to modality and seed electrode type (sensorimotor (SM) or control (C)). Note the preponderance of positive within-modality ($R_{i,j}^{B:B}$ and $R_{i,j}^{E:E}$) as well as positive cross-modality ($R_{i,j}^{B:E}$) spatial correlations when both seed electrodes are sensorimotor ($i,j \in$ sensorimotor; 4 left-most blocks). By distinction, comparing maps obtained with sensorimotor vs. control seed electrodes yielded spatial correlations that were either homogeneously near zero or a mixture of positive and negative values (4 right-most blocks). The bar graphs under the colored grid displays represent spatial correlations (R values) averaged over various blocks. Thus, "BOLD-BOLD SM-SM" corresponds to the average over the set, $\{R_{ij}^{B:B}, i,j \in$ sensorimotor, $i \neq j\}$. "BOLD-ECoG SM-C" corresponds to the average over the sets, $\{R_{ij}^{B:E}, i \in$ sensorimotor, $j \in$ control$\}$ and $\{R_{ij}^{B:E}, i \in$ control, $j \in$ sensorimotor$\}$. The number of bar graphs (6) is less than the number of blocks (8) because of partial redundancy in the grid displays. Error bars denote SEM. The asterisks denote significantly non-zero mean spatial correlations for both seed electrodes within the sensorimotor system (***: P < .0001; **: P < .001; *: P < .05, one-sample t-test). The over-bracketed P values indicate unpaired t-tests comparing seed electrodes within (SM-SM) vs. across (SM-C) functional systems. The results obtained in Patient 1 using waking ECoG data are also shown in Main Text Fig. 5b.

Supplementary Figure 7 Control for the effect of inter-seed distance in spatial correlation analysis. Data are from Patient 2, ECoG signals are < 0.5 Hz from awake state. (**a**) Spatial correlations plotted against the distance between seed electrodes, all SM-SM (red) and SM-C (blue) seed electrode pairs are included. Spatial correlations were computed between two BOLD maps (left), a BOLD map and an ECoG map (middle), or two ECoG maps (right). (**b**) Format as in (**a**). Seed electrode pairs separated by < 2 cm or > 7.5 cm were excluded, so that the inter-seed distances in both SM-SM and SM-C groups range from 2 cm to 7.5 cm. (**c**) As in (**b**), except that the trend of distance

was taken out by a linear regression for each group (SM-SM and SM-C). (**d**) Data in (c) were subjected to a similar test as in Figs. 5b and S6. The result is very similar to that shown in Fig. S6 (Patient 2, awake ECoG).
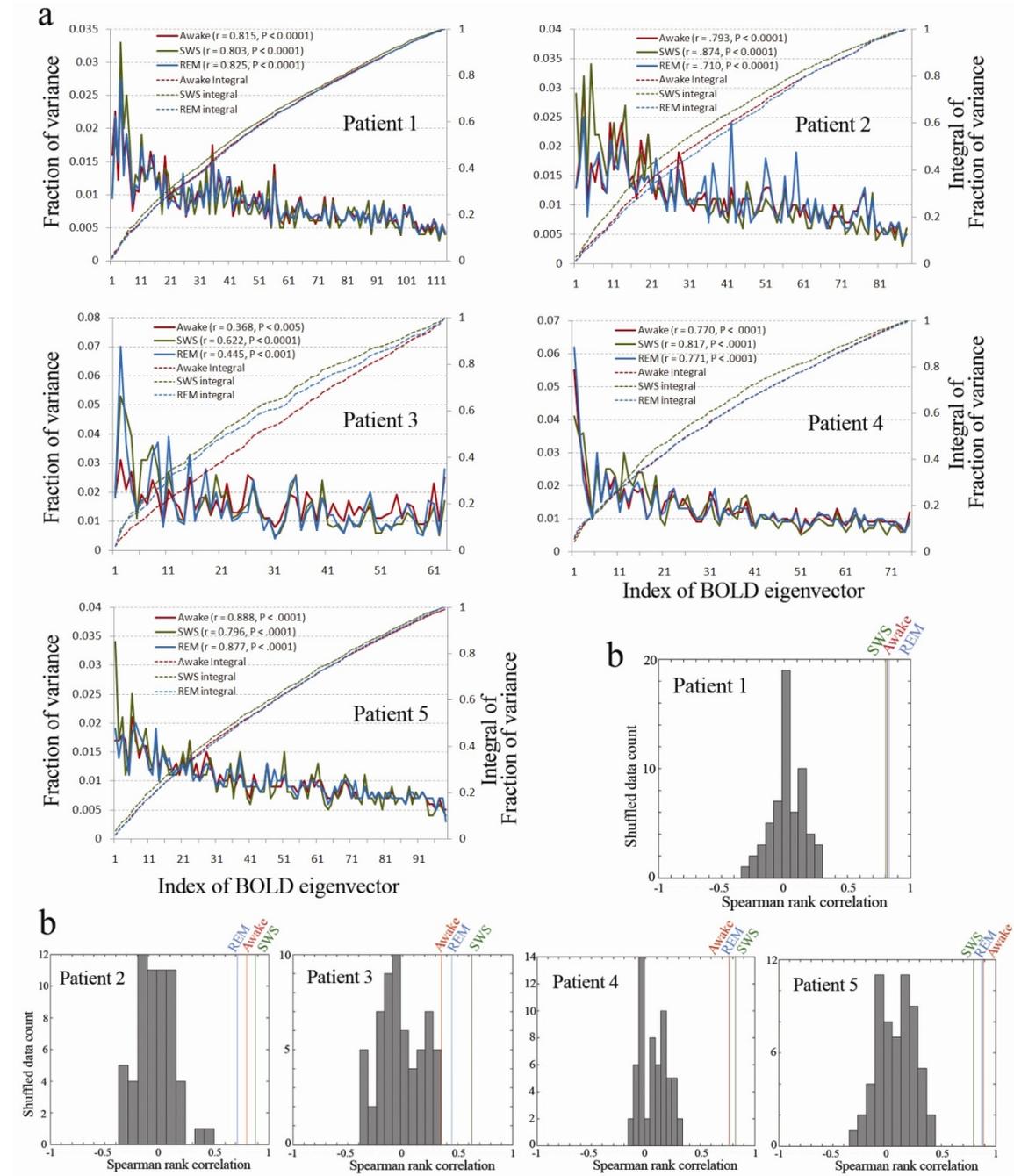
Supplementary Figure 8 Similarity of BOLD and ECoG (< 0.5 Hz band) covariance matrices assessed by means of eigenvector decomposition (see Supplementary methods).

(**a**) In each plot, the solid lines (left ordinate) show the fraction of ECoG variance captured by eigenvectors derived by diagonalization of the BOLD covariance matrix. In the present notation, the ordinate is ϕ_{Ei}/S, where $S = \sum_i \phi_{Ei}$ and the abscissa is i where i corresponds to the BOLD covariance matrix eigenvalue ordering (greatest variance in first eigenvalue). Similarity of covariance structures is indicated by the decreasing trends of the plots. Lack of similarity would manifest as the absence of this relation between ϕ_{Ei} and i. The variable range of i in the plots reflects the number of usable electrodes (n) in each patient. Statistical significance was assessed using the Spearman rank order correlation test, the results of which are shown in the insets. The dashed lines (right ordinate) are the integrated curves of the solid lines. Their locations above the diagonal reinforce the impression that eigenvectors with a smaller index value (i.e., accounting for more BOLD variance) accounts for more ECoG variance. (**b**) For each patient, the Spearman rank order correlation values for ECoG data from each arousal state (from insets of panel a, shown as colored lines here) are compared to the distribution of those computed using shuffled ECoG data. The ordering of ECoG channels was shuffled 20 times for data from each arousal state, thus, the distribution of shuffled data contains 60 observations for each patient.
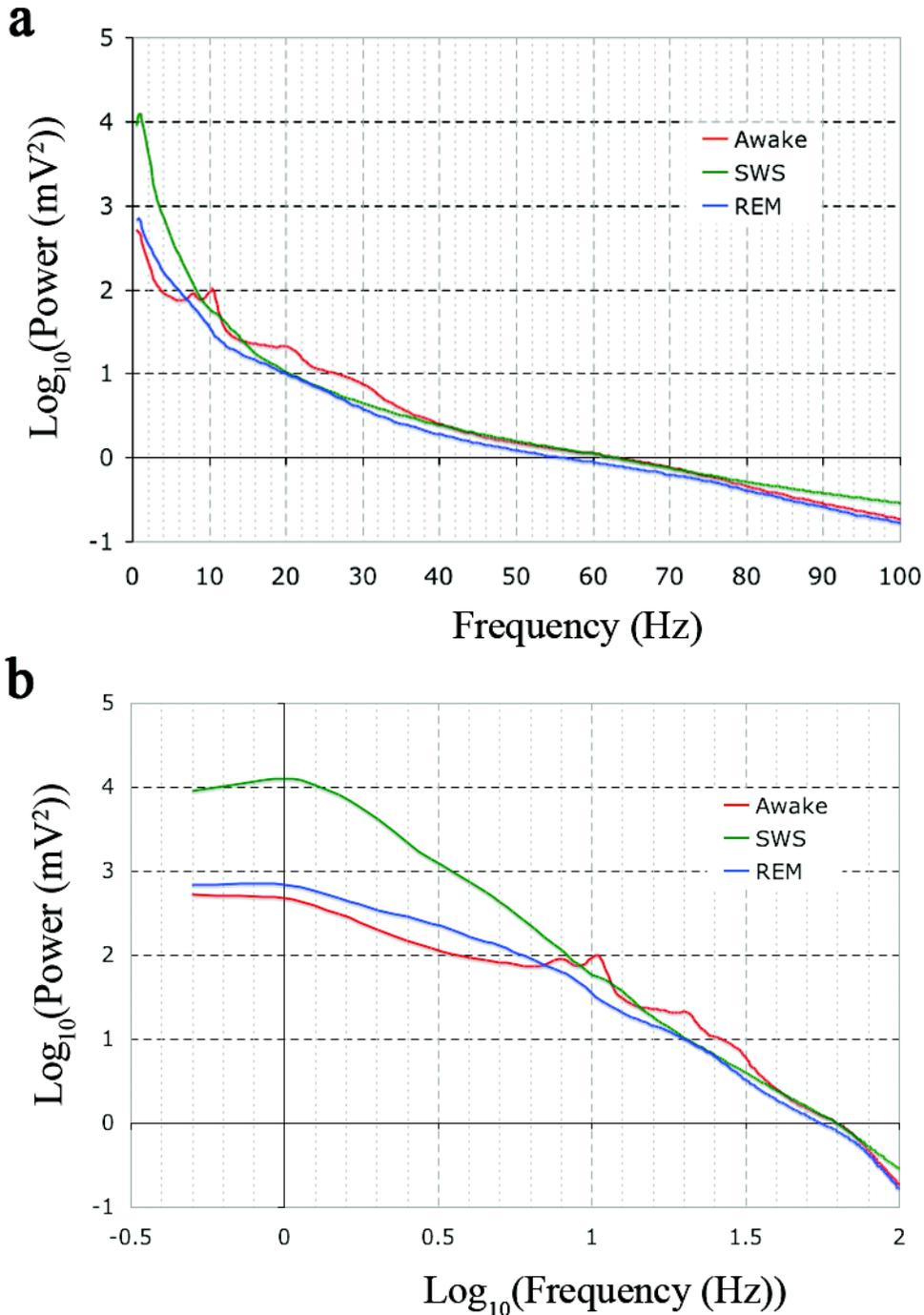
Supplementary Figure 9 Power spectra averaged over sensorimotor electrodes in wakefulness, SWS and REM. All results are from Patient 1, average reference recording. Spectra were averaged across data segments in the same arousal state. (**a**) Semi-log plot. (**b**) Log-log plot.
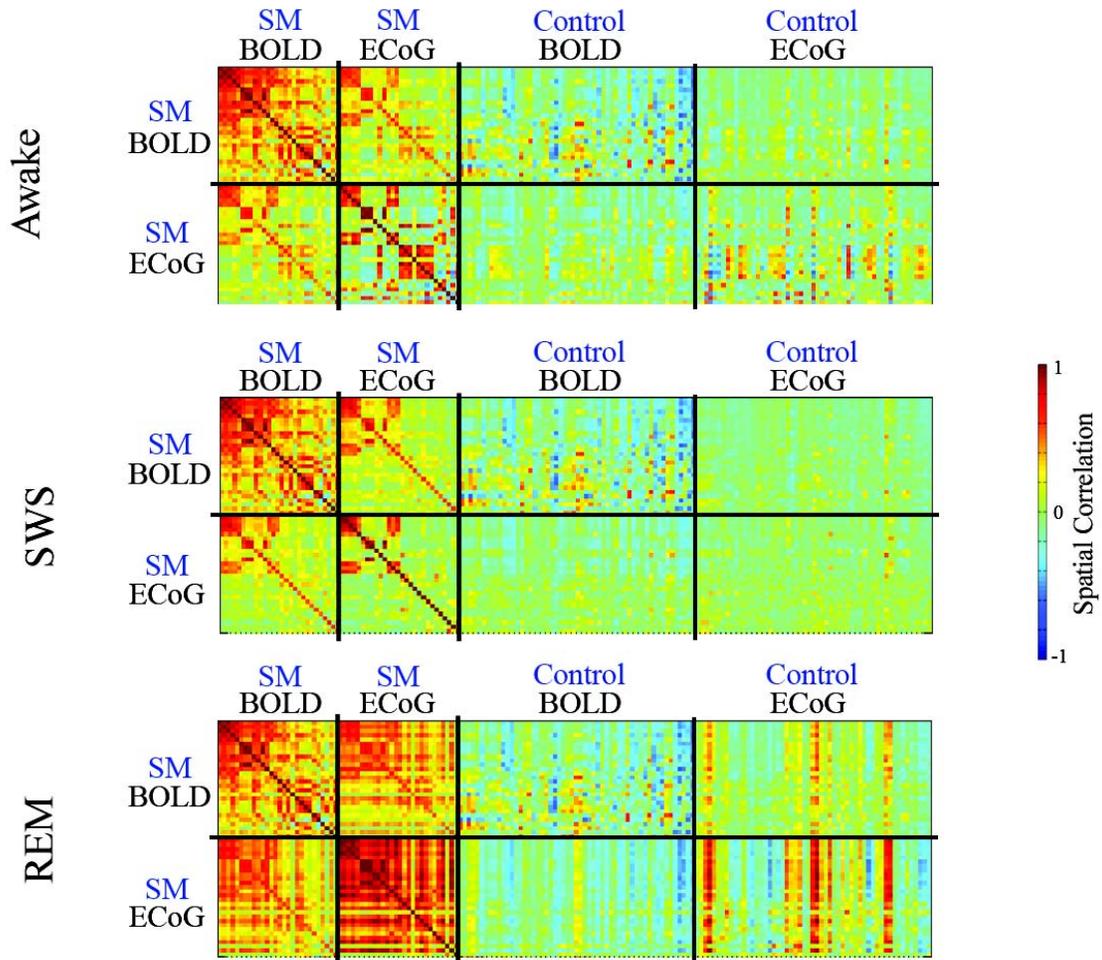
Supplementary Figure 10 Spatial correlations of BOLD and γ-BLP ECoG correlation maps obtained in Patient 1. Format as in Fig.S6 top panels. Note marked enhancement in BOLD-ECoG and ECoG-ECoG spatial correlations for both seed electrodes within the sensorimotor system (SM – SM) during REM.

References

Averbeck, B.B., Latham, P.E., and Pouget, A. (2006). Neural correlations, population coding and computation. Nat Rev Neurosci *7*, 358-366.

Birbaumer, N., Elbert, T., Canavan, A.G., and Rockstroh, B. (1990). Slow potentials of the cerebral cortex and behavior. Physiol Rev *70*, 1-41.

Birn, R.M., Diamond, J.B., Smith, M.A., and Bandettini, P.A. (2006). Separating respiratory-variation-related fluctuations from neuronal-activity-related fluctuations in fMRI. Neuroimage *31*, 1536-1548.

Biswal, B., Yetkin, F.Z., Haughton, V.M., and Hyde, J.S. (1995). Functional connectivity in the motor cortex of resting human brain using echo-planar MRI. Magn Reson Med *34*, 537-541.

Boly, M., Balteau, E., Schnakers, C., Degueldre, C., Moonen, G., Luxen, A., Phillips, C., Peigneux, P., Maquet, P., and Laureys, S. (2007). Baseline brain activity fluctuations predict somatosensory perception in humans. Proc Natl Acad Sci U S A *104*, 12187-12192.

Cordes, D., Haughton, V.M., Arfanakis, K., Carew, J.D., Turski, P.A., Moritz, C.H., Quigley, M.A., and Meyerand, M.E. (2001). Frequencies contributing to functional connectivity in the cerebral cortex in "resting-state" data. AJNR Am J Neuroradiol *22*, 1326-1333.

Devrim, M., Demiralp, T., Kurt, A., and Yucesir, I. (1999). Slow cortical potential shifts modulate the sensory threshold in human visual system. Neurosci Lett *270*, 17-20.

Engel, A.K., Moll, C.K., Fried, I., and Ojemann, G.A. (2005). Invasive recordings from the human brain: clinical insights and beyond. Nat Rev Neurosci *6*, 35-47.

Fox, M.D., Corbetta, M., Snyder, A.Z., Vincent, J.L., and Raichle, M.E. (2006).

>   Spontaneous neuronal activity distinguishes human dorsal and ventral attention

>   systems. Proc Natl Acad Sci U S A *103*, 10046-10051.

Fox, M.D., Snyder, A.Z., Vincent, J.L., and Raichle, M.E. (2007). Intrinsic fluctuations

>   within cortical systems account for intertrial variability in human behavior.

>   Neuron *56*, 171-184.

Gazzaniga, M.S., Bogen, J.E., and Sperry, R.W. (1965). Observations on visual

>   perception after disconnexion of the cerebral hemispheres in man. Brain *88*, 221-

>   236.

Golanov, E.V., Yamamoto, S., and Reis, D.J. (1994). Spontaneous waves of cerebral

>   blood flow associated with a pattern of electrocortical activity. Am J Physiol *266*,

>   R204-214.

Goldring, S. (1974). DC Shifts Released by Direct and Affrent Stimulation. In Handbook

>   of Electroencephalography and Clinical Neurophysiology, A. Remond, ed.

>   (Amsterdam: Elsevier), pp. 12-24.

Greicius, M.D., Krasnow, B., Reiss, A.L., and Menon, V. (2003). Functional connectivity

>   in the resting brain: a network analysis of the default mode hypothesis. Proc Natl

>   Acad Sci U S A *100*, 253-258.

Hampson, M., Peterson, B.S., Skudlarski, P., Gatenby, J.C., and Gore, J.C. (2002).

>   Detection of functional connectivity using temporal correlations in MR images.

>   Hum Brain Mapp *15*, 247-262.

Hathout, G.M., Gopi, R.K., Bandettini, P., and Gambhir, S.S. (1999). The lag of cerebral hemodynamics with rapidly alternating periodic stimulation: modeling for functional MRI. Magn Reson Imaging *17*, 9-20.

He, B.J., Snyder, A.Z., Vincent, J.L., Epstein, A., Shulman, G.L., and Corbetta, M. (2007). Breakdown of functional connectivity in frontoparietal networks underlies behavioral deficits in spatial neglect. Neuron *53*, 905-918.

Hobson, J.A., Pace-Schott, E.F., and Stickgold, R. (2000). Dreaming and the brain: toward a cognitive neuroscience of conscious states. Behav Brain Sci *23*, 793-842; discussion 904-1121.

Horovitz, S.G., Fukunaga, M., de Zwart, J.A., van Gelderen, P., Fulton, S.C., Balkin, T.J., and Duyn, J.H. (2008). Low frequency BOLD fluctuations during resting wakefulness and light sleep: a simultaneous EEG-fMRI study. Hum Brain Mapp *29*, 671-682.

Jenkins, G.M., and Watts, D.G. (1998). Spectral analysis and its applications, 5 edn (Boca Raton, Florida: Emerson-Adams Press).

Jones, M.O., Martin, C., Boorman, L., Harris, S., Bartlett, K., Kennerley, A., Zheng, Y., Berwick, J., and Mayhew, J.E.W. (2007). Interactions between evoked and spontaneous hemodynamic fluctuations in rodent brain. In 37th Annual Meeting of Society for Neuroscience, San Diego (San Diego).

Khader, P., Schicke, T., Roder, B., and Rosler, F. (2008). On the relationship between slow cortical potentials and BOLD signal changes in humans. Int J Psychophysiol *67*, 252-261.

Lancaster, J.L., Glass, T.G., Lankipalli, B.R., Downs, H., Mayberg, H., and Fox, P.T. (1995). A modality-independent approach to spatial normalization of tomographic images of the human brain. Human Brain Mapping *3*, 209-223.

Leopold, D.A., Murayama, Y., and Logothetis, N.K. (2003). Very slow activity fluctuations in monkey visual cortex: implications for functional brain imaging. Cereb Cortex *13*, 422-433.

Llinas, R., and Ribary, U. (1993). Coherent 40-Hz oscillation characterizes dream state in humans. Proc Natl Acad Sci U S A *90*, 2078-2081.

Logothetis, N.K., Pauls, J., Augath, M., Trinath, T., and Oeltermann, A. (2001). Neurophysiological investigation of the basis of the fMRI signal. Nature *412*, 150-157.

Massimini, M., Huber, R., Ferrarelli, F., Hill, S., and Tononi, G. (2004). The sleep slow oscillation as a traveling wave. J Neurosci *24*, 6862-6870.

Mitzdorf, U. (1985). Current source-density method and application in cat cerebral cortex: investigation of evoked potentials and EEG phenomena. Physiol Rev *65*, 37-100.

Mukamel, R., Gelbard, H., Arieli, A., Hasson, U., Fried, I., and Malach, R. (2005). Coupling between neuronal firing, field potentials, and FMRI in human auditory cortex. Science *309*, 951-954.

Niessing, J., Ebisch, B., Schmidt, K.E., Niessing, M., Singer, W., and Galuske, R.A. (2005). Hemodynamic signals correlate tightly with synchronized gamma oscillations. Science *309*, 948-951.

Nunez, P.L., Srinivasan, R., Westdorp, A.F., Wijesinghe, R.S., Tucker, D.M., Silberstein, R.B., and Cadusch, P.J. (1997). EEG coherency. I: Statistics, reference electrode, volume conduction, Laplacians, cortical imaging, and interpretation at multiple scales. Electroencephalogr Clin Neurophysiol *103*, 499-515.

Petersen, C.C., Hahn, T.T., Mehta, M., Grinvald, A., and Sakmann, B. (2003). Interaction of sensory responses with spontaneous depolarization in layer 2/3 barrel cortex. Proc Natl Acad Sci U S A *100*, 13638-13643.

Raichle, M.E. (2006). Neuroscience. The brain's dark energy. Science *314*, 1249-1250.

Raichle, M.E., and Mintun, M.A. (2006). Brain work and brain imaging. Annu Rev Neurosci *29*, 449-476.

Rodriguez, E., George, N., Lachaux, J.P., Martinerie, J., Renault, B., and Varela, F.J. (1999). Perception's shadow: long-distance synchronization of human brain activity. Nature *397*, 430-433.

Seeley, W.W., Menon, V., Schatzberg, A.F., Keller, J., Glover, G.H., Kenna, H., Reiss, A.L., and Greicius, M.D. (2007). Dissociable intrinsic connectivity networks for salience processing and executive control. J Neurosci *27*, 2349-2356.

Shmuel, A., Augath, M., Oeltermann, A., and Logothetis, N.K. (2006). Negative functional MRI response correlates with decreases in neuronal activity in monkey visual area V1. Nat Neurosci *9*, 569-577.

Shmueli, K., van Gelderen, P., de Zwart, J.A., Horovitz, S.G., Fukunaga, M., Jansma, J.M., and Duyn, J.H. (2007). Low-frequency fluctuations in the cardiac rate as a source of variance in the resting-state fMRI BOLD signal. Neuroimage *38*, 306-320.

Singer, W. (2001). Consciousness and the binding problem. Ann N Y Acad Sci *929*, 123-146.

Stamm, J.S., and Gillespie, O. (1978). Task acquisition with feedback of steady potential shifts from monkeys prefrontal cortex. In Multidisciplinary Perspectives in Event-Related Brain Potential Research, D.A. Otto, ed. (Washington, DC: US Environmental Protection Agency), pp. 410-415.

Stamm, J.S., Whipple, S.C., and Born, J. (1987). Effects of spontaneous cortical slow potentials on semantic information processing. Int J Psychophysiol *5*, 11-18.

Steriade, M. (1997). Synchronized activities of coupled oscillators in the cerebral cortex and thalamus at different levels of vigilance. Cereb Cortex *7*, 583-604.

Steriade, M., Contreras, D., Amzica, F., and Timofeev, I. (1996). Synchronization of fast (30-40 Hz) spontaneous oscillations in intrathalamic and thalamocortical networks. J Neurosci *16*, 2788-2808.

Steriade, M., Nunez, A., and Amzica, F. (1993). A novel slow (< 1 Hz) oscillation of neocortical neurons in vivo: depolarizing and hyperpolarizing components. J Neurosci *13*, 3252-3265.

Talairach, J., and Tournoux, P. (1988). Co-Planar Stereotaxic Atlas of the Human Brain (New York: Thieme Medical Publishers, Inc.).

Vanhatalo, S., Palva, J.M., Holmes, M.D., Miller, J.W., Voipio, J., and Kaila, K. (2004). Infraslow oscillations modulate excitability and interictal epileptic activity in the human cortex during sleep. Proc Natl Acad Sci U S A *101*, 5053-5057.

Vincent, J.L., Patel, G.H., Fox, M.D., Snyder, A.Z., Baker, J.T., Van Essen, D.C., Zempel, J.M., Snyder, L.H., Corbetta, M., and Raichle, M.E. (2007). Intrinsic functional architecture in the anaesthetized monkey brain. Nature *447*, 83-86.

von Stein, A., Chiang, C., and Konig, P. (2000). Top-down processing mediated by interareal synchronization. Proc Natl Acad Sci U S A *97*, 14748-14753.

Wise, R.G., Ide, K., Poulin, M.J., and Tracey, I. (2004). Resting fluctuations in arterial carbon dioxide induce significant low frequency variations in BOLD signal. Neuroimage *21*, 1652-1664.

Zar, J.H. (1984). Biostatistical Analysis, 2 edn (Englewood Cliffs, New Jersey: Prentice-Hall, Inc.).

CHAPTER IV: The temporal structures and functional significance of scale-free brain activity

Summary

The arrhythmic, scale-free brain activity, with a power spectrum following $P \propto f^{\beta}$ and commonly referred to as "$1/f$ noise", is often discarded in electrophysiological research. Here we show that it contains extensive nested frequencies with phase of slower activities modulating amplitude of faster activities in an upward progression across the frequency spectrum. Importantly, the scale-free brain activity is modulated by task performance in a brain-network-specific fashion, and its power-law exponent β varies across brain regions, being largest in default network and visual cortex, and smallest in cerebellum, hippocampus and thalamus. We further show that other scale-free dynamics in nature, such as earth seismic waves and stock market fluctuations, also contain extensive nested frequencies, but their exact patterns differ from that of brain activity. These results call attention to the scale-free brain activity, and strongly encourage future investigations on its fine spatiotemporal structures and functional significance.

Introduction

Since the invention of human electroencephalography (EEG), and Berger's first demonstration of human occipital alpha rhythm (Berger, 1929), the search for brain rhythms has been a dominant theme not only in human EEG and later-developed animal local field potential (LFP) research, but also in routine clinical EEG practice. Indeed, the

133

classical frequency bands in EEG – delta (1-3 Hz), theta (4-8 Hz), alpha (9-12 Hz), beta (12-30 Hz) and gamma (>30 Hz)[1] – were demarcated based on the various oscillatory rhythms that appear conspicuously in the EEG traces from time to time, such as delta oscillation during sleep, theta oscillation under certain types of cognition, alpha oscillation during eye-closure, beta and gamma oscillations in activated states. However, as pointed out by several pioneers in the field (Bullock et al., 1995; Bullock et al., 2003; Freeman and Zhai, 2009; Logothetis, 2002), arrhythmic brain activity also constitutes a significant part of EEG and LFP records, if not the major part, but much less is known about it. Recently, it was found that broadband field potentials recorded from the human brain are modulated by task performance and correlate with neuronal spiking activity (Manning et al., 2009; Miller et al., 2009). Moreover, synchronization between different neuronal groups can occur not only by way of synchronized oscillations, but also within arrhythmic brain activity with no apparent periodicity (Eckhorn, 1994; Thivierge and Cisek, 2008).

Viewed in the frequency domain, the temporal power spectrum of arrhythmic brain activity roughly follows a straight line when plotted in coordinates of log power vs. log frequency: $\log(P) \propto -\beta \log(f)$ or $P \propto f^{\beta} (0 < \beta < 3)$. This is called a "power-law" distribution, "scale-invariance" or "scale-free" dynamics, commonly referred to as "$1/f$ noise" (note, however, that the exponent β for brain signals is not always in the vicinity of 1, see below). Periodic brain oscillations appear as local peaks that rise above the

---

[1] In this chapter, I use "delta", "theta", "alpha", "beta", and "gamma" to denote their respective frequency ranges, applied to both periodic oscillations and arrhythmic brain activity. Although the word "oscillation" has often been used to refer to band-pass filtered arrhythmic brain activity, I herein use it exclusively to refer to periodic, rhythmic brain activities before artificial filtering.

power-law distribution in the power spectrum. The scale-free brain activity ("1/f noise") is invisible in many EEG or LFP studies, since power at each frequency is routinely normalized by its value during a pre-task baseline, effectively removing the presence of the "1/f noise", or else the data is "pre-whitened" to remove the "1/f noise" and emphasize oscillations (e.g., (Buzsaki, 2006; Mitra and Pesaran, 1999)). The disregard of the "1/f noise" is partly due to its ubiquitous presence in nature, including earthquakes, solar flares, economics, evolution, ecology, epidemics, electronics, speech and music (Bak, 1996; Gisiger, 2001; Hsu and Hsu, 1991; Voss and Clarke, 1975), which often leads to doubts of any significance the "1/f noise" might have in the operations specific to the brain. In addition, the possibility that "1/f noise" might originate from instrument noise (Zarahn et al., 1997) also deters the studying of it in relation to brain function.

However, not only LFP, EEG and functional magnetic resonance imaging (fMRI) activities exhibit scale-free dynamics (Bullmore et al., 2004; Bullmore et al., 2001; Buzsaki, 2006; Freeman and Zhai, 2009; Linkenkaer-Hansen et al., 2001; Milstein et al., 2009; Monto et al., 2008) but the speed of action potentials (Ward, 2002), the dynamics of neurotransmitter release (Lowen et al., 1997) and human cognition and behaviors (Gilden, 2001; Maylor et al., 2001; Ward, 2002) also follow a power-law distribution, which are inexplicable by instrument noise. Moreover, recent work suggested that spontaneous fluctuations in the low-frequency end of the "1/f noise", termed infraslow fluctuations or slow cortical potentials, not only modulate trial-to-trial behavioral performance and the amount of higher-frequency activities ((Monto et al., 2008), for review see (He and Raichle, 2009)), but also correlate with fMRI signals (He et al., 2008).

Therefore, to understand the arrhythmic, scale-free activity of the brain – the common "1/f noise" – seems critical if a full understanding of the brain's operation is aimed for. Unfortunately, existing studies on the full frequency spectrum of the "1/f noise" remain scarce (Buiatti et al., 2007; Freeman and Zhai, 2009; Lin et al., 2006a; Manning et al., 2009; Miller et al., 2007; Milstein et al., 2009), and they usually only characterize the gross properties of the "1/f noise" such as its power-law exponent or variance. Many simulations of scale-free dynamics have been constructed (e.g., Bak, 1996; de Arcangelis et al., 2006; De Los Rios and Zhang, 1999; Lin and Chen, 2005; Mandelbrot, 1999; Ward and Greenwood, 2007), but it remains to be seen if they describe the neurophysiological processes giving rise to the "1/f noise" in the brain. Notably, scale-free properties have recently been described in the amplitude and synchronization of oscillatory brain activity (Linkenkaer-Hansen et al., 2001; Linkenkaer-Hansen et al., 2004; Stam and de Bruin, 2004), and in the temporal and spatial distributions of negative LFP peaks (Plenz and Thiagarajan, 2007). Yet, these analyses do not directly address the scale-free dynamics so prevalent in the raw fluctuations of brain field potentials, and their relationships to the latter await future investigation.

We investigated the fine temporal structures of arrhythmic, scale-free brain activity by using nested-frequency analysis. Nested frequencies refer to a systematic relationship between the phase of a lower frequency and the amplitude of a higher frequency, and has been described between phase of theta and amplitude of gamma activity (Bragin et al., 1995; Buzsaki et al., 2003; Canolty et al., 2006; Lakatos et al., 2005; Tort et al., 2008), and between phase of delta and sub-delta activity and amplitude

of higher frequencies (Lakatos et al., 2008; Monto et al., 2008; Vanhatalo et al., 2004).

Here we show that the extent of nested frequencies is much broader than previously

conceived, extending beyond the confinement of brain oscillations, and present within

arrhythmic, scale-free brain activity. These results suggest that scale-free brain activity

contains a rich temporal organization. We then provide data showing that the power-law

exponent of scale-free brain activity varies across brain regions and is modulated by task

performance. Lastly, we compared scale-free brain activity with other scale-free

dynamics in nature including earth seismic waves and stock market fluctuations, as well

as simulated time series. Although all these dynamics follow a power-law distribution,

the fine temporal structures present in them differ across systems, likely a manifestation

of the different underlying generating mechanisms. These results call attention to the "1/f

noise" in the brain, and strongly encourage future studies on the fine spatiotemporal

patterns within and functional meanings of the arrhythmic brain activity.

Methods

Electrocorticography (ECoG) Data Collection

Subjects

Eight patients undergoing surgical treatment for intractable epilepsy participated

in the study. To localize epileptogenic zones, patients underwent a craniotomy for

subdural placement of electrode grids and strips followed by 1-2 weeks of continuous

video and ECoG monitoring. The placement of the electrodes and the duration of

monitoring were determined entirely by clinical considerations. All patients gave

informed consent according to the procedures established by Washington University

Institutional Review Board. Exclusion criteria were: (1) widespread interictal spike-and-wave discharges; (2) age < 8 years old; (3) severely impaired cognitive capability; (4) diffuse brain tissue abnormality, e.g., tuberous sclerosis, cerebral palsy; (4) limited electrode coverage. See Table S1 for demographic, clinical and data collection information.

Recording apparatus

The electrode arrays (typically 8×8, 4×5 or 2×5) and strips (typically 1×6 or 1×8) consisted of platinum electrodes of 4-mm diameter (2.3 mm exposed) with a center-to-center distance of 10 mm between adjacent electrodes (AD-TECH Medical Instrument Corporation, Racine WI). ECoG signals were split and sent to both the clinical EEG system and a research EEG system (SynAmp^2, Neuroscan, DC-coupled recording with no low- or high-pass filtering). All data in the present study were from the research amplifier. Sampling frequencies for each patient (ranging from 500 to 2000 Hz) are listed in Table S1. Noisy electrodes and electrodes overlying pathologic tissue (including both the primary epileptogenic zone and areas showing active interictal discharges) were eliminated from all analyses. The remaining electrodes were re-referenced to the common average before further analyses. Number of usable electrodes in each patient ranged from 28 to 64 (see Table S1).

Spontaneous ECoG data collection

In patients #1 – #5, artifact-free, interictal-spike-free ECoG data were collected from both wakefulness and slow-wave sleep (SWS, sleep stages 3/4). Arousal state determination was based on the conjunction of ECoG and video recordings. Total lengths of data collected for each patient are listed in Table S1. In Patient #4, 30 min of

rapid-eye-movement (REM) sleep data was also collected. REM sleep was identified

based on a conjunction of active eye movements in the video record and the

electrooculogram (EOG).

Task ECoG data collection

Patients #3, #5, #6, #7 and #8 also undertook visuomotor task performance.

There were two task conditions, both of which involved pressing a button. In the first

task condition ("cued"), subjects were instructed to fixate on a white crosshair in the

center of a black background, presented on a laptop screen. The cross hair occasionally

changed from white to dark-gray for a period of 250 ms. Subjects were instructed to press

a button with their left or right index finger as quickly as possible when they saw the

crosshair dim. Both the button-press force and reaction time were recorded (but not used

in the present analyses). The inter-trial interval (ITI) varied randomly between 2 and 20

seconds, with an average ITI of 6.1 sec. Each task block contained 50 button presses, and

lasted about 5 min. The left and right hand was used in different task blocks. In the

second task condition ("self-paced"), the same white crosshair was presented in the

center of a black background, which the subject was to fixate on, but this time the

crosshair lasted without any change for the duration of a task block (5 min). Subjects

were instructed to press the button with left or right index finger at their own pace, and to

separate adjacent button presses by a few seconds. They were told to avoid rhythms and

avoid counting either the interval between successive button presses or the number of

button presses. Button press force and the timing of button presses were recorded but not

used in the current analyses. Again, the left and right hand was used in different task

blocks. Subjects practiced each task condition for a few trials before the recording session began. The number of task blocks completed by each subject is listed in Table S1.

Functional Magnetic Resonance Imaging (fMRI) Data Collection and Pre-processing

fMRI data were from Fox et al. (2007). Blood-oxygen-level dependent (BOLD) fMRI data (4 x 4 x 4 mm voxels, TE 25 ms, TR 2.16 s) were acquired in 17 normal right-handed young adults (9 females, age 18-27 years) in a 3T Siemens Allegra MR scanner. Each subject completed 4 resting-state fMRI runs, each 194 frames (7 min) in duration (the first 4 frames were discarded in analyses). Subjects were instructed to fixate at a white crosshair presented in the center of a black screen, remain still, and to not fall asleep. Anatomical MRI included a high-resolution (1 x 1 x 1.25 mm) sagittal, T1-weighted MP-RAGE (TR =2.1 s, TE = 3.93 ms, flip angle = 7°) and a T2 weighted fast spin echo scan. fMRI preprocessing steps included, 1st, compensation of systematic, slice-dependent time shifts; 2nd, elimination of systematic odd-even slice intensity differences due to interleaved acquisition; 3rd, rigid body correction for inter-frame head motion within and across runs, and 4th, intensity scaling to a yield a whole brain mode value of 1000 (with a single scaling factor for all voxels). Atlas registration was achieved by computing affine transforms connecting the fMRI run first frame (averaged over all runs after cross-run realignment) with the T2- and T1-weighted structural images (Ojemann et al., 1997). Our atlas representative template includes MP-RAGE data from 12 normal individuals and was made to conform to the 1988 Talairach atlas (Talairach

and Tournoux, 1988). Each fMRI run was transformed to atlas space and resampled to 3 mm cubic voxels. Linear trend was removed before calculating power spectrum.

Seismic Wave Data Collection

Continuous natural seismic wave data (sampling rate 100 Hz) were collected by University of Nevada, Reno seismic network, and archived and distributed by Northern California Earthquake Data Center (NCEDC) (http://www.ncedc.org/). The data analyzed in the current study were from HHE channel, BEK station, NN network (Latitude 39.87°, Longitude -120.36°, Elevation 1743.0m), collected by CMG-40 seismometers, recorded by RefTeck digitizers. Data were recorded from Jan 1 to Apr 28, 2005.

Stock Market Data Collection

The historical daily prices of Dow-Jones Industrial Average index from Oct 1, 1929 to Apr 9, 2009 were downloaded from Yahoo Finance website: (http://finance.yahoo.com/q/hp?s=%5EDJI). Daily close price adjusted for dividends and splits was used for the analyses.

Power Spectra of ECoG, Seismic, Stock and Simulated signals

Power spectra were computed using Fast Fourier Transform (FFT) applied to half-overlapping, Hanning windows, and averaged across successive windows. Window length was 300 sec for ECoG and simulated data, 8 sec for earth seismic data (the < 0.1

Hz frequency range of seismic data was attenuated by a highpass filter in the seismometer), and 1000 days for stock market data.

Power Spectra of fMRI signal

A set of 31 regions of interest (ROIs) were obtained from previous activation studies in the laboratory or from published fMRI activation studies. The anatomical locations, coordinates and references of these ROIs are listed in Table S2. The regions were grouped into 5 brain networks and a separate group consisting regions outside the neocortex based on their known anatomical/functional properties. The fMRI signal time course from each ROI was extracted for each subject and fMRI run. The time course from each run was subjected to Fourier analysis to yield the power spectrum, and then averaged across runs. The average power spectrum for each ROI was obtained by averaging across subjects, and homologous ROIs were averaged together (Fig. 5A). Finally, the power-law exponent of each average power spectrum was obtained by using a least squares fit (values in Table S2), which was then entered into an ANOVA with brain network as the main factor (Fig. 5B).

Cross-frequency phase-amplitude coupling analysis

For each frequency pair f_p and f_A, time series $x(t)$ (brain, seismic, economic activity or simulated signal) was filtered in the corresponding frequency bins $|f_p|$ and $|f_A|$ using a 3rd-order symmetrical butterworth filter after linear trend removal, to obtain filtered time series $x_{fp}(t)$ and $x_{fA}(t)$. Windows of 600-sec length were used for filtering ECoG data and simulated time series, windows of 300-sec length were used for filtering

142

seismic wave data, and windows of 1000-day length used for stock market data. We also performed the same analyses using different window lengths (including 100, 300, 1200, 3000 sec for ECoG data). Results described in our paper did not depend on window length.

Next, a standard Hilbert transform was used to obtain an instantaneous phase time series for $x_{fp}(t)$, denoted $\varphi_{fp}(t)$, and an instantaneous amplitude time series for $x_{fA}(t)$, denoted $A_{fA}(t)$. Then the values of $\varphi_{fp}(t)$ were binned into twenty 0.1π intervals from $-\pi$ to π, and the concurrent $A_{fA}(t)$ values were averaged within each phase bin (as shown in Fig. 2D). We denote as $\left\langle A_{fA} \right\rangle_{\varphi_{fp}}(j)$ the mean A_{fA} value at phase bin $\varphi_{fp}(j)$.

We then apply an inverted entropy measure to obtain a modulation index (*MI*) which describes the deviation of $\left\langle A_{fA} \right\rangle_{\varphi_{fp}}(j)$ from a uniform distribution (Tort et al., 2008): $MI = \dfrac{H_{max} - H}{H_{max}}$. H, the entropy of $\left\langle A_{fA} \right\rangle_{\varphi_{fp}}(j)$ distribution, is defined by

$$H = -\sum_{j=1}^{N} p_j \log p_j \text{,where } N = 20 \text{ (i.e., the number of phase bins), and } p_j \text{ is given by}$$

$$p_j = \frac{\left\langle A_{fA} \right\rangle_{\varphi_{fp}}(j)}{\sum_{j=1}^{N} \left\langle A_{fA} \right\rangle_{\varphi_{fp}}(j)}.$$ H_{max} is the maximum possible entropy when the distribution is

uniform, in which case $p_j = 1/20$, hence $H_{max} = \log 20$.

Therefore, *MI* represents the dependence of $A_{fA}(t)$ on $\varphi_{fp}(t)$, i.e., how strongly phase of f_p modulates amplitude of f_A. To assess the statistical significance of *MI*, it was compared against the distribution of shuffled data. Shuffling was done by cutting the time series $\varphi_{fp}(t)$ into 5 equal-length segments, and then shuffling these 5 segments (with

no segment remaining at the original place), thereby yielding 44 shuffled time series φ $_{fp}(t)_{\text{shuffle}}$ in total. This shuffling procedure preserves the temporal structure of the original signal, and therefore is a rigorous test that is less prone to false positives (Hurtado et al., 2004). Then the inverted entropy measure as described above was computed using the 44 $\varphi_{fp}(t)_{\text{shuffle}}$time series and the original $A_{fA}(t)$ to produce $MI_{shuffle}$.

Finally, the original MI was compared against the mean and s.d. of $MI_{shuffle}$, denoted as $\overline{MI_{shuffle}}$ and $\sigma(MI_{shuffle})$ respectively, to obtain the modulation index (MI Z-score):

$$MIZ-score = \frac{MI - \overline{MI_{shuffle}}}{\sigma(MI_{shuffle})}.$$

Phase-amplitude coupling was computed for every frequency pair in a 2-D frequency space. For ECoG data and simulated data, 1-Hz-width frequency bins centered at $1 - 20$ Hz in 1-Hz steps were used for phase extraction (plotted on x-axis), 4-Hz-width frequency bins centered at $5 - 200$ Hz in 5-Hz steps were used for amplitude extraction (y-axis). For seismic wave data, 1-Hz-width frequency bins centered at $1 - 10$ Hz in 1-Hz steps were used for phase extraction, 2-Hz-width bins centered at $2 - 36$ Hz in 2-Hz steps were used for amplitude extraction. For Dow-Jones Index (here frequency is cycle/day, c/d), 0.004-c/d-width frequency bins centered at $0.005 - 0.05$ c/d in 0.005 c/d steps were used for phase extraction, 0.02-c/d-width bins centered at $0.02 - 0.48$ c/d in 0.02-c/d steps were used for amplitude extraction.

All analyses were performed using custom written code in C or Matlab.

Results

Power Spectra of Electrical Field Potentials of the Brain

We collected spontaneous electrocorticography (ECoG, i.e., invasive EEG) data from five patients (Patients #1 - #5, Table S1) undergoing surgical treatment for drug-resistant epilepsy, in both quiet wakefulness and slow-wave sleep (SWS, sleep stages 3/4). Length of data collected in each arousal state ranged from 12 to 83 min. In Patient #4, 30 min of rapid-eye-movement (REM) sleep data was also collected. Electrode locations documented by plain X-ray pictures are shown in Fig. 1F. For details of clinical and data collection information see Table S1.

Power spectra of ECoG signals, plotted in log-log coordinates (Fig. 1 A-E, top graphs), roughly followed a straight line, with local peaks corresponding to well-known brain oscillations rising above this line. These oscillations included the slow oscillation (~0.8 Hz) and sleep spindles (~12 Hz) during SWS, and the theta (~7-8 Hz), alpha (~10 Hz) and beta (~20 Hz) oscillations in the awake state. Interestingly, although the slow oscillation (i.e., "up-and-down states") is traditionally considered to be absent in wakefulness or REM sleep, an oscillatory peak around its frequency (~1 Hz) is weakly present in the waking and REM-sleep power spectra, consistent with recent reports of its presence in wakefulness when sleep pressure increases (Vyazovskiy et al., 2009) and its slightly higher frequency in wakefulness (~1 Hz) compared to SWS (~0.8 Hz) (Petersen et al., 2003). Multiple brain oscillations notwithstanding, the vast majority of power (> 90%) in the ECoG signals is accounted for by the power-law distribution representing the scale-free brain activity (i.e., "$1/f$ noise").

145
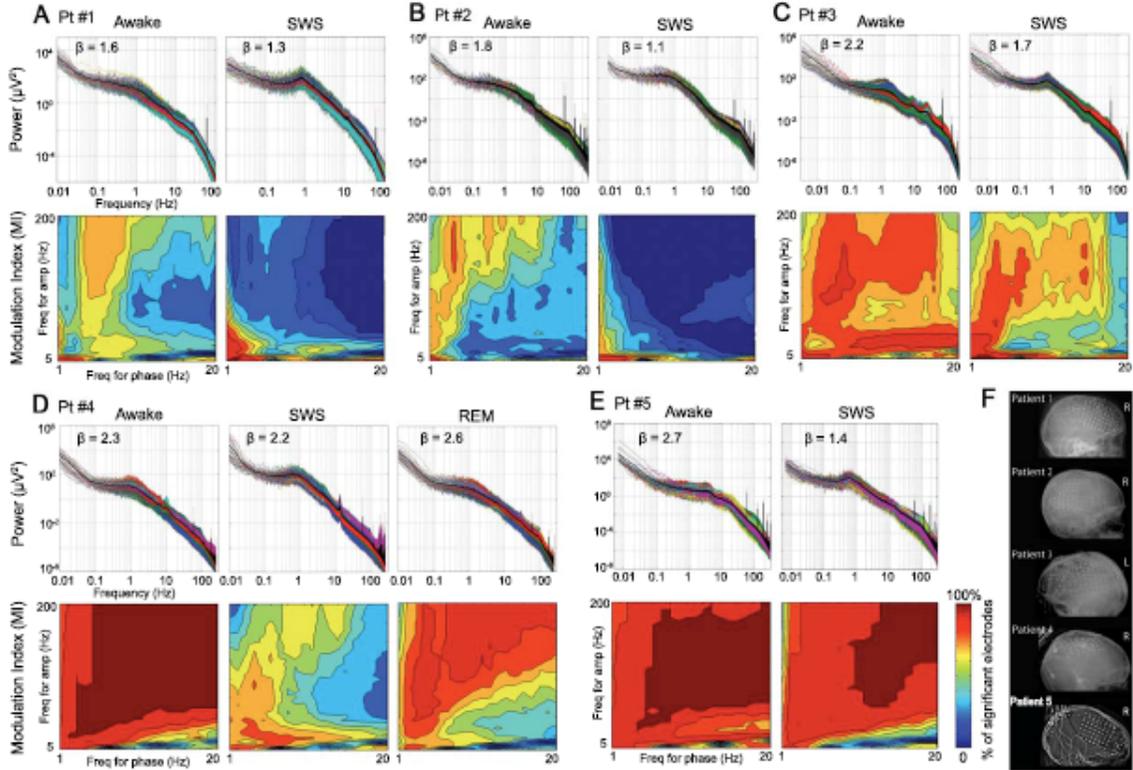
Figure 1 (A-E) Power spectra and nested frequencies in spontaneous ECoG signals recorded from different arousal states in patients #1 – #5. The top graphs show the power spectra for all electrodes plotted in a log-log plot, with the thick black line being the average across all electrodes. The low-frequency end (<0.1 Hz) of the average power spectrum was fitted with a power-law function $P(f) \propto 1/f^{\beta}$. The obtained exponent β is shown in each graph. The bottom graphs show the percentage of electrodes with significant phase-to-amplitude cross-frequency coupling. Phase was extracted from 1-Hz-width bands with center frequencies from 1 to 20 Hz in 1-Hz steps. Amplitude was extracted from 5-Hz-width bands with center frequencies from 5 to 200 Hz in 5-Hz steps. To assess the strength of cross-frequency coupling, a modulation index (MI) was computed for each electrode (see experimental procedures) and then compared with shuffled data to obtain a MI Z-score. The percentage of electrodes with a significant MI Z-score ($P < 0.05$ after Bonferroni correction) was plotted as color for each frequency pair. (**F**) Electrode locations documented by plain X-ray pictures.

To estimate the power-law exponent, we fitted the low-frequency end (<0.1 Hz) of the power spectrum with a power-law function $\log(P) \propto -\beta \log(f)$. The power-law exponents β (shown in Fig. 1) ranged from 1.1 to 2.7, with a mean of 1.84. The average exponent during wakefulness and SWS was 2.13 and 1.55 respectively ($P < 0.05$ by paired t-test). We used the low-frequency end for obtaining the power-law exponent,

146

recommended by (Eke et al., 2002), because it is less contaminated by higher-frequency oscillatory activities and aliasing effect. Since there is no current consensus in physics literature on the procedure for estimating the power-law exponent (e.g., (Clauset et al., 2009)), the values of these exponents should be taken as approximates only. Nonetheless, they correspond very well with previous reports on the power-law exponent of LFP or ECoG activity (Freeman and Zhai, 2009; Miller et al., 2007; Milstein et al., 2009).

The Widespread Presence of Nested Frequencies

To investigate temporal structures within spontaneous ECoG signals, we examined nested frequency patterns in each electrode. For a pair of frequencies, instantaneous phase and amplitude was extracted for the lower and higher frequency respectively. The lower-frequency phase at all samples was divided into 20 bins, and the concurrent higher-frequency amplitude was averaged within each bin. The resultant curve shows the dependency of the higher-frequency amplitude on lower-frequency phase, and its deviation from a uniform distribution was evaluated by using an inverted entropy measurement to yield a modulation index (MI) (Tort et al., 2008). The MI was compared with shuffled data to obtain a MI Z-score indexing the strength of cross-frequency phase-amplitude coupling. For further details on the analytical steps see Experimental Procedures.

Cross-frequency phase-amplitude coupling was investigated in a 2-D frequency space: phase was extracted from each 1-Hz-width band centered at 1, 2 … 20 Hz, and amplitude was extracted from each 5-Hz-width band centered at 5, 10 … 200 Hz. For

147

each frequency pair, the percentage of electrodes with a significant MI Z-score (P<0.05 after Bonferroni correction) is plotted as color in Fig. 1 A-E (bottom graphs). As can be seen from the figure, during wakefulness, extensive nested frequencies are present in every patient in the majority of electrodes; the extent of nested frequencies decreases during SWS, but remains highly robust across wide frequency ranges in patients #3-#5. Such widespread presence of nested frequencies is much more extensive than previously conceived, and is difficult to reconcile with a notion picturing nested frequencies only within the framework of periodic brain oscillations. For example, periodic theta oscillation is largely absent during SWS in both human EEG and animal LFP recordings (Chrobak and Buzsaki, 1998; Lin et al., 2006b; Nishida et al., 2004), consistent with the absence of local peak in theta frequency range in the power spectra of our SWS data (Fig. 1A-E, top). Nonetheless, theta-phase modulation of higher frequencies is prominent during SWS. Hence, it appears that to explain such widespread presence of nested frequencies, the arrhythmic brain activity must be invoked.

Power-law Distribution Is Not an Artifact of Averaging

As mentioned in INTRODUCTION, brain oscillations and "1/f noise" have so far remained two largely separate fields in electrophysiology research. One important, unresolved question concerns whether they pertain to separate physiological processes with different underlying mechanisms (e.g., (Bullock et al., 2003; Freeman and Zhai, 2009)), or alternatively, the "1/f noise" is the result of averaging across time of many different, transient and recurrent oscillations at different frequencies and with different amplitudes (e.g., (Buzsaki, 2006)).

To investigate this issue, we randomly picked three electrodes (from Patient #3), two with and one without rhythmic oscillations. As shown by the power spectra averaged across the entire awake record (Fig. 2A left), electrode #33 contains oscillations at ~1.5 Hz and at ~20 Hz, electrode #43 contains oscillations at ~7-8 Hz and ~20 Hz, and electrode #64 contains no periodic oscillations but only arrhythmic, scale-free activity. This impression from the power spectra is confirmed by visually inspecting the raw ECoG records. Two randomly selected 20-second segments of raw data are shown in Fig. 2C. The power spectra of these two short data segments (Fig. 2A middle and right) recapitulate the power spectra averaged over the entire 83-min record: Electrode #33 has oscillatory peaks between 1 and 2 Hz, and at ~20 Hz; electrode #43 has oscillatory peaks at ~7-8 Hz and ~20 Hz; and electrode #64 has no discernible oscillatory peak. The observation that the overall shape of the power spectrum – its power-law distribution and the presence or absence of oscillatory peaks – appears to be stable over time was obtained in many electrodes.
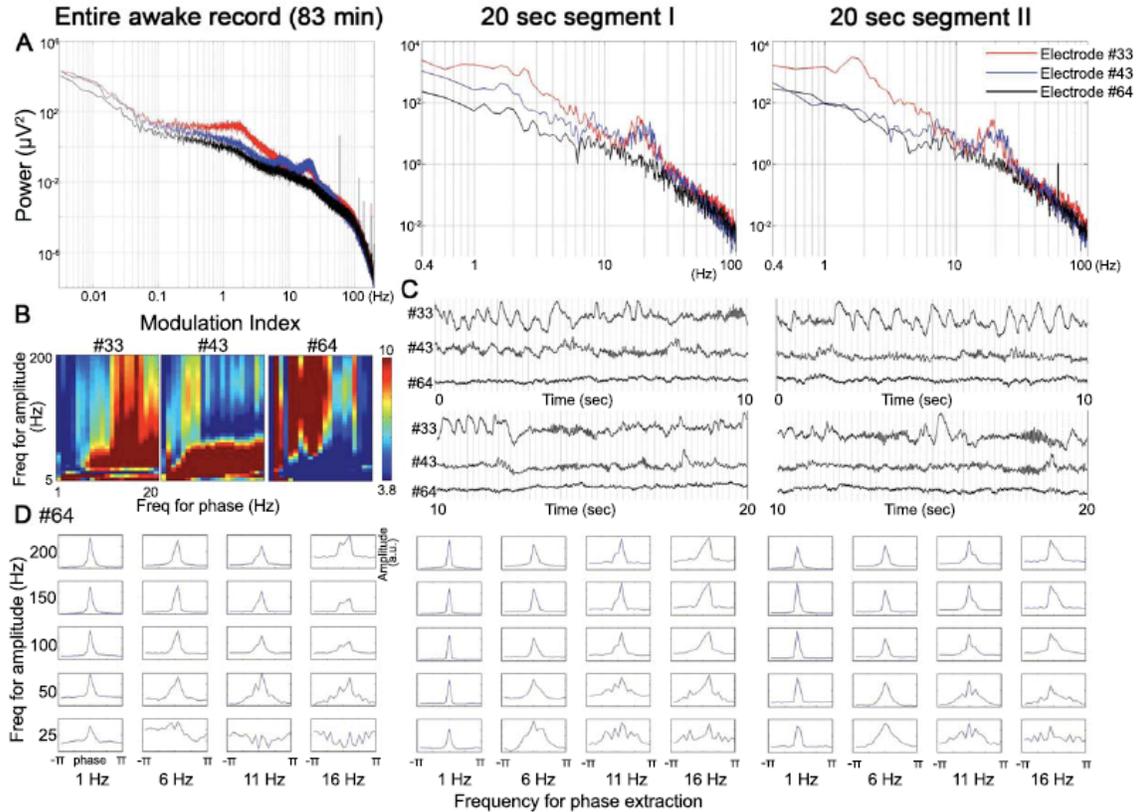
Figure 2 Stability of power-law distribution and nested frequency patterns. (**A**) Power spectra from three example electrodes in Patient #3. The left, middle and right columns are from the entire awake record (83 min total), and two randomly selected 20-sec segments, respectively. Note the difference in scales between left vs. middle and right graphs. (**B**) Phase-amplitude cross-frequency coupling for each of the three electrodes computed from the entire awake record. MI Z-score was plotted as color for each frequency pair. Only significant values (P < 0.05 after Bonferroni correction) are shown. (**C**) The raw data records for the two 20-sec segments. The whole segment was broken into half, 0-10 sec shown in the top and 10-20 sec shown in the bottom. Note the presence of ~1.5 Hz oscillation in electrode #33, and ~20 Hz oscillations in both electrodes #33 and #43, corresponding to the peaks in power spectra as shown in (A). The absence of oscillation in electrode #64 is consistent with the power-law distribution of its power spectrum without notable peaks. (**D**) Nested-frequency patterns for selected frequency pairs from electrode #64. Amplitude of the higher frequencies (5-Hz-width bands centered at 25, 50, 100, 150, 200 Hz) was averaged at different phases of the lower frequencies (1-Hz-width bands centered at 1, 6, 11, 16 Hz) and plotted. Phase $\pm\pi$ corresponds to the trough (surface negativity), and phase 0 corresponds to the peak (surface positivity) of the lower-frequency fluctuation. Nested frequency patterns from the two 20-sec segments (middle and right) are very similar to that from the entire awake record (left).

Therefore, the power-law distribution of the ECoG power spectrum does not seem to be an artifact of averaging across time of many independent, periodic oscillations, but rather appears to be the direct result of the presence of arrhythmic, scale-free brain activity. One remaining possibility is that there are hidden rhythmic activities at finer spatial resolutions than that can be observed with the ECoG electrodes. However, arrhythmic activity is present at every spatial scale in the brain: The power spectrum of spontaneous LFP activity also follows a power-law distribution (Leopold et al., 2003; Milstein et al., 2009). Moreover, cortical pyramidal neurons' spikes are usually non-rhythmic ((Ermentrout et al., 2008; Faisal et al., 2008; Freeman and Zhai, 2009; Koch, 1997; Thivierge and Cisek, 2008) but see (Maimon and Assad, 2009)) and "1/f noise" has been observed in neuronal spike trains (Gisiger, 2001; Gruneis et al., 1989; Takahashi et al., 2004; Yamamoto, 1991).

Stability of Nested Frequencies within Scale-Free Brain Activity

Next we investigated whether electrodes with only scale-free brain activity but no rhythmic oscillations also contained nested frequencies. Nested frequencies in the above three electrodes were computed in the same 2-D frequency space as shown in Fig. 1A-E. Significant cross-frequency coupling across wide frequency ranges were found in every electrode (Fig. 2B), including electrode #64, which contained no discernible periodic oscillations.

To examine the stability of nested frequency patterns within scale-free brain activity, for selected frequency pairs from electrode #64, we plotted the higher-frequency amplitude averaged at different phases of the lower frequency. Amplitude of 5-Hz-width

bands centered at 25, 50, 100, 150, 200 Hz was averaged at different phases of lower-frequency bands (1-Hz-width) centered at 1, 6, 11, 16 Hz and plotted in Fig. 2D. This analysis was repeated for the entire awake record (Fig. 2D, left) and the two 20-sec segments shown in Fig. 2C (Fig. 2D, middle and right). The nested frequency patterns from the two short data segments are each similar to the pattern from the entire record, suggesting that the nested frequencies present within scale-free brain activity appear to be stable over time. Similar results from a few other representative electrodes from each patient are shown in Fig. S1. Importantly, the pattern of nested frequencies varied across electrodes, despite that all of them contained mainly arrhythmic brain activity (Fig. S1).

Nested Frequency Patterns Across Brain Surface

To characterize nested frequency patterns across electrodes, for the same frequency pairs as in Fig. 2D, we obtained the MI Z-score, which indexes the strength of cross-frequency phase-amplitude coupling, for each of the 259 electrodes from all five patients. Averaged across the 20 frequency pairs, 80% and 65% electrodes had a significant MI Z-score in wakefulness and SWS respectively. For each electrode and frequency pair we also determined the preferred phase of the lower frequency, which denotes the phase of the lower frequency fluctuation at which the higher frequency has the largest amplitude.

Plotting the MI Z-score against preferred phase on an electrode-by-electrode basis for each patient and frequency pair, we found that the preferred phase tends to cluster around phase 0 and phase $\pm\pi$, that is, the peak and trough of the lower-frequency fluctuation respectively (see Fig. 3A for results from Patients #3&4, Fig. S2 for Patients

#1&5, Patient #2 was not used in this analysis due to lesser amount of electrodes). This raised the question of whether the electrodes with preferred phase around 0 and those with preferred phase around ±π situated in different cortical regions. Thus, for each frequency pair, we plotted the preferred phase of the lower frequency as color on a 2-D representation of the electrode grid (Patient #3 in Fig. 3B, Patients #1, 4&5 in Fig. S3). Indeed, electrodes with preferred phase around 0 and those with preferred phase around±π formed largely separate clusters, which to a rough degree respected cortical anatomy such as the location of Sylvian fissure and central sulcus (marked in Fig. 3B). Moreover, these spatial patterns were relatively stable across arousal states.

It should be noted that the results of this analysis were contributed by both scale-free brain activity and periodic brain oscillations, because, unlike in Fig. 2, the spontaneous ECoG signals from all electrodes were used. When the periodic brain oscillations and scale-free brain activity are already mixed in collected data, as is the case for many electrodes in our recordings, there are no *a posteriori* mathematical tools to separate them while preserving their respective biologically meaningful phases. The influence of brain oscillations on the results in Fig. 3 can be most clearly seen in 1-Hz-phase modulation of higher frequency amplitudes (the leftmost column in each sub-panel). During wakefulness, the preferred 1-Hz phase is a bimodal distribution, clustered around both 0 and±π; however, during SWS it becomes a unimodal distribution with most electrodes having their preferred phase around 0. This is in full accordance with known neurophysiology: during SWS, the slow oscillation at around 1 Hz becomes very prominent, which modulates higher frequencies strongly. The surface positive (phase-0)

ECoG activity at ~1 Hz corresponds to the intracellular "up-state", during which higher-

frequency activities are dramatically increased (Vyazovskiy et al., 2009).
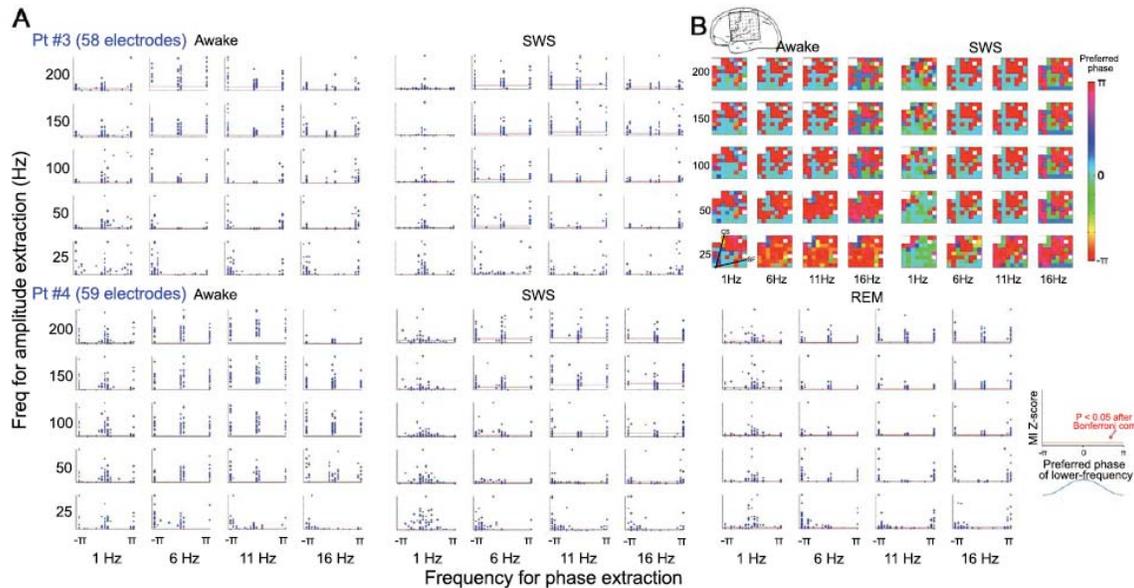
Figure 3 (**A**) Nested frequency patterns from two example patients, #3 and #4, with 2 and 3 arousal states each. Phase was extracted from 1-Hz-width bands centered at 1, 6, 11, and 16 Hz. Amplitude was extracted from 5-Hz-width bands centered at 25, 50, 100, 150, 200 Hz. For each phase-amplitude frequency pair, the subplot shows a scatter-plot of all electrodes, each represented by one dot. The ordinate value shows the cross-frequency coupling strength as indexed by MI Z-score. The red horizontal line indicates significance level ($P < 0.05$ after Bonferroni correction). The abscissa value shows the preferred phase of the lower frequency, i.e., the phase of the lower-frequency fluctuation at which the amplitude of the higher frequency is the largest. (**B**) For Patient #3, the preferred phase for each frequency pair in (A) and each electrode are plotted as color on a 2-D representation of the 8 ×8 electrode grid. The orientation and location of this grid on the cortical surface is shown in the top diagram. The six white cells in the grid are bad electrodes that have been eliminated from all analyses. The approximate locations of the central sulcus (CS) and the sylvian fissure (SF) are denoted on the bottom left grid.

Task Modulation of Scale-Free Brain Activity

We tested whether scale-free brain activity has any functional significance by

recording ECoG signals during both quiet wakefulness and task performance in Patients

#3 & #5 and three additional subjects (#6-#8, see Table S1). The task included a cued

button press condition and a self-paced button press condition. In the cued condition, a

visual cue prompted the subject to press a button as soon as they saw the cue, the inter-trial interval varied randomly between 2 and 20 seconds (mean 6.1 sec). In the self-paced condition, the subject was instructed to press the button at their own pace, separating adjacent button presses by a few seconds but to avoid either counting or regular rhythms (which could entrain scale-free brain activity to oscillations, see, e.g., (Elbert et al., 1991; Lakatos et al., 2008)). The button press was performed by either the left or right index finger, corresponding to either the contralateral or ipsilateral hand, as the electrodes covered only one hemisphere in each patient.

We searched blindly for electrodes whose power spectrum was significantly altered by task performance. Significant deviation of power-law exponent during task from that during rest was found in 11 electrodes, including four over hand motor area, one over the lower motor cortex (representation of tongue/face), three over premotor area, one over Broca's area, one over lateral occipital cortex, and one over lateral temporal lobe (Fig. 4 A-C & Fig. S4). All five electrodes over motor cortex were confirmed by cortical stimulation as part of patients' routine clinical care. Compared to rest, the power-law exponent of all these electrodes decreased during all four trial types, suggesting that scale-free brain activity is modulated by task performance. Interestingly, there was no systematic difference between the four trial types.
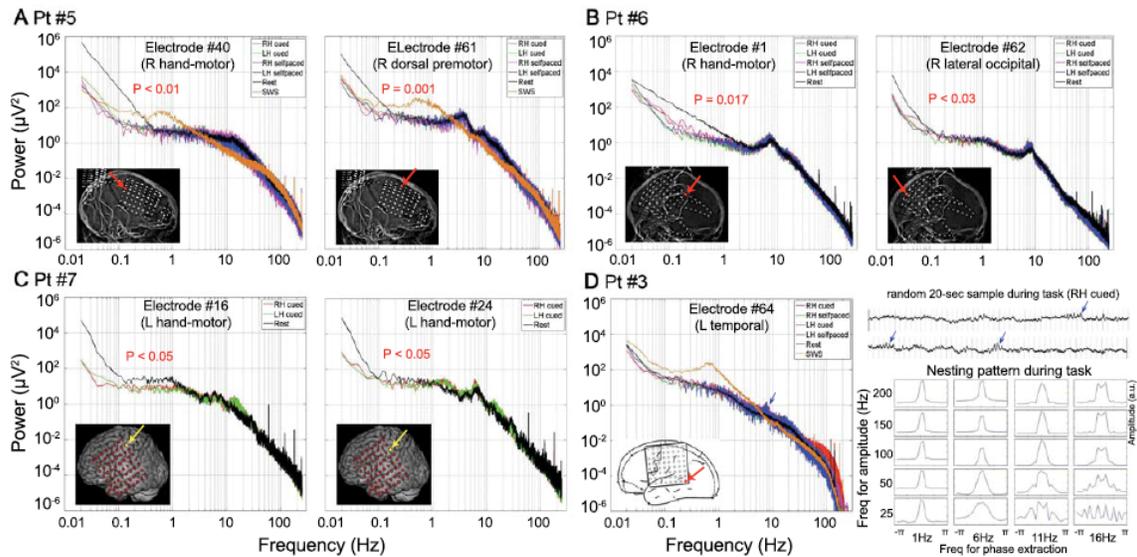
Figure 4 Changes of power-law distribution during task. (**A-C**) Power-law exponent changes during task performance in electrodes over task-relevant brain areas. The task consisted of a 2 × 2 design: visual-cued button press (cued) or self-paced button press (selfpaced); and the button press was performed by either the left (LH) or right (RH) index finger. Six example electrodes from three patients are shown. Five additional electrodes with significant alteration of power spectrum during task are shown in Fig. S4. Significance levels of the difference of power-law exponent between rest and task conditions are indicated in the graphs (t-tests). In Pt #5, SWS power spectrum was presented for comparison, but not used for statistical analysis. (**D**) Emergence of an oscillation from scale-free brain activity during task performance. Results are from electrode #64 in Pt #3, same as electrode #64 in Fig. 2.Left: Power spectra from the spontaneous awake state (black), SWS (orange), and four trial types of the task. An oscillatory peak at ~8 Hz emerges during all four task conditions (blue arrow). Top right: Randomly selected 20-sec raw data record during task performance. The presence of ~8 Hz oscillation is readily seen (arrows). Bottom right: Nested-frequency pattern for selected frequency pairs during task-performance (averaged across all task blocks), which are very similar to those during spontaneous awake state (see Fig. 2D). The location of all electrodes are shown by X-ray pictures (**A&B**), reconstructed image from anatomical MRI and CT scan (**C**) and clinical diagram (**D**). The electrodes whose power spectra are shown are indicated by red and yellow arrows.

In one of the electrodes that contained only scale-free brain activity spontaneously (electrode #64 in Pt #3, same as #64 in Fig. 2), we found an oscillation at ~8 Hz emerges during task performance, in all four trial types. This oscillatory activity can be seen in both the power spectrum and the raw data records (Fig. 4D). Nonetheless, the nested frequency patterns did not change (compare Fig. 4D bottom right graph to Fig. 2D, and

see Fig. S5 for 8-Hz phase modulation of higher frequencies during rest and task). Since our task contained no rhythmic structure, the emergence of this 8-Hz oscillation was not a result of entrainment by external stimuli, but rather reflected intrinsic properties of the underlying neural network.

Spontaneous fMRI Signal is also Scale-Free, and its Power-Law Exponent Varies Across Brain Regions

Next we tested whether the power-law exponent of scale-free brain activity was the same across brain regions. For this we utilized fMRI, which provides whole brain coverage, in contrast to the limited cortical surface coverage of ECoG electrodes. Resting-state fMRI (with visual fixation) was acquired in 17 consenting healthy volunteers in a 3T scanner. Each subject completed 4 fMRI runs, each run lasted 7 min.

A set of 31 regions of interest (ROIs) were obtained from previous works by the authors or published articles (see Table S2), among which there were 10 pairs of homologous brain regions. Other than three ROIs located outside the neocortex – hippocampus, cerebellum and thalamus, the remaining regions resided in five known brain networks (attention, default, motor, saliency, and visual) (Fox and Raichle, 2007).

For each ROI, the fMRI signal from each run was subjected to Fourier analysis to yield the power spectrum, which was then averaged across runs and across subjects, and power spectra from homologous brain regions were averaged together. The resultant power spectra, plotted in log-log coordinates in Fig. 5A, suggested that the spontaneous fMRI signal is also scale-free. The power-law exponents of the fMRI signals, obtained by a least squares fit, are listed in Table S2, with a mean of 0.69, which differed

significantly from the power-law exponents of ECoG signals (mean 1.84) (P < 0.0001). We note that the power-law exponent of ECoG signals was obtained from the < 0.1 Hz range, similar to the frequency range of the fMRI signal, and this low-frequency range of the ECoG signal, the slow cortical potential, has been shown to be a correlate of the fMRI signal (He and Raichle, 2009; He et al., 2008). Hence, the difference between ECoG and fMRI signal power-law exponent is curious, and its origin warrants future investigation (one potential factor being the constraints imposed by the neurovascular coupling mechanisms).

Intriguingly, the power-law exponent of the fMRI signal was found to differ between brain networks. The visual regions, the default network and the dorsal anterior cingulate cortex (dACC) had the steepest power spectra, characterized by the largest power-law exponent. On the contrary, the cerebellum, thalamus and hippocampus had the shallowest power spectra, characterized by the smallest power-law exponent. The motor and attention regions were in between. An ANOVA suggested that the effect of network on power-law exponent was highly significant ($F_{5,15}$ = 5.05, P = 0.006). In contrast, when the variances of the fMRI signal (see Table S2) instead of power-law exponents were entered into the ANOVA, no significant network effect was found. It is worth noting that the small power-law exponents of the cerebellum, thalamus and hippocampus reflected a proportionally smaller amount of low-frequency activity as compared to the neocortex, consistent with previous neurophysiological observations and their different anatomical structures (Bullock and Basar, 1988; He and Raichle, 2009).
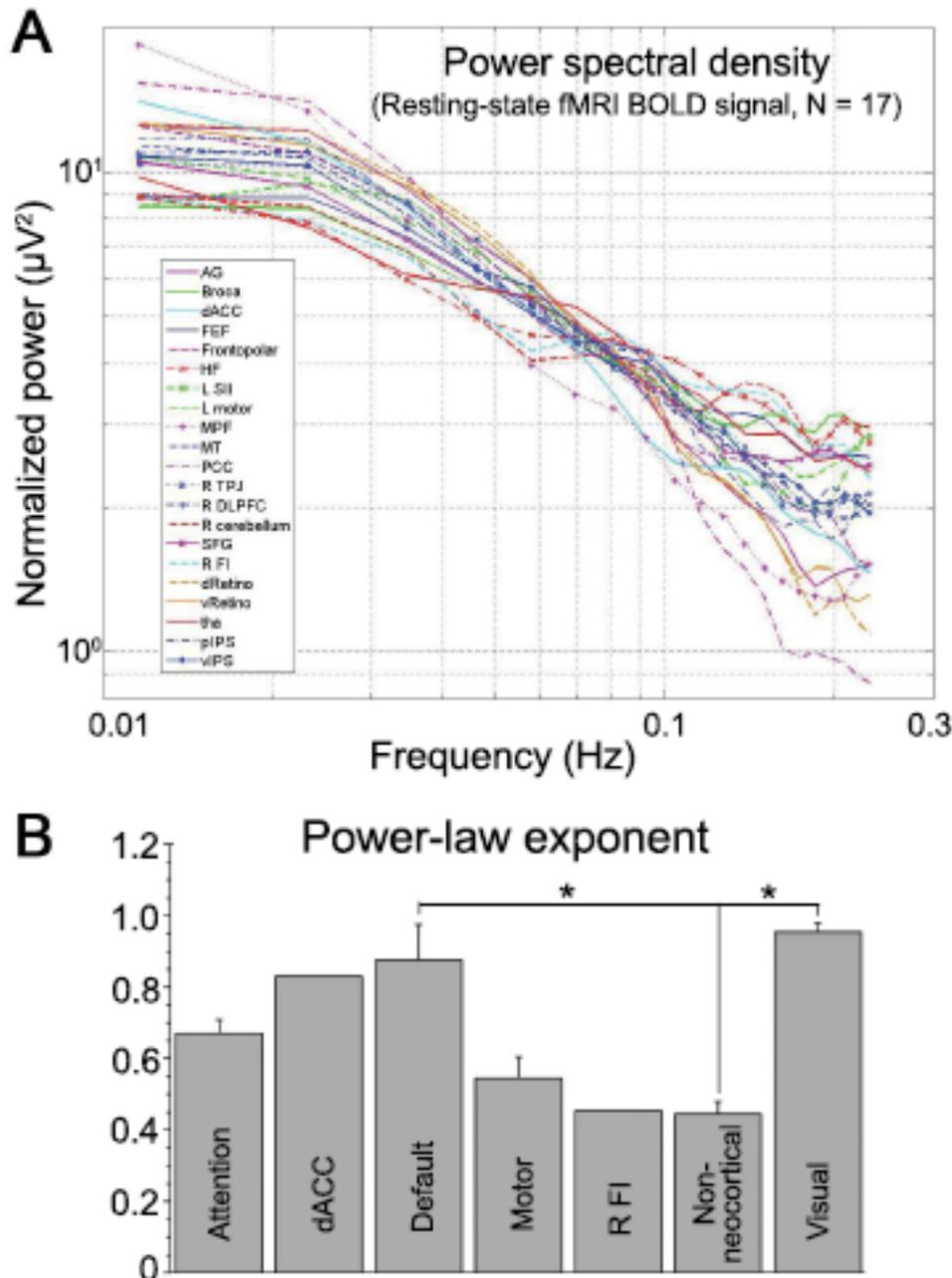
Figure 5 Power-law distribution of spontaneous fMRI signal. fMRI signal power spectrum was computed for 31 brain regions (10 pairs of homologous regions were each averaged together, for details see Table S2) in a resting-state fMRI data set from 17 young healthy volunteers. (**A**) Power spectrum (normalized by total variance) was averaged across all subjects for each brain region and plotted in a log-log plot. (**B**) Each power spectrum in (A) was fitted with a power-law function $P(f) \propto 1/f^{\beta}$. The exponent β was then averaged across brain regions in the same network (for mapping from region to network see Table S2). Error bars denote S.E.M. The two regions belonging to the saliency network, R FI and dACC, were plotted separately for visualization, given the wide difference between their exponents. The non-neocortical group includes the cerebellum, hippocampus and thalamus. The effect of network was highly significant

($F_{5,15} = 5.05$, $P = 0.006$). Using Tukey/Kramer post-hoc test, significant differences were found between the default network and the non-neocortical group, and between the visual and non-neocortical regions.

Control Recordings

Because fluctuations of resistivity in electronic conducting materials can also exhibit "1/f noise" (Weissman, 1988), it is important to demonstrate that our data were not contributed by instrument noise. Therefore, we conducted a dummy ECoG recording in a standard epilepsy in-patient monitoring room without the presence of a patient. Two types of recordings were performed over a duration of 46 min: in the first, a resistor was connected into the amplifier to record the internal noise in the recording system; in the second the circuit was left open to record the noise pattern in the room. The power spectrum from neither recording showed a power-law distribution (Fig. 7A). Our fMRI data were previously published in (Fox et al., 2007). In this study the authors acquired fMRI signals from a water phantom in the same scanner, the power spectrum of which was close to white noise (see Fig. S4 in (Fox et al., 2007)), which differs significantly from the power spectrum of fMRI signals recorded from the brain (see Fig. 5A herein and Fig. S4 in (Fox et al., 2007)).

Scale-Free Dynamics and Nested Frequencies in Earth Seismic Waves and Stock Market Fluctuations

The above results showing nested frequencies in brain ECoG activity raise the following question: Since the brain and many other natural processes all exhibit scale-free dynamics, and nested frequencies are present in brain activity, do other natural

processes that are characterized by "1/f noise" also contain nested frequencies? Hence, we conducted nested frequency analysis on spontaneous earth seismic waves (collected over 4 months) and the fluctuations of daily close price of Dow-Jones Industrial Average Index (collected over 80 years). Both earth seismic waves and stock market fluctuations exhibited scale-free dynamics and followed a power-law distribution in their temporal power spectrum (Fig. 6A). Moreover, the power-law exponents of both data types (2.1 for seismic waves and 1.9 for stock market) were close to that of the brain ECoG activity (mean 2.13 during awake state).

Intriguingly, both earth seismic waves and stock market fluctuations contained extensive nested frequencies (Fig. 6B). However, the exact pattern of nested frequencies in these signals differed from that in brain activity. For example, a bimodal nested – frequency distribution with two preferred phases is seldom seen in the ECoG signals (< 10% of all electrodes), but it was prominent in earth seismic waves. This bimodal distribution in earth waves might be due to different generators in the earth propagating to the same surface location; by contrary, the lack of a bimodal nested-frequency pattern in the ECoG signal might imply a more homogeneous source of generators. The observation that nested frequencies are prominent in these natural and economic scale-free dynamics reinforces the above conclusion that the widespread nested frequencies seen in the ECoG signals were contributed primarily by scale-free brain activity and not by isolated, periodic brain oscillations.
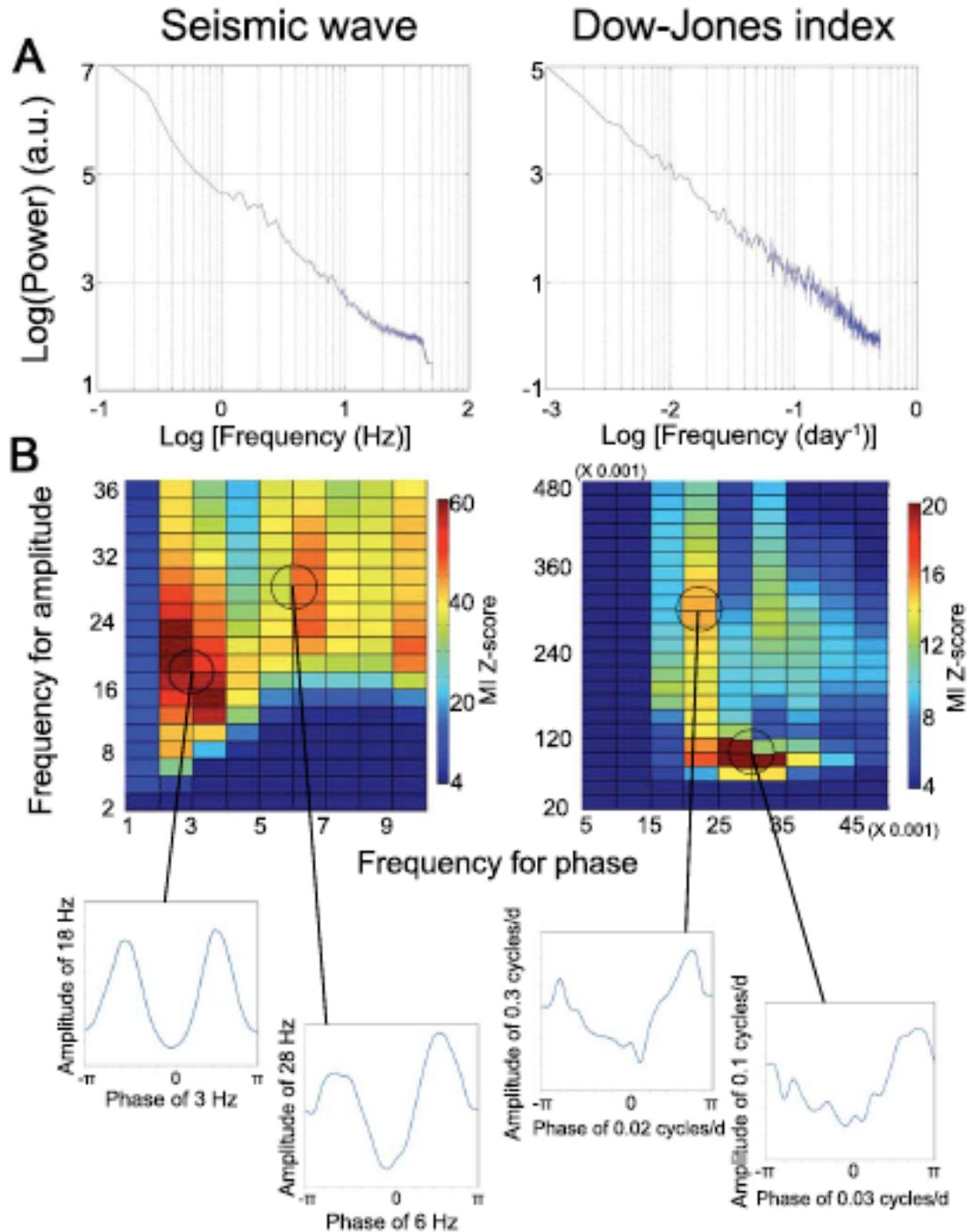
Figure 6 Power-law distribution and nested frequencies in earth seismic waves (left column) and stock market fluctuations (right column). (**A**) Power spectra plotted in a log-log plot. For seismic data, frequency is in Hz (cycle/sec). For stock market data, frequency is in cycle/day. The power-law exponent β for seismic and stock market data was 2.1 and 1.9 respectively.(**B**) **Top:** Phase-amplitude cross-frequency coupling assessed by MI Z-score, plotted as color in the 2-D frequency space. Only significant values (P < 0.05 after Bonferroni correction) are shown. **Bottom**: Example nested

frequency patterns for selected frequency pairs. Amplitude of the higher frequency was averaged at different phases of the lower frequency and plotted.

Simulations of Scale-Free Dynamics

Finally, to better understand the relationship between nested frequencies and scale-free dynamics, we constructed a few simulations of scale-free time series and examined whether they contained nested frequencies. All simulated time series were analyzed in a manner similar to the ECoG data for temporal power spectrum and nested frequencies.

First, a scale-free time series was constructed by filtering white noise (created by drawing independent samples from a zero-mean, unit-variance Gaussian distribution) in the frequency domain to yield a power-law distribution of $\log(P) \propto -\beta \log(f)$ ($\beta = 1.8$), while maintaining the random phase of the white noise. This spectrally generated scale-free time series with a power-law exponent close to that of brain ECoG activity did not contain any nested frequencies (Fig. 7B).

Second, because the power-law exponent of the ECoG signals was close to 2, which is typical of a random walk process (i.e., Brownian motion), we constructed a random walk model by summing over a white noise time series: $x(t) = x(t-1) + \varepsilon(t)$, where $\varepsilon(t)$ is the same white noise time series as used in Fig. 7B. To our surprise, this random walk process contained statistically significant nested frequencies (Fig. 7C). When we substituted the input white noise by drawing independent samples from a zero-mean, uniform distribution in the range [-0.5, 0.5), the resulted scale-free time series also had significant nested frequencies (Fig. 7D).
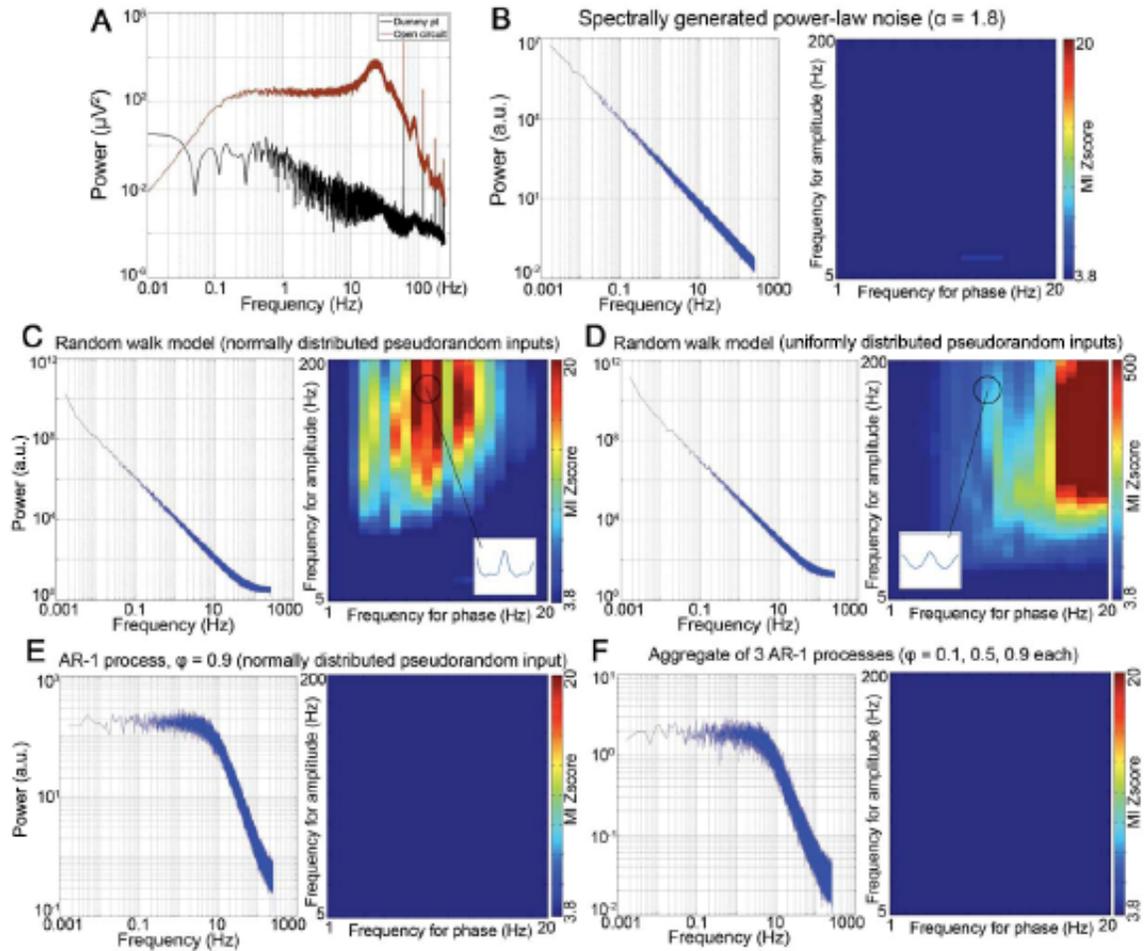
Figure 7 (**A**) Power spectrum of dummy recording conducted in a standard ECoG-video in-patient monitoring room (duration: 46 min). Black: a resistor was connected into the amplifier to record the internal noise in the recording system. Red: the circuit between the electrode and the reference ends of the amplifier was left open, in order to record the noise pattern in the room. Neither spectrum follows power-law distribution. (**B**) Power spectrum and the absence of nested frequency in a spectrally generated scale-free time series. First, a white noise time series was generated by drawing independent samples from a zero-mean, unit-variance Gaussian distribution. This time series was then filtered in the frequency domain by the function $P(f) \propto 1/f^{\beta}$ ($\beta = 1.8$), and inverse-Fourier transformed, then subjected to the same nested frequency analysis as the ECoG data. (**C**) Power spectrum and the presence of nested frequencies in a random-walk model: $x(t) = x(t\text{-}1) + \varepsilon(t)$, where $\varepsilon(t)$ is as in (B). (**D**) Power spectrum and the presence of nested frequencies in a random-walk model: $x(t) = x(t\text{-}1) + \varepsilon(t)$, where $\varepsilon(t)$ is a white noise time series generated by drawing independent samples from a uniform distribution in the range [-0.5, 0.5]. (**E**) Power spectrum and the absence of nested frequencies in an AR-1 process: $x(t) = \varphi x(t\text{-}1) + \varepsilon(t)$, where $\varphi = 0.9$ and $\varepsilon(t)$ is as in (B) and (C). (**F**) Power spectrum and the absence of nested frequencies in a time series generated by aggregating three first-order autoregressive (AR-1) processes: $x(t) = \sum_{i=1}^{3} [\varphi_i x_i(t\text{-}1) + \varepsilon_i(t)]$, where $\varphi_1 = 0.1$, $\varphi_2 = 0.5$, $\varphi_3 = 0.9$, and $\varepsilon_i(t)$ is normally distributed white noise as in (B) (C) and (E).

We then added a single parameter to the above random-walk model to change it into a first-order autoregressive (AR-1) process: $x(t) = 0.9\,x(t-1) + \varepsilon(t)$, where $\varepsilon(t)$ is the same white noise time series as used in Fig. 7B&C. The addition of this single parameter eliminated nested frequency patterns (Fig. 7E). Despite the seemingly small change in the model, an important difference between this AR-1 process and the random walk process in Fig. 7C is that the random walk process has long-range temporal dependence (also called "long memory", see discussions in (Linkenkaer-Hansen et al., 2001)) whereas the AR-1 process does not.

Lastly, we constructed a model of an aggregate of AR-1 processes (Fig. 7F). The approach of aggregating a few AR-1 processes to model scale-free dynamics (in a relatively restricted frequency range) has been used extensively in economics (Erland and Greenwood, 2007; Granger, 1980), and has been applied with considerable success to modeling the power-law distribution of psychological data, such as the fluctuations of reaction times in a decision making task (Wagenmakers et al., 2004; Ward, 2002). Contrary to our initial conjecture, such a model did not contain any statistically significant nested frequencies (Fig. 7F). Importantly, although a mixture of AR-1 processes could produce the appearance of "$1/f$ noise", such dynamics do not have genuine long-range temporal dependence (Wagenmakers et al., 2004).

It might be counterintuitive that a random-walk model contained structures. We suggest that this is because of the higher-order statistical regularities present in the arithmetic pseudorandom number generator used for generating white noise, which are invisible in most applications but produce interesting patterns under the sensitive nested

frequency analyses and when the modeled process contains long memory. Hence, it appears that the combination of even very weak structures in the underlying generative process and a long-range temporal dependence are sufficient to produce nested frequencies in scale-free dynamics.

We caution that the simulations constructed here constitute only a subset of all models that can give rise to scale-free dynamics (for reviews see (Bak, 1996; Frank, 2009; Mandelbrot, 1999; Ward and Greenwood, 2007; Weissman, 1988)) and it is certainly out of the scope of the present paper to exhaust these models, without which the above tentative conclusion that long memory is crucial for nested frequencies to emerge in scale-free dynamics remains of a limited scope.

Discussion

In summary, we have shown that, contrary to common assumption, the arrhythmic, scale-free activity, which makes up a significant portion of the spontaneous field potentials recorded from the brain, contains a rich temporal organization with phase of lower frequencies modulating amplitude of higher frequencies in an upward progression across the frequency spectrum. Moreover, these nested frequency patterns varied across electrodes. Importantly, the power-law exponent of scale-free brain activity is modulated by task performance in a brain-network-specific fashion, suggesting a potential functional significance. We further show that power-law exponent of spontaneous fMRI signal varied across brain regions, being largest in visual and default-network regions and smallest in cerebellum, thalamus and hippocampus. Other scale-free dynamics in nature, such as earth seismic waves and stock market fluctuations, also

contained extensive nested frequencies, whose exact patterns differed from that of brain activity. Hence, it appears that different mechanisms in a variety of systems can give rise to scale-free dynamics (Frank, 2009), but the fine temporal structures in these dynamics, such as nested frequencies, differ across systems, possibly a footprint of the different underlying generating mechanisms (Fig. 8).
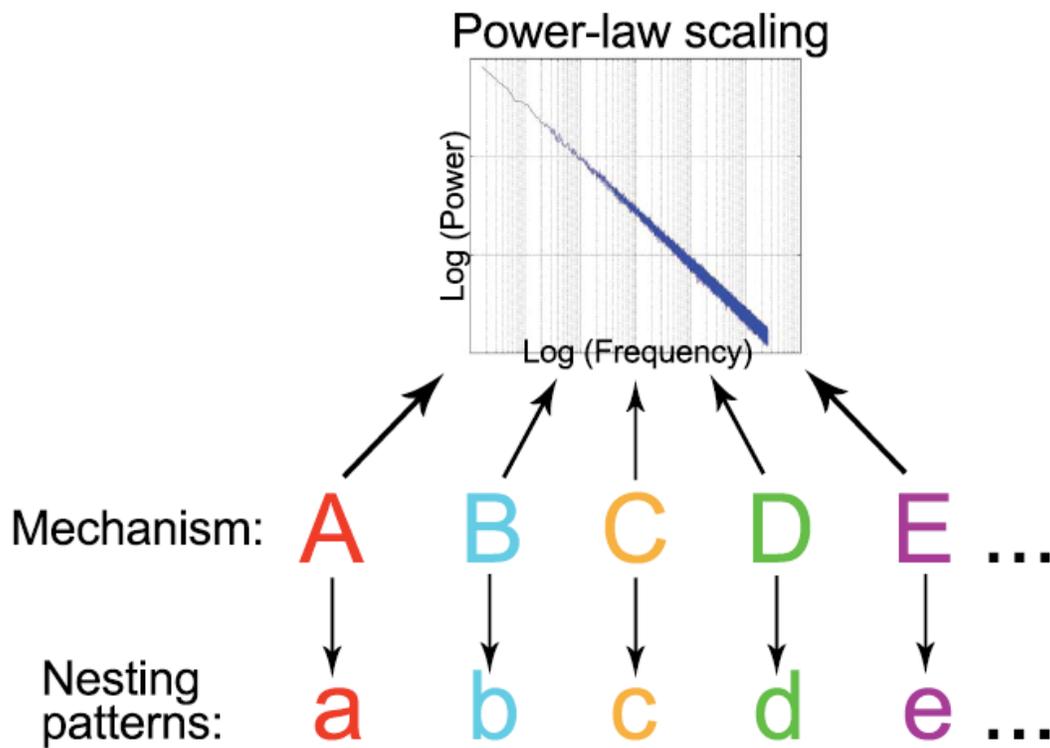
Figure 8 A general picture emerging from the present results. Different mechanisms in a variety of systems – including the human brain, earth seismic activity, stock market, and simulated long-memory processes – can all give rise to scale-free signals exhibiting $1/f^{\beta}$ power spectrum, but these different signals have different nested-frequency patterns. Hence, the different nested-frequency patterns might be thought of as footprints of the different underlying generating mechanisms, even when the gross property of the power spectrum is similar across these systems.

These results suggest that investigations on scale-free brain activity should go beyond characterizing the gross $1/f^{\beta}$ power spectrum, and aim at revealing the fine spatiotemporal structures and functional meanings in these signals. We strongly

encourage future empirical and theoretical work to bring the arrhythmic, scale-free brain activity together with the rest of ongoing electrophysiological brain research, such as brain oscillations and EEG event-related potentials.

The Interpretation of Nested Frequencies in Scale-Free Dynamics

Whereas the interpretation of nested brain oscillations is relatively straightforward (Jensen and Colgin, 2007; Schroeder and Lakatos, 2009), that of nested frequencies in scale-free brain activity is less intuitive. In general, nested frequencies in scale-free dynamics should also mean that at a particular phase of the lower-frequency fluctuation, such as its trough or peak, the amount of higher frequency activity increases. For example, the troughs of surface recorded slow cortical potentials are known to index increased cortical excitability and are correlated with increased amount of higher frequencies (Birbaumer et al., 1990; He and Raichle, 2009; Rockstroh et al., 1989; Vanhatalo et al., 2004). This is in line with comments on "1/f noise" in the physics literature suggesting that perturbations at long wavelength cause energy dissipations at all length scales (Bak et al., 1987). Furthermore, the non-random distribution of preferred phase of the lower frequency in our data (Figs. 3 & S2), which clustered around either trough or peak of the lower frequency, is indicative of the underlying neurobiological mechanisms.

Nonetheless, as pointed out by Kramer et al. (Kramer et al., 2008), complex waveforms such as edges or triangular waves could also produce significant results in nested frequency analysis. While artifacts in EEG recordings can certainly create sharp edges, we emphasize that an artifact-free EEG record (such as electrode #64 in Fig. 2C)

is also full of complex waveforms that are non-sinusoidal, indeed waveforms that make up the "1/f noise". These complex waveforms produced by the brain should not be considered artifact or noise because they do not fit in an oscillation-centric view of the brain, and their functional meaning deserves future investigation. Our view is similar to that of Bullock et al.(2003), who suggested that "the wide-band, apparently stochastic background activity in the EEG may in part consist of structured events or sequences, as in speech or music", and "one is compelled to presume that the power spectrum is an inadequate descriptor, as it would be for speech or music". Under this view, the scale-free brain activity most likely plays an important role in the brain's operation, and one important goal for future work is to crack the code contained therein. We would not be surprised if new mathematical tools will have to be developed before this goal is within reach. The present study, by showing unique nested-frequency patterns in different systems, all hiding beneath a similar $1/f^\beta$ power spectrum, constitutes an initial, modest step toward this direction.

The Genesis of Scale-Free Brain Activity

The power-law distribution is a common attractor distribution that can emerge out of many different generative mechanisms (Frank, 2009), and a variety of different models have been built which give rise to scale-free dynamics (for reviews see (Bak, 1996; Frank, 2009; Mandelbrot, 1999; Ward and Greenwood, 2007; Weissman, 1988)). It would be out of the scope of the present paper to exhaustively discuss existing models on scale-free dynamics (denoted also as $1/f^\beta$ noise from here on). Thus, we focus on

potential neurobiological mechanisms that might underlie scale-free field potentials recorded from the brain.

One obvious candidate is the $1/f^{\beta}$ noise present in neurotransmitter release (Lowen et al., 1997) and neuronal spike trains (Gisiger, 2001; Gruneis et al., 1989; Takahashi et al., 2004; Yamamoto, 1991). However, since these phenomena remain isolated observations (we urge more systematic investigations on them), they might not be sufficient to account for the ubiquitous scale-free dynamics in EEG or LFP recordings, and a brain-network perspective is likely also important.

Notably, functional brain networks extracted from voxel-by-voxel spontaneous fMRI signal correlations have a connectivity distribution that follows power-law scaling with an exponent close to 2, suggesting a scale-free network topology (Eguiluz et al., 2005; van den Heuvel et al., 2008). Furthermore, the geometry of axonal and dendritic trees exhibits self-similarity and scale-invariance properties (Bok, 1959; Freeman, 2007). While an important future direction in complexity science concerns the bridging of complex networks with complex dynamics (Barabasi, 2009) and the relation between scale-free and small-world networks remains an area of active research (Bullmore and Sporns, 2009), we here tentatively propose that scale-free brain electrical field potentials could be produced by random, Poission-like spike trains propagating through scale-free brain networks, and that the addition of inhibitory neurons introduces a time constant to the network and thus produces periodic brain oscillations added to the scale-free brain activity (another mechanism of producing oscillations is cellular pacemakers). In line with recent neurophysiological observations (Logothetis et al., 2007), this mechanism does not involve frequency-dependent cortical tissue filtering of field potentials. While

our proposal remains to be tested explicitly, it is consistent with recent results from optogenetic manipulations showing that activation of fast-spiking interneurons selectively amplifies gamma oscillations and activation of pyramidal neurons amplifies lower frequencies, the profile of which resembled $1/f^{\beta}$ noise (see Fig. 3d in (Cardin et al., 2009)). This proposal is also consistent with recent models of brain networks (Freeman and Zhai, 2009; Thivierge and Cisek, 2008). In Freeman and Zhai (2009), Poission-like spike trains were convolved with an impulse response function representing dendritic response and summed, the result was scale-free dynamics similar to that recorded by ECoG. Moreover, addition of inhibitory neurons introduced narrow-band oscillations that appeared as local peaks above the $1/f^{\beta}$ distribution in the power spectrum. Similarly, in Thivierge and Cisek (2008), arrhythmic network spikes were shown to be a direct result of heterogeneity among modeled pyramidal neurons, and the addition of inhibitory pathways introduced higher-frequency activities. This model also elegantly showed that global synchronization can emerge out of arrhythmic activity and that neuronal spikes have long memory – a hallmark of scale-free dynamics.

An influential model of "$1/f$ noise" is the self-organized criticality (SOC) theory (Bak, 1996; Bak et al., 1987), which has been applied extensively to simulate brain networks (Shin and Kim, 2006), neuronal avalanches and "$1/f$ noise" (de Arcangelis et al., 2006; Levina et al., 2007; Lin and Chen, 2005). Although the SOC theory might be more suited to describe neuronal avalanches (Petermann et al., 2009), in our view, convincing evidence suggesting that it is the underlying mechanism giving rise to the "$1/f$ noise" in raw EEG/LFP records is still lacking. Moreover, the SOC theory emphasizes the power-law exponent being close to 1, which is rarely met in empirical

electrophysiological recordings (Fig. 1, also see (Freeman and Zhai, 2009; Miller et al., 2007; Milstein et al., 2009)). Nonetheless, the recent extension of the SOC theory to include a broader range of power-law exponents (De Los Rios and Zhang, 1999) might aid in expanding its explanatory power.

Lastly, the relation between scale-free brain activity investigated herein and neuronal avalanches manifested in negative LFP (nLFP) peaks (Plenz and Thiagarajan, 2007) is worthy of future investigation. Although it was commented that the power-law distribution of nLFPs was not predicted by the $1/f^{\beta}$ noise in raw LFP traces (Petermann et al., 2009), given that both phenomena are extrapolated from the same brain records, a relationship between them would be illuminating. Since neuronal avalanches are specific to superficial layers of the cortex (Stewart and Plenz, 2006), a first step might be to investigate whether the $1/f^{\beta}$ noise in raw LFP traces has any heterogeneity across cortical layers. Surprisingly, we are not aware of any published record on this, and urge such a systematic investigation, which would not only shed light onto the potential relationship between $1/f^{\beta}$ noise and neuronal avalanches, but also be informative on the mechanisms underlying $1/f^{\beta}$ noise itself.

Implications for Psychology and Cognitive Sciences

$1/f^{\beta}$ noise is widely present in the fluctuations of human cognitive and behavioral performances (Gilden, 2001). Because the brain evolved through organisms' struggles in coping with the external world and its main function is to proactively act upon the world through its sense and motor organs for the sake of the organism's survival, it is hardly surprising that the statistical properties of the brain's dynamics reflect the statistical

properties of the environment and the universally present scale-invariance thereof; and in turn it is hardly surprising that the cognition and behavior as well as music produced by the human brain follow the same statistical properties. Indeed, several most established psychological laws applicable across domains and species, including Weber's law, can be derived simply from a scale-free principle (Buzsaki, 2006; Chater and Brown, 1999). In line with our results showing that the power-law exponent decreased (i.e., the slope of the power spectrum becomes shallower) during task performance in activated brain regions, it was found that the slope of $1/f^{\beta}$ noise in the fluctuations of reaction times during working memory and decision making tasks varied parametrically with task difficulty, being steepest for easiest tasks and shallower as the task difficulty increased (Clayton and Frey, 1997; Ward, 2002). Lastly, given that the power-law exponent of spontaneous ECoG signal was close to 2 (Fig. 1, also see (Freeman and Zhai, 2009; Miller et al., 2007; Milstein et al., 2009)), it is of interest to note that the power spectra of some cartoons are approximately $1/f^{1}$, whereas those of "realistic" paintings and photographs are close to $1/f^{2}$, and impressionist paintings have spectra somewhere in between (Balboa and Grzywacz, 2003; Ward, 2002).

Conclusions

By showing fine temporal structures within and potential functional significance of the scale-free brain activity, our results draw attention to the arrhythmic, scale-free brain activity, and emphasize the importance of investigating its fine spatiotemporal patterns and functional meanings beyond the mask of its $1/f^{\beta}$ power spectrum. These

results strongly encourage incorporating the arrhythmic brain activity, so prevalent in

electrophysiological recordings, into both empirical research and theoretical frameworks.

Supplementary Data
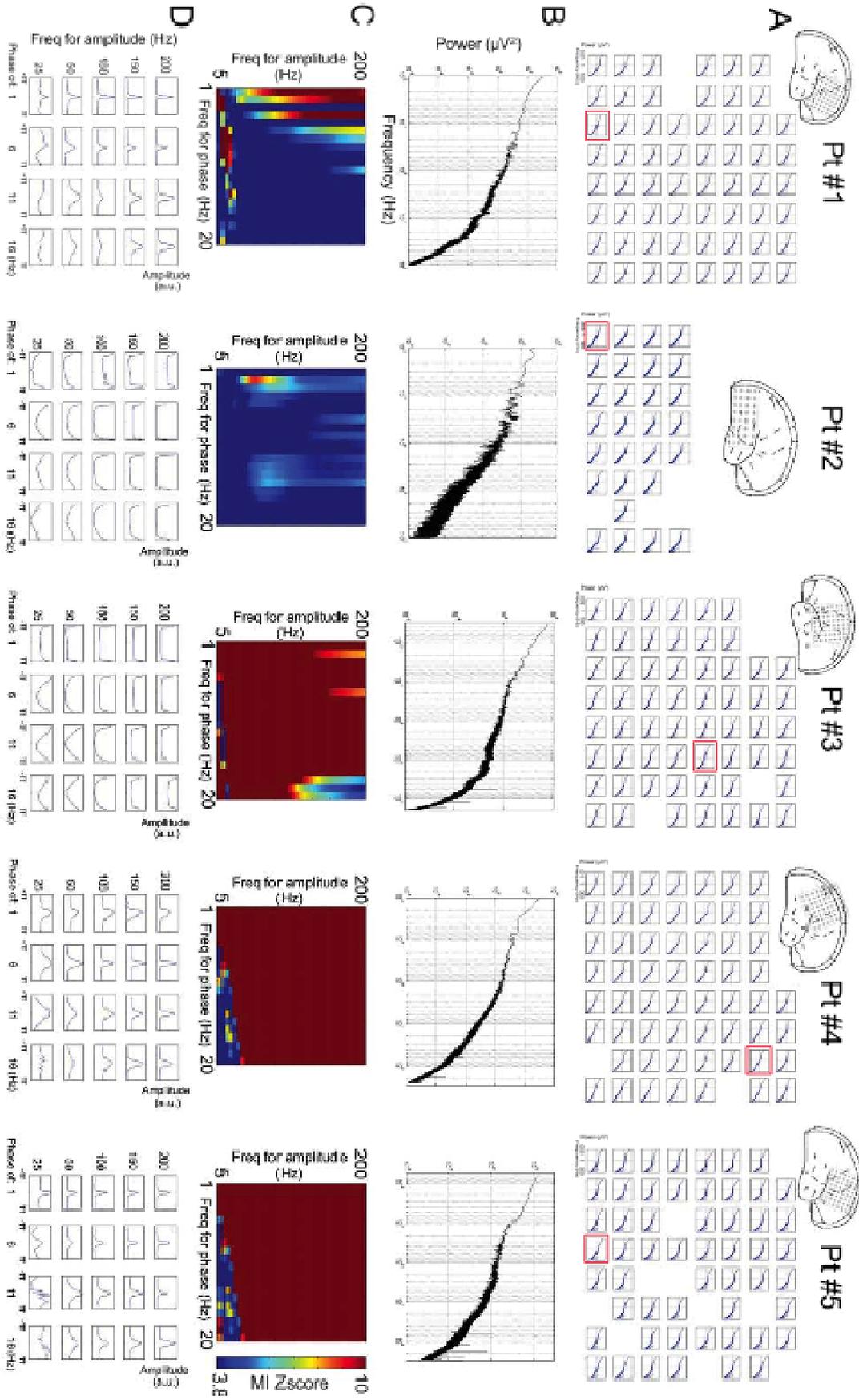
Fig. S1 Waking power spectra from all electrodes and example nested frequency patterns in Patients #1 through #5 (each patient in a separate column). (**A**) Power spectra of waking ECoG data from every electrode, aligned to the electrode's position in the 2-D electrode grid. Bad electrodes are eliminated. The orientation and position of the electrode grid on the cortical surface is indicated in the top diagram. Red squares indicate the representative electrode selected in each patient for analyses in (B) to (D). (**B**) Waking ECoG power spectrum plotted in log-log coordinates for the example electrode. (**C**) Cross-frequency phase-amplitude coupling in each example electrode. Phase was extracted in 1-Hz-width bands centered at 1, 2, … 20 Hz. Amplitude was extracted from 5-Hz-width bands centered at 5, 10, … 200 Hz. Color plots the strength of cross-frequency coupling as indexed by MI Z-score. Only significant values ($P<0.05$ after Bonferroni correction) are shown. (**D**) Nested-frequency patterns for selected frequency pairs in each example electrode. Amplitude of the higher frequencies (25, 50, 100, 150, 200 Hz) was averaged at different phases of the lower frequencies (1, 6, 11, 16 Hz) and plotted. Phase $\pm\pi$ corresponds to the trough (surface negativity), and phase 0 corresponds to the peak (surface positivity) of the lower-frequency fluctuation.
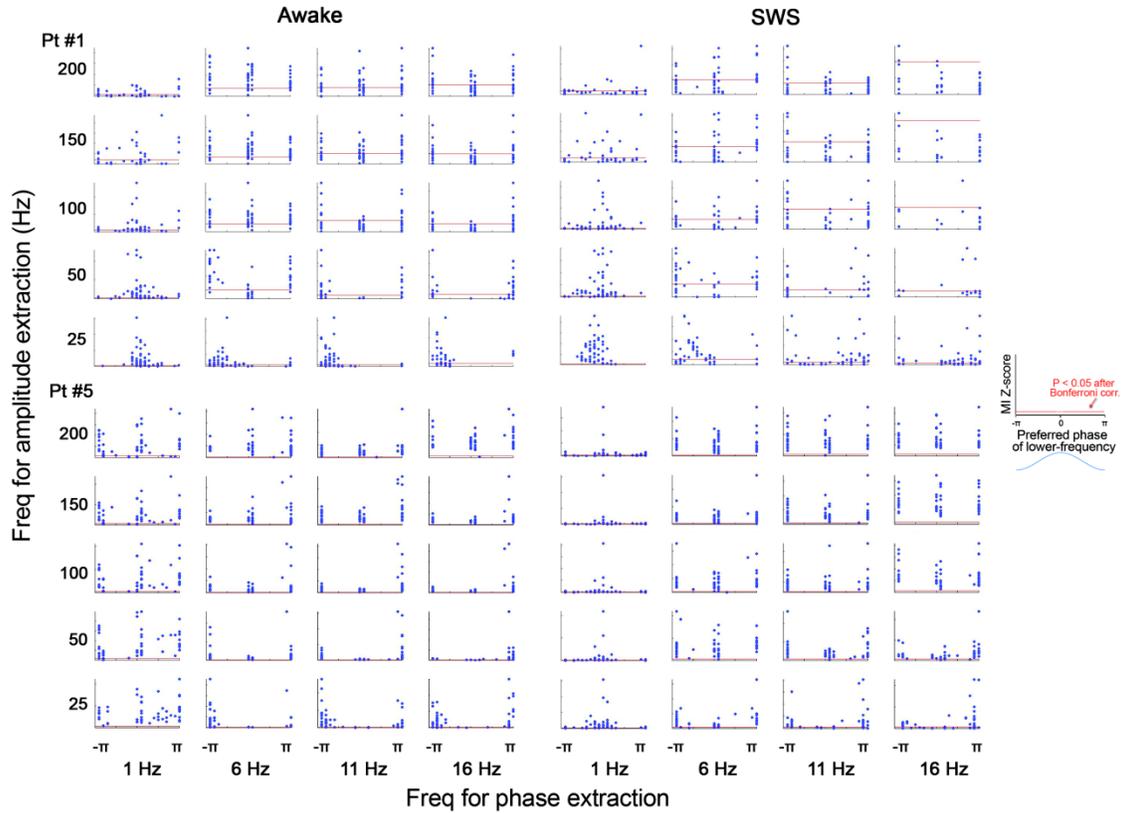
Fig. S2 Complement to Fig. 3A, nested frequency patterns from patients #1 (top) and #5 (bottom). Phase was extracted from 1-Hz-width bands centered at 1, 6, 11, and 16 Hz. Amplitude was extracted from 5-Hz-width bands centered at 25, 50, 100, 150, 200 Hz. For each frequency pair, the subplot shows a scatter-plot of all electrodes, each represented by one dot. The ordinate value shows the cross-frequency coupling strength indexed by MI Z-score. The red horizontal line indicates significance level (P < 0.05 after Bonferroni correction). The abscissa value shows the preferred phase of the lower frequency, i.e., the phase of the lower-frequency fluctuation at which the amplitude of the higher frequency is the largest. Phase ±π corresponds to the trough (surface negativity), and phase 0 corresponds to the peak (surface positivity) of the lower-frequency fluctuation. Patient #2 was not used in this analysis because of the lesser number of electrodes.

177
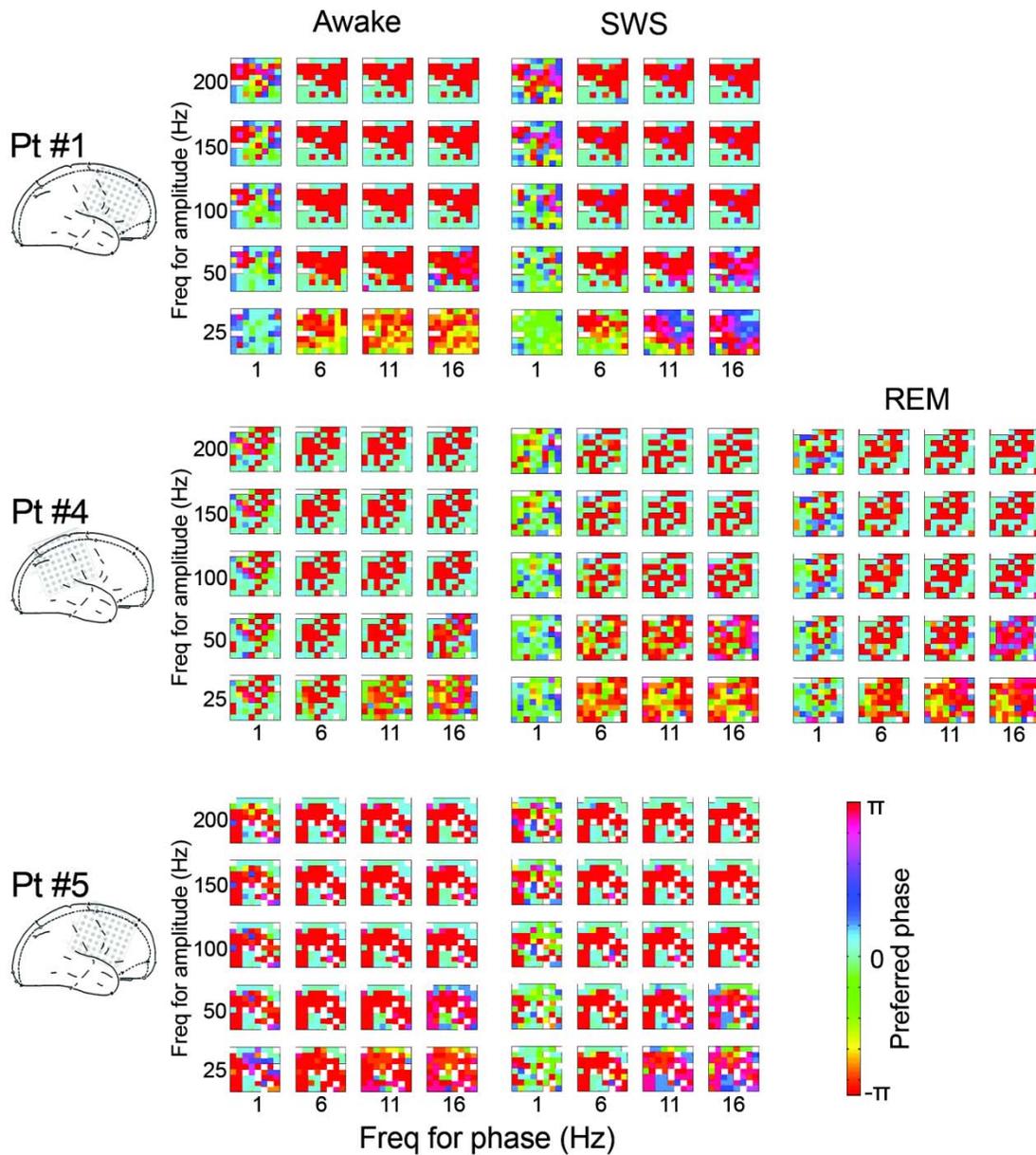
Fig. S3 Complement to Fig. 3B, results from Patients #1, #4, and #5. For each frequency pair (phase from 1, 6, 11 and 16 Hz; amplitude from 25, 50, 100, 150, and 200 Hz),the preferred phase of the lower frequency in each electrode was plotted as color on a 2-D representation of the 8 ×8 electrode grid. The orientation and location of this grid on the cortical surface is shown in the diagram to the left. The white cells in the grids are bad electrodes that have been eliminated from all analyses. Patient #2 was not used in this analysis because of the lesser number of electrodes.
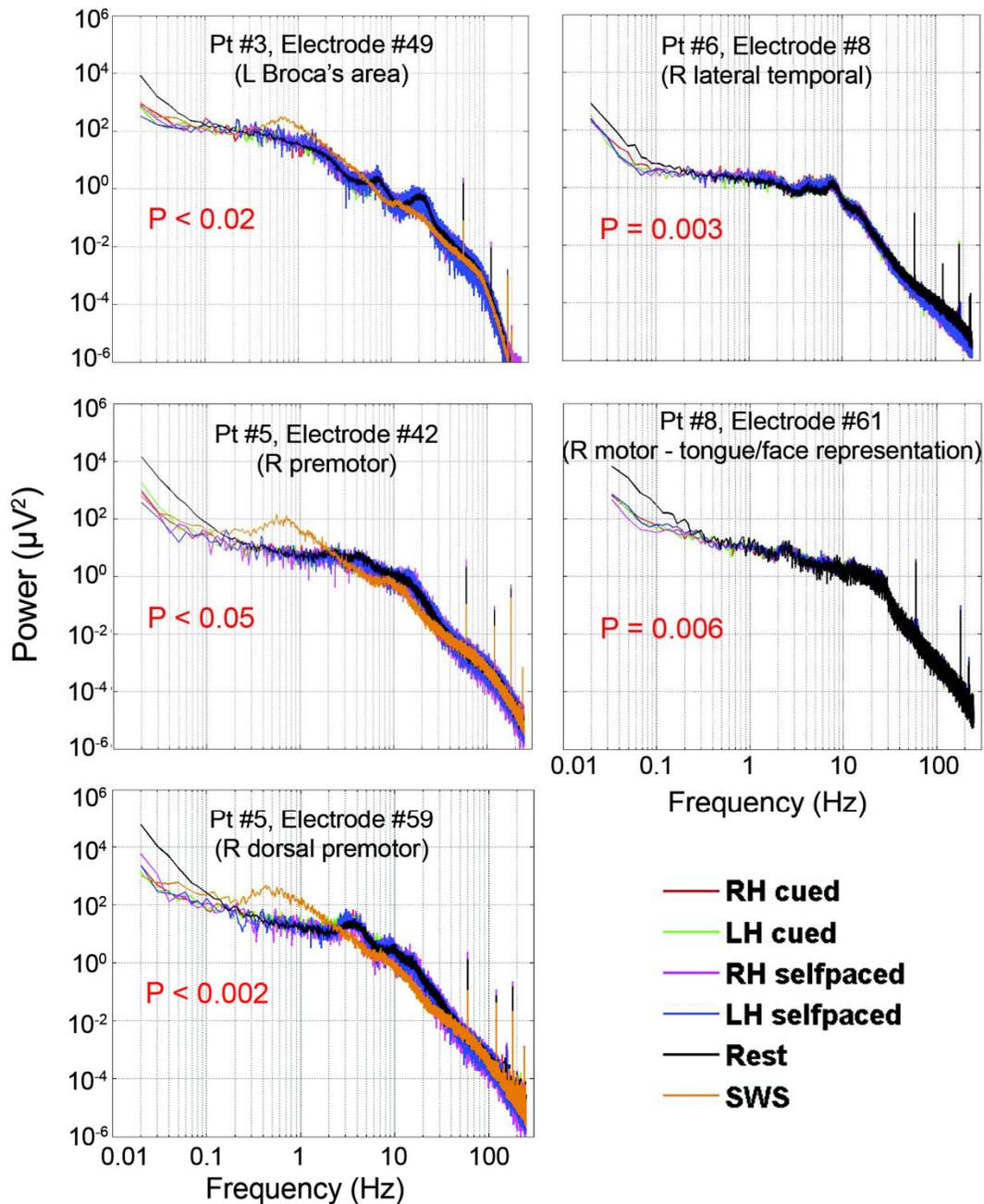
Fig. S4 Complement to Fig. 4A-C, power-law exponent changes during task performance. The task consisted of a 2 × 2 design: visual-cued button press (cued) or self-paced button press (selfpaced); and the button press was performed by either the left (LH) or right (RH) index finger. Significance levels of the difference of power-law exponent between rest and task conditions are indicated in the graphs (t-tests). In Pt #3&#5, SWS power spectrum was presented for comparison, but not used for statistical analysis. The anatomical locations of each electrode are indicated in the graphs.
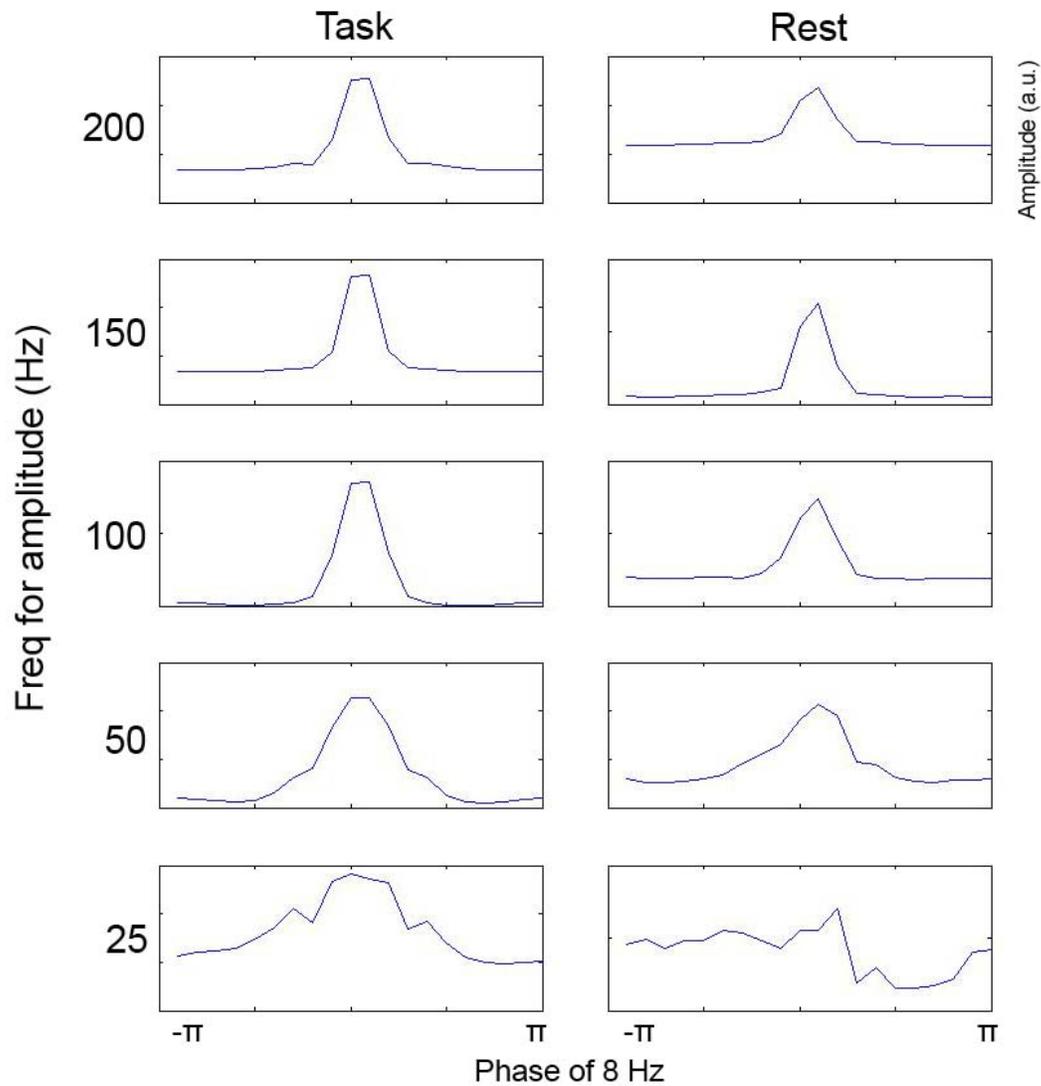
Fig. S5 Complement to Fig. 4D, results from electrode #64 in Patient #3. Amplitude of 5-Hz-width bands centered at 25, 50, 100, 150 and 200 Hz were each averaged at different phases of 8-Hz fluctuation (extracted from a 1-Hz-width band). Phase 0 corresponds to peak of 8-Hz activity; phase $\pm\pi$ to trough of 8-Hz activity. The left column was from ECoG data during task performance, averaged across all task blocks. The right column was from spontaneous ECoG signals in the awake state.

180

Table S1. Demographic, clinical and data collection information of the patients.

Pt.	Age	Gender	Handed-ness	Seizure type	Seizure focus	Total length of spontaneous ECoG data (min)			Collection of task ECoG data (No. of task blocks completed, each block ~ 5 min)				SR (Hz)	No. of usable electrodes
						Awake	SWS	REM	LH cued	RH cued	LH self-paced	RH self-paced		
#1	12	M	R	Complex partial	R inferior frontal	30	20						2000	60
#2	8	M	R	Complex partial	R basal temporal and mesial occipital	19	12						1000	28
#3	16	M	R	Complex partial	L frontal	83	69		2	2	1	2	500	58
#4	9	F	R	Complex partial	R somatosensory	69	28	30					1000	59
#5	28	F	R	Complex partial	R frontal	28	24		1	1	1	1	1000	54
#6	59	F	L	Complex partial	R inferior lateral parietal	33			3	3	3	3	1000	62
#7	45	F	R	Complex partial	L temporal	15			3	3			1000	64
#8	58	F	R	Complex partial	L frontal	5			2	2	2	2	1000	56

Pt., Patient; SR, sampling rate.

Table S2. Brain regions used for fMRI data analysis in Fig. 5

Region	full name	Network	Power-law exponent	Variance	Talairach coordinates/References
FEF	(L and R) frontal eye field	attention	0.507	7.637235	-26, -9, 48 & 32, -9, 48 (He et al., 2007)
MT	(L and R) middle temporal region	attention	0.685	9.387676	-43, -70 -3 & 42 -68 -6 (He et al., 2007)
R TPJ	R temporoparietal junction	attention	0.709	11.15353	49, -50, 28 (He et al., 2007)
R DLPFC	R dorsolateral prefrontal cortex	attention	0.693	11.44678	43, 22, 34 (Dosenbach et al., 2006)
pIPS	(L and R) posterior intraparietal sulcus	attention	0.766	14.6165	-25, -63, 47 & 23 -65 48 (He et al., 2007)
vIPS	(L and R) ventral intraparietal sulcus	attention	0.676	6.940647	-24, -69, 30 & 30, -80, 16 (He et al., 2007)
AG	(L and R) angular gyrus	default	0.898	14.24665	-51, -54, 30 & 45, -66, 27 (Shulman et al., 1997)
FP	frontopolar cortex	default	0.777	6.981706	-3, 45, 36 (Shulman et al., 1997)
MPF	medial prefrontal cortex	default	0.969	22.73547	-6, 51, -9 (Shulman et al., 1997)
PCC	Posterior cingulate cortex	default	1.164	28.97818	-6, -45, 33 (Shulman et al., 1997)
SFG	(L and R) superior frontal cortex	default	0.573	7.268529	-15, 33, 48 & 18, 27, 48 (Shulman et al., 1997)
Broca	Broca's area	motor	0.436	6.447941	-42, 13, 14
L SII	L parietal operculum	motor	0.639	9.27823	-57, -27, 21

L motor	L primary motor cortex	motor	0.557	5 7.856588	-39, -27, 48
dACC	dorsal anterior cingulate cortex	saliency	0.831	21.58818	-1, 10, 46 (Dosenbach et al., 2006)
R FI	R frontoinsular cortex	saliency	0.454	14.60935	36, 21, -6 (Seeley et al., 2007)
HF	(L and R) hippocampal formation	Non-neocortical	0.414	20.77979	-21, -25, -14 & 23, -23, -14 (Vincent et al., 2007)
R cerebellum	R cerebellum	Non-neocortical	0.413	6.481176	21, -54, -21
tha	(L and R) thalamus	Non-neocortical	0.513	7.751618	-15, -21, 6 & 9, -18, 9
d Retino	(L and R) dorsal retinal region	visual	0.981	10.08076	-6, -75, 9 & 9, -75, 12
v Retino	(L and R) ventral retinal region	visual	0.924	5.991588	-15, -75, -9 & 15, -75, -9

References for Table S2:

Dosenbach, N.U., Visscher, K.M., Palmer, E.D., Miezin, F.M., Wenger, K.K., Kang, H.C., Burgund, E.D., Grimes, A.L., Schlaggar, B.L., and Petersen, S.E. (2006). A core system for the implementation of task sets. Neuron *50*, 799-812.

He, B.J., Snyder, A.Z., Vincent, J.L., Epstein, A., Shulman, G.L., and Corbetta, M. (2007). Breakdown of functional connectivity in frontoparietal networks underlies behavioral deficits in spatial neglect. Neuron *53*, 905-918.

Seeley, W.W., Menon, V., Schatzberg, A.F., Keller, J., Glover, G.H., Kenna, H., Reiss, A.L., and Greicius, M.D. (2007). Dissociable intrinsic connectivity networks for salience processing and executive control. J Neurosci *27*, 2349-2356.

Shulman, G.L., Fiez, J.A., Corbetta, M., Buckner, R.L., Miezin, F.M., Raichle, M.E., and Petersen, S.E. (1997). Common blood flow changes across visual tasks: II. Decreases in cerebral cortex. Journal of Cognitive Neuroscience *9*, 648-663.

Vincent, J.L., Patel, G.H., Fox, M.D., Snyder, A.Z., Baker, J.T., Van Essen, D.C., Zempel, J.M., Snyder, L.H., Corbetta, M., and Raichle, M.E. (2007). Intrinsic functional architecture in the anaesthetized monkey brain. Nature *447*, 83-86.

References

Bak, P. (1996). How nature works (New York: Springer).

Bak, P., Tang, C., and Wiesenfeld, K. (1987). Self-organized criticality: An explanation of the 1/f noise. Phys Rev Lett *59*, 381-384.

Balboa, R.M., and Grzywacz, N.M. (2003). Power spectra and distribution of contrasts of natural images from different habitats. Vision Res *43*, 2527-2537.

Barabasi, A.L. (2009). Scale-free networks: a decade and beyond. Science *325*, 412-413.

Berger, H. (1929). Uber das Elektroenkephalogramm des Menschen. Arch. Psyhiatr. Nervenkr. *87*, 527-570.

Birbaumer, N., Elbert, T., Canavan, A.G., and Rockstroh, B. (1990). Slow potentials of the cerebral cortex and behavior. Physiol Rev *70*, 1-41.

Bok, S.T. (1959). Histonomy of the Cerebral Cortex (Amsterdam: Elsevier).

Bragin, A., Jando, G., Nadasdy, Z., Hetke, J., Wise, K., and Buzsaki, G. (1995). Gamma (40-100 Hz) oscillation in the hippocampus of the behaving rat. J Neurosci *15*, 47-60.

Buiatti, M., Papo, D., Baudonniere, P.M., and van Vreeswijk, C. (2007). Feedback modulates the temporal scale-free dynamics of brain electrical activity in a hypothesis testing task. Neuroscience *146*, 1400-1412.

Bullmore, E., Fadili, J., Maxim, V., Sendur, L., Whitcher, B., Suckling, J., Brammer, M., and Breakspear, M. (2004). Wavelets and functional magnetic resonance imaging of the human brain. Neuroimage *23 Suppl 1*, S234-249.

Bullmore, E., Long, C., Suckling, J., Fadili, J., Calvert, G., Zelaya, F., Carpenter, T.A., and Brammer, M. (2001). Colored noise and computational inference in

neurophysiological (fMRI) time series analysis: resampling methods in time and wavelet domains. Hum Brain Mapp *12*, 61-78.

Bullmore, E., and Sporns, O. (2009). Complex brain networks: graph theoretical analysis of structural and functional systems. Nat Rev Neurosci *10*, 186-198.

Bullock, T.H., and Basar, E. (1988). Comparison of ongoing compound field potentials in the brains of invertebrates and vertebrates. Brain Res *472*, 57-75.

Bullock, T.H., McClune, M.C., Achimowicz, J.Z., Iragui-Madoz, V.J., Duckrow, R.B., and Spencer, S.S. (1995). Temporal fluctuations in coherence of brain waves. Proc Natl Acad Sci U S A *92*, 11568-11572.

Bullock, T.H., McClune, M.C., and Enright, J.T. (2003). Are the electroencephalograms mainly rhythmic? Assessment of periodicity in wide-band time series. Neuroscience *121*, 233-252.

Buzsaki, G. (2006). Rhythms of the Brain. (New York, NY: Oxford University Press), pp. 111-135.

Buzsaki, G., Buhl, D.L., Harris, K.D., Csicsvari, J., Czeh, B., and Morozov, A. (2003). Hippocampal network patterns of activity in the mouse. Neuroscience *116*, 201-211.

Canolty, R.T., Edwards, E., Dalal, S.S., Soltani, M., Nagarajan, S.S., Kirsch, H.E., Berger, M.S., Barbaro, N.M., and Knight, R.T. (2006). High gamma power is phase-locked to theta oscillations in human neocortex. Science *313*, 1626-1628.

Cardin, J.A., Carlen, M., Meletis, K., Knoblich, U., Zhang, F., Deisseroth, K., Tsai, L.H., and Moore, C.I. (2009). Driving fast-spiking cells induces gamma rhythm and controls sensory responses. Nature *459*, 663-667.

Chater, N., and Brown, G.D. (1999). Scale-invariance as a unifying psychological principle. Cognition *69*, B17-24.

Chrobak, J.J., and Buzsaki, G. (1998). Gamma oscillations in the entorhinal cortex of the freely behaving rat. J Neurosci *18*, 388-398.

Clauset, A., Shalizi, C.R., and Newman, M.E.J. (2009). Power-law distributions in empirical data. SIAM Review *arXiv:0706.1062v2 [physics.data-an]*.

Clayton, K., and Frey, B. (1997). Studies of mental "noise". Nonlinear Dynamics, Psychology, and Life Sciences *1*, 173-180.

de Arcangelis, L., Perrone-Capano, C., and Herrmann, H.J. (2006). Self-organized criticality model for brain plasticity. Phys Rev Lett *96*, 028107.

De Los Rios, P., and Zhang, Y.-C. (1999). Universal 1/f noise from dissipative self-organized criticality models. Physical Review Letters *82*, 472-475.

Eckhorn, R. (1994). Oscillatory and non-oscillatory synchronizations in the visual cortex and their possible roles in associations of visual features. Prog Brain Res *102*, 405-426.

Eguiluz, V.M., Chialvo, D.R., Cecchi, G.A., Baliki, M., and Apkarian, A.V. (2005). Scale-free brain functional networks. Phys Rev Lett *94*, 018102.

Eke, A., Herman, P., Kocsis, L., and Kozak, L.R. (2002). Fractal characterization of complexity in temporal physiological signals. Physiol Meas *23*, R1-38.

Elbert, T., Ulrich, R., Rockstroh, B., and Lutzenberger, W. (1991). The processing of temporal intervals reflected by CNV-like brain potentials. Psychophysiology *28*, 648-655.

Erland, S., and Greenwood, P.E. (2007). Constructing 1/omegaalpha noise from reversible Markov chains. Phys Rev E Stat Nonlin Soft Matter Phys *76*, 031114.

Ermentrout, G.B., Galan, R.F., and Urban, N.N. (2008). Reliability, synchrony and noise. Trends Neurosci *31*, 428-434.

Faisal, A.A., Selen, L.P., and Wolpert, D.M. (2008). Noise in the nervous system. Nat Rev Neurosci *9*, 292-303.

Fox, M.D., and Raichle, M.E. (2007). Spontaneous fluctuations in brain activity observed with functional magnetic resonance imaging. Nat Rev Neurosci *8*, 700-711.

Fox, M.D., Snyder, A.Z., Vincent, J.L., and Raichle, M.E. (2007). Intrinsic fluctuations within cortical systems account for intertrial variability in human behavior. Neuron *56*, 171-184.

Frank, S.A. (2009). The common patterns of nature. J Evol Biol *22*, 1563-1585.

Freeman, W.J. (2007). Scale-free neocortical dynamics. Scholarpedia *2*, 1357.

Freeman, W.J., and Zhai, J. (2009). Simulated power spectral density (PSD) of background electrocorticogram (ECoG). Cogn Neurodyn *3*, 97-103.

Gilden, D.L. (2001). Cognitive emissions of 1/f noise. Psychol Rev *108*, 33-56.

Gisiger, T. (2001). Scale invariance in biology: coincidence or footprint of a universal mechanism? Biol Rev Camb Philos Soc *76*, 161-209.

Granger, C.W.J. (1980). Long memory relationships and the aggregation of dynamic models. Journal of Econometrics *14*, 227-236.

Gruneis, F., Nakao, M., Yamamoto, M., Musha, T., and Nakahama, H. (1989). An interpretation of 1/f fluctuations in neuronal spike trains during dream sleep. Biol Cybern *60*, 161-169.

He, B.J., and Raichle, M.E. (2009). The fMRI signal, slow cortical potential and
consciousness. Trends Cogn Sci *13*, 302-309.

He, B.J., Snyder, A.Z., Zempel, J.M., Smyth, M.D., and Raichle, M.E. (2008).
Electrophysiological correlates of the brain's intrinsic large-scale functional
architecture. Proc Natl Acad Sci U S A *105*, 16039-16044.

Hsu, K.J., and Hsu, A. (1991). Self-similarity of the "1/f noise" called music. Proc Natl
Acad Sci U S A *88*, 3507-3509.

Hurtado, J.M., Rubchinsky, L.L., and Sigvardt, K.A. (2004). Statistical method for
detection of phase-locking episodes in neural oscillations. J Neurophysiol *91*,
1883-1898.

Jensen, O., and Colgin, L.L. (2007). Cross-frequency coupling between neuronal
oscillations. Trends Cogn Sci *11*, 267-269.

Koch, C. (1997). Computation and the single neuron. Nature *385*, 207-210.

Kramer, M.A., Tort, A.B., and Kopell, N.J. (2008). Sharp edge artifacts and spurious
coupling in EEG frequency comodulation measures. J Neurosci Methods *170*,
352-357.

Lakatos, P., Karmos, G., Mehta, A.D., Ulbert, I., and Schroeder, C.E. (2008).
Entrainment of neuronal oscillations as a mechanism of attentional selection.
Science *320*, 110-113.

Lakatos, P., Shah, A.S., Knuth, K.H., Ulbert, I., Karmos, G., and Schroeder, C.E. (2005).
An oscillatory hierarchy controlling neuronal excitability and stimulus processing
in the auditory cortex. J Neurophysiol *94*, 1904-1911.

Leopold, D.A., Murayama, Y., and Logothetis, N.K. (2003). Very slow activity fluctuations in monkey visual cortex: implications for functional brain imaging. Cereb Cortex *13*, 422-433.

Levina, A., Herrmann, J.M., and Geisel, T. (2007). Dynamical synapses causing self-organized criticality in neural networks. Nature Physics *3*, 857-860.

Lin, D.C., Sharif, A., and Kwan, H.C. (2006a). Scaling and organization of electroencephalographic background activity and alpha rhythm in healthy young adults. Biol Cybern *95*, 401-411.

Lin, M., and Chen, T. (2005). Self-organized criticality in a simple model of neurons based on small-world networks. Phys Rev E Stat Nonlin Soft Matter Phys *71*, 016133.

Lin, S.C., Gervasoni, D., and Nicolelis, M.A. (2006b). Fast modulation of prefrontal cortex activity by basal forebrain noncholinergic neuronal ensembles. J Neurophysiol *96*, 3209-3219.

Linkenkaer-Hansen, K., Nikouline, V.V., Palva, J.M., and Ilmoniemi, R.J. (2001). Long-range temporal correlations and scaling behavior in human brain oscillations. J Neurosci *21*, 1370-1377.

Linkenkaer-Hansen, K., Nikulin, V.V., Palva, J.M., Kaila, K., and Ilmoniemi, R.J. (2004). Stimulus-induced change in long-range temporal correlations and scaling behaviour of sensorimotor oscillations. Eur J Neurosci *19*, 203-211.

Logothetis, N.K. (2002). The neural basis of the blood-oxygen-level-dependent functional magnetic resonance imaging signal. Philos Trans R Soc Lond B Biol Sci *357*, 1003-1037.

Logothetis, N.K., Kayser, C., and Oeltermann, A. (2007). In vivo measurement of
cortical impedance spectrum in monkeys: implications for signal propagation.
Neuron *55*, 809-823.

Lowen, S.B., Cash, S.S., Poo, M., and Teich, M.C. (1997). Quantal neurotransmitter
secretion rate exhibits fractal behavior. J Neurosci *17*, 5666-5677.

Maimon, G., and Assad, J.A. (2009). Beyond Poisson: increased spike-time regularity
across primate parietal cortex. Neuron *62*, 426-440.

Mandelbrot, B.B. (1999). Multifractals and 1/f Noise (New York: Springer).

Manning, J.R., Jacobs, J., Fried, I., and Kahana, M.J. (2009). Broadband shifts in local
field potential power spectra are correlated with single-neuron spiking in humans.
J Neurosci *29*, 13613-13620.

Maylor, E.A., Chater, N., and Brown, G.D. (2001). Scale invariance in the retrieval of
retrospective and prospective memories. Psychon Bull Rev *8*, 162-167.

Miller, K.J., Leuthardt, E.C., Schalk, G., Rao, R.P., Anderson, N.R., Moran, D.W.,
Miller, J.W., and Ojemann, J.G. (2007). Spectral changes in cortical surface
potentials during motor movement. J Neurosci *27*, 2424-2432.

Miller, K.J., Zanos, S., Fetz, E.E., den Nijs, M., and Ojemann, J.G. (2009). Decoupling
the cortical power spectrum reveals real-time representation of individual finger
movements in humans. J Neurosci *29*, 3132-3137.

Milstein, J., Mormann, F., Fried, I., and Koch, C. (2009). Neuronal shot noise and
Brownian 1/f2 behavior in the local field potential. PLoS One *4*, e4338.

Mitra, P.P., and Pesaran, B. (1999). Analysis of dynamic brain imaging data. Biophys J
76, 691-708.

Monto, S., Palva, S., Voipio, J., and Palva, J.M. (2008). Very slow EEG fluctuations predict the dynamics of stimulus detection and oscillation amplitudes in humans. J Neurosci *28*, 8268-8272.

Nishida, M., Hirai, N., Miwakeichi, F., Maehara, T., Kawai, K., Shimizu, H., and Uchida, S. (2004). Theta oscillation in the human anterior cingulate cortex during all-night sleep: an electrocorticographic study. Neurosci Res *50*, 331-341.

Petermann, T., Thiagarajan, T.C., Lebedev, M.A., Nicolelis, M.A., Chialvo, D.R., and Plenz, D. (2009). Spontaneous cortical activity in awake monkeys composed of neuronal avalanches. Proc Natl Acad Sci U S A *106*, 15921-15926.

Petersen, C.C., Hahn, T.T., Mehta, M., Grinvald, A., and Sakmann, B. (2003). Interaction of sensory responses with spontaneous depolarization in layer 2/3 barrel cortex. Proc Natl Acad Sci U S A *100*, 13638-13643.

Plenz, D., and Thiagarajan, T.C. (2007). The organizing principles of neuronal avalanches: cell assemblies in the cortex? Trends Neurosci *30*, 101-110.

Rockstroh, B., Elbert, T., Canavan, A., Lutzenberger, W., and Birbaumer, N. (1989). Slow Brain Potentials and Behaviour II, 2 edn (München, Germany: Urban & Schwarzenberg).

Schroeder, C.E., and Lakatos, P. (2009). Low-frequency neuronal oscillations as instruments of sensory selection. Trends Neurosci *32*, 9-18.

Shin, C.W., and Kim, S. (2006). Self-organized criticality and scale-free properties in emergent functional neural networks. Phys Rev E Stat Nonlin Soft Matter Phys *74*, 045101.

Stam, C.J., and de Bruin, E.A. (2004). Scale-free dynamics of global functional connectivity in the human brain. Hum Brain Mapp *22*, 97-109.

Stewart, C.V., and Plenz, D. (2006). Inverted-U profile of dopamine-NMDA-mediated spontaneous avalanche recurrence in superficial layers of rat prefrontal cortex. J Neurosci *26*, 8148-8159.

Takahashi, K., Koyama, Y., Kayama, Y., Nakamura, K., and Yamamoto, M. (2004). Is state-dependent alternation of slow dynamics in central single neurons during sleep present in the rat ventroposterior thalamic nucleus? Neurosci Res *48*, 203-210.

Talairach, J., and Tournoux, P. (1988). Co-Planar Stereotaxic Atlas of the Human Brain (Stuttgart - New York: Georg Thieme Verlag).

Thivierge, J.P., and Cisek, P. (2008). Nonperiodic synchronization in heterogeneous networks of spiking neurons. J Neurosci *28*, 7968-7978.

Tort, A.B., Kramer, M.A., Thorn, C., Gibson, D.J., Kubota, Y., Graybiel, A.M., and Kopell, N.J. (2008). Dynamic cross-frequency couplings of local field potential oscillations in rat striatum and hippocampus during performance of a T-maze task. Proc Natl Acad Sci U S A *105*, 20517-20522.

van den Heuvel, M.P., Stam, C.J., Boersma, M., and Hulshoff Pol, H.E. (2008). Small-world and scale-free organization of voxel-based resting-state functional connectivity in the human brain. Neuroimage *43*, 528-539.

Vanhatalo, S., Palva, J.M., Holmes, M.D., Miller, J.W., Voipio, J., and Kaila, K. (2004). Infraslow oscillations modulate excitability and interictal epileptic activity in the human cortex during sleep. Proc Natl Acad Sci U S A *101*, 5053-5057.

Voss, R.F., and Clarke, J. (1975). '1/f noise' in music and speech. Nature *258*, 317-318.

Vyazovskiy, V.V., Olcese, U., Lazimy, Y.M., Faraguna, U., Esser, S.K., Williams, J.C., Cirelli, C., and Tononi, G. (2009). Cortical firing and sleep homeostasis. Neuron *63*, 865-878.

Wagenmakers, E.J., Farrell, S., and Ratcliff, R. (2004). Estimation and interpretation of 1/falpha noise in human cognition. Psychon Bull Rev *11*, 579-615.

Ward, L.M. (2002). Dynamical Cognitive Science (London: The MIT Press).

Ward, L.M., and Greenwood, P.E. (2007). 1/f noise. Scholarpedia *2*, 1537.

Weissman, M.B. (1988). 1/f noise and other slow, nonexponential kinetics in condensed matter. Reviews of Modern Physics *60*, 537-571.

Yamamoto, M. (1991). Fluctuations observed in biological time series signals and their functional significance. Front Med Biol Eng *3*, 135-137.

Zarahn, E., Aguirre, G.K., and D'Esposito, M. (1997). Empirical analyses of BOLD fMRI statistics. I. Spatially unsmoothed data collected under null-hypothesis conditions. Neuroimage *5*, 179-197.

CHAPTER V: Implications of the current work (i) - The role of impaired neuronal communication in neurological disorders

<u>Summary</u>

Basic and translational neuroscience findings indicate that normal brain function depends on activity synchronization within distributed brain networks. This conclusion suggests a view of how brain injury causes behavioral deficits that differs from traditional localizationist views. Novel functional neuroimaging methods demonstrate coherent activity in large-scale networks not only during task performance but also, surprisingly, at rest (i.e. in the absence of stimuli, tasks, or overt responses). Furthermore, breakdown of activity coherence at rest, even in regions of the brain that are structurally intact, correlates with behavioral deficits and their recovery after injury. Breakdown of functional connectivity appears to occur not just after local injury but also in other conditions that affect large-scale neural communication. Therefore, a network perspective is fundamental to appreciating the pathophysiology of brain injury at the systems level and the underlying mechanisms of recovery, and for developing novel strategies of rehabilitation.

<u>Introduction</u>

Clinicians commonly localize behavioral deficits to focal lesions in the brain. This principle of '*cortical localization of function'* is a cornerstone of clinical practice based on two theoretical principles that were articulated in the 1800's: *One*, specific functions are represented in specific parts of the brain (Brodmann, 1909). *Two*, injuries to the brain

disrupt localized functions and give rise to corresponding behavioral deficits (Broca, 1863). While there remains debate concerning precisely 'what' is localized within a given patch of brain, the general consensus is that complex functions such as language and memory emerge from the combination of much simpler 'elementary operations' (Brodmann, 1909; Posner et al., 1988; Ullman, 1984). These principles have supported serial models of brain function in which stimuli (e.g., a word) are first analyzed in sensory areas, then associated with more abstract representations (e.g., meaning) in higher-order associative areas and finally reach the motor system where a response is generated. Even more sophisticated cognitive-anatomical models (see (Price, 2000) for language) assume a feed-forward stream of information processing in which each region contributes a specific input/output operation. While these localizationist ideas remain the theoretical backbone of clinical neurology, recent advances in neuroscience suggest a much more distributed, parallel, and recursive view of brain function that has deep implications for clinical practice.

It is well accepted that the brain is anatomically organized in widely distributed and highly parallel networks. For example, the visual system is arranged as a hierarchy of cortical areas, each connected bidirectionally with areas below and above it (Felleman and Van Essen, 1991). Moreover, many areas are horizontally connected with other areas at the same level. Critically, this anatomical arrangement emphasizes not just a bidirectional flow of information (bottom-up from sensory to cognitive to motor areas, and top-down from cognitive to sensory levels), but also local and long-range recursive processing through cortico-cortical or cortico-subcortical loops. In other words,

perception of a stimulus or performance of a task requires the temporal coordination of multiple regions as the behavior unfolds.

Efficient transfer of information within the brain has long been assumed to depend on changes in mean rate of spike discharge. Thus, pre-synaptic neurons transfer information by modulating their mean firing rate, which is integrated dendritically and which ultimately leads to a change of the firing rate of post-synaptic neurons (Shadlen et al., 1996). However, more recent results emphasize the importance of rhythmic synchronization, which is a universal property of neural systems at the scale of neurons, small circuits, and widely distributed networks. Synchronization results in alternating periods of excitation and inhibition that can respectively facilitate or inhibit the transfer of information (Buzsaki, 2006). Neurons likely communicate most effectively when their excitability fluctuations are synchronized. Conversely, a given anatomical connection is relatively ineffective when the connected neuronal groups are not synchronized (reviewed in (Fries, 2005)). There is a substantial and growing body of evidence that rhythmic synchronization plays a functional role in many cognitive functions (reviewed in (Engel et al., 2001; Varela et al., 2001)) as well as brain disorders (Uhlhaas and Singer, 2006). Furthermore, recent evidence indicates that brain networks exhibit synchronized spontaneous activity, i.e., are 'functionally connected', even in the absence of specific task performance, i.e., at 'rest' (see below).

These findings indicate that the functions of any brain region cannot be understood in isolation but only in conjunction with the ensemble of other regions ('network') with which it interacts at rest and during active behavior. The large-scale organization of the brain into distributed networks has important implications for our

understanding of central nervous system disorders and brain-behavioral relationships after brain injury. Some of these implications were foreseen many years ago by early neurologists like Jackson, Andral, Prince, von Monakoff, and Head (reviewed in (Finger, 1994)) who proposed that neurologic deficits do not simply reflect the primary effect of a lesion but also the secondary effects of the lesion on other structures: "*Hence it follows that at the place where you discover a lesion there does not always reside the direct cause of the effects which are produced* (Andral, 1833)". Furthermore, the damaged brain must be viewed as a whole new system, and not simply as the old system minus the lesioned parts: "*So far as the loss of function or negative manifestations are concerned...it is a new condition, the consequences of a fresh readjustment of the organism as a whole to the factors at work at the particular functional level disturbed by the local lesion*" (Head, 1920).

Functional connections in healthy brains

Functional neuroimaging techniques, especially positron emission tomography (PET) and functional magnetic resonance imaging (fMRI) have greatly enhanced our understanding of the brain. Classically, neuroimaging experiments demonstrated focal physiological responses induced by performance of externally imposed tasks. Such responses indirectly reflect changes in synaptic activity which manifest in PET as changes in regional cerebral blood flow and in fMRI as changes in the blood oxygenation level dependent (BOLD) signal (Raichle and Mintun, 2006). The accumulated functional neuroimaging experience indicates that anatomically consistent networks comprised of widely distributed regions activate and deactivate in concert across a wide range of tasks.

For example, eye movements associated with viewing objects in the visual environment lead to consistently coupled activations in frontal and posterior parietal cortex (Corbetta, 1998). While co-occurrence of activations in different regions is suggestive of network structure, more definitive evidence has come from analyses of the temporal interactions between regions.

Over the past decade, several techniques have been developed to determine if interactions between jointly activated regions produce enhanced temporal correlations in task-evoked responses. (For an earlier review see (Lee et al., 2006). Unfortunately, these methods require an *a priori* model of how regions are connected (for detailed reviews see (Penny et al., 2004; Stephan et al., 2007)). Moreover, they are (invariably) contingent upon the specific task used, as changes in the system caused by external inputs are an integral part of the model (for examples of applications to patient populations see (Hinrichs et al., 2006; Mechelli et al., 2007; Schlosser et al., 2003; Seminowicz et al., 2004)).

Because of these complicating factors, the strongest evidence for network structure based on temporal interactions between brain regions has come from the study of 'intrinsic' neural activity, that is, spontaneous activity observed as subjects lie quietly with the eyes either closed or simply fixated on a cross-hair. '*Functional connectivity MRI'* (fcMRI) is model-free strategy that measures the temporal correlation of the BOLD signal between brain regions, usually in the resting state (Biswal et al., 1995; De Luca et al., 2005; Fox et al., 2006; Fox et al., 2005; Greicius et al., 2003; Hampson et al., 2002; Hampson et al., 2006; Mantini et al., 2007; Vincent et al., 2006).

fcMRI studies in neurologically normal, resting young adults have shown that spontaneous fluctuations of the BOLD signal are correlated within widely distributed networks that reproduce the topography typically seen in responses to controlled tasks. For example, regions commonly recruited by directed attention to environmental stimuli or during performance of controlled cognitive tasks, show higher temporal correlations among themselves than with other regions even in the resting state (Dosenbach et al., 2007; Fox et al., 2006; Fox et al., 2005). These intrinsic signal fluctuations are in part related to the underlying anatomical connectivity. For example, in monkeys, fcMRI correlation maps involving parietal area LIP, the frontal eye fields and functionally related temporal areas closely resemble the pattern of anatomical connectivity revealed by tract tracing (Vincent et al., 2007). Similarly, in humans as well as monkeys, homologous regions of the cortex typically show high functional connectivity (Salvador et al., 2005), a finding that appears to reflect inter-hemispheric connections through the corpus callosum. However, the correspondence between functional and anatomical connectivity is not one-to-one. For instance, while area MT has strong direct connections to both area V1 and LIP, it has a stronger resting-state temporal correlation with parietal than visual areas. These considerations suggest that fcMRI reflects anatomical connections that are somehow 'weighted' by function.

Recent studies have investigated the neural signals that underlie the observed temporal correlations of the BOLD signal. While BOLD fluctuations are slow (< 0.1 Hz) some evidence indicates they might be related to power fluctuations of oscillatory neuronal activity at higher frequencies (1-200 Hz) (Leopold et al., 2003). Recent studies

show that different networks defined by fcMRI at rest are characterized by power fluctuations of EEG signals (Laufs et al., 2003; Mantini et al., 2007**).**

Critically, resting state fcMRI has been shown to be functionally significant in health, disease and normal development. Thus, in healthy adult subjects, functional connectivity in a language network correlated with reading ability (Hampson et al., 2006). Conversely, in stroke patients with spatial neglect, impaired functional connectivity in attention networks was observed to correspond to the severity of spatial perceptual deficits (see below) (He et al., 2007). Finally, the functional connectivity of networks involved in cognitive control was shown to be immature in children, which corresponds to the fact that children normally perform less well than adults in controlled cognitive tasks (Fair et al., 2007).

Functional connections in injured brains

The identification of complex and distributed brain networks, identified by measuring temporal correlations in activity at rest and during behavior, suggests strong predictions concerning the effects of a lesion on the brain's functional architecture. *First*, a focal injury will disrupt the synchronization between the site of damage and other connected regions, upstream and downstream, leading to changes in excitability throughout the network. Furthermore, changes in the state of one network may affect the dynamic state of other connected networks. *Second*, these altered patterns of activity in large-scale networks, whether measured at rest or during active behavior, should correlate with the observed neurological deficits. Behavioral deficits will reflect not only structural damage to a local part of a network, but functional imbalances throughout the network

and in other connected networks. *Third*, recovery of function involves the reorganization of entire brain networks. Rehabilitation may restore the networks to a normal state or enable a new state in which functions are performed through compensatory strategies.

To-date, the most common functional pattern observed in patients with focal injury is a dynamic reorganization of the topography of task-related functional responses. For instance, Saur *et al*. (Saur et al., 2006) tested a group of post-stroke aphasic patients (N=14) with an auditory comprehension task at three stages: acute (1.8 days post-stroke), subacute (12 days) and chronic (321 days). They observed in parallel with an improvement of language performance increased activation over time of left hemisphere language regions (inferior frontal gyrus (IFG) and middle temporal gyrus). In contrast, the homologous right hemisphere regions showed an early increase from acute to subacute stages that correlated with improvement, followed by a decrement at the chronic stage. A similar pattern of functional reorganization has been observed in primary motor cortices (M1) in patients with motor impairment after subcortical strokes (reviewed in (Ward, 2006)). These findings carry implications for treatment. Enhancement of excitability in ipsilesional M1 by transcranial direct current stimulation (tDCS) significantly improves motor performance (Fregni et al., 2005; Hummel et al., 2005). In contralesional M1, increased excitability at the acute stage (< 1 month post-stroke) was correlated with functional recovery (Butefisch et al., 2003), whereas at the chronic stage (> 12 months post-stroke) a decrease of excitability significantly correlated with motor improvement (Fregni et al., 2005).

The typical interpretation of these findings is that recruitment of contralesional and ipsilesional associative regions may be helpful for recovery at the acute and subacute

stages but may be maladaptive at the chronic stage, and that preservation or reactivation of ipsilesional activity affords the best chances of optimal recovery. A 'connectionist' interpretation suggests that these dynamic patterns of activation in the two hemispheres are linked and underlie changes in the functional communication within and between hemispheres caused by the lesion. For example, the lesion may abolish inhibitory influences over homologous areas in the opposite hemisphere mediated by callosal connections.

Changes in connectivity following a lesion occur rapidly and presumably depend on unmasking and changes in synaptic weights of pre-existing connections rather than the creation of new pathways. The rapidity of these changes is evident from a recent TMS study in healthy subjects demonstrating that suppression of activity in left premotor cortex induces an immediate increase of activity in the contralateral premotor area which facilitates behavioral performance (O'Shea et al., 2007).

Inter- or intra-hemispheric functional imbalances may also account for disrupted functional connectivity between two structurally intact regions that are directly or indirectly connected to an area of damage. A recent study of spatial neglect shows that asymmetries in spatial attention correlate with imbalanced functional response in structurally intact left and right parietal cortex. At the subacute stage, activity in right ipsilesional parietal cortex was relatively depressed during a spatial orienting task whereas activity in contralesional left parietal cortex was relatively enhanced. This imbalance was behaviorally significant as the magnitude of activation in left parietal cortex correlated with the degree of spatial neglect (Corbetta et al., 2005). A recent follow-up study showed that this functional imbalance was manifested also in fcMRI

measures (Fig. 1). Specifically, low inter-hemispheric coherence in parietal cortex correlated with worse neglect (He et al., 2007). Critically, in both studies the anatomical damage was in the frontal cortex and underlying white matter, far removed from the parietal regions where the functional signals were measured.
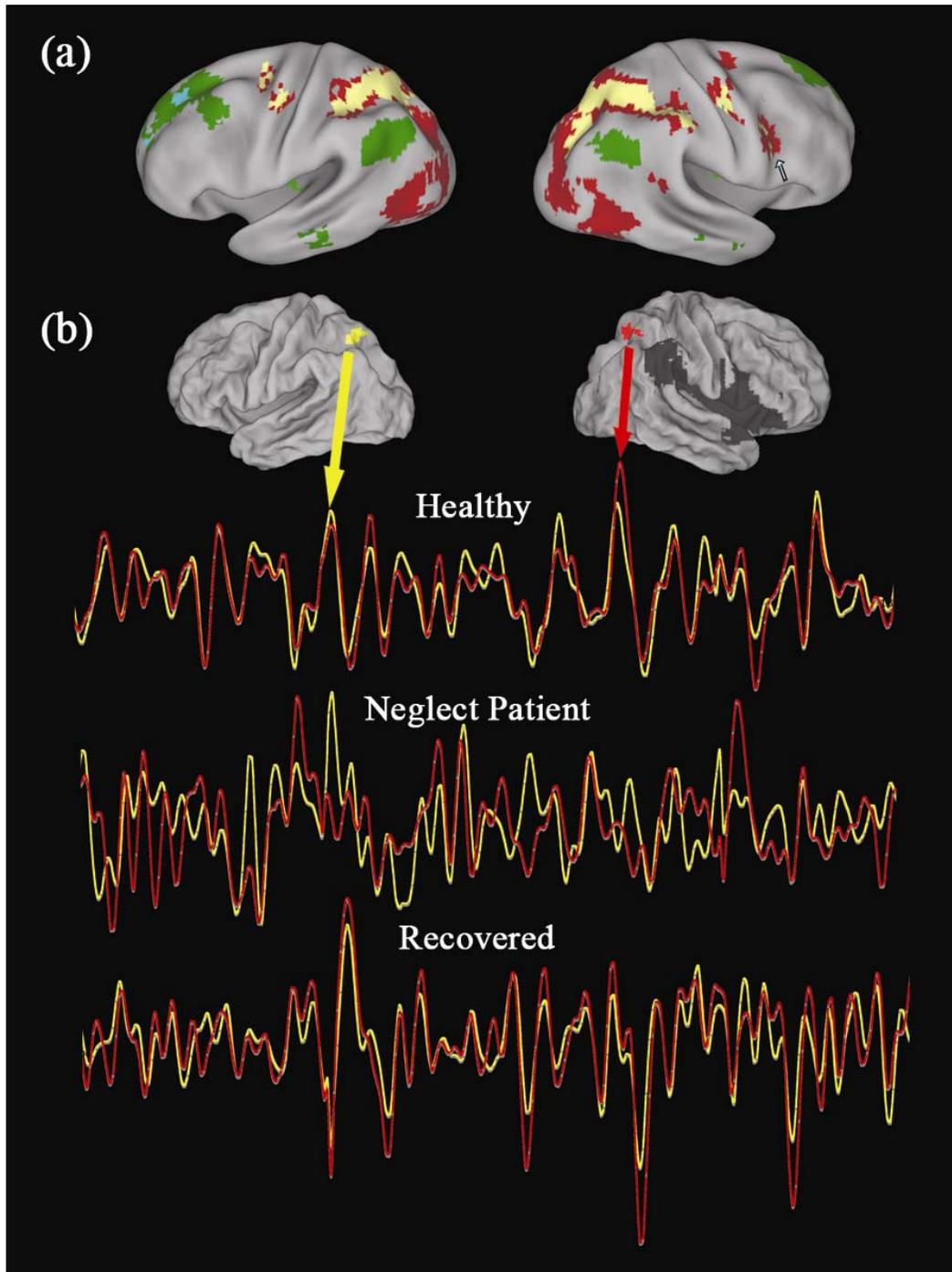
Figure 1 (**a**) An example of functional connectivity obtained by measuring spontaneous blood oxygenation level dependent (BOLD) signal fluctuations with functional magnetic resonance imaging (fMRI) in healthy subjects. Areas in yellow/red are temporally correlated, and correspond to the 'dorsal attention network' important for the control of spatial attention. Areas in green/blue are negative correlated with the dorsal attention network, and correspond to the 'default' network. (**b**) Randomly selected 10-min records of fMRI signals from the left (shown in yellow) and right (in red) posterior parietal cortex in an elderly healthy subject (top), an acute stroke patient with spatial neglect (middle), and the same patient 9 months later when the behavioral deficits have recovered (bottom). Both regions are part of the dorsal attention network, and were outside of the lesion in this patient, which is shown in black. In healthy subjects, these two regions are coherent in their spontaneous fMRI fluctuations. Such temporal relationship is disrupted in patients with acute spatial neglect, but is regained during course of recovery.

<u>Conclusions</u>

These novel findings provide a neurobiological basis for the intuition of early neurologists that what ultimately matters is the state of the network and not only what happens at the locus of injury. Knowing that a frontal lesion can cause functional changes in parietal cortex and that these changes are behaviorally significant not only provides a more complete understanding of brain-behavior relationships, but also opens up the possibility of novel interventions. For instance, preliminary evidence indicates that rebalancing of activity across the hemisphere by suppressive TMS improves performance (Brighina et al., 2003; Naeser et al., 2005).

This network approach also explains why stroke patients present acutely with a multiple deficits that are not easily attributable to the locus of injury. For instance, a subcortical lesion may not only present with motor deficits but also with a variety of impairments of language, attention, working memory, and task control. It is the rule that cognitive functions are almost never normal in patients with a focal brain injury. While traditional explanations invoke non-neuronal factors such as edema, vascular

dysregulation, etc, a network perspective explains this multitude of problems by invoking disrupted neuronal communication within brain networks. fcMRI, potentially in association with simultaneous EEG recordings, is an especially promising approach for studying these network-level abnormalities because of its robustness (networks can be normally seen in a single subject after 5-15 min scanning), reproducibility, and minimal task requirements that enable patients with a large range of deficits to be tested.

A final important point is that a network approach can be applied as well to the study of non-focal disorders such as Alzheimer's disease (Greicius et al., 2004), depression (Greicius et al., 2007) or schizophrenia (Buckholtz et al., 2007; Kubicki et al., 2007; Zhou et al., 2007). In Alzheimer's disease (AD) a breakdown of functional connectivity has been reported in the 'default' network (Greicius et al., 2004) a set of brain regions that normally show task-related deactivations during controlled task performance (Shulman et al., 1997) and that also are involved in memory retrieval (Buckner et al., 2005). In primary progressive aphasia, weakened functional connectivity during a language task between Broca's and Wernicke's regions correlated with the degree of language impairment (Sonty et al., 2007). It is likely that a network approach using either fcMRI or more task-driven methods (see review by (Lee et al., 2006)) will be helpful in other disorders that affect large-scale cortical communication as in the case of white matter lesions in multiple sclerosis (Cader et al., 2006) or disrupted interaction of basal ganglia and cortex in Huntington's disease (Thiruvady et al., 2007).

References

Andral, G. (1833). Clinique Medicale, Vol 4 (Paris: Librairie fe Deville).

Biswal, B., Yetkin, F., Haughton, V., and Hyde, J. (1995). Functional connectivity in the motor cortex of resting human brain using echo-planar MRI. Magnetic Resonance in Medicine *34*, 537-541.

Brighina, F., Bisiach, E., Oliveri, M., Piazza, A., La Bua, V., Daniele, O., and Fierro, B. (2003). 1 Hz repetitive transcranial magnetic stimulation of the unaffected hemisphere ameliorates contralesional visuospatial neglect in humans. Neurosci Lett *336*, 131-133.

Broca, P. (1863). Localisation des fonctions cerebrales. Siege du langage articule. Bullettins del la Societe d'Anthropologie (Paris) *4*, 200-203.

Brodmann, K. (1909). Vergleichende lokalisationlehre der grosshirnrinde in inren prinzipien dargestellt auf grund des zellenbaues (Leipzig: J. A. Barth).

Buckholtz, J.W., Meyer-Lindenberg, A., Honea, R.A., Straub, R.E., Pezawas, L., Egan, M.F., Vakkalanka, R., Kolachana, B., Verchinski, B.A., Sust, S.*, et al.* (2007). Allelic variation in RGS4 impacts functional and structural connectivity in the human brain. J Neurosci *27*, 1584-1593.

Buckner, R.L., Snyder, A.Z., Shannon, B.J., LaRossa, G., Sachs, R., Fotenos, A.F., Sheline, Y.I., Klunk, W.E., Mathis, C.A., Morris, J.C., and Mintun, M.A. (2005). Molecular, structural and functional characterization of Alzheimer's disease: evidence for a relationship between default activity, amyloid, and memory. Journal of Neuroscience *25*, 7709-7717.

Butefisch, C.M., Netz, J., Wessling, M., Seitz, R.J., and Homberg, V. (2003). Remote changes in cortical excitability after stroke. Brain *126*, 470-481.

Buzsaki, G. (2006). Rhythms of the Brain. (New York, NY: Oxford University Press), pp. 119-135.

Cader, S., Cifelli, A., Abu-Omar, Y., Palace, J., and Matthews, P.M. (2006). Reduced brain functional reserve and altered functional connectivity in patients with multiple sclerosis. Brain *129*, 527-537.

Corbetta, M. (1998). Frontoparietal cortical networks for directing attention and the eye to visual locations: identical, independent, or overlapping neural systems. Proceedings of the National Academy of Science, USA *95*, 831-838.

Corbetta, M., Kincade, M.J., Lewis, C., Snyder, A.Z., and Sapir, A. (2005). Neural basis and recovery of spatial attention deficits in spatial neglect. Nat Neurosci *8*, 1603-1610.

De Luca, M., Smith, S., Nicola De, S., Antonio, F., and Paul, M.M. (2005). Blood oxygenation level dependent contrast resting state networks are relevant to functional activity in the neocortical sensorimotor system. Experimental Brain Research *167*, 587-594.

Dosenbach, N.U., Fair, D.A., Miezin, F.M., Cohen, A.L., Wenger, K.K., Dosenbach, R.A., Fox, M.D., Snyder, A.Z., Vincent, J.L., Raichle, M.E.*, et al.* (2007). Distinct brain networks for adaptive and stable task control in humans. Proc Natl Acad Sci U S A *104*, 11073-11078.

Engel, A.K., Fries, P., and Singer, W. (2001). Dynamic predictions: oscillations and synchrony in top-down processing. Nat Rev Neurosci *2*, 704-716.

Fair, D.A., Dosenbach, N.U., Church, J.A., Cohen, A.L., Brahmbhatt, S., Miezin, F.M., Barch, D.M., Raichle, M.E., Petersen, S.E., and Schlaggar, B.L. (2007). Development of distinct control networks through segregation and integration. Proc Natl Acad Sci U S A *104*, 13507-13512.

Felleman, D.J., and Van Essen, D.C. (1991). Distributed hierarchical processing in the primate cerebral cortex. Cerebral Cortex *1*, 1-47.

Finger, S. (1994). Origins of Neuroscience. O.U. Press, ed. (New York Oxford), pp. 51-62.

Fox, M.D., Corbetta, M., Snyder, A.Z., Vincent, J.L., and Raichle, M.E. (2006). Spontaneous neuronal activity distinguishes human dorsal and ventral attention systems. Proc Natl Acad Sci U S A *103*, 10046-10051.

Fox, M.D., Snyder, A.Z., Vincent, J.L., Corbetta, M., Van Essen, D.C., and Raichle, M.E. (2005). The human brain is intrinsically organized into dynamic, anticorrelated functional networks. Proc Natl Acad Sci U S A *102*, 9673-9678.

Fregni, F., Boggio, P.S., Mansur, C.G., Wagner, T., Ferreira, M.J., Lima, M.C., Rigonatti, S.P., Marcolin, M.A., Freedman, S.D., Nitsche, M.A., and Pascual-Leone, A. (2005). Transcranial direct current stimulation of the unaffected hemisphere in stroke patients. Neuroreport *16*, 1551-1555.

Fries, P. (2005). A mechanism for cognitive dynamics: neuronal communication through neuronal coherence. Trends Cogn Sci *9*, 474-480.

Greicius, M.D., Flores, B.H., Menon, V., Glover, G.H., Solvason, H.B., Kenna, H., Reiss, A.L., and Schatzberg, A.F. (2007). Resting-state functional connectivity in major

depression: abnormally increased contributions from subgenual cingulate cortex and thalamus. Biol Psychiatry *62*, 429-437.

Greicius, M.D., Krasnow, B., Reiss, A.L., and Menon, V. (2003). Functional connectivity in the resting brain: a nework analysis of the default mode hypothesis. Proc Natl Acad Sci U S A *100*, 253-258.

Greicius, M.D., Srivastava, G., Reiss, A.L., and Menon, V. (2004). Default-mode network activity distinguishes Alzheimer's disease from healthy aging: evidence from functional MRI. Proc Natl Acad Sci U S A *101*, 4637-4642.

Hampson, M., Peterson, B.S., Skudlarski, P., Gatenby, J.C., and Gore, J.C. (2002). Detection of functional connectivity using temporal correlations in MR images. Hum Brain Mapp *15*, 247-262.

Hampson, M., Tokoglu, F., Sun, Z., Schafer, R.J., Skudlarski, P., Gore, J.C., and Constable, R.T. (2006). Connectivity-behavior analysis reveals that functional connectivity between left BA39 and Broca's area varies with reading ability. Neuroimage *31*, 513-519.

He, B.J., Snyder, A.Z., Vincent, J.L., Epstein, A., Shulman, G.L., and Corbetta, M. (2007). Breakdown of functional connectivity in frontoparietal networks underlies behavioral deficits in spatial neglect. Neuron *53*, 905-918.

Head, H. (1920). Studies in Neurology (London).

Hinrichs, H., Heinze, H.J., and Schoenfeld, M.A. (2006). Causal visual interactions as revealed by an information theoretic measure and fMRI. Neuroimage *31*, 1051-1060.

Hummel, F., Celnik, P., Giraux, P., Floel, A., Wu, W.H., Gerloff, C., and Cohen, L.G. (2005). Effects of non-invasive cortical stimulation on skilled motor function in chronic stroke. Brain *128*, 490-499.

Kubicki, M., McCarley, R., Westin, C.F., Park, H.J., Maier, S., Kikinis, R., Jolesz, F.A., and Shenton, M.E. (2007). A review of diffusion tensor imaging studies in schizophrenia. J Psychiatr Res *41*, 15-30.

Laufs, H., Krakow, K., Sterzer, P., Eger, E., Beyerle, A., Salek-Haddadi, A., and Kleinschmidt, A. (2003). Electroencephalographic signatures of attentional and cognitive default modes in spontaneous brain activity fluctuations at rest. Proc Natl Acad Sci U S A *100*, 11053-11058.

Lee, L., Friston, K., and Horwitz, B. (2006). Large-scale neural models and dynamic causal modelling. Neuroimage *30*, 1243-1254.

Leopold, D.A., Murayama, Y., and Logothetis, N.K. (2003). Very slow activity fluctuations in monkey visual cortex: implications for functional brain imaging. Cereb Cortex *13*, 422-433.

Mantini, D., Perrucci, M.G., Del Gratta, C., Romani, G.L., and Corbetta, M. (2007). Electrophysiological signatures of resting state networks in the human brain. Proc Natl Acad Sci U S A *104*, 13170-13175.

Mechelli, A., Allen, P., Amaro, E., Jr., Fu, C.H., Williams, S.C., Brammer, M.J., Johns, L.C., and McGuire, P.K. (2007). Misattribution of speech and impaired connectivity in patients with auditory verbal hallucinations. Hum Brain Mapp.

Naeser, M.A., Martin, P.I., Nicholas, M., Baker, E.H., Seekins, H., Kobayashi, M., Theoret, H., Fregni, F., Maria-Tormos, J., Kurland, J.*, et al.* (2005). Improved

picture naming in chronic aphasia after TMS to part of right Broca's area: an

open-protocol study. Brain Lang *93*, 95-105.

O'Shea, J., Johansen-Berg, H., Trief, D., Gobel, S., and Rushworth, M.F. (2007).

Functionally specific reorganization in human premotor cortex. Neuron *54*, 479-

490.

Penny, W.D., Stephan, K.E., Mechelli, A., and Friston, K.J. (2004). Modelling functional

integration: a comparison of structural equation and dynamic causal models.

Neuroimage *23 Suppl 1*, S264-274.

Posner, M.I., Petersen, S.E., Fox, P.T., and Raichle, M.E. (1988). Localization of

cognitive operations in the human brain. Science *240*, 1627-1631.

Price, C.J. (2000). The anatomy of language: contributions from functional

neuroimaging. J Anat *197 Pt 3*, 335-359.

Raichle, M.E., and Mintun, M.A. (2006). Brain work and brain imaging. Annu Rev

Neurosci *29*, 449-476.

Salvador, R., Suckling, J., Coleman, M.R., Pickard, J.D., Menon, D., and Bullmore, E.

(2005). Neurophysiological architecture of functional magnetic resonance images

of human brain. Cereb Cortex *15*, 1332-1342.

Saur, D., Lange, R., Baumgaertner, A., Schraknepper, V., Willmes, K., Rijntjes, M., and

Weiller, C. (2006). Dynamics of language reorganization after stroke. Brain *129*,

1371-1384.

Schlosser, R., Gesierich, T., Kaufmann, B., Vucurevic, G., Hunsche, S., Gawehn, J., and

Stoeter, P. (2003). Altered effective connectivity during working memory

performance in schizophrenia: a study with fMRI and structural equation modeling. Neuroimage *19*, 751-763.

Seminowicz, D.A., Mayberg, H.S., McIntosh, A.R., Goldapple, K., Kennedy, S., Segal, Z., and Rafi-Tari, S. (2004). Limbic-frontal circuitry in major depression: a path modeling metanalysis. Neuroimage *22*, 409-418.

Shadlen, M., Britten, K.H., Newsome, W.T., and Movshon, J.A. (1996). A computational analysis of the relationship between neuronal and behavioral responses to visual motion. Journal of Neuroscience *16*, 1486-1510.

Shulman, G.L., Fiez, J.A., Corbetta, M., Buckner, R.L., Miezin, F.M., Raichle, M.E., and Petersen, S.E. (1997). Common blood flow changes across visual tasks: II. Decreases in cerebral cortex. Journal of Cognitive Neuroscience *9*, 648-663.

Sonty, S.P., Mesulam, M.M., Weintraub, S., Johnson, N.A., Parrish, T.B., and Gitelman, D.R. (2007). Altered effective connectivity within the language network in primary progressive aphasia. J Neurosci *27*, 1334-1345.

Stephan, K.E., Harrison, L.M., Kiebel, S.J., David, O., Penny, W.D., and Friston, K.J. (2007). Dynamic causal models of neural system dynamics:current state and future extensions. J Biosci *32*, 129-144.

Thiruvady, D.R., Georgiou-Karistianis, N., Egan, G.F., Ray, S., Sritharan, A., Farrow, M., Churchyard, A., Chua, P., Bradshaw, J.L., Brawn, T.L., and Cunnington, R. (2007). Functional connectivity of the prefrontal cortex in Huntington's disease. J Neurol Neurosurg Psychiatry *78*, 127-133.

Uhlhaas, P.J., and Singer, W. (2006). Neural synchrony in brain disorders: relevance for cognitive dysfunctions and pathophysiology. Neuron *52*, 155-168.

Ullman, S. (1984). Visual routines. Cognition *18*, 97-159.

Varela, F., Lachaux, J.P., Rodriguez, E., and Martinerie, J. (2001). The brainweb: phase

synchronization and large-scale integration. Nat Rev Neurosci *2*, 229-239.

Vincent, J.L., Patel, G.H., Fox, M.D., Snyder, A.Z., Baker, J.T., Van Essen, D.C.,

Zempel, J.M., Snyder, L.H., Corbetta, M., and Raichle, M.E. (2007). Intrinsic

functional architecture in the anaesthetized monkey brain. Nature *447*, 83-86.

Vincent, J.L., Snyder, A.Z., Fox, M.D., Shannon, B.J., Andrews, J.R., Raichle, M.E., and

Buckner, R.L. (2006). Coherent spontaneous activity identifies a hippocampal-

parietal memory network. J Neurophysiol *96*, 3517-3531.

Ward, N.S. (2006). The neural substrates of motor recovery after focal damage to the

central nervous system. Arch Phys Med Rehabil *87*, 30-35.

Zhou, Y., Liang, M., Jiang, T., Tian, L., Liu, Y., Liu, Z., Liu, H., and Kuang, F. (2007).

Functional dysconnectivity of the dorsolateral prefrontal cortex in first-episode

schizophrenia using resting-state fMRI. Neurosci Lett *417*, 297-302.

CHAPTER VI: Implications of the current work (ii) and a hypothesis for future work –The fMRI signal, slow cortical potential and consciousness

Summary

As functional magnetic resonance imaging (fMRI) has become a driving force in cognitive neuroscience, it is critical to understand the neural basis of the fMRI signal. We here discuss a novel neurophysiological correlate of the fMRI signal, the slow cortical potential (SCP), which also appears to modulate the power of higher-frequency activity, the more established neurophysiological correlate of the fMRI signal. We further propose a hypothesis for the involvement of the SCP in the emergence of consciousness, and review existing data that lend support to our proposal. This hypothesis, unlike several previous theories of consciousness, is firmly rooted in physiology and as such is entirely amenable to empirical testing.

Introduction

Since its introduction in the early 1990's, fMRI has become the most widely used tool in human cognitive neuroscience and has produced a formidable array of brain maps depicting both localization (as in traditional activation studies) and integration (as in more recent functional connectivity studies) of brain activity. As the fMRI signal measures directly blood oxygenation and only indirectly neuronal activity, an important need for understanding the neural events contributing to the fMRI signal has been widely recognized. Such a need is further stressed by the inconsistencies between a number of

human fMRI and monkey unit physiological studies employing the same tasks (Logothetis, 2002).

Responding to this need, a number of studies have compared the fMRI signal (reviewed in (Logothetis, 2008)) or its close relatives (including tissue oxygenation (Viswanathan and Freeman, 2007), blood flow (Lauritzen and Gold, 2003), optical intrinsic signals (Niessing et al., 2005)) with simultaneously recorded electrophysiological signals. The convergent results from these studies suggest that the fMRI signal is contributed predominantly by synaptic activity representing inputs and local processing in an area as measured by local field potentials (LFP) (Arthurs and Boniface, 2002; Lauritzen and Gold, 2003; Logothetis, 2008; Raichle and Mintun, 2006; Viswanathan and Freeman, 2007). The spiking activity, though often correlated with both the LFP and the fMRI signal, can be dissociated from the latter two in a number of conditions including adaptation (Logothetis et al., 2001), drug modulation (Rauch et al., 2008), manipulations of excitatory and inhibitory inputs (Lauritzen and Gold, 2003), and a spatial separation between input and output activity (Raichle and Mintun, 2006).

Whereas multiple frequency ranges of the LFP (e.g., 5-30 Hz (Maier et al., 2008), 20-60 Hz (Goense and Logothetis, 2008; Kayser et al., 2004), ~25-90 Hz (Logothetis et al., 2001; Mukamel et al., 2005; Niessing et al., 2005; Rauch et al., 2008; Viswanathan and Freeman, 2007)) have been correlated with the fMRI signal in different conditions, all of these studies have only assessed power modulations of the LFP because only the power of these frequency ranges has a comparable temporal scale to that of the fMRI signal (< 0.5 Hz). We here add a new dimension to this evolving story by bringing in the low-frequency end of field potentials (<4 Hz), which, with a temporal scale overlapping

that of the fMRI signal, appears to correlate with the fMRI signal in its raw fluctuations. This signal, termed the "slow cortical potential" (SCP) by us and others (Birbaumer et al., 1990; He et al., 2008; Khader et al., 2008), appears optimally positioned for carrying out large-scale information integration in the brain. Since conscious experience (see Glossary) is always a unitary and undivided whole (Searle, 2000; Tononi, 2008), segregated information processing in the brain cannot contribute to the conscious awareness of "I". Hence, we propose that the SCP may contribute directly to the emergence of consciousness[*] and review existing empirical evidence supporting this idea. As the current hypothesis is based on a well-defined, well-characterized physiological process, it is entirely amenable to empirical testing.

Evidence for a relationship between the SCP and the fMRI signal

The SCP is the slow end (mainly <1 Hz, can extend up to ~4 Hz) of the field potential that can be recorded using either depth (Goldring, 1974; Rebert, 1973) or surface (He et al., 2008; Rosler et al., 1997) electrodes (Box 1). Negative shift in surface-recorded SCP indexes increased cortical excitability (for detailed physiology please see the following section). Since the SCP frequency range is subject to artifacts due to sweating (in scalp-electroencephalography (EEG) recordings), movement and electrode drift (if polarizable electrodes are used), it has been eliminated in most animal physiology as well as human EEG studies by online high-pass filtering. This is

---

[*] In this chapter, I use "consciousness" or "conscious awareness" synonymously as "subjective awareness". I use "conscious experience" to refer to the experience of subjective awareness. Lastly, "conscious state" refers to the physiological states under which conscious awareness is present.

unfortunate because, as was recognized in the 1970's, "If DC [i.e., direct-current] recording is used, virtually every stimulus-bound cortical activity is seen to be accompanied by a change in cortical steady potentials" (P.12 in (Goldring, 1974)). As a result of this methodological neglect, studies on the relationship between SCP and the fMRI signal are scarce. Nonetheless, despite the limited data available, a correlation between the SCP and the fMRI signal no less intimate than that between higher-frequency (>5 Hz) LFP power and fMRI signal can be observed (He et al., 2008; Khader et al., 2008; Nagai et al., 2004).

Investigations of the relationship between LFP power and the fMRI signal have generally showed one of the following: (i) covariation of simultaneously recorded LFP power and the fMRI signal during a task or electrical stimulation (Goense and Logothetis, 2008; Kayser et al., 2004; Logothetis et al., 2001; Niessing et al., 2005; Rauch et al., 2008; Viswanathan and Freeman, 2007); (ii) covariation of simultaneously recorded *spontaneous* LFP power and the fMRI signal (Shmuel and Leopold, 2008); and (iii) similar correlation patterns in the spontaneous fluctuations of LFP power and the fMRI signal measured separately (He et al., 2008; Lu et al., 2007; Nir et al., 2008).

To our knowledge, the only available data that demonstrate covariation of simultaneously recorded SCP and the fMRI signal during task stimulation (type (*i)* above) has been provided by Nagai and colleagues using simultaneously recorded EEG and fMRI (Nagai et al., 2004).These authors found a trial-by-trial correlation between the amplitude of a negative SCP response indexing expectancy ("contingent negative variation", CNV) and the fMRI signal amplitude in anterior cingulate cortex (Fig. 1a). The anterior cingulate has previously been determined as a generator region of CNV

(Nagai et al., 2004). Evidence for SCP-fMRI correlation of the above type (*ii*) is provided by Jones et al.(Jones et al., 2007), who showed that spontaneously fluctuating total hemoglobin concentration (a signal tightly linked to the fMRI signal) and low-pass filtered LFP (i.e., depth recorded SCP) are temporally correlated. Data of the above type (*iii*) is provided by He et al. using invasive EEG (i.e., electrocorticography, ECoG) and fMRI in neurosurgical patients(He et al., 2008). It was shown that large-scale (2-10 cm on cortical surface) correlation patterns in the spontaneous SCP and fMRI signals were similar (Fig. 1b). This finding has since been extended to inter-hemispheric correlations as well (unpublished data). Taken together, all three types of evidence for the correlation between LFP power and the fMRI signal are also available for a correlation between SCP and the fMRI signal.

Beyond the above approaches, there is an extensive literature showing similar modulation patterns of the SCP and the fMRI signal in a wide range of cognitive tasks (Birbaumer et al., 1990; Khader et al., 2008; Rosler et al., 1997). For example, visual working memory tasks elicit a negative-going slow potential over the parietal cortex, the amplitude of which scales with the load of working memory (Vogel and Machizawa, 2004). This pattern is very similar to that observed for the fMRI signal in posterior parietal cortex during the same task (Song and Jiang, 2006).

In summary, convergent results suggest that the SCP has a close correspondence to the fMRI signal in different experimental conditions. Like many advances in science, the relationship between SCP and fMRI signal is not without prescient conjecture. In 1975, H.W. Shipton wrote: "the work of Cooper, which showed slow rhythmic changes in brain pO_2 and in blood flow (e.g., (Cooper et al., 1966)), is of interest in the context of

slow [cortical] potential change"(Shipton, 1975). Next, we consider the physiological

mechanisms underlying the SCP.
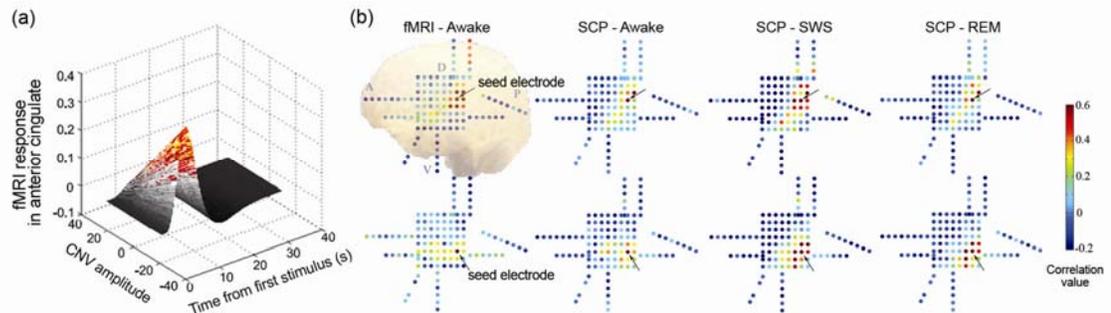
Figure 1. Evidence for a correlation between the slow cortical potential (SCP) and the fMRI signal.**(a)**Simultaneous fMRI and EEG was used to identify fMRI signal activation correlated with trial-by-trial measurement of contingent negative variation (CNV) amplitude. CNV is a negative slow potential that relates to the anticipation of a stimulus and it is maximal over frontal midline electrodes. Trial-by-trial covariation between CNV amplitude and fMRI signal timecourse in anterior cingulate cortex is shown in a 3-D plot. Adapted with permission from Nagai et al. (2004). **(b)**Correlation patterns in the spontaneous fMRI signals and spontaneous SCPs are similar. A group of 5 patients with intractable epilepsy underwent approximately a week of continuous video-monitored electrocorticography (ECoG) for the purpose of determining the epileptic focus before surgical resection. Artifact-free, spontaneous ECoG data were collected from three arousal states: wakefulness, slow-wave sleep (SWS), and rapid-eye-movement (REM) sleep, and then low-pass filtered at <0.5 Hz to yield spontaneous SCPs. In addition, patients underwent a session of resting-state fMRI before the implantation of electrode grids. SCP correlation maps were obtained by computing Pearson correlation coefficients between a seed electrode (arrow) and all other electrodes. For corresponding fMRI correlation maps, the fMRI signal was averaged across a group of voxels centered at each electrode, and correlation coefficients were computed between the fMRI signal associated with the seed electrode and that from all other electrodes. Representative maps from one patient are shown. A 2-D representation of the electrode grid is shown with each dot representing one electrode. Color represents the correlation value between each electrode and the seed electrode (arrow). Maps in the top row seed at a same electrode, those in the bottom row seed at another electrode 2 cm apart. Note that correlation maps with the same seed electrode are similar regardless of whether the fMRI signal or the SCP was used in computing the map. A, anterior; D, dorsal; P, posterior; V, ventral. Adapted with permission from He et al.(He et al., 2008)

The physiological basis of the SCP

Simultaneous recordings of surface potentials, field potentials in different cortical layers, and intracellular membrane potentials have clearly demonstrated that synaptic activities at apical dendrites in superficial layers are the main factor contributing to the SCP. Specifically, long-lasting excitatory postsynaptic potentials (EPSPs) at these apical dendrites underlie negative-going surface-recorded SCPs (Birbaumer et al., 1990; Goldring, 1974; Mitzdorf, 1985). As an example, we consider the effect of visual stimulation in V1 – a standard model for the investigation of fMRI-electrophysiology correspondence (Goense and Logothetis, 2008; Kayser et al., 2004; Logothetis et al., 2001; Niessing et al., 2005; Rauch et al., 2008; Viswanathan and Freeman, 2007). Specific thalamic inputs terminate first on the soma of layer-IV stellate cells and layer-III pyramidal cells, and then follow one of two pathways to depolarize the apical dendrites of superficial- or deep-layer pyramidal cells (Mitzdorf, 1985) (Fig. 2a). Given the geometry of cortical fields, the earlier processes – excitations of pyramidal cells at their soma, produce positive-going surface potentials (Fig. 2b i). The later processes, excitations of pyramidal cells at their apical dendrites, produce surface negative potentials (Fig. 2b ii and iii). However, EPSPs at apical dendrites of deep layer pyramidal cells create closed fields and thus have rather small influence on surface potentials (Fig. 2b ii). By contrast, depolarizations of superficial layer apical dendrites contribute greatly to negative SCPs (Fig. 2b iii). The contribution of inhibitory interneurons to SCP or field potentials in general is also small because of the low amplitude of membrane current flow during inhibitory activity and a lack of laminar specificity (Fig. 2b iv) (Birbaumer et al., 1990; Mitzdorf, 1985). In summary, the later component of sensory evoked potentials in EEG or ECoG recordings – a negative slow-

potential shift – is primarily due to long-lasting depolarizations of superficial layer apical dendrites.

Other than activations by specific thalamic inputs described above, the superficial layers are also where long-range intracortical and cortico-cortical connections preferentially terminate (Braitenberg and Schuz, 1998; Douglas and Martin, 2004; Mitzdorf, 1985). First, only in superficial layers do pyramidal cells make extensive horizontal arborizations (Douglas and Martin, 2004). Thus, EPSPs in superficial layers spread over a considerable spatial extent and manifest themselves as "depolarization fields" (~several mm^2) in optical imaging recordings (Roland, 2002). Second, long-range inter-areal feedback connections also terminate mainly in superficial layers. Hence, it is not surprising that the SCP and the correlated fMRI signal reveal large-scale brain networks in their spontaneous fluctuations (He et al., 2008). Moreover, superficial-layer apical dendrites are also the main target of nonspecific thalamic inputs that originate from "matrix cells" spread throughout the thalamus (Jones, 1998). Interestingly, the reticular thalamic nucleus, which the nonspecific thalamocortical projections must pass through, exerts a low-pass filter influence that may facilitate the emergence of slow activity (Scheibel and Scheibel, 1967). In summary, long-range intracortical and feedback cortico-cortical connections, as well as the nonspecific thalamic inputs, all contribute directly and significantly to the SCP.
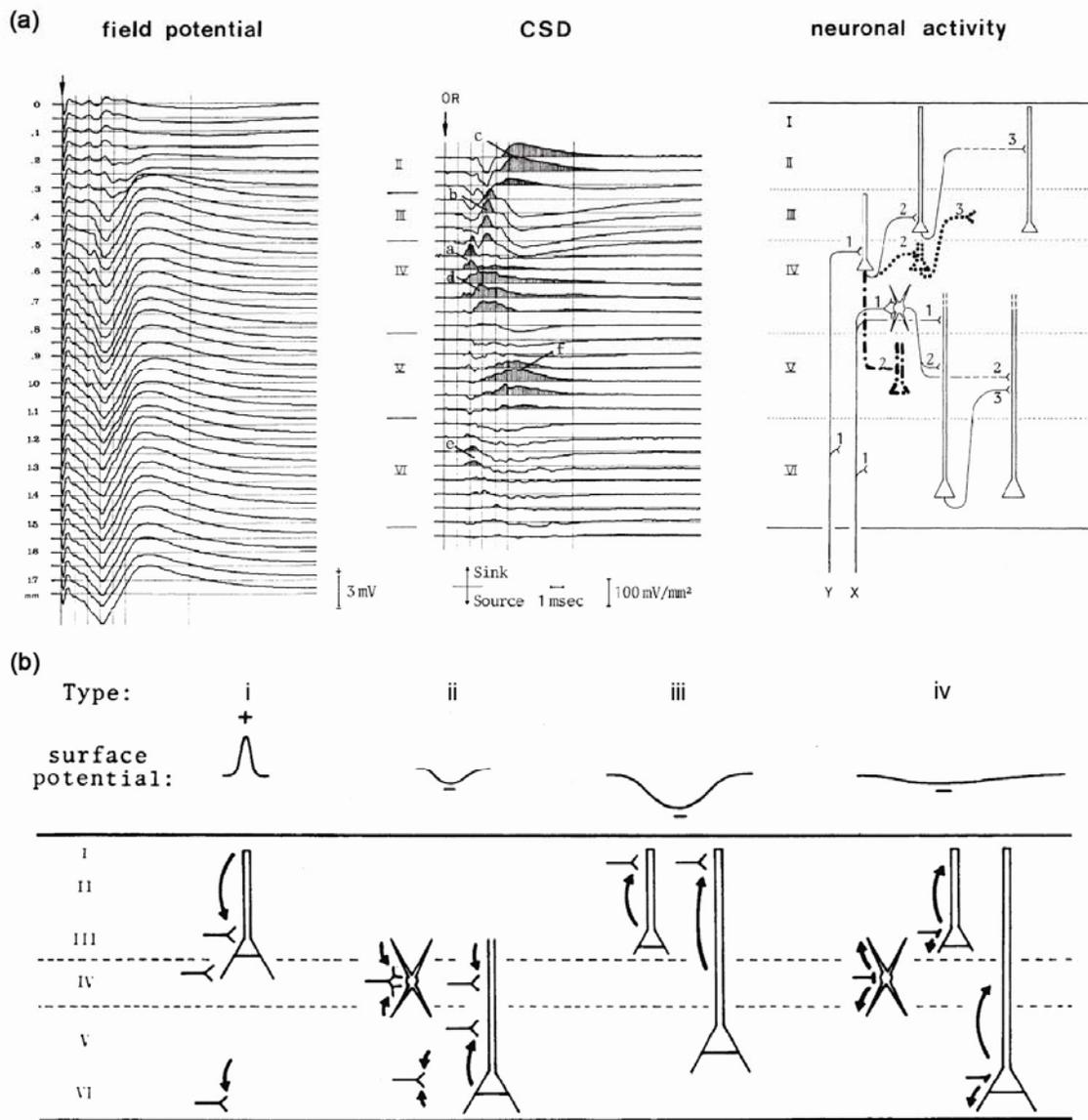
Figure 2. The physiological basis of the SCP.**(a)***Left*: field potential in primary visual cortex of the cat evoked by electrical stimulation of optical radiation. Each trace is the average of 20 responses. Distance between adjacent recordings is 50 μm. *Middle*: current source-density (CSD) distribution obtained from the potential profile on the left. Sinks, corresponding to active EPSPs, are shaded. Cortical laminae are indicated. Sinks a, b, and c reflect mono-, di-, and trisynaptic Y-type activity as shown in the right panel; sinks d and f reflect mono-, di-, and trisynaptic X-type activity shown in the right panel; sink e reflects Y-type and X-type monosynaptic activity. Sinks a, b, and e contribute to type *i* activity in **(b)**; sinks d and f contribute to type *ii* activity in **(b)**; sink c contributes to type *iii* activity in **(b)**. *Right*: schematic diagram of successive intracortical excitatory relay stations as well as cell types involved. Long-range feedback connections and nonspecific thalamic inputs are not depicted. **(b)** Schematic diagram of 4 main types of cortical activities and their reflection in surface potential (recorded by ECoG or EEG). *i*:

223

Depolarization of pyramidal cells at their deeper extremities, which generates a surface-positive potential deflection. *ii*: Depolarization of deep-layer pyramidal cells at their apical dendrites or stellate cells. This type of activity generates a sink in the middle layers and a surface-negative potential deflection. But because of the closed-field arrangement of CSD components, its contribution to surface potential is rather small. *iii*: Depolarization of superficial layer pyramidal cells at their apical dendrites. This is the main contributor to long-lasting surface-negative potentials. This type of activity involves long-distance connections and depends greatly on the general state of cortical excitability. *iv*: Inhibitory activity does not usually cause significant CSD contributions, because of the low amplitudes of membrane currents involved and a general lack of lamina specificity. Adapted with permission from Mitzdorf (Mitzdorf, 1985).

Given that negative SCPs index increased cortical excitability, it should not come as a surprise that during the negative shift of spontaneous SCP fluctuations there are increased multi-unit activity (Rebert, 1973), increased higher-frequency field potentials (Vanhatalo et al., 2004) (B.J. He *et al.*, unpublished), higher amplitude of short-latency evoked potentials such as P300 (Ergenoglu et al., 1998), and better behavioral performance ((Devrim et al., 1999) and see references in (Birbaumer et al., 1990)). The recently observed phase-coding in the delta frequency range (Lakatos et al., 2008; Montemurro et al., 2008) is likely of the same origin as information carried in the SCP phase. Of particular interest in the current context, since the SCP modulates the power of higher-frequency activities, it may be a more fundamental correlate of the fMRI signal than LFP power is, as implicated in a previous study (He et al., 2008).

The SCP is one important and substantial contributor to the fMRI signal (but not the only one—see Box 2). In addition to advancing our understanding of the fMRI signal and bridging the fMRI field and neurophysiological fields, this observation is also of particular interest in the study of consciousness. For example, fMRI experiments and single-unit recordings often show discordant results during manipulations of consciousness; this disagreement has been most dramatic in V1 (Logothetis, 2002; Maier

et al., 2008; Tong, 2003; Tononi and Koch, 2008). These puzzling results are at least partially illuminated when we bring the SCP and its underlying physiology into the picture. In the remainder of this article, we discuss these data and further propose a specific hypothesis on the involvement of the SCP in engendering conscious awareness.

The SCP and consciousness – a neurophysiological hypothesis of consciousness

From a theoretical perspective, information has to be integrated to contribute to conscious awareness, for conscious experience is always a unitary and undivided whole (Searle, 2000; Tononi, 2008). We suggest that the SCP may be an optimal neural substrate to carry such information integration across wide cortical areas because 1) its slow time scale allows synchronization across long distance despite axonal conduction delays (Buzsaki, 2006; He et al., 2008; Leopold et al., 2003; von Stein and Sarnthein, 2000); 2) long-range intracortical and corticocortical connections terminate preferentially in superficial layers and thus contribute significantly to the SCP. Furthermore, for each patch of superficial-layer pyramidal neurons (for definition of "patch", see Fig. 1 in (Douglas and Martin, 2004)), corresponding deep layer neurons could provide additional information through specialized local processing. These local deep-layer loops may constitute neural substrates for unconscious processes that can affect and be affected by conscious experience (for discussions on the relation between conscious and unconscious processes see Refs (Baars, 2005; Tononi, 2008)). A rough schematic depicting our hypothesis is shown in Fig. 3a.
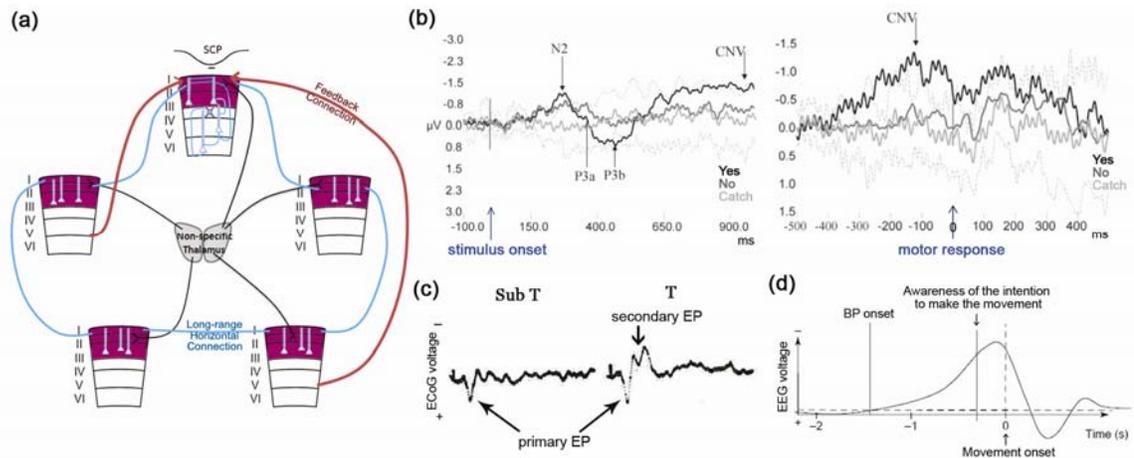
Figure 3. SCP and consciousness.**(a)**Schematic illustration of our hypothesis. Superficial layers of the cerebral cortex (shown in purple)are the only layers containing extensive long-range horizontal connections (thick blue lines); they are also the main target for nonspecific thalamocortical inputs (black lines) as well as long-range inter-areal feedback connections (thick red arrows). We propose that long-lasting synaptic activities in superficial layers, manifesting as SCPs in surface recording or low-frequency current source density (CSD) activity in superficial layers, carry large-scale information integration in the brain and contribute directly to conscious awareness. Neuronal circuits in deep layers (thin blue lines) provide specialized local processing that assist superficial-layer computations and send output to subcortical structures. Two specific predictions made by this hypothesis are provided in Conclusions. **(b)** Subjects performed a target detection task in which a visual grating stimulus at threshold was briefly presented. Following a variable delay, the subject was prompted by an auditory cue to press one of two buttons to indicate whether they saw the stimulus. A small percentage of catch trials in which no grating was presented were randomly interleaved. EEG potential from the left parietal electrode (P3, using Laplacian derivation, which emphasizes local vertical currents underneath the electrode) was averaged around the onset of grating stimulus (*left panel*), or around the motor response (*right panel*). The evoked potentials for "Yes, I saw", "No, I did not see", and catch trials are shown in black, dark grey and light grey respectively. The inter-subject s.d. for catch trials are shown as dotted lines. A negative slow potential builds up between stimulus onset and motor response during "Yes" trials but not catch trials nor the trials during which the stimulus was present but not perceived. Adapted with permission from Pins and ffytche et al.(Pins and Ffytche, 2003)**(c)** Average evoked-potentials (EPs) in response to single stimulus pulses at the skin, recorded from the surface of somatosensory cortex. EPs to 500 stimulus presentations were averaged for each condition. Sub T: subthreshold stimuli, none of the 500 stimuli were felt by the subject. T: threshold stimuli, subject reporting feeling some of the 500 stimuli. Each recording trace is 500 milliseconds long. Primary EP: a transient, surface-positive deflection that occurs ~30 ms after the stimulus, was present in both cases. Secondary EP: a later slower surface-negative component, only occurs when the stimulus was at times felt. Adapted with permission from Libet et al. (Libet et al., 1967)**(d)** The Bereitschaft potential (BP) is a negative SCP shift preceding the onset of a voluntary movement (Kornhuber and Deecke, 1965). It was shown by Libet (Libet et al., 1983)

that the onset of the BP also precedes the subject's subjective awareness of the intention to make the movement by a few hundred milliseconds. Adapted with permission from Haggard (Haggard, 2008).

Interestingly, the cerebellum, generally considered nonessential for consciousness (Tononi, 2008; Tononi and Koch, 2008), is notably weak in its low-frequency activity as compared to the neocortex (Bullock, 1997). The cerebellar cortex also lacks the "crowning mystery" – layer I, which is one major target for long-range feedback connections and nonspecific thalamic inputs (Douglas and Martin, 2004; Jones, 1998).

In what follows we review existing empirical data supporting a functional role of the SCP in the emergence of conscious awareness.

Attention

Although attention and consciousness are distinct and dissociable phenomena (Tononi and Koch, 2008), attention clearly affects which information has better access to conscious awareness. The top-down effect of attention in early sensory cortex is largely invisible to spike recordings, but is readily seen in the fMRI signal (Logothetis, 2002). Consistent with a close correspondence between the SCP and the fMRI signal as argued here, top-down influence in V1 can be seen with measurements of the SCP using either optical imaging or field potential recordings (Lakatos et al., 2008; Roland et al., 2006). In the first case, a feedback wave of depolarization was found to traverse the superficial layers from higher-order to lower-order visual areas (Roland et al., 2006). In the second case, top-down attention was found to modulate the phase of delta-frequency activity which further modulated the power of higher frequencies (Lakatos et al., 2008). Importantly, this effect was found only in superficial layers, consistent with the

physiology of the SCP and with the laminar preference of feedback connections (Douglas and Martin, 2004).

Perception

Many studies have investigated the neural correlates of conscious visual perception (for a recent review see (Tononi and Koch, 2008)), however, only a handful presented data including the SCP, which we will focus on here. Pins and ffytche (Pins and Ffytche, 2003) presented visual stimulation at threshold to normal subjects, so that an identical stimulus would sometimes be perceived and at other times not. In trials during which the subject perceived the stimulus, a negative slow potential builds up over parietal electrodes between the stimulus onset and the response. This slow potential was next to nonexistent in trials during which the stimulus escaped conscious perception (Fig. 3b). Using a visual illusion task and depth recording in V1, Leopold and colleagues (Leopold et al., 2008) showed that perceptual suppression was only associated with changes in the lowest frequencies in upper cortical layers when the current source density (CSD) method (which has much better localizing power than raw field potentials, see Fig. 2a) was used. Similar to the SCP, the fMRI signal also tracks perceptual changes, whereas spiking activity was unaffected (Maier et al., 2008). Furthermore, momentary fluctuations in the spontaneous SCP have an effect on whether a stimulus at threshold is consciously perceived or not (Devrim et al., 1999). An active involvement of the SCP in conscious perception is also supported by early experiments in the somatosensory domain. Through a series of elegant experiments using skin stimuli, electrical stimulations applied to the subcortical pathway and the cortex itself, Libet (Libet et al., 1967) showed that the

secondary evoked response (i.e., a long-lasting negative potential in surface-recordings), but not the primary response (i.e., the short-latency positive potential), was essential for conscious perception (Fig. 3c). These findings have since received support from more recent studies (Rossion et al., 2000; Sergent et al., 2005).

Volition

If consciousness is a two-sided coin, then on one side it is occupied by perception/experience; on the other side by volition/agency (Gray et al., 2007). Similar to perception, volition (i.e., voluntary actions) also has a long recognized association with the SCP. It was discovered more than 20 years ago that a negative SCP shift preceded voluntary movement (Kornhuber and Deecke, 1965) and even the subjective awareness of the intention to make the movement (Libet et al., 1983) (Fig. 3d). Though the implications of these results were highly debated by philosophers, the essential findings have been replicated numerous times and extended (Haggard, 2008; Libet, 2000). Specifically, recent fMRI experiments have determined both the brain regions underlying the intention to make a movement and those underlying the awareness of such intention (Haggard, 2008). Important in the current context, recent results showed that the outcome of a free choice can be decoded using the fMRI signal up to 6 sec before the decision outcome enters conscious awareness (Soon et al., 2008). Future experiments should illuminate whether this early fMRI signal is related to the early negative SCP shift preceding a voluntary action.

The unconscious states

One of the most dramatic experimental manipulations of consciousness comes from stimulations of intralaminar thalamic nuclei in minimally conscious patients (Schiff et al., 2007) and anesthetized rats (Alkire et al., 2007). In both cases of impaired consciousness, stimulation of nonspecific thalamic pathways significantly improved behavioral responsiveness. As mentioned previously, nonspecific thalamic afferents terminate preferentially on apical dendrites in cortical superficial layers. Therefore, stimulation of these pathways would drive negative shifts of the SCP (i.e., increased excitability) and thus may restore long-range communications carried by this signal. Similarly, recovery from persistent vegetative state (PVS) was accompanied by restoration of functional connectivity between the intralaminar thalamic nuclei and prefrontal cortex (Laureys et al., 2000). These experiments lend important support for the current hypothesis of a relation between the SCP and conscious awareness. Further support comes from DC-recordings of auditory evoked potentials (AEP) in humans undergoing propofol anesthesia (Fitzgerald et al., 2001). Whereas the early positive component of AEP was preserved during anesthesia, the later component – a negative shift in the SCP was abolished under anesthesia and reappeared during emergence from anesthesia.

These results however do not suggest that the negative SCP, whenever it appears, is an index of conscious awareness. Instead, key brain regions may be required (Box 3) (Bud Craig, 2009; Dehaene et al., 2006; Tononi and Koch, 2008). For example, the negative SCP can occur in primary sensory cortex under anesthesia (Fig. 2a) without propagating to higher-order areas (Fitzgerald et al., 2001). In parallel, fMRI signal activation in response to sensory stimulation is usually found in primary sensory but not

higher-order areas in anesthetized or PVS patients (Heinke et al., 2004; Laureys et al., 2005).

Large-scale coherent structures in the spontaneous fluctuations of both the SCP and the fMRI signal (Box 3) have been described under unconscious states – slow-wave sleep (SWS) and deep anesthesia respectively (He et al., 2008; Vincent et al., 2007). Do these findings contradict the current hypothesis? We suggest not. These coherent fluctuations could reflect spontaneous synaptic activity constrained by anatomical connections that continue to maintain homeostasis in the brain (Marder and Goaillard, 2006), but which lack sufficient information content (such as the bistable dynamics of "up-and-down states" (Tononi, 2008)) or the integration necessary for the emergence of consciousness. In fact, in both cases, the patterns of SCP or fMRI signal coherence were weaker in the unconscious state as compared to the conscious states (He et al., 2008; Vincent et al., 2007). A decreased baseline level of cortical excitability (not assessed by temporal correlation measurements) may also contribute to loss of consciousness, as supported by aforementioned experiments in which stimulation of nonspecific thalamic pathways restored responsiveness in subjects with impaired consciousness (Alkire et al., 2007; Schiff et al., 2007).

Concluding remarks

Studies on the neural basis of the fMRI signal have focused on the LFP power. We here present evidence for another neurophysiological signal underlying the fMRI signal that has received much less attention – the slow cortical potential (SCP). The linkage between the SCP and the fMRI signal not only advances our understanding of

cortical physiology but also provides a different vantage point to many experimental results. I further propose that the SCP may carry large-scale information integration in the neocortex that contributes to the emergence of conscious awareness. Experiments on consciousness have seldom included the SCP, but whenever it was included, the results appear to be consistent with the above hypothesis. Given that this hypothesis involves a specific physiological process, it is clearly amenable to empirical testing.

Specifically, the hypothesis put forward makes two testable predictions:

I) Whenever there is a change in the content of conscious awareness, there should also be a concurrent change in the SCP in corresponding essential brain regions (which yet need to be determined for different forms of conscious awareness – we offer a speculation on this in Box 3).

II) In altered states of consciousness, such as deep slow-wave sleep, under anesthesia, or in patients with severe brain injury, the spontaneous organization of the SCP that is important for large-scale information integration should be altered compared to the fully conscious state. This should also apply to systems with reduced consciousness, such as the cerebellum (in comparison to the cerebrum), and maybe organisms lower on the evolutionary tree (see Box 3).

I look forward to future work that confirms or falsifies this hypothesis.

Box 1. Is the SCP an oscillation?

The SCP frequency band has also been referred to as "infraslow oscillations" (Vanhatalo et al., 2004), but is the SCP really an oscillation? EEG can be classified in

three distinct groups (Logothetis, 2002): rhythmic, arrhythmic and dysrhythmic. The first two appear in normal subjects and refer to waves of approximately constant frequency and no stable rhythms, respectively. The latter refers to pathological rhythms in patient groups. Rhythmic EEG is further subdivided into frequency bands known as delta, theta, alpha, beta and gamma, etc. The SCP frequency range does not normally contain any true rhythmic activity, except the "up-and-down states" (also called the "slow oscillation" by its discoverer (Steriade et al., 1993)) that occurs during deep sleep (~0.8 Hz). The "up-and-down states" is a distinct phenomenon that can be easily differentiated from the SCP (for detailed discussions see supplementary materials in He et al. (He et al., 2008)). Therefore SCP is a fluctuation rather than oscillation (Monto et al., 2008) (B.J. He *et al.*, unpublished). The confusion between fluctuations and oscillations, or, arrhythmic and rhythmic activities, is quite common. This is largely because time-frequency analyses widely adopted create artificial rhythmic signals. However, as pointed out by T.H. Bullock, "Most of the time in most animals there is little evidence of really rhythmic oscillators in the ongoing cerebral activity, let alone that rhythms account for much of the total energy" (Bullock, 1997). We here avoid using terms such as "delta" or "infra-delta" to describe the SCP, because these terms have connotations of oscillations that are not present in an arrhythmic signal.

Box 2: Other contributors to the fMRI signal

The arguments we have put forward for a close correspondence between the SCP and the fMRI signal do not imply that the SCP is the sole contributor to the fMRI signal. Because excitatory synaptic activities contribute to an increased fMRI signal irrespective

of cortical depth (the mechanisms of which are reviewed in details elsewhere (Lauritzen and Gold, 2003; Raichle and Mintun, 2006)), the short-latency positive components of sensory evoked potentials, indexing the initial excitations of mid-layer cell bodies, should also contribute to the fMRI signal activation (e.g., Eichele et al., 2005; Mobascher et al., 2009). Accordingly, fMRI signal increases were found to spread first from layer IV during sensory stimulation in anaesthetized animals (Silva and Koretsky, 2002). The contribution of inhibitory neurons to the fMRI signal remains undetermined, even though their activity is clearly accompanied by changes in blood flow and glucose metabolism (Buzsaki et al., 2007; Lauritzen and Gold, 2003).

Box 3. Brain networks, information integration and consciousness.

Spontaneous SCP and fMRI signals are temporally correlated within a set of large-scale functional brain networks such as those associated with visual, auditory, somato-sensory/motor, language, attention, executive, and self-reflective functions (see (He et al., 2008) and the references therein). The temporal correlation or independent component maps normally presented to describe these networks tend to leave an impression that these networks are separate entities. This impression overlooks the cross-network interactions that are constantly taking place. If one watches the raw fluctuations of the spontaneous fMRI signal, the signal increases appear to move from one network to another with different time-lags in different nodes within a network (see ftp://imaging.wustl.edu/pub/raichlab/Spontaneous_fMRI_signal_movies/). The exact physiology underlying cross-network interaction is yet unclear, though one specific example might be the anti-correlation between the attention/cognitive-control networks

234

and the default network (Fox et al., 2009). Interestingly, though both sets of networks were present in anesthetized monkeys (Vincent et al., 2007), this anti-correlation between networks was gone (unpublished data). Both cross-network and within-network interactions should play a role in large-scale information integration that contributes to conscious awareness.

Not all brain networks contribute to consciousness equally, as discussed in the text. We speculate that the anterior cingulate and anterior insular cortices, as well as the default network, might be more pivotal than the sensory/motor networks and maybe even the dorsal attention network (including the dorsal visual stream and frontal eye field) in the emergence of consciousness. This conjecture mainly comes from a thought experiment comparing the largely unconscious state – slow-wave sleep (SWS), with the conscious states including wakefulness and rapid-eye-movement (REM) sleep. Whereas the sensory/motor regions and the dorsal attention network are as active in SWS as in wakefulness; the anterior cingulate, anterior insular and the midline regions of the default network are deactivated in SWS and reactivated in both REM sleep and wakefulness (Braun et al., 1997; Maquet et al., 2005). To the best of our knowledge, this conjecture is also consistent with existing data from persistent vegetative patients, blindsight patients (Laureys et al., 2005; Milner and Goodale, 2008), and from manipulations of momentary conscious perception (Bud Craig, 2009; Dehaene et al., 2006).

Finally, a corollary prediction of the present hypothesis is that in most invertebrates (except octopus which does not conform to the following characterization), consciousness, if present, might be very different from that in vertebrates because the invertebrate nervous systems are similar to the vertebrate cerebellum, spinal cord or brain

stem, but distinct from the vertebrate cerebrum, in two aspects: (i) with much pronounced fast activity but notably weak slow activity; (ii)seems to consist of a population of relatively independent neurons with little integration across the population (Bullock and Basar, 1988). This prediction is not formalized herein because we consider it to be non-testable by current empirical means, for a human being cannot be an invertebrate and experience what it experiences from inside, therefore to judge what a fruit fly experiences by observing its exhibited behaviors from outside is ill-defined by empirical standards.

References:

Alkire, M.T., McReynolds, J.R., Hahn, E.L., and Trivedi, A.N. (2007). Thalamic microinjection of nicotine reverses sevoflurane-induced loss of righting reflex in the rat. Anesthesiology *107*, 264-272.

Arthurs, O.J., and Boniface, S. (2002). How well do we understand the neural origins of the fMRI BOLD signal? Trends Neurosci *25*, 27-31.

Baars, B.J. (2005). Global workspace theory of consciousness: toward a cognitive neuroscience of human experience. Prog Brain Res *150*, 45-53.

Birbaumer, N., Elbert, T., Canavan, A.G., and Rockstroh, B. (1990). Slow potentials of the cerebral cortex and behavior. Physiol Rev *70*, 1-41.

Braitenberg, V., and Schuz, A. (1998). In Cortex: Statistics and Geometry of Neuronal Connectivity (Germany: Springer).

Braun, A.R., Balkin, T.J., Wesenten, N.J., Carson, R.E., Varga, M., Baldwin, P., Selbie, S., Belenky, G., and Herscovitch, P. (1997). Regional cerebral blood flow

throughout the sleep-wake cycle. An H2(15)O PET study. Brain *120 (Pt 7)*, 1173-1197.

Bud Craig, A.D. (2009). How do you feel--now? The anterior insula and human awareness. Nat Rev Neurosci *10*, 59-70.

Bullock, T.H. (1997). Signals and signs in the nervous system: the dynamic anatomy of electrical activity is probably information-rich. Proc Natl Acad Sci U S A *94*, 1-6.

Bullock, T.H., and Basar, E. (1988). Comparison of ongoing compound field potentials in the brains of invertebrates and vertebrates. Brain Res *472*, 57-75.

Buzsaki, G. (2006). Rhythms of the Brain. (New York, NY: Oxford University Press), pp. 119-135.

Buzsaki, G., Kaila, K., and Raichle, M. (2007). Inhibition and brain work. Neuron *56*, 771-783.

Cooper, R., Crow, H.J., Walter, W.G., and Winter, A.L. (1966). Regional control of cerebral vascular reactivity and oxygen supply in man. Brain Res *3*, 174-191.

Dehaene, S., Changeux, J.P., Naccache, L., Sackur, J., and Sergent, C. (2006). Conscious, preconscious, and subliminal processing: a testable taxonomy. Trends Cogn Sci *10*, 204-211.

Devrim, M., Demiralp, T., Kurt, A., and Yucesir, I. (1999). Slow cortical potential shifts modulate the sensory threshold in human visual system. Neurosci Lett *270*, 17-20.

Douglas, R.J., and Martin, K.A. (2004). Neuronal circuits of the neocortex. Annu Rev Neurosci *27*, 419-451.

Eichele, T., Specht, K., Moosmann, M., Jongsma, M.L., Quiroga, R.Q., Nordby, H., and Hugdahl, K. (2005). Assessing the spatiotemporal evolution of neuronal

activation with single-trial event-related potentials and functional MRI. Proc Natl Acad Sci U S A *102*, 17798-17803.

Ergenoglu, T., Demiralp, T., Beydagi, H., Karamursel, S., Devrim, M., and Ermutlu, N. (1998). Slow cortical potential shifts modulate P300 amplitude and topography in humans. Neurosci Lett *251*, 61-64.

Fitzgerald, R.D., Lamm, C., Oczenski, W., Stimpfl, T., Vycudilik, W., and Bauer, H. (2001). Direct current auditory evoked potentials during wakefulness, anesthesia, and emergence from anesthesia. Anesth Analg *92*, 154-160.

Fox, M.D., Zhang, D., Snyder, A.Z., and Raichle, M.E. (2009). The Global Signal and Observed Anticorrelated Resting State Brain Networks. J Neurophysiol.

Goense, J.B., and Logothetis, N.K. (2008). Neurophysiology of the BOLD fMRI signal in awake monkeys. Curr Biol *18*, 631-640.

Goldring, S. (1974). DC Shifts Released by Direct and Affrent Stimulation. In Handbook of Electroencephalography and Clinical Neurophysiology, A. Remond, ed. (Amsterdam: Elsevier), pp. 12-24.

Gray, H.M., Gray, K., and Wegner, D.M. (2007). Dimensions of mind perception. Science *315*, 619.

Haggard, P. (2008). Human volition: towards a neuroscience of will. Nat Rev Neurosci *9*, 934-946.

He, B.J., Snyder, A.Z., Zempel, J.M., Smyth, M.D., and Raichle, M.E. (2008). Electrophysiological correlates of the brain's intrinsic large-scale functional architecture. Proc Natl Acad Sci U S A *105*, 16039-16044.

Heinke, W., Fiebach, C.J., Schwarzbauer, C., Meyer, M., Olthoff, D., and Alter, K. (2004). Sequential effects of propofol on functional brain activation induced by auditory language processing: an event-related functional magnetic resonance imaging study. Br J Anaesth *92*, 641-650.

Jones, E.G. (1998). Viewpoint: the core and matrix of thalamic organization. Neuroscience *85*, 331-345.

Jones, M.O., Martin, C., Boorman, L., Harris, S., Bartlett, K., Kennerley, A., Zheng, Y., Berwick, J., and Mayhew, J.E.W. (2007). Interactions between evoked and spontaneous hemodynamic fluctuations in rodent brain. In 37th Annual Meeting of Society for Neuroscience, San Diego (San Diego).

Kayser, C., Kim, M., Ugurbil, K., Kim, D.S., and Konig, P. (2004). A comparison of hemodynamic and neural responses in cat visual cortex using complex stimuli. Cereb Cortex *14*, 881-891.

Khader, P., Schicke, T., Roder, B., and Rosler, F. (2008). On the relationship between slow cortical potentials and BOLD signal changes in humans. Int J Psychophysiol *67*, 252-261.

Kornhuber, H.H., and Deecke, L. (1965). [Changes in the Brain Potential in Voluntary Movements and Passive Movements in Man: Readiness Potential and Reafferent Potentials.]. Pflugers Arch Gesamte Physiol Menschen Tiere *284*, 1-17.

Lakatos, P., Karmos, G., Mehta, A.D., Ulbert, I., and Schroeder, C.E. (2008). Entrainment of neuronal oscillations as a mechanism of attentional selection. Science *320*, 110-113.

Laureys, S., Faymonville, M.E., Luxen, A., Lamy, M., Franck, G., and Maquet, P. (2000). Restoration of thalamocortical connectivity after recovery from persistent vegetative state. Lancet *355*, 1790-1791.

Laureys, S., Perrin, F., Schnakers, C., Boly, M., and Majerus, S. (2005). Residual cognitive function in comatose, vegetative and minimally conscious states. Curr Opin Neurol *18*, 726-733.

Lauritzen, M., and Gold, L. (2003). Brain function and neurophysiological correlates of signals used in functional neuroimaging. J Neurosci *23*, 3972-3980.

Leopold, D.A., Aura, C., and Maier, A.V. (2008). Laminar analysis of local field and current source density during physical and perceptual events in monkey V1. In 38th Annual Meeting of Society for Neuroscience, Washington D.C. (Washington, DC).

Leopold, D.A., Murayama, Y., and Logothetis, N.K. (2003). Very slow activity fluctuations in monkey visual cortex: implications for functional brain imaging. Cereb Cortex *13*, 422-433.

Libet, B. (2000). Time factors in conscious processes: reply to Gilberto Gomes. Conscious Cogn *9*, 1-12.

Libet, B., Alberts, W.W., Wright, E.W., Jr., and Feinstein, B. (1967). Responses of human somatosensory cortex to stimuli below threshold for conscious sensation. Science *158*, 1597-1600.

Libet, B., Gleason, C.A., Wright, E.W., and Pearl, D.K. (1983). Time of conscious intention to act in relation to onset of cerebral activity (readiness-potential). The unconscious initiation of a freely voluntary act. Brain *106 (Pt 3)*, 623-642.

Logothetis, N.K. (2002). The neural basis of the blood-oxygen-level-dependent

    functional magnetic resonance imaging signal. Philos Trans R Soc Lond B Biol

    Sci *357*, 1003-1037.

Logothetis, N.K. (2008). What we can do and what we cannot do with fMRI. Nature *453*,

    869-878.

Logothetis, N.K., Pauls, J., Augath, M., Trinath, T., and Oeltermann, A. (2001).

    Neurophysiological investigation of the basis of the fMRI signal. Nature *412*,

    150-157.

Lu, H., Zuo, Y., Gu, H., Waltz, J.A., Zhan, W., Scholl, C.A., Rea, W., Yang, Y., and

    Stein, E.A. (2007). Synchronized delta oscillations correlate with the resting-state

    functional MRI signal. Proc Natl Acad Sci U S A *104*, 18265-18269.

Maier, A., Wilke, M., Aura, C., Zhu, C., Ye, F.Q., and Leopold, D.A. (2008). Divergence

    of fMRI and neural signals in V1 during perceptual suppression in the awake

    monkey. Nat Neurosci *11*, 1193-1200.

Maquet, P., Ruby, P., Maudoux, A., Albouy, G., Sterpenich, V., Dang-Vu, T., Desseilles,

    M., Boly, M., Perrin, F., Peigneux, P., and Laureys, S. (2005). Human cognition

    during REM sleep and the activity profile within frontal and parietal cortices: a

    reappraisal of functional neuroimaging data. Prog Brain Res *150*, 219-227.

Marder, E., and Goaillard, J.M. (2006). Variability, compensation and homeostasis in

    neuron and network function. Nat Rev Neurosci *7*, 563-574.

Milner, A.D., and Goodale, M.A. (2008). Two visual systems re-viewed.

    Neuropsychologia *46*, 774-785.

Mitzdorf, U. (1985). Current source-density method and application in cat cerebral cortex: investigation of evoked potentials and EEG phenomena. Physiol Rev *65*, 37-100.

Mobascher, A., Brinkmeyer, J., Warbrick, T., Musso, F., Wittsack, H.J., Saleh, A., Schnitzler, A., and Winterer, G. (2009). Laser-evoked potential P2 single-trial amplitudes covary with the fMRI BOLD response in the medial pain system and interconnected subcortical structures. Neuroimage *45*, 917-926.

Montemurro, M.A., Rasch, M.J., Murayama, Y., Logothetis, N.K., and Panzeri, S. (2008). Phase-of-firing coding of natural visual stimuli in primary visual cortex. Curr Biol *18*, 375-380.

Monto, S., Palva, S., Voipio, J., and Palva, J.M. (2008). Very slow EEG fluctuations predict the dynamics of stimulus detection and oscillation amplitudes in humans. J Neurosci *28*, 8268-8272.

Mukamel, R., Gelbard, H., Arieli, A., Hasson, U., Fried, I., and Malach, R. (2005). Coupling between neuronal firing, field potentials, and FMRI in human auditory cortex. Science *309*, 951-954.

Nagai, Y., Critchley, H.D., Featherstone, E., Fenwick, P.B., Trimble, M.R., and Dolan, R.J. (2004). Brain activity relating to the contingent negative variation: an fMRI investigation. Neuroimage *21*, 1232-1241.

Niessing, J., Ebisch, B., Schmidt, K.E., Niessing, M., Singer, W., and Galuske, R.A. (2005). Hemodynamic signals correlate tightly with synchronized gamma oscillations. Science *309*, 948-951.

Nir, Y., Mukamel, R., Dinstein, I., Privman, E., Harel, M., Fisch, L., Gelbard-Sagiv, H., Kipervasser, S., Andelman, F., Neufeld, M.Y.*, et al.* (2008). Interhemispheric correlations of slow spontaneous neuronal fluctuations revealed in human sensory cortex. Nat Neurosci *11*, 1100-1108.

Pins, D., and Ffytche, D. (2003). The neural correlates of conscious vision. Cereb Cortex *13*, 461-474.

Raichle, M.E., and Mintun, M.A. (2006). Brain work and brain imaging. Annu Rev Neurosci *29*, 449-476.

Rauch, A., Rainer, G., and Logothetis, N.K. (2008). The effect of a serotonin-induced dissociation between spiking and perisynaptic activity on BOLD functional MRI. Proc Natl Acad Sci U S A *105*, 6759-6764.

Rebert, C.S. (1973). Slow potential correlates of neuronal population responses in the cat's lateral geniculate nucleus. Electroencephalogr Clin Neurophysiol *35*, 511-515.

Roland, P.E. (2002). Dynamic depolarization fields in the cerebral cortex. Trends Neurosci *25*, 183-190.

Roland, P.E., Hanazawa, A., Undeman, C., Eriksson, D., Tompa, T., Nakamura, H., Valentiniene, S., and Ahmed, B. (2006). Cortical feedback depolarization waves: a mechanism of top-down influence on early visual areas. Proc Natl Acad Sci U S A *103*, 12586-12591.

Rosler, F., Heil, M., and Roder, B. (1997). Slow negative brain potentials as reflections of specific modular resources of cognition. Biol Psychol *45*, 109-141.

Rossion, B., de Gelder, B., Pourtois, G., Guerit, J.M., and Weiskrantz, L. (2000). Early extrastriate activity without primary visual cortex in humans. Neurosci Lett *279*, 25-28.

Scheibel, M.E., and Scheibel, A.B. (1967). Structural organization of nonspecific thalamic nuclei and their projection toward cortex. Brain Res *6*, 60-94.

Schiff, N.D., Giacino, J.T., Kalmar, K., Victor, J.D., Baker, K., Gerber, M., Fritz, B., Eisenberg, B., Biondi, T., O'Connor, J.*, et al.* (2007). Behavioural improvements with thalamic stimulation after severe traumatic brain injury. Nature *448*, 600-603.

Searle, J.R. (2000). Consciousness. Annu Rev Neurosci *23*, 557-578.

Sergent, C., Baillet, S., and Dehaene, S. (2005). Timing of the brain events underlying access to consciousness during the attentional blink. Nat Neurosci *8*, 1391-1400.

Shipton, H.W. (1975). EGG analysis: a history and a prospectus. Annu Rev Biophys Bioeng *4*, 1-13.

Shmuel, A., and Leopold, D.A. (2008). Neuronal correlates of spontaneous fluctuations in fMRI signals in monkey visual cortex: Implications for functional connectivity at rest. Hum Brain Mapp *29*, 751-761.

Silva, A.C., and Koretsky, A.P. (2002). Laminar specificity of functional MRI onset times during somatosensory stimulation in rat. Proc Natl Acad Sci U S A *99*, 15182-15187.

Song, J.H., and Jiang, Y. (2006). Visual working memory for simple and complex features: an fMRI study. Neuroimage *30*, 963-972.

Soon, C.S., Brass, M., Heinze, H.J., and Haynes, J.D. (2008). Unconscious determinants of free decisions in the human brain. Nat Neurosci *11*, 543-545.

Steriade, M., Nunez, A., and Amzica, F. (1993). A novel slow (< 1 Hz) oscillation of neocortical neurons in vivo: depolarizing and hyperpolarizing components. J Neurosci *13*, 3252-3265.

Tong, F. (2003). Primary visual cortex and visual awareness. Nat Rev Neurosci *4*, 219-229.

Tononi, G. (2008). Consciousness as integrated information: a provisional manifesto. Biol Bull *215*, 216-242.

Tononi, G., and Koch, C. (2008). The neural correlates of consciousness: an update. Ann N Y Acad Sci *1124*, 239-261.

Vanhatalo, S., Palva, J.M., Holmes, M.D., Miller, J.W., Voipio, J., and Kaila, K. (2004). Infraslow oscillations modulate excitability and interictal epileptic activity in the human cortex during sleep. Proc Natl Acad Sci U S A *101*, 5053-5057.

Vincent, J.L., Patel, G.H., Fox, M.D., Snyder, A.Z., Baker, J.T., Van Essen, D.C., Zempel, J.M., Snyder, L.H., Corbetta, M., and Raichle, M.E. (2007). Intrinsic functional architecture in the anaesthetized monkey brain. Nature *447*, 83-86.

Viswanathan, A., and Freeman, R.D. (2007). Neurometabolic coupling in cerebral cortex reflects synaptic more than spiking activity. Nat Neurosci *10*, 1308-1312.

Vogel, E.K., and Machizawa, M.G. (2004). Neural activity predicts individual differences in visual working memory capacity. Nature *428*, 748-751.

von Stein, A., and Sarnthein, J. (2000). Different frequencies for different scales of

cortical integration: from local gamma to long range alpha/theta synchronization.

Int J Psychophysiol *38*, 301-313.

EPILOGUE

I came to St. Louis in the summer of 2004 to pursue a Ph.D. in neurosciences. Over the past five and a half years, other than having grown a good deal personally (it was a long time!), I consider that I have made the following scientific contributions:

1) Established the functional significance of spatiotemporal structures present in spontaneous fMRI signals;

2) Discovered a novel neurophysiological correlate of the fMRI signal, the slow cortical potential (SCP);

3) Proposed a neurophysiologically based hypothesis on the emergence of conscious awareness;

4) Demonstrated a rich temporal organization present within and a potential functional significance of the arrhythmic, scale-free brain activity (commonly called "$1/f$ noise").

A rough idea of my next-step research, which has to be qualified by the totally unpredictable nature of where science takes one, is to test the hypothesis on SCP and consciousness, and to bring it together with my work on scale-free brain activity, as well as other neurophysiological phenomena of the brain.

A brief Curriculum Vitae at this point is attached below.

Biyu Jade He

BIOGRAPHICAL INFORMATION:

Birth date / place: December 2nd, 1985 / China

Work address: Department of Radiology
Washington University School of Medicine
4525 Scott Ave. St. Louis, MO, 63110

E-mail: biyu.jade.he@gmail.com

EDUCATION:

2004 – Present   Neurosciences program, Division of Biology and Biomedical Sciences.
Ph.D. Candidate   Washington University School of Medicine, St. Louis, U.S.
Advisiors: Marcus E. Raichle and Maurizio Corbetta

2000 –2004   Tsinghua University, Beijing, China.   Major: Biology.
B. Sci.   Research Advisors: Yi Zhong and Zuoping Xie

FELLOWSHIPS, AWARDS AND HONORS:

2008   Fellowship, Summer Institute in Cognitive Neuroscience, Lake Tahoe, California.
(Was not able to attend due to visa background security check.)

2008   James L. O'Leary Prize finalist, Washington University

2007   C-WIN graduate student travel award, Society for Neuroscience

2007   Fellowship and Presentation, Workshop on Cognitive Neurobiology,
Okinawa Institute of Science and Technology, Okinawa, Japan.

2007   Fine Science Travel Fellowship,
Neuroscience graduate program, Washington University

2006   Hope Center for Neurological Disorders Award,
Washington University School of Medicine

2006   Fellowship, Summer Institute in Cognitive Neuroscience, Dartmouth College.
"Conscious and unconscious cognition and their interface with artificial devices."

2006   Fellowship, John Merck Fund Summer Insitute on the Biology of Developmental
Disabilities, Princeton University. (Could not attend due to conflict of schedule)

2002	Zhou Huiqi Scholarship for Academic Excellence (Highest award for academic achievement in the Dept. of Biology), Tsinghua University
2001	Zhou Huiqi Scholarship for Academic Excellence, Tsinghua University
2000	Zhou Huiqi Scholarship for Academic Excellence, Tsinghua University
2000	Scholarship for Excellent Freshman, Tsinghua University
2000	Champion in the National College Entrance Exams, China (equivalent to SAT)
1998	National Mathematics Olympiad, First prize in the all-China finals

TEACHING POSITION:

| 2005 | Teaching assistant to Washington University course "Principles of the Nervous System" |

PEER-REVIEWED JOURNAL ARTICLES:

Biyu J. He and Marcus E. Raichle. The fMRI signal, slow cortical potential and consciousness. **Trends in Cognitive Sciences.** 2009 Jul; 13(7):302-9
With cover illustration.

Biyu J. He, Abraham Z. Snyder, John M Zempel, Matthew D. Smyth, and Marcus E. Raichle. Electrophysiological correlates of the brain's intrinsic large-scale functional architecture. **Proc Natl Acad Sci U S A.** 2008 Oct;105(41):16039-44
Preview in Balduzzi, Riedner and Tononi. PNAS. 2008 Oct;105(41):15641-2

Biyu J. He, Abraham Z. Snyder, Justin L. Vincent, Adrian Epstein, Gordon L. Shulman, and Maurizio Corbetta. Breakdown of functional connectivity in frontoparietal networks underlies behavioral deficits in spatial neglect. **Neuron.** 2007 Mar;53(6): 905-918
Preview in: Gabrieli and Whitfield-Gabrieli. Neuron. 2007 Mar;53(6):776-7

James M. Johnston, S. Neil Vaishnavi, Matthew D. Smyth, Dongyang Zhang, **Biyu J. He**, John M. Zempel, Joshua S. Shimony, Abraham Z. Snyder, and Marc E. Raichle. Loss of resting interhemispheric functional connectivity after complete section of the corpus callosum. **Journal of Neuroscience**. 2008 Jun;28(25):6453-8

Ayelet Sapir, Julie Kaplan, **Biyu J. He**, and Maurizio Corbetta. Neuroanatomical correlates of directional hypokinesia in patients with hemispatial neglect. **Journal of Neuroscience.** 2007 Apr; 27(15): 4045-4051

BOOK CHAPTERS, REVIEWS AND COMMENTARIES:

Biyu J. He and Marcus E. Raichle. Response to Koch: Elaborations on the SCP hypothesis. **Trends in Cognitive Sciences.** 2009 Sep; 13(9):368-9

Biyu J. He, Gordon L. Shulman, Abraham Z. Snyder, and Maurizio Corbetta. The role of impaired neuronal communication in neurological disorders. **Current Opinion in Neurology.** 2007 Dec; 20(6):655-60

Gaurav Patel, **Biyu J. He**, and Maurizio Corbetta. Attentional networks in the parietal cortex. In **Encyclopedia of Neuroscience**, Larry Squire (editor). Academic Press. 2008

PRESENTATIONS:

    2009   Complexity Workshop, Sage Center for the Study of the Mind,
                   University of Santa Barbara, CA, U.S.

CONFERENCE PROCEEDINGS:

B.J. He, A. Z. Snyder, J.M. Zempel, M.D. Smyth, M.E. Raichle. Cross-frequency coupling in human electrocorticorgraphy. Society for Neuroscience meeting, 2008, Washington D.C., U.S.

B.J. He, A.Z. Snyder, J. Zempel, M.D. Smyth, M.E. Raichle.Electrophysiological correlates of the brain's intrinsic large-scale functional architecture. Organization for Human Brain Mapping annual meeting, 2008, Melbourne, Australia.

B.J. He, A.Z. Snyder, J. Zempel, M.D. Smyth, M.E. Raichle. Electrophysiological underpinnings of spontaneous fMRI correlation maps. Society for Neuroscience meeting, 2007, San Diego, U.S.

J.M. Johnston, S.N. Vaishnavi, **B.J. He**, M.D. Smyth, J.M. Zempel, J.S. Shimony, A.Z. Snyder, M.E. Raichle. Loss of resting interhemispheric functional connectivity after complete corpus callosotomy in a six year old child with intractable epilepsy. Society for Neuroscience meeting, 2007, San Diego, U.S.

P. Ramkumar, L. Parkkonen, **B.J. He**, M.E. Raichle, M. Hämäläinen, R. Hari. Identification of stimulus-related and intrinsic networks by spatial independent component analysis of MEG signals. Society for Neuroscience meeting, 2007, San Diego, U.S.

B.J. He, A.Z. Snyder, J.L. Vincent, G.L. Shulman, M.Corbetta. Breakdown of frontoparietal functional connectivity characterizes spatial neglect. Oral Presentation in Society for Neuroscience meeting, 2006, Atlanta, U.S.

AD HOC REVIEWER FOR SCIENTIFIC JOURNALS:

Neuroimage.

PROFESSIONAL MEMBERSHIPS:

Society for Neuroscience
Orgination for Human Brain Mapping
American Association for the Advancement of Science (AAAS)